# An Internal Variable Constitutive Model for the Hot Working of Metals

by

**Stuart Bryan Brown**

B.S., Mechanical Engineering, Washington University, St. Louis (1977)
A.B., English Literature, Washington University, St. Louis (1977)
M.B.A., Stanford University (1979)
M.S., Mechanical Engineering, Stanford University (1980)

SUBMITTED IN PARTIAL FULFILLMENT
OF THE REQUIREMENTS FOR THE
DEGREE OF
DOCTOR OF PHILOSOPHY
IN MECHANICAL ENGINEERING

at the

MASSACHUSETTS INSTITUTE OF TECHNOLOGY
April 1987



Signature of Author _____
Department of Mechanical Engineering
April 9, 1987

Certified by _____
Professor Lallit Anand
Thesis Supervisor

Accepted by _____
Professor Ain Ants Sonin, Chairman
Departmental Committee on Graduate Studies

# AN INTERNAL VARIABLE CONSTITUTIVE MODEL FOR THE HOT WORKING METALS

by

STUART B. BROWN

Submitted to the Department of Mechanical Engineering
on April 15, 1987 in partial fulfillment of the
requirements for the Degree of Doctor of Philosophy in
Mechanical Engineering.

## ABSTRACT

An internal variable constitutive model has been developed for the deformation of metals at high homologous temperatures and moderate strain rates. A high temperature mechanical test system was designed and assembled, incorporating a vacuum/inert environment furnace mounted in a tension/torsion servohydraulic test machine. The system is capable of tests at temperatures up to approximately 1200 degrees Celsius and at strain rates up to 1 $sec^{-1}$. A set of tests appropriate to evaluating constitutive behavior within the context of an internal variable framework were performed. The tests were on an Fe - 2% Si alloy, and consisted of strain rate jump tests, constant true strain rate tests, and load-unload-hold-reload tests.

An internal variable model is formulated based on the test results, and a procedure is proposed for evaluating the model parameters. The correlation between the model and the experimental results is found to be excellent. Additional tests are performed to validate the model. These test results and the model predictions are in excellent agreement. An additional specimen configuration is proposed and tested to provide a gradient in internal structure which may then be correlated with a predicted state variable gradient. The state variable gradient predicted by the model duplicates the gradient of room temperature yield stress in the deformed and quenched specimen.

Thesis Supervisor: Dr. Lallit Anand

Title: Professor of Mechanical Engineering

VITA

## Education

- Master of Science in Mechanical Engineering, Stanford University, March, 1980.
- Master of Business Administration, Stanford University, May, 1979.
- Bachelor of Science in Mechanical Engineering, Washington University in Saint Louis, May, 1977.
- Bachelor of Arts in English Literature, Washington University in Saint Louis, May, 1977.

## Professional

- Senior Engineer, Failure Analysis Associates, Palo Alto, California, 1980 to 1982.

## Personal

- Born, August 15, 1955 in Cleveland, Ohio.
- Residence at time of publication of this document:
  784 Main Street, Apt. 6, Cambridge, Massachusetts 02139.

## ACKNOWLEDGEMENTS

It is impossible in this page to adequately thank all of the people who have helped me. Certainly, my greatest appreciation goes to Lallit Anand who provided support and guidance during my stay here at M.I.T. I hope that in the future I may find a way to repay his generosity.

I would also like to thank the Army Materials Testing Laboratory, Watertown, Massachusetts, the Shell Foundation, and M.I.T. for providing funds for my graduate studies. Dave Jablonski of Instron Corporation also provided much needed assistance at the commencement of this project.

Next I must acknowledge the help of my officemates. Charles White, Mehrdad Haghi, Mary Boyce, Kwon Kim, Tresa Pollock, Curt Bronkhurst and Shoichi Hashimoto all provided help and guidance. They all also provided cheerful help to a sometimes somewhat invalid me. Loads have been carried on my behalf which people had no obligation to bear; it was appreciated.

Many other individuals, either through their friendship or advice have made the last four years more pleasureable. Among these are Bill Henry, David Gladstone, Ann St. Onge, David Parks, Frank McClintock, Ali Argon, and Jay Keyser.

I hope that we will stay friends.

# Contents

# Chapter 1

# Introduction

Hot working refers to a collection of metal forming processes which take advantage of the lower flow stress and greater ductility of metals at high temperatures. It encompasses such operations as hot rolling, extrusion, and forging, where metals are heated to a large fraction of their melting temperatures and then subjected to large deformations. Hot working is a common operation in the processing of metals. It has been estimated that well over 80 percent of all metallic products undergo some form of hot working during their fabrication history [Semiatin et al. 1981].

The benefits of hot working are extensive. Large changes in shape may be achieved with each processing step. The machine loads required to achieve these changes are much lower than would be encountered at room temperature. There can be substantial savings in material, with properly designed processes producing little waste metal. There is also the opportunity to control material properties during the working operation. Many hot working processes produce beneficial distributions of oriented grains and introduce deformation-induced microstructures which increase the subsequent deformation and fracture resistance of the material.

There are several features common to most hot working processes. Most hot

working produces large deformations, with equivalent strains easily exceeding 1 or 2. Most processes, to achieve lower working loads, heat the worked metal to temperatures from one-half to nine-tenths its melting (homologous) temperature. Strain rates are similarly high, ranging from $10^{-2}$ per second for isothermal forgings to $10^{3}$ or more per second in finish rolling and high speed hammer operations. Many working processes are interrupted, incorporating multiple deformation passes on the same workpiece with hold periods between passes. Temperatures may vary dramatically, as a function of both time and position within the workpiece. Temperature changes may occur due to both heat losses to tooling and the atmosphere and the conversion of plastic work into heat. Finally, the mode of deformation may be extremely inhomogeneous, with very complex material flow paths involving large rotations, strains, and changes in strain rate.

Partially due to the conservatism of the industry and partially due to the complexity of the hot working process, much of the knowledge for the design of hot working processes has been both experiential and proprietary. The modelling of such processes requires the solution of very complex, strongly coupled mechanical and thermal boundary value problems. The advent of digital modelling techniques such as the finite element method is beginning to permit the simulation of working operations which before were frequently designed on a trial-and-error basis. The problems associated with such simulations, however, are far from resolved. Several difficulties remain, many which encompass experimental, theoretical, and computational disciplines. These difficulties include the proper accomodation of kinematics of large deformation, the complexity of material behavior possible in hot working, coupled thermo-mechanical deformation, the complex friction and thermal boundary conditions, and element distortion and remeshing.

This investigation concentrates on the central issue of appropriate large deformation constitutive equations for the high temperature deformation of metals. Currently used constitutive models (e.g. in the F.E.M. program ALPID) are usually simple three dimensional generalizations of uniaxial stress versus strain rate

relationships of the power law form where the stresses and strain rates are those obtained as "steady state" values after any transients have decayed [Thomsen, et. al. 1965; Jonas, 1969, Sellars 1972, 1978]. Although these models consider only steady state behavior, conditions described above for hot working are inherently non-steady. The interrupted, inhomogeneous deformations resulting from hot working may prevent the numerous operative physical mechanisms and thermally activated processes from ever reaching a steady state. The final state of a hot worked piece of metal therefore is strongly affected by its deformation history. This history dependence suggests a constitutive model of the internal variable type, where the current state or condition of the microstructure is tracked via a list of variables which evolve with the deformation and temperature history. These internal variables are not necessarily directly measureable, but may represent some averaged material property, such as a generalized resistance to plastic deformation. At any point, the internal variables are assumed to represent the condition of the metal; there is no need to know the prior thermo-mechanical history. A second list of variables is added to the list of internal variables to complete the constitutive model. These imposed or "external" variables such as strain rate, stress, and temperature are assumed, with the internal variables, to be sufficient to represent the current mechanical response of the material and the evolution of both the external and internal variables. The form of the model consists of a list of both external $e_i$ and internal $s_i$ variables, and evolution equations for each variable:

$$\frac{de_i}{dt} = \hat{e}_i(e_i, s_i)$$

$$\frac{ds_i}{dt} = \hat{s}_i(e_i, s_i)$$

Several investigators have recently proposed internal variable constitutive models for the high temperature deformation of metals [Hart, 1970, Bodner and Partom, 1975; Kocks, 1976; and Anand 1982]. Virtually all models except that of Anand have been proposed for application in the creep deformation regime, at temperatures and strain rates lower than that encountered in hot working. The issues associated with formulating an internal variable model in either regime are the same. However,

due to lack of experimental data in the hot working regime, it is not evident that a model formulated for creep may be extrapolated for hot working simulation. The model proposed by Anand for hot working was based on a reduced set of moderate strain, material tests representing a small subset of the hotworking regime. Anand by necessity assumed functional forms for his material model which he then fit to the experimental data. No data were available for model validation independent of that used for the fitting of model parameters.

The goals of the research represented by this thesis are therefore:

1. Develop a high temperature mechanical test system to characterize metal behavior in the hot working regime, including high homologous temperatures, moderate strain rates, and large strains.

2. Perform experiments necessary to investigate the constitutive response of a representative metal in the hot working regime.

3. Formulate an internal variable constitutive model from the experimental data, with the following considerations:

   a. The model should represent large, three dimensional deformations in the hot working regime.

   b. The model should be able to represent the most significant aspects of the underlying microstructural state of the metal and its evolution during deformation. Physical phenomena to be modelled include strain hardening, strain rate and temperature sensitivity including history effects, and both dynamic and static recovery processes.

   c. Material parameter determination should be straightforward and require a minimum of experimental testing. This should of course be commensurate with the degree of complexity that is to be modelled.

   d. Finally, the model should be formulated with due consideration of issues regarding its numerical implementation in finite element programs.

4. Evaluate the model through appropriate validation experiments, including an investigation of the model's ability to predict some aspects of the internal state of the material.

The following chapter surveys the field of internal variable models for high temperature metal deformation. Chapter 3 describes a high temperature test system and describes the compression testing procedures associated with an iron – 2% silicon alloy. Chapter 4 discusses the structure of the constitutive model, describes a set of experiments used to evaluate the material functions, and proposes specific forms for those functions. Chapter 5 discusses the reduction of the data obtained from the mechanical tests and presents a procedure for determining material constants for the constitutive model. Chapter 6 presents a comparison of material response predicted by the constitutive model with experiments involving boundary conditions not used for the material parameter evaluation. This chapter also discusses means of correlating predicted values of the internal variable with physically measureable quantities. Finally, we conclude this paper with some final remarks and discussion in Chapter 7.

# Chapter 2

# Review of Current Internal Variable Constitutive Models for the High Temperature Deformation of Metals

A legion of internal variable constitutive models for the high temperature deformation of metals have been proposed over the last decade. The form of each proposed model, not surprisingly, has to a large extent been influenced by the proposing investigator's particular scientific community. This chapter reviews a number of the current models and places them within one of three categories: empirical, mechanistically inspired, and alternative analytic framework models. The empirical model category incorporates those models which attempt to duplicate the behavior of the material through empirical relations which may not necessarily represent physical deformation processes. Investigators such as Miller [1976] and Bodner and Partom [1975] have proposed empirical models where the forms of the rate equations are inspired by steady state strain rate and stress response, and evolution equation(s) for the internal variable(s) are structured after the Bailey-Orowan [Bailey, 1926; Orowan, 1940] model for steady state creep, incorporating hardening and softening terms to accomodate competing mechanisms. The mechanistically inspired model

category includes those which attempt to construct a comprehensive constitutive model by assembling models for different physical mechanisms into a single set of equations. Investigators such as Prinz and Argon [1984], and Nix and Gibeling [1985] have constructed multiple internal variable constitutive models by considering the dynamics and evolution of dislocation structure in single phase materials. The alternative analytic framework models category is meant to include those models whose forms are motivated primarily by analytic convenience, with little attention given to representing actual physical mechanisms. Investigators such as Krempl [Cernocky and Krempl, 1979] and Valanis [1971] have proposed models which one may place within this category, their models also differing from the normal differential, state-space constitutive models represented by the first two categories.

The above three categories are not mutually exclusive. The separation of models which occurs below is therefore only approximate, suggesting only part of the continuum of models which exist for simulating the high temperature deformation of metals.

Appendix A contains a set of model summaries, providing equations, experimental data, and references for several models.

## 2.1 Empirical Models

The vast majority of internal variable models appear to fall within this broad classification. The list seemingly grows daily, but a complete list should certainly include models by

1. L. Anand
2. S. R. Bodner and Y. Partom
3. J. L. Chaboche

4. E. W. Hart

5. U. F. Kocks, H. Mecking, and Y. Estrin

6. R. D. Krieg and J. C. Swearengen

7. D. Lee and F. Zaverl

8. A. K. Miller

9. K. P. Walker

If we consider just the portions of the models which represent isotropic behavior and limit the deformations to infinitesimal plastic strains, all of the above models fall within the following structure. The plastic strain rate is assumed to be proportional to the deviatoric stress according to the functional dependence:

$$\dot{\epsilon}^p_{ij} = f\left(\frac{\tilde{\sigma}}{s}, \theta\right) \frac{\sigma'_{ij}}{\tilde{\sigma}} \qquad 2.1.1$$

where

$\dot{\epsilon}^p_{ij}$ = plastic strain rate,
$\sigma'_{ij}$ = deviatoric stress,
$\tilde{\sigma}$ = $\sqrt{(1/2)\sigma'_{ij}\sigma'_{ij}}$, equivalent stress
$f\left(\frac{\tilde{\sigma}}{s}, \theta\right)$ = scaling function,
$\theta$ = absolute temperature,
$s$ = stress valued, scalar internal variable.

The function

$$f\left(\frac{\tilde{\sigma}}{s}, \theta\right)$$

incorporates rate, temperature, and structure dependence of the material. Notice that the internal variable enters into the rate equation only as a ratio with the equivalent stress, and only through the scaling function $f$.

The evolution equation for the scalar internal variable in the above models assumes one of two forms. The first assumes that the rate of change of the internal variable is a function of the difference between its current value and a saturation value:

$$\frac{ds}{dt} = \hat{s}(s_{sat} - s), \qquad 2.1.2$$

which is justified by the observation of steady state strain rates in creep experiments or constant value of stress in isothermal, constant strain rate experiments. The second assumes that the rate of change of the internal variable is proportional to the equivalent plastic strain rate, $\dot{\bar{\epsilon}}^p$, minus a function dependent on the external and internal variables:

$$\frac{ds}{dt} = h_0 \dot{\bar{\epsilon}}^p - \hat{s}(\tilde{\sigma}, \theta, s). \qquad 2.1.3$$

This second form is generally justified via the Bailey-Orowan assumption of competing hardening and recovery mechanisms coupled with the observation of strain hardening data where the rate of plastic hardening at high strain rates or low temperatures approaches a constant, athermal value [Mecking and Kocks, 1981]. The magnitude of the second term on the right hand side of 2.1.3 therefore generally increases as the strain rate decreases or the temperature increases.

Several of the above investigators [1-4, 6-9] have included even-ranked, tensor-valued internal variables to accomodate anisotropy, although there is substantial variation in both the internal variables and how they are incorporated into the rate equations of their respective models. Anand and Chaboche propose a stress-valued backstress tensor which is subtracted fr[illegible] the deviatoric stress, Hart proposes a strain-valued anisotropy tensor, and Cernocky employs the accumulated plastic strain tensor. Bodner and Partom employ a fourth order tensor which operates linearly on the deviatoric stress, while Lee and Zaverl employ both a second and a fourth order tensor.

The choice of the higher order internal variable has been governed by the nature of the anisotropy to be modelled. Most of the investigators have considered small scale effects associated with Bauschinger type phenomena which typically saturate

after a few percent plastic strain. Evolution equations for the higher order internal variables vary dramatically between models. Large deformation effects such as the development of crystalline texture have not been included in any of the models. Of the above models, only Anand has presented a formulation which both includes the effect of elasticity and develops the equations in terms of finite deformations.

## 2.2 Mechanistically Inspired Models

An ideal internal variable model directly represents physical deformation processes and assigns internal variables to actual features of a material's microstructure. One procedure to produce such a model would be to assemble equations representing the different operative physical processes into a single unified constitutive model. A knowledge of these processes therefore should guide the construction of a mechanistically inspired models.

Much of the high temperature mechanical behavior of metals may be explained in terms of the thermally activated motion of dislocations and evolution of dislocation structures. The mechanical response of metals under these conditions is highly dependent on strain rate and temperature, primarily a consequence of the thermally activated glide and climb of dislocations neccessary to accomodate plastic deformation. The mechanical response is also dependent on such structural features as dislocation structure, grain size, secondary phases, and defect density. Several physical mechanisms operate to enhance and reduce the effect of the above characteristics. Hardening results from the accumulation of dislocation structures which then may act as obstacles to the displacement of mobile dislocations. Dislocation multiplication occurs through the development and activation of dislocation sources.

Reduction in dislocation density may result from several thermally activated processes. Dislocations may be annihilated via the approach and cancelling of like dislocations of opposite sign, commonly referred to as recovery. Recovery is

generally classified into two categories, static and dynamic [Swearengen, 1985]. Dynamic recovery is assumed to be the result of the motion of mobile dislocations and therefore requires plastic deformation. It is furthermore associated with cross-slip processes which permit screw dislocations to encounter other screw dislocations of opposite sign. Static recovery is assumed to result from climb-associated processes and therefore may occur is the absence of an imposed load or strain rate. Its activation energy is expected to be close to that of self-diffusion. Since cross-slip may be thermally activated, dynamic recovery is expected to be thermally activated as well, although much more weakly than static recovery. Materials of high stacking fault energy ($\alpha$-Fe and all BCC metals, Al) demonstrate high rates of recovery, since undissociated dislocations may climb and cross-slip with relative ease. Low stacking fault energy materials ($\gamma$-Fe and most FCC metals: Ni, Cu) due to the formation of partial dislocations should recover more slowly.

Dislocations may also be erased via recrystallization. Materials with relatively low rates of recovery may accumulate a sufficient stored strain energy to initiate recrystallization during deformation. This "dynamic" recrystallization causes macroscopic strain softening which may lead to deformation localization. Both low and high stacking fault energy metals may recrystallize statically, although, as in dynamic recrystallization, depending on the initial microstructure, some initial deformation may be necessary for initiation.

Essential aspects of metal behavior during hot working extend beyond those associated with average dislocation density or arrangement. Strong anisotropy may develop due to deformation-induced crystalline texture and grain distortion. Small strain anisotropy associated with substructure polarization and Bauschinger-type effects certainly develops.

Relatively few investigators have formulated internal variable models from fundamental relationships assumed about dislocation motion and evolution. The choice, number, and interpretation of the internal variables selected is not self-evident. As-

sumptions concerning the physical deformation processes may suggest a large number of internal variables. For example, given that the dislocation distribution in many metals at high temperatures is not random, it seems reasonable to assign at least two isotropic state variables which in some way express both the density and arrangement of dislocations. Since both static and dynamic recovery processes are occurring, and since static recovery is generally assumed to involve edge dislocations in cell walls, while dynamic recovery is associated with screw dislocations, perhaps in dislocation cell interiors, it is also desirable to propose two dislocation densities, one edge and one screw. Since models for the thermally activated glide of dislocations in a slip plane frequently involve both mobile and immobile dislocations, both of which may act as obstacles, it may be preferable to express the densities of these two types of dislocations as internal variables as well.

Of course, given particular assumptions, one may relate one dislocation pair mentioned above to another pair and thus reduce the number of internal variables. None of the above internal variable candidates is necessarily scalar, incapable of being polarized. In real materials they certainly are capable of producing anisotropic behavior.

In an attempt to resolve some of the above uncertainties, the investigators below have proposed models based on dislocation evolution for high temperature metal deformation. The mechanistic models proposed are derived from conditions of a single phase material where the dislocation motion is essentially unidirectional. There is no generalization to three dimensional deformation. None of the mechanistic models additionally proposes a relationship either for small scale anisotropy associated with Bauchinger type effects or for large scale anisotropy associated with the development of crystalline texture.

Prinz and Argon [1984], and Nix and Gibeling [1985], and Bergstrom and Hallen [1982] have proposed mechanistically-inspired internal variable models. The Bergstrom and Hallen model is the simplest of the three models proposed, employ-

ing a single internal variable representing a total dislocation density. The model considers dislocation creation, accumulation, and annihilation processes to evolve dislocation density with accumulated strain. The model does not consider static recovery, nor does it propose *a priori* a specific function for dynamic recovery. choosing evaluate a dynamic recovery function from experimental data.

The former two pairs of investigators, Prinz and Argon, and Nix and Gibeling, assume a one dimensional composite material structure consisting of an alternating cell wall/interior structure. Both employ two internal variables which represent the material state within the cell wall and cell interior, respectively. Both propose evolution equations where the rate of accumulation of dislocations in both the cell wall and interior is geometrical and depends on the current dislocation densities. Recovery within cell walls in both cases is assumed to occur via diffusion controlled climb; neither model proposes a stress dependence for the static recovery within cell walls. Prinz and Argon propose a geometric recovery mechanism within cell interiors as well, while Nix and Gibeling propose a recovery term assuming thermally activated cross-slip. Both investigators assume that the rate of static recovery is dependent only on the internal variables and temperature; there is no assumed effect of externally applied stresses in either model. Nix and Gibeling add the additional feature of two rate equations, one for cell walls and one for cell interiors, which produces a compatibility requirement where the two strain rates yield the macroscopic strain rate.

The models described above represent certain characteristics of high temperature deformation well. None of the models however is able to reproduce the behavior of actual metallic materials without employing empirical parameters to scale model predictions with actual material data. The latter two models differ in that the Prinz model predicts eventual steady state conditions while the Nix model permits continued hardening at large strains. None of the models demonstrates the transition in steady state stress dependence characteristic of power law breakdown, nor do they necessarily predict the power law dependence associated with steady state

creep.

## 2.3 Alternative Analytic Framework Models

Two classes of models which have been applied to the high temperature deformation of metals in addition to the differential state variable formulation are the overstress and endochronic models, proposed by Krempl [1979] and Valanis [1971], respectively.

Krempl's overstress model incorporates rate dependence by assuming that viscoplastic behavior is composed of two components, a component which may be represented by material response at an "infinitely slow strain rate", and a second component which is added to the first to accomodate the rate dependent response. The infinitely slow strain rate response acts as an internal variable which may evolve. In contrast to the convention that rate dependent, thermally activated processes act to *decrease* the resistance to plastic deformation associated with a given state, viscoplastic behavior in the overstress model acts to *increase* the stress over that of the internal variable.

Valanis's integral, endochronic theory assumes a modified "time scale", based on a measure of accumulated plastic strain, $d\xi$, which is then combined with time to form an "intrinsic time measure", $d\varsigma$:

$$d\varsigma^2 = \alpha^2 d\xi^2 + \beta^2 dt^2,$$

where $\alpha$ and $\beta$ are scalar material parameters. This "time scale" is not associated with any particular deformation mechanism. Material response, however, is assumed to track with the evolution of this variable.

Both models have been applied to rate dependent metal deformation where material constants have been evaluated at a single temperature. Temperature dependence has not been explicitly included in either constitutive model, nor has either

been applied to hot working applications.

## 2.4 Discussion

As is perhaps evident from the above discussion, this author has an affinity towards mechanistically inspired models, in part since such models seem to be a natural (and desirable) consequence of the use of internal variables. Any effort to correlate internal variables to measures of material microstructure suggests a reciprocal effort to use such measures to formulate internal variable models.

Unfortunately, the mechanistically inspired models, as stated above, have yet to accomodate all of the features of high temperature mechanical behavior. The dilemma then is that compromises must be made both in terms of complexity and phenomenology to produce a model which may be easily correlated with material data and incorporated into a finite element program for process modelling.

The model which will be presented in Chapter Four of this thesis represents such a compromise. Its objective is to duplicate the major features of metal behavior during hot working within a simple internal variable framework, in this case employing a single scalar internal variable. Some correlation with mechanistically inspired models will certainly be possible, and such correlations will be presented. The model, though, falls within the first category discussed above, that of empirical models.

# Chapter 3

# Experimental Apparatus

This chapter begins with a description of the high temperature test system designed and used to evaluate material response under hot working conditions. Issues related to compression testing are discussed, and the model material used in this investigation, an iron - 2% silicon alloy, is described.

## 3.1 High Temperature Test System

Any system used for basic high temperature mechanical testing and for the simulation of hot working should possess the following minimal characteristics:

1. Isothermal testing to temperatures exceeding .9 $T_m$ of the material of interest, where $T_m$ is the melting temperature in degrees absolute.
2. True strain rates ranging from $10^{-4}$ to at least $10^{0}$ $sec^{-1}$ and preferably greater.
3. Variable testing modes, including compression, torsion, and tension.
4. Rapid quenching of specimens from test temperatures.

5. Complex loading histories, both to evaluate material response and to simulate non-steady forging operations.

6. Controllable environments to reduce the effect of oxidation.

7. High speed data collection.

Figure 3.1 shows a photograph of the test system constructed to meet the above characteristics. The basic system consists of an Instron Corporation, Model 1322 tension/torsion servohydraulic test machine. The system actuator has a frequency response of approximately 10 hertz, which effectively limits the maximum controllable strain rate for ordinary, laboratory sized axial specimens to approximately 1 per second. The lower strain rate limit is approximately $10^{-4}$ per second due to the limits of resolution for the actuator displacement and hydraulic servovalve. Approximately the same strain rates are obtainable in torsion.

The analog controllers for the servohydraulic machine permit external control signals in the form of voltages. These may be provided either by digital or analog function generators, permitting arbitrarily complex loading histories. Most of the control signals for this investigation were obtained from an analog function generator, designed and assembled by Mehrdad Haghi (of our laboratory), following a simpler design used by Immarigeon and Jonas [Immarigeon and Jonas 1975]. The function generator uses a simple RC circuit to provide a decaying exponential voltage which simulates a constant true strain rate compression test. The function generator is also designed with set points which may either hold the voltage at that point or change the strain rate, which enables strain rate jump and recovery tests.

The temperature and environmental control for the test system is provided by a high temperature, vacuum furnace built by Centorr Associates, Suncook, New Hampshire, according to our specifications. The furnace, pictured in Figures 3.2 through 3.4 is a stainless steel, double-walled chamber with a center heat zone. The furnace is mounted in the frame of the servohydraulic machine, as illustrated

in Figure 3.1. The vacuum system consists of a roughing pump and a 4 inch diffusion pump which is attached to the back plate of the furnace. Maximum vacuum attainable was approximately $10^{-6}$ torr. The furnace is equipped with flexible bellows above and below through which pass loading rods composed of a high temperature molybdenum alloy, TZM. The loading rods pass into the furnace through the bellows and are hermetically sealed with a pair of differentially pumped Viton quad rings. The lower seal is designed to permit the lower loading rod to both rotate and move in and out of the furnace without disturbing the vacuum.

Heating is provided by a cylindrical heating zone consisting of tungsten mesh heating elements surrounded by a multiple layer set of molybdenum heat shields. Power is provided by an SCR-controlled A/C power supply which caused extensive problems with electrical noise. Electrical noise is a continual, unavoidable problem with SCR controllers. In retrospect the system should have been designed with a D/C power supply. A Leeds and Northrup Electromax V temperature controller is used with chromel-alumel thermocouples to maintain specimen temperatures. A thermocouple spot welded to each specimen serves as the feedback transducer to the controller. The heat zone is designed to reach temperatures up to 1800 Celsius, but the loading rod materials, i.e., 94% alumina and TZM begin to creep and recrystallize, respectively, at approximately 1200 Celsius. All tests were therefore run at or below 1200 Celsius. The furnace is water-cooled, water being circulated between the double walls of the furnace while at temperature.

The furnace was also equipped with an insulated Conflat induction heating feedthrough. Induction heating in atmosphere or vacuum is therefore another possible means of reaching high temperatures. Tests involving quenching require induction heating since the tungsten mesh heating elements and molybdenum heat shields can not withstand the rapid contraction associated with quench cooling. Induction heating possesses the same disadvantage as the SCR heating system in that it generates a significant amount of electrical noise, obscuring transducer signals.

Other features of the furnace include ports to accomodate gas quenching, 12 thermocouple feedthroughs, and mounting brackets and feedthroughs appropriate for a high temperature, MTS extensometer.

Data acquisition for most of this project was accomplished with an IBM PC/XT equipped with a Metrabyte Corporation DASH-16 analog-to-digital converter. The DASH-16 was provided with BASIC language callable subroutines which permitted sampling rates exceeding 1 kilohertz. An approximate limit of 30,000 data points could be collected during one sampling session, the maximum number controlled by the memory remaining after subtracting the memory requirements of the BASIC language and the BASIC sampling program from a 64K sector of IBM/PC memory. All data was transferred to a Data General MV4000 computer for analysis; the IBM/PC was used only for data acquisition.

The high temperature system is unique in the variety of high temperature test capabilities. Other systems exist which permit one mode of testing, heating, or control, but we know of no other system with the same collected capabilities. All of the data presented in this thesis were obtained using this test system.

## 3.2 Compression Testing

The role of the compression test in the study of the large deformation of metals is well established [ASTM Standard E209-65; Chait and Papirno, 1983; Hsu, 1969]. Compression testing achieves large strains due to the absence of necking and permits a fairly simple means of measuring strain by determining the relative displacement of the compression platens. Also it is also easier to perform relative to torsion testing since it requires simpler and more common experimental apparatus and requires less complicated alignment of loading fixtures. Compression testing is particularly appropriate for large deformation testing at high temperatures, where temperature uniformity is difficult to maintain in tension and torsion specimens, and strain

measurement in tension and torsion requires complex extensometry.

Unlike tension and, to a lesser extent, torsion testing, compression testing frequently is not selected for material testing due to its propensity for different modes of inhomogeneous deformation. Temperature gradients, lateral buckling, and friction between the compression specimen and compression platen all may create inhomogeneous deformation.

When a material demonstrates substantial rate sensitivity, temperature gradients, specifically axial gradients, may produce conical specimens, illustrated in Figure 3.5. The gradient in this case was caused by the quenching of the upper end of the specimen by a cooler compression platen. Extensive finite element heat transfer analyses of the Centorr furnace heat zone and the initially installed TZM alloy loading rods provided with the furnace indicated that the greatest source of heat loss was through the water-cooled loading rods. The conduction through the rods was enough to produce temperature gradients in excess of 20 degrees Celsius along the length of the compression specimens. This gradient was reduced to $\pm 2$ degrees Celsius by installing one inch diameter, 94% alumina ceramic rods in place of the TZM loading rods. The alumina rods fit within the mounting sockets of the TZM rods, which were withdrawn from the furnace heat zone. The change to alumina rods reduced the thermal conductivity of the heat zone loading rod material from approximately 100 W/m $^0$K to 5 W/m $^0$K. The new loading rod system is shown in Figure 3.6. TZM was still used as the compression platen material, since it could be easily polished to provide a smooth compression surface, and since it acted to distribute the specimen contact load evenly over the alumina rod crossection. It should be noted that a much easier method to eliminate temperature gradients is to employ a three zone furnace. Such a furnace eliminates any sensitivity to load train materials, permitting the use of high temperature materials, such as thoriated tungsten or graphite without concern for these materials' high thermal conductivities.

Lateral buckling was encountered in compression specimens whose height to diameter ratio exceeded 1.5. This height-to-diameter limit appears rather inflexible, for we frequently obtained shear buckling in specimens with a 1.6 ratio. A ratio of 1.5 eliminated any ostensible buckling.

A more significant deformation inhomogeneity resulted from friction between the specimen and the compression platens. Figure 3.7 indicates the deformation pattern which results from excessive friction between the specimen and platens. Figure 3.9 illustrates the shape of a comparably barrelled specimen. The effect of friction in preventing homogeneous compression was reduced through the use of grooves in the ends of the compression specimens in conjunction with high temperature lubricants. This technique has been used by many investigators [Uvria, 1968; Sherby, 1980; Hsu, 1969] and appears to work very well in producing homogeneous compression for compressive true strains exceeding $-1.0$. Shallow, concentric grooves are machined on the end faces of the specimens to hold high temperature lubricant. Figure 3.10 provides the dimensions of the specimen and the grooves on the specimen faces. The specimen dimensions were selected to provide sufficient grains in the cross-section to permit a continuum assumption, the number of grains encountered across the diameter being approximately fifteen.

The lubricants used were mixtures of powdered glass and boron nitride powder. This particular combination of glass and boron nitride appears to act as a high temperature analog to the common room temperature lubricants of molybdenum disulfide or graphite in a grease carrier. At high temperatures the glass melts to form a viscous, lubricating film which also carries the boron nitride. Boron nitride possesses a hexagonal basal plane crystalline structure, providing lubrication in the same manner as graphite or molybdenum disulfide [Niedenzu, et al. 1965]. The particular glass/boron nitride mixtures used as lubricants at the different test temperatures are listed in Table 3.1. Our general experience indicates that the general criteria for lubricant selection is that the melted glass should have a viscosity of approximately $10^4$ poise at test temperature, and that the glass-to-boron nitride

weight ratio should be greater than 4-to-1, and should probably be closer to 8 or 10-to-1.

It is also possible to eliminate the boron nitride completely and still obtain uniform deformation using only glass. Boron nitride extends the effective usable lubrication temperature range of a particular glass. Boron nitride may also react with oxygen at high temperatures, so its usefulness may be limited to vacuum or inert environments.

Figure 3.11 shows a typical compression specimen before and after an essentially homogeneous, isothermal, constant true strain rate compression test to a true strain of -100%. Notice that the deformed specimen is still cylindrical, and that there is no noticeable rollover of the sides of the specimen, which would have resulted were there friction between the specimen end faces and the compression platens. Figure 3.12 shows the microstructure of one such specimen. Notice that all of the grains possess approximately the same aspect ratio as the deformed specimen.

Additional factors influenced deformation homogeneity of the compression specimens. It appears to be very important for the compression platens to be well polished. The TZM platens used for the experiments described within were polished for each experiment to an approximately 10 micron surface finish. The ends of the compression specimens were also finished to a 600 grit roughness. It is also important for the opposing surfaces of the load train to be parallel and remain so during the test. The end of the compression specimens should also be parallel. Groove spacing and depth appeared to be less sensitive controlling parameters than was initially anticipated. Approximate bounds for these dimensions are a groove spacing of fifteen to thirty thousandths of a inch and a groove depth of four to eight thousandths of an inch.

Compressive strains throughout this investigation were measured by subtracting the effect of test machine compliance from the displacement of the servohydraulic actuator. The large displacements required for large strain compression tests per-

mitted this indirect means of measuring deformation, since the errors associated with variations and nonlinearities in compliance and the resolution of the actuator LVDT were relatively small. The errors were more significant, however, at the beginning of each test when the tolerances were taken up, and when we desired very accurate strain measurements. Extensive digital smoothing techniques permitted greater resolution in measuring displacements than was possible using analog data collection equipment. Using smoothing, we could resolve strains easily less than $10^{-4}$, although the degree of resolution was sensitive to both strain rate and rate of data acquisition. More exact resolution of strains would be aided by some means of measuring the relative displacement of the compression platens, such as a high temperature LVDT, extensometer, or strain gauge. Implementation of these transducers is not trivial, although they are necessary for small strain resolution.

## 3.3 Iron – 2% Silicon Model Material

An iron silicon alloy was selected as the model material in this investigation for several reasons. First, although an iron based material, it retains a body-centered cubic structure up to the solidus temperature. This is an useful property, for we wished to be able to deform our model material at hot working temperatures and then rapidly quench the test specimens to preserve the hot worked microstructure. The martensitic transformation associated with many iron alloys would erase any deformation-induced microstructure. The equilibrium diagram for the iron/silicon system shown in Figure 3.13 indicates the persistence of the alpha phase at all temperatures for the above composition.

The iron 2% silicon was also selected for the high stacking fault energy associated with body-centered cubic materials. Our intention was to model the evolution of structure including the mechanisms of hardening, dynamic recovery, and static recovery. We wished to avoid dynamic recrystallization, which can introduce such complications as an oscillating stress/strain response and deformation localization

[Jonas, 1969]. Figure 3.14 illustrates the oscillations which result during the deformation of a material which exhibits dynamic recrystallization, in this case 1018 plain carbon steel. Dynamic recrystallization and the consequent localization is generally avoided during hot working; hot working schedules are frequently designed expressly to prevent its occurence [op. cit.]. High stacking fault materials generally do not demonstrate dynamic recrystallization since the rate of recovery is believed to be sufficiently high to prevent the accumulation of a deformation structure which may trigger recrystallization [McQueen, 1982].

The deformation response of iron silicon alloys has also been studied extensively using both transmission electron microscopy [e.g. Hu, 1964] and dislocation etch pits [Lytton, et al., 1965]. We felt that extensive experience in the examination of iron silicon microstructures would facilitate efforts at similar examinations should we wish to do so.

The particular alloy used in this investigation was provided by Armco Steel Company, Middletown, Ohio. It was provided in rolled plates, approximately 1 inch thick, 12 inches wide, and 3 to 4 feet long. The nominal composition is listed in Table 3.2. All specimens were machined such that their axis of symmetry was oriented across the width of the plate, illustrated in Figure 3.15. The material possessed a large grain size. Figure 3.16 illustrates the polished and etched (Fry's reagent) cross-section of a typical compression specimen.

All specimens were annealed for 1 hour at 700 degrees Celsius. This schedule is identical to that used by Young and Sherby [Young and Sherby, 1973] in an investigation of a similar iron silicon alloy. Annealing at higher temperatures and for a longer time was avoided to prevent excessive grain growth.

TABLE 3.1

Lubricant Composition

| Temperature (Celsius) | Constituents | Composition Ratio by Weight |
|---|---|---|
| 700 | BN:1190:Acetone | 1:4:16 |
| 800 | BN:1190:Acetone | 1:4:16 |
| 900 | BN:0010:Acetone | 1:8:32 |
| 1000 | BN:0010:Acetone | 1:8:32 |
| 1100 | BN:0010:Acetone | 1:8:32 |
| 1200 | BN:0010:Acetone | 1:8:32 |

Notes:

1. BN = boron nitride powder, purchased from Union Carbide Corporation, Grade HCP.
2. Four digit number refer to glass classification codes. Glass was purchased as a powder, 325 screen size, from Corning Corporation, Corning, New York.

TABLE 3.2

Composition of Iron - 2% Silicon

| Element | Weight % |
|---|---|
| Si | 1.98 |
| Al | 0.56 |
| C | 0.0023 |
| Mn | 0.16 |
| Cu | 0.26 |
| Cr | 0.13 |
| Ni | 0.14 |
| S | 0.0012 |
| P | 0.009 |
| T | 0.0041 |
| N | 0.0050 |
| Mo | 0.038 |

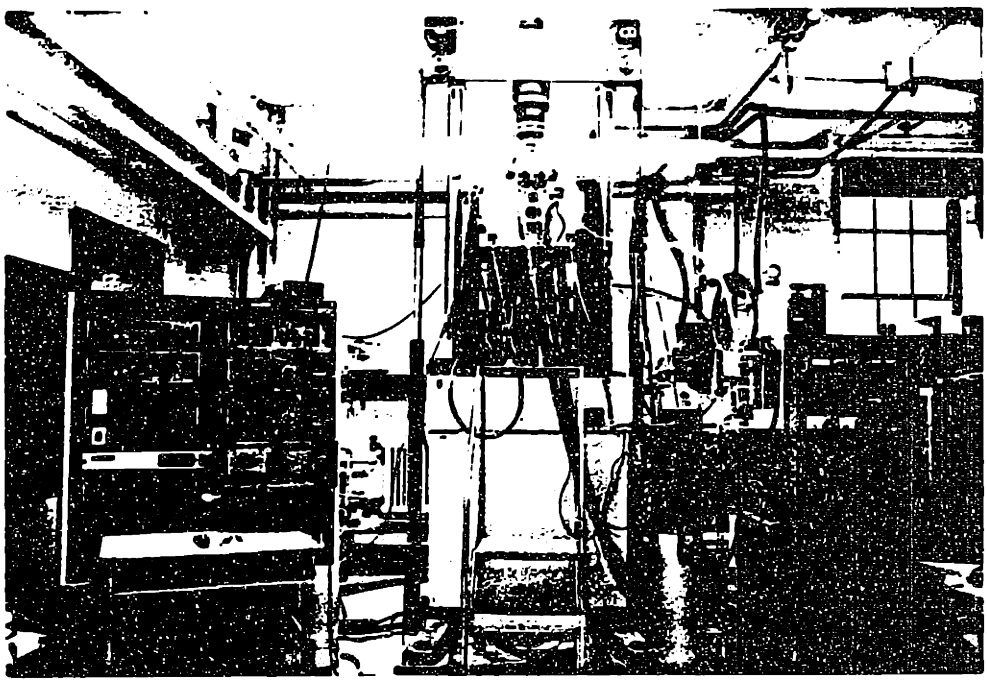

**Figure 3.1 High temperature mechanical test system.**

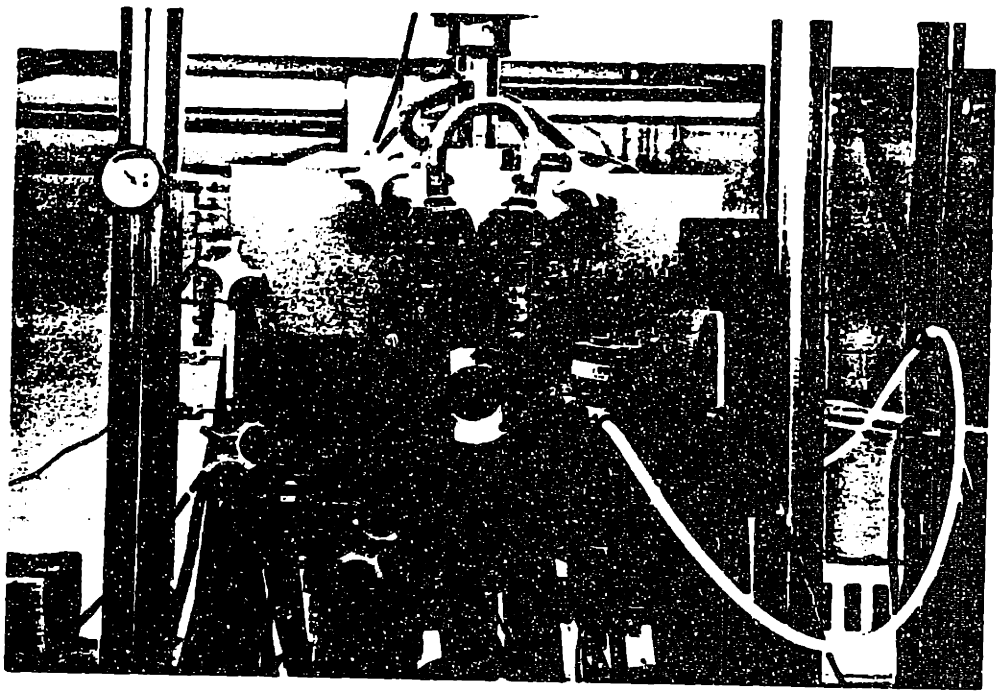

**Figure 3.2 Vacuum furnace exterior**

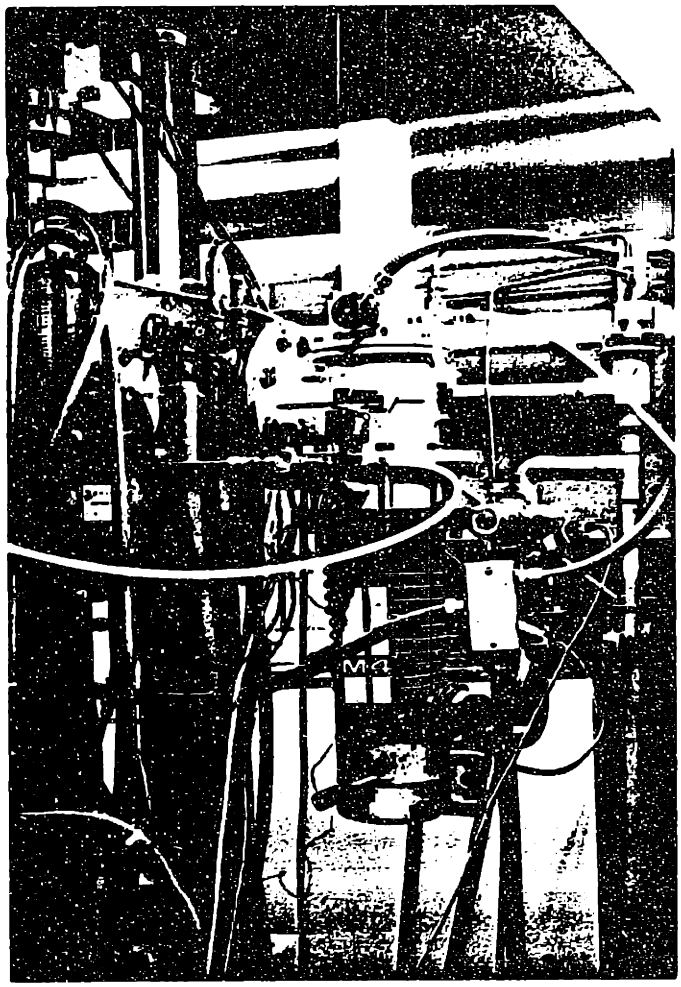

**Figure 3.3 Vacuum system for high temperature furnace.**

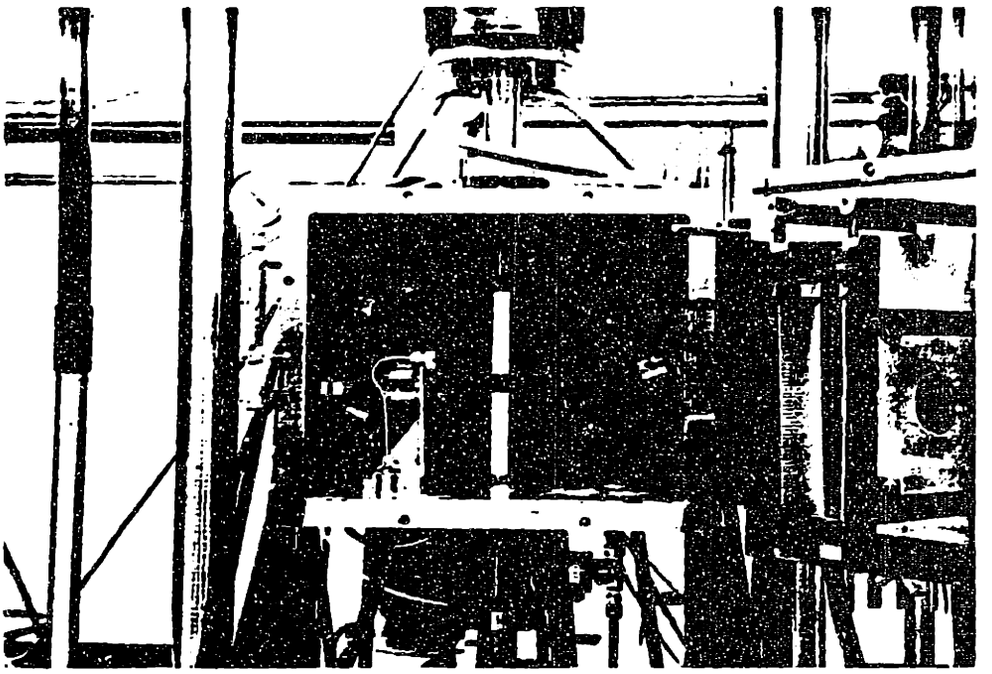

**Figure 3.4 Vacuum furnace interior.**

**Figure 3.5 Conical specimen resulting from axial temperature gradient.**

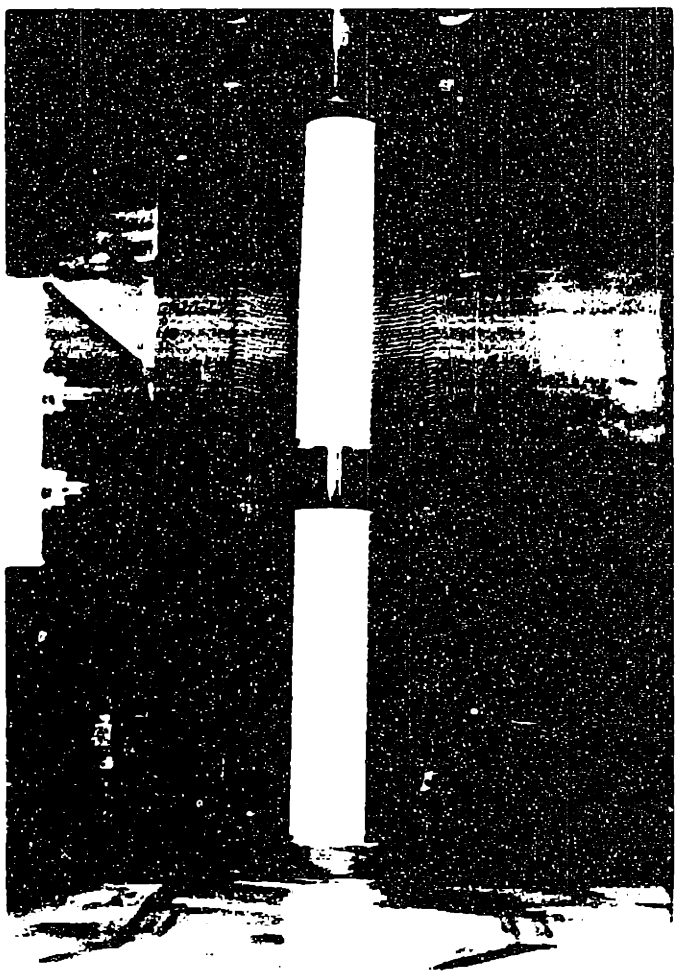

**Figure 3.6 Load train for isothermal compression testing.**

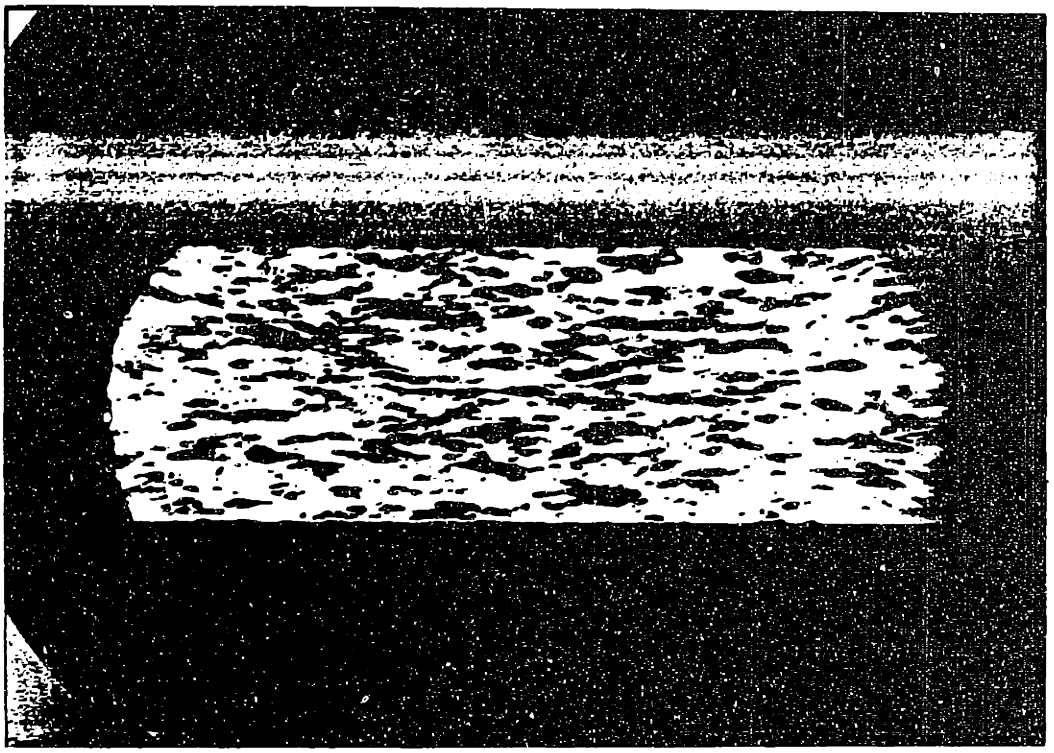

**Figure 3.7 Pattern of grain deformation in compression specimen with significant friction between specimen and compression platen.**

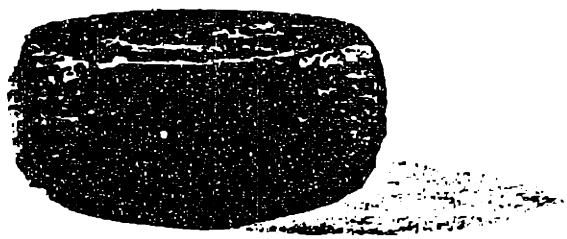

**Figure 3.8 Barrelled compression specimen resulting from friction between specimen and compression platen.**

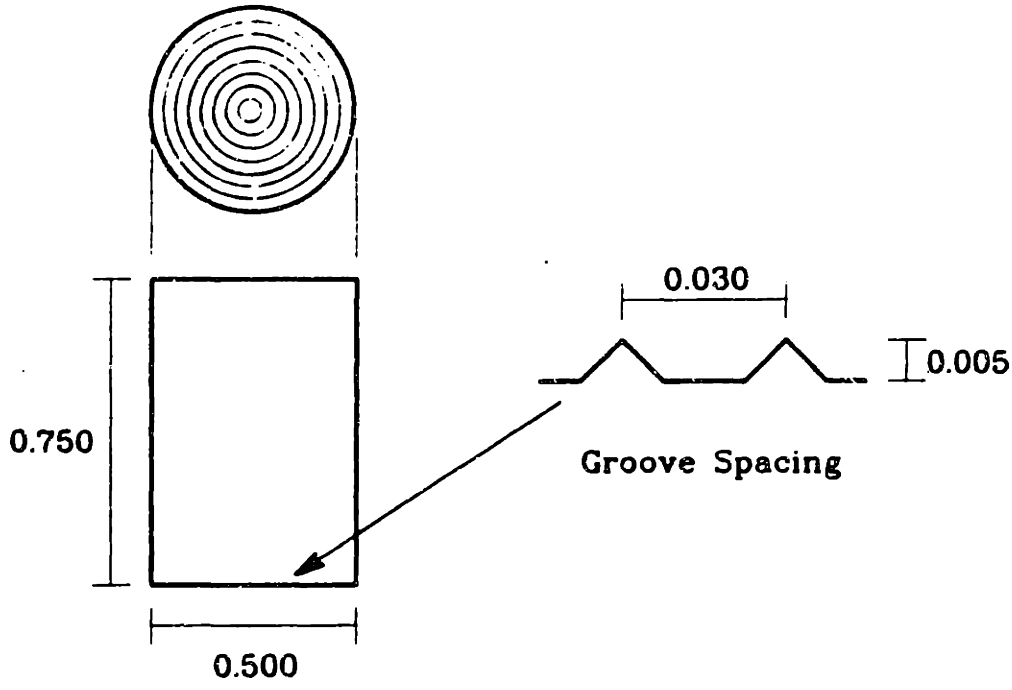


**Figure 3.10** Compression specimen dimensions and groove specifications.

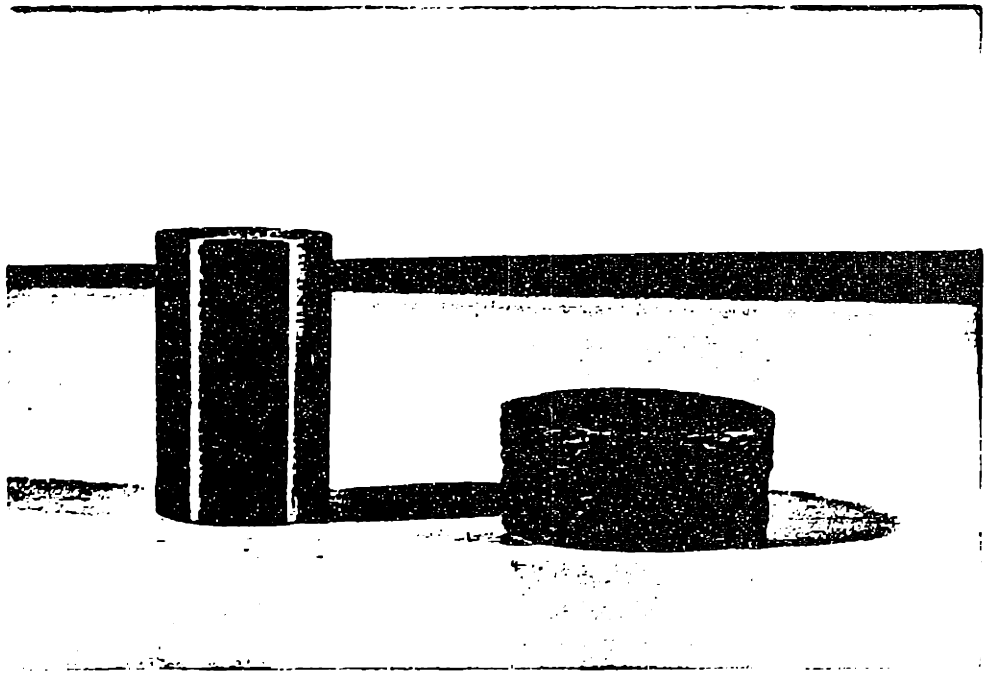

**Figure 3.11 Compression specimen before and after a homogeneous, isothermal, constant true strain rate compression test.**

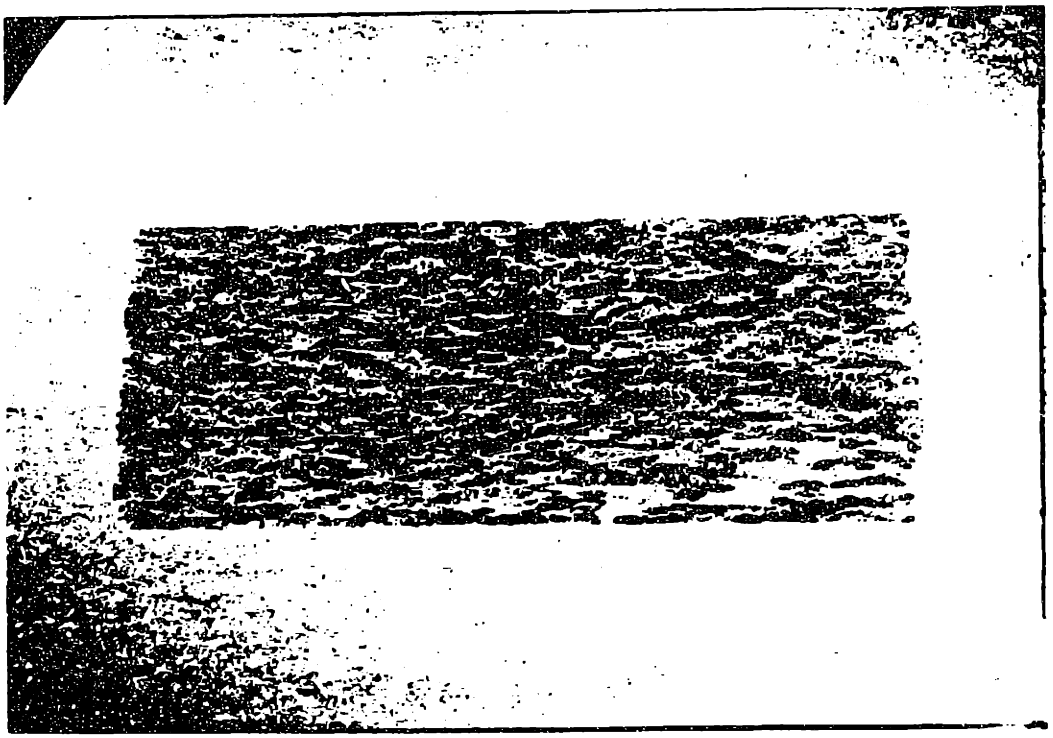

**Figure 3.12 Grain deformation obtained from a homogeneous, isothermal, constant true strain rate compression test.**

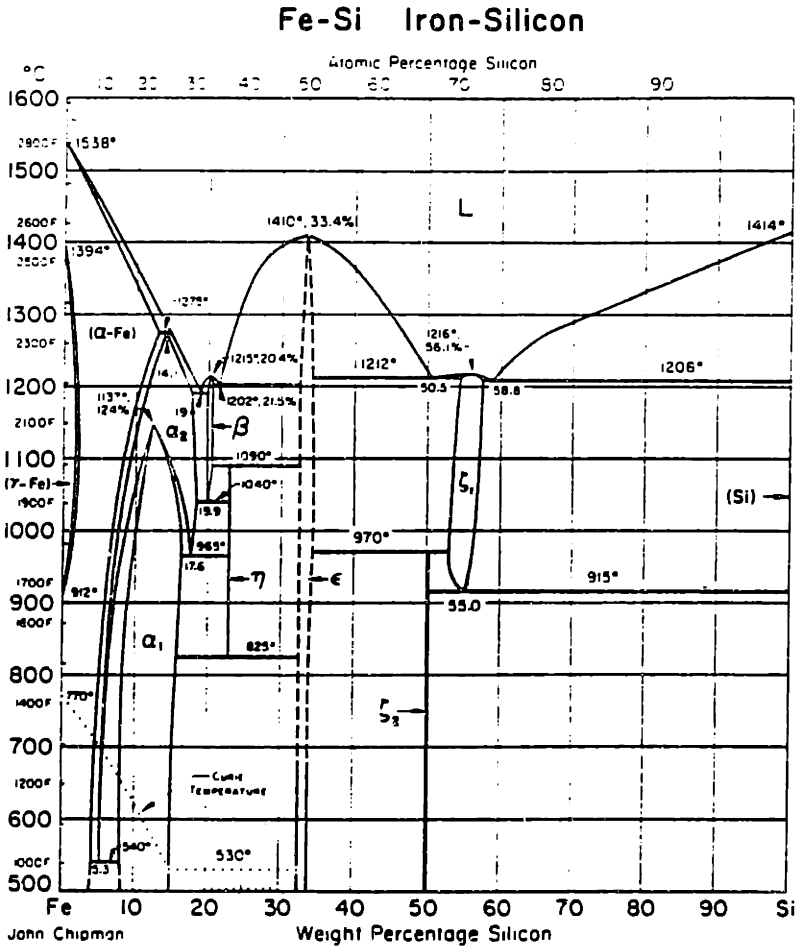


**Figure 3.13 Equilibrium diagram of iron/silicon system.**

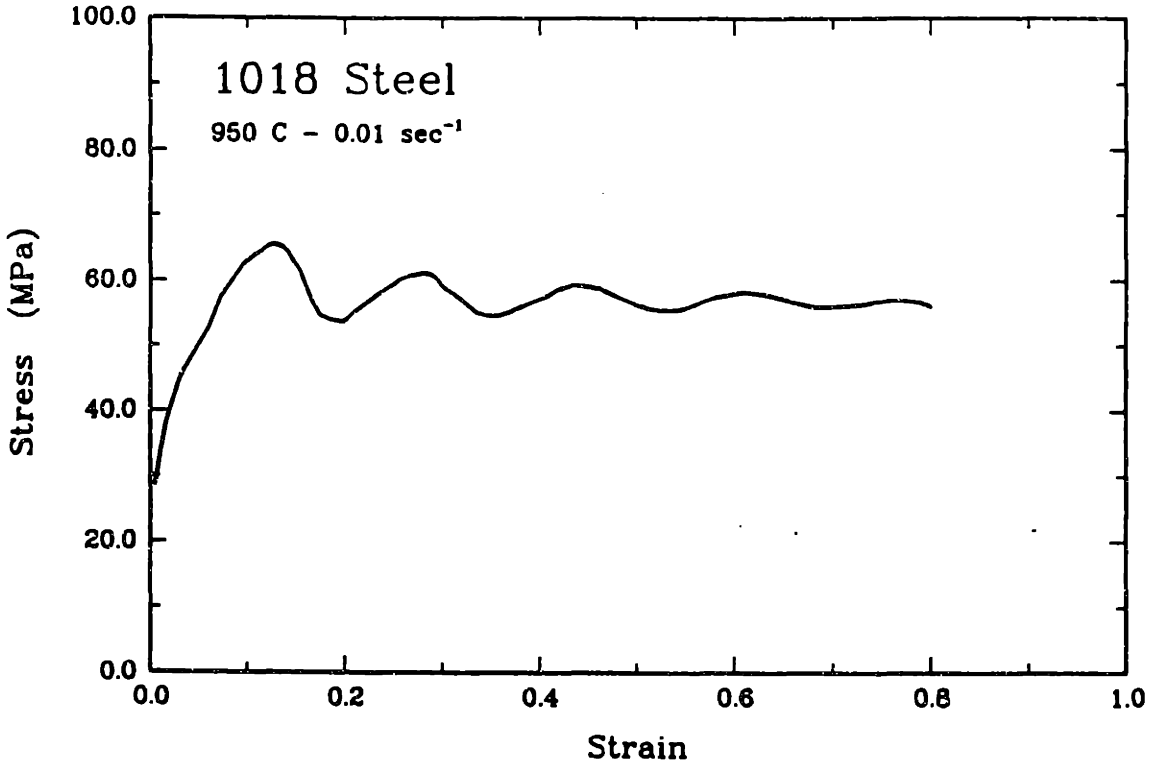


**Figure 3.14** True stress/strain curve for isothermal compression of 1018 carbon steel, indicating oscillations associated with dynamic recrystallization.

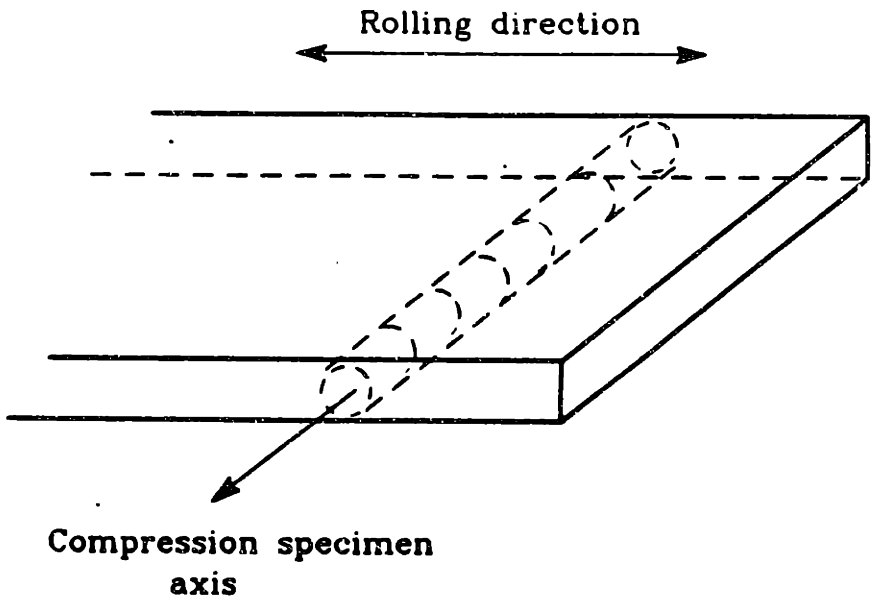


**Figure 3.15 Orientation of compression specimens relative to furnished rolled plate of Fe - 2% Si.**

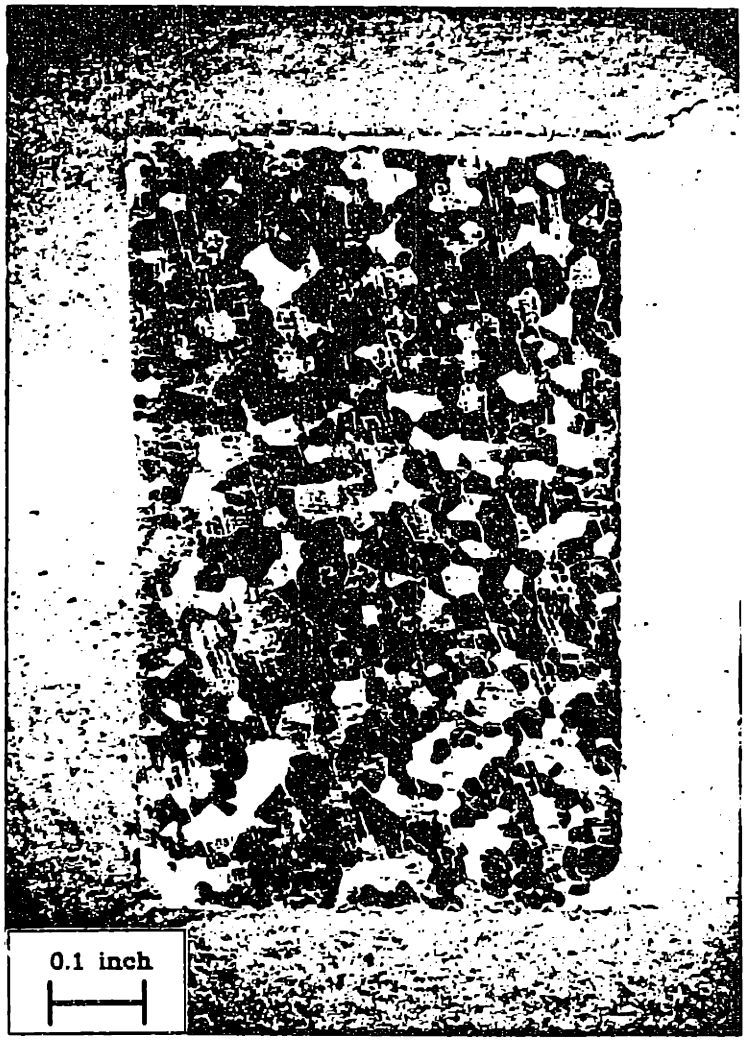


**Figure 3.16 Crosssection of compression specimen etched to indicate grain size.**

# Chapter 4

# Experimental Determination of the Material Response Functions

The basic form of the constitutive model follows the mathematical structure proposed by Anand for an isotropic metal [Anand, 1985]. The model assumes three state variables:

$$\{\mathbf{T}, s, \theta\},$$

where $\mathbf{T}$ is the Cauchy stress, $\theta$ is the absolute temperature, and $s$ is a scalar internal variable which represents an isotropic resistance to plastic deformation. Evolution equations for the three variables are:

- Evolution equation for the stress:

$$\mathbf{T}^{\nabla} = \mathcal{L}[\mathbf{D} - \mathbf{D}^{\mathrm{p}}] - \mathbf{\Pi}\dot{\theta},$$

where

| | |
|---|---|
| $\mathbf{T}^{\nabla} \equiv \dot{\mathbf{T}} - \mathbf{W}\mathbf{T} + \mathbf{T}\mathbf{W}$ | Jaumann derivative of Cauchy stress $\mathbf{T}$; |
| $\mathcal{L} \equiv 2\mu\mathcal{I} + \{\kappa - (2/3)\mu\}\mathbf{1} \otimes \mathbf{1}$ | fourth order isotropic elasticity tensor; |
| $\mu = \hat{\mu}(\theta), \quad \kappa = \hat{\kappa}(\theta)$ | shear and bulk moduli; |
| $\mathbf{\Pi} \equiv (3\kappa\alpha)\mathbf{1}$ | stress-temperature tensor; |
| $\alpha = \hat{\alpha}(\theta)$ | coefficient of thermal expansion; |

| | |
|---|---|
| $\mathbf{L} \equiv \text{grad } \mathbf{v}$ | spatial gradient of velocity; |
| $\mathbf{D} \equiv \text{sym } (\mathbf{L})$ | stretching tensor; |
| $\mathbf{W} \equiv \text{skew } (\mathbf{L})$ | spin tensor; |
| $\theta$ | absolute temperature; |
| $I$ | fourth order identity tensor; |
| $\mathbf{1}$ | second order identity tensor. |

The constitutive equation for $\mathbf{D}^p$ is:

$$\mathbf{D}^p = \dot{\tilde{\epsilon}}^p \left( \frac{3}{2} \frac{\mathbf{T}'}{\tilde{\sigma}} \right),$$

where

| | |
|---|---|
| $\dot{\tilde{\epsilon}}^p = f(\tilde{\sigma}, \theta, s) > 0, \quad \tilde{\sigma} < s$ | equivalent plastic tensile strain rate; |
| $\mathbf{T}'$ | deviator of the Cauchy stress; |
| $\tilde{\sigma} = \sqrt{(3/2)\mathbf{T}' \cdot \mathbf{T}'}$ | equivalent tensile stress. |

- Evolution equation for the internal variable $s$:

$$\dot{s} = \dot{s}(\tilde{\sigma}, \theta, s),$$

- Evolution equation for the absolute temperature:

  Given by the following approximate energy balance equation (this is not a constitutive equation):

$$\dot{\theta} \doteq (\rho c)^{-1} \left( k \, \Delta \theta + \omega \, \mathbf{T} \cdot \mathbf{D}^p \right)$$

  Here $\rho = \rho(\theta)$ is the mass density, $c = \hat{c}(\theta)$ is the specific heat, $k = \hat{k}(\theta)$ is the thermal conductivity (here assumed to be independent of the position), $\Delta\theta$ is the Laplacian of $\theta$, and $\omega$, a scalar in the range $0.85 \leq \omega \leq 1.0$, is the fraction of plastic work converted to heat.

The main task of this investigation then is to evaluate the functional forms for the equivalent plastic strain rate $f(\tilde{\sigma}, \theta, s)$ and the evolution equation for the internal variable $s$: $\dot{s}(\tilde{\sigma}, \theta, s)$.

This constitutive model employs only one scalar internal variable, $s$, for several reasons. First, we wished to determine whether one scalar internal variable would be sufficient to describe the major features of metal behavior during hot working. The well-known correlation between the dislocation density and flow stress suggested that a single internal variable might be adequate. There is additionally sufficient uncertainty of what role a second internal variable would play. Some investigators [Kocks, 1966] suggest that obvious secondary parameters such as dislocation cell size may not contribute to deformation resistance and are merely consequences of dislocation density.

Second, the task of determining the evolution of internal variables is much more straightforward if there is only one. We wished to be able to perform tests which would suggest the functional form for the evolution equation for the internal variable. More than one internal variable would necessitate tests which would somehow decouple the evolution of the two or more internal variables. We felt that the extent of knowledge concerning the development of state during large deformations provides very little guidance for performing such experiments.

The internal variable was selected to be scalar since the task of accomodating the largest source of anisotropy, deformation-induced texture, is computationally very difficult and not well understood. Small strain anisotropy associated with Bauschinger type effects were ignored since its effect was assumed to saturate at a small fraction of the strains encountered in hot working.

Here, we focus our attention on the two undetermined response functions of the constitutive model, the rate equation:

$$\dot{\bar{\epsilon}}^p = f(\tilde{\sigma}, s, \theta), \tag{4.1}$$

and the evolution equation:

$$\dot{s} = g(\tilde{\sigma}, s, \theta). \tag{4.2}$$

Given the above structure, we now must deduce the functional forms of the two equations. Ideally, we would like to have an adequate understanding of the underlying mechanisms governing high temperature behavior such that our task would be only to perform the experiments to determine the few specific material constants for the metal of interest. Realistically, our limited knowledge of these mechanisms precludes this, both because our understanding of the different mechanisms is incomplete and because the actual mechanisms are associated with complex structures and processes certainly not totally representable by a single internal variable model. We therefore choose to motivate functional forms, where possible, from elementary assumptions about deformation mechanisms, guided by appropriate experimentation to modify these forms and provide material parameters.

We make the following assumptions concerning the forms of equations 4.1 and 4.2:

1. We define the scalar internal variable $s$ to be a stress valued quantity called the *deformation resistance.* As a structure parameter, it represents a generalized isotropic resistance to plastic flow which contains contributions from dislocation structure, grain size, solid solution strengthening, intrinsic lattice resistance, etc. For pure, single phase materials, we expect it to be highly correlated with the dislocation density, which is expected to be the primary contribution to deformation resistance at these temperatures.

2. The state variable enters into the rate equation only as a *ratio* with the equivalent tensile stress. That is,

$$\dot{\bar{\epsilon}}^p = f\left(\frac{\tilde{\sigma}}{s}, \theta\right). \tag{4.3}$$

This form has been suggested by Kocks, Argon, and Ashby [1975] in conjunction with a model for mechanically-activated dislocation glide. Rice [1970] and others have suggested this structure as well, although there seems to be no fundamental requirement for a scalar internal variable to be incorporated in this way. We shall consider functional forms for which equation 4.3 may be inverted such that we may write $\sigma = cs$, where $c$ is a function of strain rate and temperature. This structure parallels an expanding or shrinking isotropic yield surface, where the plastic resistance acts as the flow strength. Of course, the model presented here does not include a yield surface; plastic deformation is assumed to occur at any non-zero value of equivalent stress.

3. The evolution equation for the internal variable is assumed to be of the form:

$$\dot{s} = h(\tilde{\sigma}, s, \theta)\dot{\bar{\epsilon}}^p - \dot{r}(s, \theta). \tag{4.4}$$

Assuming three primary mechanisms, hardening, dynamic recovery, and static recovery, we associate $h(\tilde{\sigma}, s, \theta)$ with dynamic processes, i.e., hardening and dynamic recovery. Static recovery is accommodated through $\dot{r}(s, \theta)$. This form is reminiscent of the Bailey-Orowan equation [Bailey, 1926, Orowan, 1945], and is almost universally employed in internal variable evolution equations for high temperature deformation. The assumption that the static recovery function is independent of stress reflects our desire for this function to represent evolution processes which occur in unloaded material.

Given the above assumptions about the forms of the rate and evolution equations, we now ask what experiments may be performed to complete their specification. Given that the two differential equations 4.3 and 4.4 are coupled, it seems reasonable that we should seek some way of decoupling the two equations so that the functional forms may be investigated separately. Given two equations of the form 4.3 and 4.4, then following a similar development presented by Ruina [1983], we may make the statements:

- The value of the internal variable is uniquely determined if *all* of the external variables $(\tilde{\sigma}, \theta, \dot{\tilde{\epsilon}}^p)$ are known. This is portrayed in Figure 4.1 where dotted lines of constant internal variable $s$ are indicated in stress/strain rate/temperature space. The lines are straight only for illustration, there is no physical reason why they should be straight. The dashed line exists for those materials which reach some saturation condition where the value of the internal variable attains some constant value, here denoted as $s^*$.

- Experiments where we apply fast changes in the external variables (so that we may assume constant structure) should produce the relationship between them expressed by 4.3. If we are confident that the structure has not changed in the time necessary to apply the change, then the changes in the external variables are governed only by the rate equation. This then suggests a series of experiments where we rapidly change either the strain rate, temperature, or stress to different values, with the values of the other external variables being the same just before the change. This guarantees that the initial state is unchanged, and the rate equation is decoupled from the evolution equation.

Using the assumptions listed above and exploiting the characteristics of the functional forms outlined, the following sections propose a series of tests for evaluating

the constitutive functions. At least three modes of testing are required to evaluate the functional form of both the rate equation and evolution equation for the internal variable. The following sections detail the three series of tests used in this investigation: (a) isothermal strain rate jump tests from the same state to evaluate $g$ in 4.3, (b) isothermal load-unload-hold-reload tests to evaluate $\dot{r}$ in 4.4, and (c) isothermal, constant true strain rate tests to evaluate $h$ in 4.4.

## 4.1 Evaluation of the Rate Equation: $f(\frac{\sigma}{s}, \theta)$

As just argued, if one wishes to experimentally probe the behavior of the rate equation expressed by 4.3, one must design experiments such that material state is held constant. One can not otherwise separate the effect of an evolving structure from the instantaneous response at constant structure. Very few experiments have been performed, particularly within the hot working regime, which accomplished this separation. This is probably due to the fact that internal variable models have not been applied to hot working; experimentalists therefore have not designed their investigations with an internal variable formulation in mind. It is striking, however, that there are not more constant structure data associated with the creep regime, for internal variables have been applied to creep constitutive models for many years.

Investigators have used different experimental techniques to characterize the rate dependent deformation of metals at assumed constant internal state. Most techniques involve an abrupt change in either strain rate or stress and measurement of the instantaneous or "short time" response in the associated stress or strain rate. None of the techniques, whether stress-drop, relaxation, or jump tests, is without experimental uncertainties. These uncertainties range from difficulty in extracting the effect due to a particular mechanism when many possible mechanisms may be operating, to operational problems associated with test machine compliance, resolution of small strains, acquisition of data from rapid transients, and computational uncertainties in determining rate measures from data obtained as a function of time. As a result no one technique is universally accepted, and the type of test performed by an investigator is generally a function of the type of test equipment which is available instead of the most desirable test technique. All of the tests mentioned herein assume that internal state does not change significantly during the period of

the transient, an assumption which is only approximately satisfied in all tests.

The following paragraphs describe briefly the different tests used to correlate stress and strain rate at constant structure, list some of the investigators associated with each test type, and also give some of the uncertainties associated with each type. The section finally presents some arguments proposing that the strain rate jump test may have some clear advantages over stress-drop and relaxation tests in determining isostructural properties.

Mitra and McLean [1967] used stress-drop tests to evalute the stress dependence of the creep strain rate in aluminum and nickel by correlating the strain rate resulting after the stress drop with the magnitude of the stress after the drop. Mitra and McLean assumed an initial incubation period after which they measured the strain rate. Assuming that the state of the material has not changed significantly during the incubation period, the resulting stress/strain rate curve may be taken to be the stress dependence for the given initial internal state. Investigators have used the same procedure but have measured the "instantaneous creep rate" at the new stress without any assumed incubation period, e.g. Sherby [1957] and Robinson [1969,74,75], summarized by Takeuchi and Argon [1976] and Sherby [1977]. The above mentioned incubation period is problematic in the interpretation of stress drop data. The incubation period is assumed necessary to let anelastic effects subside, but there is no clear, and certainly no consensus, criterion on what that period should be. Frequently investigators do not indicate what delay, if any, they have employed before determining the post-stress-drop, strain rate. Complicating the uncertainty about incubation is the obvious possibility of structure evolution occurring during the incubation period, thereby voiding the constant structure assumption of the test.

Of the investigators who have used stress drop tests to evaluate rate dependence,

most of the results mentioned in the papers listed above indicate a constant structure power law stress dependence of the strain rate of 6 to 8. Figures 4.2a and 4.2b illustrate the power law dependence of constant structure, stress drop data. *This dependence in all cases was greater than the steady state stress exponent obtained for each material.* The power law strain rate/stress relationship for constant structure has not been universally confirmed. Gibeling and Nix [1982], recently performed a set of stress drop tests on pure aluminum and found that the isostructural stress dependence of the strain rate followed an exponential relationship. [Figure 4.2c]

Stress drop tests are difficult to perform for hot working investigations due to the magnitude of the associated strain rates. Evaluation of strain rates following a change in stress requires numerical differentiation of a strain versus time record, which in turn requires sampling of strain over very small time intervals. Typical current microcomputer data acquisition hardware can not sample a sufficient number of data points at a sufficiently fast rate (> 10 kHz) to permit differentiation of the strain versus time signal.

Hart [1979] and others have popularized the relaxation test as another test of stress dependence at constant structure. In this procedure, a specimen is deformed to a given strain and the test machine is halted. The specimen strain rate may be determined by subtracting a machine compliance effect from the load versus time curve obtained during relaxation. Hart estimates that the inelastic strain accumulated during a typical relaxation test is about $10^{-4}$. From this Hart states that such a small strain increment produces negligible strain hardening, so the test can be considered to be at a constant state. *This assumption is valid only as long as recovery effects can be neglected, which is certainly not possible in the range of homologous temperatures associated with hot working.* Other investigators using this technique include Alexopoulos [1982] and C. Li [1981]. The relaxation test

is problematic in that some investigators have proposed using it to characterize recovery mechanisms, an application directly contrary to Hart's assumption of zero state change. Other investigators have suggested that the small strains associated with relaxation tests do not accurately probe the large strain constitutive response of a material since little dislocation motion is required to unload the test specimen [Rhode et al. 1973].

Another procedure used to measure the constant structure, strain rate or stress dependence is to suddenly change the strain rate. The instantaneous change in stress accompanying a change in strain rate may be a more faithful representation of the stress dependence than that which results from the stress drop test, since there is no associated incubation time. Klepaczko and Duffy [1977, 1982, 1986] have probably performed the most comprehensive set of strain rate jump tests, having documented the behavior of both FCC and BCC materials over a wide range of temperatures and strain rates, although most of their test temperatures were below one half the homologous temperature.

It should be noted that very few of the investigators mentioned above have employed any of the "jump" tests described above in a manner appropriate to decoupling state from instantaneous rate dependence. Such decoupling requires jumps from the same initial state. In the context of the single, isotropic internal variable model under consideration here, this means from the same value of temperature, strain rate, and stress. Given that the real material may (and probably does) exhibit history dependence beyond that representable by a single internal variable, the jumps should occur after identical deformation histories to assure as identical a state as possible. In a case where a steady state is reached, it is useful to impose the sudden change from steady state conditions where the jump state is more reliably reproduced. A set of such jump tests is indicated in Figure 4.3. Figure 4.4

illustrates a set of jump tests on the schematic introduced in Figure 4.1, where the test begins with the value of the internal variable $s_0$ and eventually saturates at $s^*$.

Interpretation of jump test data is complicated by different back-extrapolation methods used to determine the instantaneous stress dependence, especially when there is an overshoot and subsequent drop in stress. Kocks, Argon, and Ashby [1975] review the different methods and conclude provisionally that the method of extrapolation is not of critical importance. The jump test data obtained in this investigation does not demonstrate any overshoot. The data show a linear segment which then increases monotonically with increasing strain. One may therefore select a simple and straightforward technique of defining the instantaneous stress response as that resulting from a 0.2 percent strain offset, illustrated in a schematic strain rate jump test in Figure 4.9, where $\sigma_f$ is used as the constant structure stress response. This necessarily assumes that one, there is no change in state during this strain increment, and two, that the transition to the new strain rate has been accomplished over the small strain increment. The 0.2% strain offset criteria was chosen over some back extrapolation procedure since the presence of extensive hardening made extrapolation from some point further from the jump point difficult to justify.

Very few investigators have attempted to examine the constant structure temperature dependence of the flow behavior of metals within the regime of temperatures and strain rates associated with creep or hot working. Direct measurement of this dependence, and thus the activation energies associated with the dislocation glide mechanisms, requires temperature jump tests. The activation energies obtained from steady state data represent the combined contribution of both glide kinetics and the thermal processes controlling the evolution of microstructure. We did not perform any temperature jump testing in this investigation because the time constant associated with changing temperatures in the test equipment was

significantly larger than the recovery rates associated with the model material.

### 4.1.1 Strain Rate Jump Tests

As discussed in the previous section, jump tests measure material response at a given constant structure, thereby characterizing the rate equation associated with our constitutive model. A series of strain rate jump tests were performed on the test system described in Chapter 3. All strain rate jumps were programmed to occur at the same value of strain for a given temperature, after the stress variation with strain had reached an apparent constant value at the initial strain rate. Jumping from such apparently steady state conditions minimized the variation in initial state among tests at the same temperature and initial strain rate. Figures 4.5 to 4.8 show the strain rate jump test results at 700, 800, 900 and 1000 degrees Celsius. All jumps in strain rate were from the same initial strain rate of $0.2 \times 10^{-4}$ per second. The maximum final strain rate was selected to be 1 per second due to the limit of the servohydraulic dynamic response. This strain rate also corresponded to the rate at which noticeable adiabatic heating occurred, producing an effective limit to the isothermal, constant true strain rate test conditions.

The displacement command signal for the strain rate jump tests was provided by the analog function generator described in Chapter 3. Data acquisition was performed on a IBM PC/XT equipped with a Metrabyte Dash-16 data acquisition board. Two programs were used on the PC/XT, both of which are listed and described in Appendix B . Both the load cell and LVDT output signals were also conditioned by a 60 Hertz cut-off, low pass filter to reduce the electrical noise generated by the vacuum furnace heating elements. The filter frequency was selected to permit as much noise reduction as possible without distorting transducer output signals.

Once stored on the PC/XT, the load/displacement data were transferred to a Data General 4000 where they were converted to true stress/strain data. The stress and strain values were then independently smoothed, using sample number as the independent variable, and then the plastic strain and strain rate were calculated at each sample point. The programs and procedures used for this analysis is described in Appendix B.

The stress before and immediately after the jump was then measured. The stress after the jump was selected to be the stress corresponding to a 0.002 offset from the jump strain, as illustrated in Figure 4.9. It was frequently difficult to determine this value precisely due to the absence of a clearly linear, elastic, initial portion of the jump in stress. The initial portion of the curve, although linear, decreased in slope between tests as the final strain rate was increased. In any event, the linear section of the curve was assumed to be elastic, and the offset was taken from this section. The uncertainty in this linear region did not significantly change the value of this offset stress. Examination of the strain rate data indicated that the final strain rate was achieved at approximately the same time as the 0.002 strain offset stress was reached. Given the assumption of no change in state up to that point, the offset stress could then be assumed to indicate the stress sensitivity of the material at a given internal state. Figure 4.10 shows the constant state lines constructed from this stress/strain rate data. Table 4.1 lists the data associated with these tests which were used to produce Figure 4.10.

Three rate equations were considered for correlation with the constant structure data. One, a simple model representing a stress and structure dependent thermal activation:

$$\dot{\tilde{\epsilon}} = A \exp\left[-\frac{Q}{R\theta}\left(1 - \frac{\tilde{\sigma}}{s}\right)\right]. \qquad 4.1.1$$

Here, $A$ and $Q$ are material parameters. Two, a modification of 4.1.1 to reflect the phenomena of power law breakdown:

$$\dot{\bar{\epsilon}} = A\left(\frac{\sigma}{s}\right)^q \exp\left[-\frac{Q}{R\theta}\left(1-\frac{\tilde{\sigma}}{s}\right)\right], \qquad 4.1.2$$

where an additional parameter $q$ has been added. Three, an alternative to 4.1.1 which separates temperature and stress dependence into a simple Arrhenius term involving a constant activation energy and a function depending only on stress and the internal variable:

$$\dot{\bar{\epsilon}} = A\exp\left(-\frac{Q}{R\theta}\right)\left[\sinh\left(\xi\frac{\tilde{\sigma}}{s}\right)\right]^{1/m}. \qquad 4.1.3$$

Four material parameters are required: $A, Q, \xi$, and $m$. $R$ is the gas constant in these equations ($8.314\times10^{-3}$ kJoules/mole). Equation 4.1.1 reflects a simplification of a form proposed by Kocks, Argon, and Ashby [1975] for the jerky glide of dislocations. Here, $s$ represents a generalized obstacle resistance to dislocation motion. Equation 4.1.2, proposed by Lee and Zaverl [1978], follows the same motivation, but assumes a priori that the rate equation should reflect the transition from power law to exponential behavior, and therefore includes a stress-dependent pre-exponential to accommodate the power law. Equation 4.1.3 makes the same a priori assumption but uses a modification of the following hyperbolic sine form first proposed by Garofalo [1963] to model steady state behavior into the power law breakdown regime:

$$\dot{\epsilon}_{ss} = A_{ss}\exp\left(-\frac{Q_{ss}}{R\theta}\right)[\sinh(\alpha\sigma_{ss})]^{1/m}, \qquad 4.1.4$$

where the "ss" subscript denotes quantities relevant only to steady state conditions. This form accomodates power law breakdown since for low values of $(\alpha\sigma_{ss})$ it approximates:

$$\dot{\epsilon}_{ss} = A_{ss}\exp\left(-\frac{Q_{ss}}{R\theta}\right)(\alpha\sigma_{ss})^{1/m}, \qquad 4.1.5$$

and for large values of the same argument it approaches:

$$\dot{\epsilon}_{ss} = \frac{A_{ss}}{2^{1/m}} \exp\left(-\frac{Q_{ss}}{R\theta}\right) \exp\left(\frac{\alpha}{m}\sigma_{ss}\right). \qquad 4.1.6$$

There appears to be no widely accepted mechanistic derivation of the hyperbolic sine form of the rate equation represent by 4.1.3. Gittus [1976] has proposed an explanation of power law breakdown founded on the dominance of forward and backward vacancy formation rates. A hyperbolic sine form results naturally from this assumption of forward and backward mechanical activation. Many other investigators, [Sherby, 1968; Frost and Ashby, 1982] associate power law breakdown with a transition from climb-dominated deformation to dislocation glide domination. In any event, it is well-known that the hyperbolic sine form provides a convenient phenomenological representation of power law breakdown.

We settled upon the hyperbolic sine form, 4.1.3, for the rate equation for the following reasons:

1. The steady state stress/strain rate relationship for pure aluminum and Fe - 2% Si suggests a constant activation energy. Figure 4.11 illustrates the steady state stress/strain rate relationship for aluminum over a wide range of strain rates and temperatures, where the steady state strain rate is normalized by a constant activation energy [Jonas, 1969]. In light of the success of this normalization, we found it reasonable to extend this relationship to the rate equation and assume a relationship of the form of 4.1.3.

   The jump test data for the Fe - 2% Si further suggests a functional dependence of the form of 4.1.3. Figure 4.12 plots the constant structure jump test data where the strain rate has been normalized by a constant activation energy, taken in this case to be that for self diffusion in alpha iron. It is obvious that

a power law does not represent the dependence between stress and the normalized strain rate. With the exception of the 700 degree Celsius data, each constant structure curve is concave upward in a manner commensurate with power law breakdown. The 700 degree data is suspect for reasons associated with the dynamic response of the servohydraulic; it is included however for both for completeness and because we are not certain that the data is actually incorrect. It would be interesting to perform constant structure tests at higher strain rates to investigate this behavior.

Although the constant structure data for the Fe - 2% Si may be represented by an exponential, constant structure stress drop tests performed on other metals suggest a power law asymptote in the low strain rate creep regime [Sherby et al. 1977]. For this reason we selected equation 4.1.3 which may accomodate this transition from an exponential to a power law.

2. Regardless of the form of the rate equation, we insist that the steady state value of the internal variable ($s_{ss}$) increase monotonically with steady state stress ($\sigma_{ss}$). This not only makes sense physically but also corresponds to measurements of room temperature yield stress as a function of steady state stress [Young and Sherby, 1973]. One may check whether the three proposed rate equations accomodate this requirement by *assuming steady state conditions* and equating each rate equation to *known* empirical relations for steady state behavior. By eliminating strain rate as the common variable we may determine whether the resulting functional dependence between the steady state values of stress and the internal variable is reasonable.

Following this procedure, equation 4.1.1 requires an unreasonable relationship between steady state stress and steady state value of the internal variable in

order to reproduce power law breakdown. The steady state strain rate/stress relationship for many materials including most metals in the hot working regime may be represented by equation 4.1.4:

$$\dot{\epsilon}_{ss} = A_{ss} \exp\left(-\frac{Q_{ss}}{R\theta}\right) [\sinh(\alpha\sigma_{ss})]^{1/m}, \qquad 4.1.4$$

where the "$ss$" subscript denotes quantities relevant only to steady state conditions. If we assume steady state conditions and then apply 4.1.4 for the steady state strain rate in 4.1.1, we obtain:

$$s_{ss} = \frac{Q}{R\theta}\sigma_{ss}\left[\ln\left\{\frac{A_{ss}}{A}\exp\left(\frac{Q-Q_{ss}}{R\theta}\right)[\sinh(\alpha\sigma_{ss})]^{1/m}\right\}\right]^{-1}. \qquad 4.1.7$$

Wong and Jonas [1968] have fit 4.1.4 to pure aluminum within a wide range of temperatures, strain rates, and stresses to find the following constants:

$Q_{ss}$ = 156.0 kJ/mole,

$\alpha$ = .0446 $MPa^{-1}$,

$1/m$ = 4.70,

$A_{ss}$ = $2.34 \times 10^{10}$ $sec^{-1}$.

If we assume additionally the following values for equation 4.1.1:

$A$ = $1 \times 10^{10}$ $sec^{-1}$, and

$Q$ = 142.0 kJ/mole, (self-diffusion),

then substitution of these values into 4.1.7 yields, for a representative temperature of 200 degrees Celsius:

$$s_{ss} = 36.0\sigma_{ss}\left[\ln\left\{0.067[\sinh(.0446\sigma_{ss})]^{4.7}\right\}\right]^{-1}. \qquad 4.1.8$$

The steady state stress/internal variable relationship expressed by 4.1.8 is shown in Figure 4.13. The negative values of state and the singularity indicates

that, while attractive (based on modelling of physical mechanisms), equation 4.1.1 is inadequate, given our assumption of power law breakdown, to simulate hot working.

3. Generally accepted notions of the stress dependence of the pre-exponential create a situation for equation 4.1.2 similar to that described in item 2 above for equation 4.1.1. Stress dependence of the pre-exponential is generally derived to be proportional to stress raised to a low power, either one or two [Argon, 1975]. If we assume two to be an upper bound and then follow a procedure identical to that followed in reason two above, we obtain the following expression correlating steady state stress and steady state deformation resistance:

$$A_{ss}\exp\left(-\frac{Q_{ss}}{R\theta}\right)[\sinh(\alpha\sigma_{ss})]^{1/m} = A\left(\frac{\sigma_{ss}}{s_{ss}}\right)^{n}\exp\left[-\frac{Q}{R\theta}\left(1-\frac{\sigma_{ss}}{s_{ss}}\right)\right], \quad 4.1.9$$

where the variables have the same interpretations as in item 1. Rearranging and using the same values for aluminum used before yields:

$$0.067[\sinh(.0446\sigma_{ss})]^{4.7} = \left(\frac{\sigma_{ss}}{s_{ss}}\right)^{2}\exp\left[36.0\frac{\sigma_{ss}}{s_{ss}}\right]. \quad 4.1.10$$

The values of $s_{ss}$ corresponding to variation in $\sigma_{ss}$ may be determined numerically from 4.1.10. Figure 4.14 plots the relationship resulting from such a determination. Once again the variation in the value of the internal variable at steady state with respect to steady state stress is not what we should reasonably expect.

4. The fact that the ratio of equivalent stress/internal variable appears twice in equation 4.1.2 complicates the determination of material parameters significantly when fitting the rate equation to actual material data. As will be seen,

much of the following analysis exploits a desirable feature of the rate equation to be inverted to produce an analytic relationship of the form:

$$\sigma = cs,$$

where $c$ depends only on temperature and strain rate. Equation 4.1.2 does not permit such an inversion.

The material parameters associated with equation 4.1.3 may be evaluated directly from the jump test data. The procedures and numerical routines used to obtain these parameters are described in Chapter 5. Figure 4.15 illustrates the correspondence between the experimental data and the rate equation with the following values for the material parameters:

$$Q = 247.5 \text{ kJ/mole}$$
$$A = 1.26 \times 10^8 \text{ sec}^{-1}$$
$$m = .22793$$

The value of $Q$ is within the range of activation energies obtained by other investigators for self-diffusion in alpha iron: 239 to 251 kJ/mole [Frost and Ashby, 1982]. It is lower than the value of 333.6 kJ/mole obtained by Uvira and Jonas [1968] by fitting equation 4.1.4 to a set of steady state stress and stress rate data on a Fe - 3% Si alloy. There is no reason to expect the activation energies obtained in this investigation and by Uvira and Jonas to be similar. The value obtained through the jump tests is a consequence of constant structure rate dependence while that obtained from steady state data provides a weighted average of both this dependence and the thermally activated processes controlling the evolution of state. The correlation between the data and the fit rate equation is excellent. We therefore adopted equation 4.1.3 as the rate equation throughout the remainder of the investigation.

The parameter $\xi$ in the rate equation is indeterminate. We chose to include $\xi$ in order to restrict values of the internal variable $s$ to be at all times greater than $\tilde{\sigma}$. This corresponds to requiring the proportionality constant $c$ to be less than one, where $\tilde{\sigma} = cs$ for isothermal, constant true strain rate conditions. For 4.1.3, $c$ is:

$$c = \frac{1}{\xi} \sinh^{-1} \left[ \left\{ \frac{\dot{\tilde{\epsilon}}^p}{A} \exp\left(\frac{Q}{R\theta}\right) \right\}^m \right]. \qquad 4.1.12$$

For the rest of this investigation we assume a value of $\xi = 5.0$.

To recapitulate, the rate equation which will be used throughout the rest of this investigation is:

$$\dot{\tilde{\epsilon}} = A \exp\left(-\frac{Q}{R\theta}\right) \left[\sinh\left(\xi \frac{\tilde{\sigma}}{s}\right)\right]^{1/m}. \qquad 4.1.3$$

where $A, Q$, and $m$ are material parameters which should be determined from constant structure, jump test data.

## 4.2 Evaluation of the Static Recovery Function: $\dot{r}(\theta, s)$

Several means are available for decoupling the dynamic and static terms of the evolution equation for $s$ represented by equation 4.4, restated here:

$$\dot{s} = h(\tilde{\sigma}, s, \theta)\dot{\bar{\epsilon}}^p - \dot{r}(s, \theta). \tag{4.4}$$

Certainly, one may assume that one term predominates within a particular temperature/strain rate regime. We expect the effect of the static recovery function $\dot{r}$ to diminish as the strain rate increases or as the temperature decreases. One may therefore assign a regime where static recovery may be neglected and the strain hardening data used to characterize only the dynamic term of the evolution equation. We may similarly perform tests where the hardening function $h$ may be considered neligible. As will be shown below, this may be accomplished either via some extrapolation technique or by static hold tests which enforce a zero plastic strain rate.

Experimental determination of a static recovery function of the form

$$\dot{r} = \dot{r}(\theta, s) \tag{4.2.1}$$

is particularly arduous since recovery testing typically yields only one data point, i.e. a "recovered" state, per test. Characterization of a recovery function therefore requires numerous tests to completely capture the effect of each of the relevant parameters. Different investigators have proposed different experiments to examine static recovery phenomena. Most assume a Bailey-Orowan form for the combined effect of hardening and recovery, and then propose a procedure whereby the hardening rate may be considered to be negligible relative to the recovery term. We

have not found any investigator who has evaluated recovery data directly in order to determine an internal variable based, static recovery function.

Perhaps the first comprehensive phenomenological investigation of hardening and recovery was performed by Mitra and McLean [1966], who, following a suggestion of Cottrell and Aytekin [1950], used stress drop experiments to evaluate a recovery function based on stress. They assumed that the recovery function could be represented as:

$$\dot{r} = \left(\frac{d\sigma}{dt}\right)_{\epsilon}.$$

They then performed a series of stress drop tests from the same initial stress, temperature, and strain, and then associated the drop in stress ($\triangle\sigma$) with the time increment ($\triangle t$) required to reach a new steady state strain rate. Figure 4.16 illustrates one such stress drop test. They then plotted the stress reductions versus the associated recovery time. The instantaneous recovery rate was assumed to be slope of the resulting curve extrapolated back to a zero stress reduction:

$$\dot{r} = \lim_{\Delta\sigma \to 0} (\Delta\sigma / \Delta t), \qquad 4.2.2$$

which is illustrated in Figure 4.17.

Kocks [1975] proposed two methods of evaluating $\dot{r}$. Method one consisted of imposing strain rate jumps from identical steady state conditions and measuring the associated instantaneous rate of change in stress. Back extrapolation of the resulting data to zero strain rate as illustrated in Figure 4.18 would then provide the recovery rate. Method two consisted of measuring the rate of change of stress immediately following a large drop in strain rate from steady state conditions (where the rate of recovery supposedly equals that of hardening). If the drop in strain rate is at least one order of magnitude, then Kocks hypothesized that since the rate of hardening is assumed in a Bailey-Orowan formulation to be proportional to the strain rate,

then the hardening term would be negligible relative to the static softening term, which would be unaffected by the reduction in strain rate. The rate of change of stress would therefore be due purely to static recovery in the absence of significant hardening or dynamic recovery. Both of these methods possess the operational disadvantage of attempting to measure the rate of change of stress associated with a very short transient. No investigations have been found which used either of these two methods to evaluate the recovery function $\dot{r}$.

An additional test of static softening mechanisms which has been employed extensively in investigations of metal working behavior is the load-unload-hold-reload test [McQueen, 1985; Luton, et al., 1980; Petkovic, 1979]. Employed primarily to simulate multistage hot working, specimens are deformed, usually isothermally, either in compression or torsion to a given strain, unloaded, held for varying time periods, then reloaded. The load-unload-reload cycle may be repeated many times sequentially on the same specimen to simulate complicated, multistage hot working processes. The change in state resulting from a particular hold period may be characterized by the yield stress obtained on reloading the specimen. The test possesses the benefit of avoiding the multiple uncertainties (and controversies) associated with both measuring and interpreting the transients associated with changing the stress or strain rate. The test, however, suffers the same shortcoming as the jump test, since some semi-arbitrary criteria must be used to measure the yield stress upon reloading. The same arguments can be made as in the case of the jump test that the variation in yield stress is relatively small given sufficient resolution on the reloading transient.

Rather than fixing a final form for the recovery function $\dot{r}$ and then using recovery data to determine the parameters of that function, the following technique is proposed to characterize the static recovery function assuming the following in-

termediate structure for the evolution equation for the internal variable:

$$\dot{s} = h(\sigma, \theta, s)\dot{\bar{\epsilon}}^{p} - \hat{r}(s)\exp\left(-\frac{Q_r}{R\theta}\right). \qquad 4.2.4$$

Here, we assume that the dependence of static recovery on the temperature and the internal variable may be expressed through the product of an Arrhenius term with a constant activation energy, $Q_r$, and a function depending only on $s$. The activation energy $Q_r$ is expected to be different from that associated with the rate equation, $Q$. Since static recovery is generally assumed to be the result of dislocation climb [Hirth, 1982] $Q_r$ should be close to the activation energy for the self-diffusion of vacancies. We therefore assume $Q_r = 300$ kJ/mole, which is an average value for self-diffusion in alpha iron [Frost and Ashby, 1982]. Chapter 5 describes a series of tests which validates this assumption. The expectation is that we may design an appropriate technique so that we only assume a priori equations 4.3 and 4.2.4, and then let the experimental data suggest a form for $\hat{r}(s)$.

The proposed procedure exploits the consequence of the above equations that the internal variable $s$ is at all times proportional to the stress $\sigma$ during an isothermal, constant true strain rate test. That is,

$$\sigma = cs, \qquad 4.2.5$$

where $c$ is a function of the rate equation which includes strain rate and temperature dependence (equation 4.1.12). *This proportionality is central to the evaluation of both the static recovery function $\dot{r}$ and the hardening function $h$, for it allows us to use a measure of stress to determine the internal variable $s$ through the constant $c$. We therefore do not have to measure $s$ directly; we need only measure stress and assure that isothermal, constant true strain rate conditions exist.* This assumption may be made as long as the functional dependence in the rate equation between

the equivalent stress and the internal variable is one-to-one for a given temperature and strain rate.

If we now perform load-unload-hold-reload experiments in isothermal, constant true strain rate conditions, the difference between the stress just before unloading and the yield stress upon reloading represents the change in state due only to static recovery. We can then vary temperature ($\theta$), hold time ($\Delta t$), and stress before unloading ($\sigma_i$), maintaining a constant value of $c$, and thus determine the temperature and state dependence of the recovery function by measuring the value of stress upon reloading ($\sigma_f$).

The procedure proposed assumes that we have already determined the functional dependence on temperature, which as stated, will be represented by an Arrhenius expression with an activation energy *equal to that of self-diffusion.* The data required is a set of load-unload-hold-reload tests, where the stress before unloading, the temperature, and strain rate are held constant. Figure 4.19 illustrates a series of such load-unload-hold-reload tests. The only variable changed between tests is the hold time, $\Delta t$. The dependent variable is the stress obtained upon reloading the specimen, $\sigma_f$. The procedure effectively measures the integrated effect of recovery, then differentiates it to obtain the recovery function. This is in contrast to the methods described at the beginning of this section which attempt to measure recovery function directly.

In the absence of hardening or dynamic recovery ($\dot{\bar{\epsilon}}^p = 0$), the evolution equation becomes:

$$\dot{s} = -\hat{r}(s) \exp\left(-\frac{Q_r}{R\theta}\right). \qquad 4.2.6$$

Integration yields

$$\exp\left(\frac{Q_r}{R\theta}\right) \int_{s_i}^{s_f} \frac{ds}{\hat{r}(s)} = -\Delta t. \qquad 4.2.7$$

However, since we only know $\sigma$ and not $s$, we may express this as:

$$\exp\left(\frac{Q_r}{R\theta}\right)\int_{\sigma_i/c}^{\sigma_f/c}\frac{d(\sigma/c)}{\hat{r}(\sigma/c)} = -\Delta t. \qquad 4.2.8$$

From load-unload-hold-reload tests we may determine $\sigma_i, \sigma_f$, and $\Delta t$. Differentiating the integral on the left hand side of 4.2.8 with respect to $\sigma_f/c$ yields:

$$\frac{d}{d(\sigma_f/c)}\int_{\sigma_i/c}^{\sigma_f/c}\frac{d(\sigma/c)}{\hat{r}(\sigma/c)} = \frac{1}{\hat{r}(\sigma_f/c)}, \qquad 4.2.9$$

or,

$$\exp\left(\frac{Q_r}{R\theta}\right)\frac{1}{\hat{r}(\sigma_f/c)} = -\frac{d}{d(\sigma_f/c)}\Delta t. \qquad 4.2.10$$

If we now know (or assume) $Q_r$, we may use 4.2.8 to plot the hold period $-\Delta t$ versus $\sigma_f/c$, the derivative of which, according to 4.2.10, is the reciprocal of the recovery function:

$$\hat{r}(\sigma_f/c) = \exp\left(\frac{Q_r}{R\theta}\right)\frac{1}{\frac{-d\Delta t}{d(\sigma_f/c)}}. \qquad 4.2.11$$

Figure 4.20 shows a schematic plot of hold period ($\Delta t$) versus the stress measured upon reloading ($\sigma_f$), which may be obtained from a series of tests like those illustrated in Figure 4.19. Figure 4.21 illustrates the result of treating the data in Figure 4.20 in the manner proposed by equation 4.2.11. The data plotted in Figure 4.21 then represents the recovery function $\hat{r}(s,\theta)$.

This procedure may be applied to the static recovery function proposed by both Prinz and Argon [1984] and Nix and Gibeling [1985]. Slightly generalized, the form of the function is:

$$\dot{r} = -\mu B \exp\left(-\frac{Q_r}{R\theta}\right)\left(\frac{s}{\mu}\right)^p. \qquad 4.2.12$$

Here, $\mu$ is the shear modulus and $B$ and $p$ and material constants. There is an additional temperature dependence of the pre-exponential in the Prinz and Argon

and the Nix and Gibeling models which has been neglected in 4.2.12. Given load-unload-hold-reload data as described above, 4.2.12 applied to 4.2.10 yields:

$$\frac{-d\Delta t}{d(\sigma_f/c)} = \exp\left(\frac{Q_r}{R\theta}\right)\frac{\mu^p}{\mu B}\left(\frac{\sigma_f}{c}\right)^{-p}. \qquad 4.2.13$$

The above procedure requires enough tests at a given temperature to be able to determine the derivative on the right hand side of 4.2.10. It also presupposes knowledge of the value of $c$ and $Q_r$. Once again, $c$ is the proportionality constant defined by equation 4.1.12 and obtained from the strain rate equation. $Q_r$ may be estimated as the activation energy for self-diffusion for the material of interest. It may also be determined by a series of tests where through trial and error the same values of $\sigma_i$ and $\sigma_f$ are obtained for two tests at different temperatures but the same value of $c$. This can be accomplished only by allowing a longer recovery time for the lower temperature test. If these conditions are met, then for the two tests at two temperatures:

$$\exp\left(-\frac{Q_r}{R\theta_1}\right)\Delta t_1 = \exp\left(-\frac{Q_r}{R\theta_2}\right)\Delta t_2, \qquad 4.2.14$$

and $Q_r$ may be determined.

### 4.2.1 Recovery Tests

A set of load-unload-hold-reload tests were performed on the silicon iron according to the paradigm described above. Before performing these tests, however, we performed a series of tests to determine the temperature and strain at which static recrystallization initiated. We then selected a temperature and strain below these values to assure that the softening measured due to the hold period would be due solely to static recovery.

The initiation of static recrystallization was determined phenomenologically according to a procedure described by McQueen [McQueen, 1982; Ryan et al., 1983].

A series of tests were performed at increments of 100 degrees Celsius where a compression specimen was deformed at a constant strain rate and temperature for a given strain increment, unloaded, and held for a specified time. This was repeated for the same strain increment until a true strain of approximately $-1.2$. The fractional softening for each hold period was then plotted as a function of strain for each test. Fractional softening is defined as:

$$FS_n = \frac{\sigma_{un} - \sigma_{r(n+1)}}{\sigma_{un} - \sigma_{y0}} \qquad 4.2.15$$

where

$\sigma_{un}$ = stress before unloading nth strain increment,

$\sigma_{r(n+1)}$ = yield stress upon reloading from nth hold period,

$\sigma_{y0}$ = original yield stress.

McQueen found that during a given test, fractional softening remained relatively constant if only static recovery was present. Static recrystallization, however, past a certain initiation strain caused the fractional softening to increase.

The results of our multiple hold tests are included in Figures 4.22 to 4.25. The fractional softening versus strain is plotted in Figure 4.26. Notice that the fractional softening begins to increase at 1000 degrees Celsius at a true strain of 0.6. We therefore chose our recovery test conditions to be at 900 degrees Celsius, at a strain rate less than that used for the multiple hold tests, ($-0.02$ per second instead of $-0.1$ per second), and at a strain of $-0.3$. Examination of the etched grains of specimens tested at this conditions did not show any regions of recrystallized grains.

The results of the recovery tests for these conditions are presented in Figure 4.27. One obvious result of these tests is that the stress measured upon reloading is not significantly different from that measured just before unloading, even for

relatively long hold periods. We should therefore expect the rate of static recovery to be commensurately low.

Another result from these recovery tests is that when the "yield stress" is measured upon reloading, the greatest incremental decrease in stress occurs during the shortest hold period. In other words, the rate of static recovery decreases dramatically as the hold period increases. This is not necessarily unexpected, for we may hypothesize short range rearrangements due to the polarization of a deformation-induced microstructure or anelastic effects which produce a rapid apparent initial rate of recovery. This result was not obtained by Petkovic [1979] who performed similar load-unload-hold-reload tests on polycrystalline copper. Petkovic found that some incubation time was necessary after unloading before any noticeable recovery was obtained upon reloading. This incubation period extended to as long as 100 seconds at 500 degrees Celsius (0.6 homologous temperature).

The question arises however whether we should model this behavior. We decided to ignore this initial rapid unloading to the following reasons:

1. Insufficient recovery testing was performed to characterize the extent of this effect.

2. If this initial high recovery rate is due to microstructure polarization or anelastic effects, we do not expect these effects to significantly alter the large deformation material response.

3. If the procedure described in Section 4.2 for evaluation of the static recovery function is followed, the high apparent initial recovery rate produces an unreasonably strong dependence of recovery on the internal variable. This dependence corresponds to a power law dependence of recovery rate on the internal variable $s$ raised to a power exceeding 100.

We therefore chose to consider data for recovery hold periods exceeding 20 seconds to fit a material function for static recovery.

Following the procedure described in Section 4.2, a 0.002 strain offset stress was measured from the reloading segment of each test. The variation in this "yield" stress was then used as a measure of the variation in state due to different hold periods. This data is plotted in Figure 4.28. Continuing with the development presented in Section 4.2, we assume that the recovery function may be represented by equation 4.2.6:

$$\dot{s} = -\hat{r}(s) \ \exp\left(-\frac{Q_r}{R\theta}\right). \qquad 4.2.6$$

Equation 4.2.11 then expresses the recovery function in terms of the derivative of the data in Figure 4.28:

$$\hat{r}(\sigma_f/c)\exp\left(-\frac{Q_r}{R\theta}\right) = \frac{1}{\frac{-d\Delta t}{d(\sigma_f/c)}}. \qquad 4.2.11$$

Figure 4.29 contains the data treated in the manner suggested by 4.2.11, which then represents the recovery function. Due to the small number of tests the derivative was taken to be the slope of the line drawn between sequential data points.

The static recovery function which we considered is a generalized form of a function proposed both by Nix and Gibeling [1985] and Prinz and Argon [1984] based on models of dislocation climb causing static recovery in dislocation cell walls:

$$\dot{r} = -\mu B \exp\left(\frac{Q_r}{R\theta}\right)\left(\frac{s}{\mu}\right)^p, \qquad 4.2.12$$

where $\mu$ is the shear modulus and $B$ and $p$ are material parameters. Both of the above pairs of investigators hypothesize a value of $p$ between four and six.

Fitting equation 4.2.13 to the recovery data illustrated in Figure 4.29 produced the following values for the material parameters:

$B \quad = 1.08 \times 10^{60}$ MPA/sec

$Q_r$ = 300 kJ/mole,

$p$ = 20.6.

The procedures and numerical routines used to obtain these parameters are described in Chapter 5. Figure 4.30 indicates the fit of equation 4.2.12 to the recovery data using the above parameters. The lack of correlation with the high recovery rate portion of the data reflects the previously described decision to ignore the initial rapid static recovery data.

Notice that the exponent $p$ is significantly greater than that predicted by Argon and Nix. It is unclear whether this is due to a stronger dependence of recovery on state than was anticipated or whether some characteristic of the experimental procedure produces this dependence. Since these experiments are rather arduous when performed with Fe - 2% Si, further investigation of both the phenomena and the experimental method would be easier if the model material were a lower melting temperature metal such as aluminum.

Nevertheless, equation 4.2.12 with the above material parameters provides a measure of static recovery, we believe the first measure of static recovery employing an internal variable formulation. To summarize, the static recovery function for the internal variable $s$ is:

$$\dot{r} = -B\mu \exp\left(-\frac{Q_r}{R\theta}\right)\left(\frac{s}{\mu}\right)^p, \qquad 4.2.12$$

where $B, Q_r$, and $p$ are material parameters.

## 4.3 Evaluation of Dynamic Hardening and Recovery Function: $h(\tilde{\sigma}, s, \theta)$

If we now consider an experiment where the temperature and true strain rate are held constant, then according to section 4.1 for fully developed flows where $\dot{\tilde{\epsilon}} \approx \dot{\tilde{\epsilon}}^p$ there is a unique proportional relationship between the equivalent stress and the internal variable throughout the test:

$$s = \frac{\tilde{\sigma}}{c}, \tag{4.3.1}$$

where $c$ is constant for a given temperature/strain rate pair. We can therefore express the evolution equation for the internal variable in terms of stress:

$$\dot{\tilde{\sigma}} = ch\left(\tilde{\sigma}, \frac{\tilde{\sigma}}{c}, \theta\right)\dot{\tilde{\epsilon}}^p - c\dot{r}\left(\frac{\tilde{\sigma}}{c}, \theta\right), \tag{4.3.2}$$

or

$$\frac{d\tilde{\sigma}}{d\tilde{\epsilon}^p} = ch\left(\tilde{\sigma}, \frac{\tilde{\sigma}}{c}, \theta\right) - \frac{c}{\dot{\tilde{\epsilon}}^p}\dot{r}\left(\frac{\tilde{\sigma}}{c}, \theta\right). \tag{4.3.3}$$

The slope of the stress versus plastic strain data $(\tilde{\sigma}, \tilde{\epsilon}^p)$, or hardening data, from an isothermal, constant true strain rate test therefore reflects the internal variable evolution equation for the above model. The hardening data however incorporates contributions from both functions $h$ and $\dot{r}$ representing the evolution of structure. Additional testing or assumptions must be made to further separate these equations for evaluation. Figure 4.31 illustrates an isothermal, constant true strain rate test path on the schematic introduced in Figure 4.1.

A series of isothermal, constant true strain rate tests have been performed on the iron - 2% silicon. These tests were performed over a temperature range of 700 to 1200 degrees Celsius (.55 to .83 $T_m$) and a strain rate range of $10^{-3}$ to 1 $sec^{-1}$. 700 Celsius represented the lowest temperature at which tests could be performed

due to the load limit of the ceramic load train. We did not perform tests above 1200 Celsius due to excessive creep of the load train. The lower limit on the strain rate of $10^{-3}$ $sec^{-1}$ was lowest true strain rate obtainable with the analog function generator. The highest strain rate represented both the limit of the frequency response of the servohydraulic and the strain rate where adiabatic heating invalidates isothermal test conditions.

Figures 4.32 through 4.36 contain the stress/strain data for the different temperatures at constant strain rate, while Figures 4.37 through 4.40 illustrate the same data, except for the various strain rates at constant temperature. Notice that the stress eventually reaches an apparent steady state value at strains approaching 0.5. Notice also that we have chosen to neglect data below an *initial* strain of 0.01. Since the specimens are grooved at the ends, we anticipate that at the test start, some "settling" of the ends will occur, rendering accurate interpretation of the small initial strains doubtful if not impossible. Table 4.2 lists the isothermal, constant true strain rate test parameters and values of saturation stress ($\sigma^*$) reached in each test.

Figures 4.41 through 4.44 represent the hardening data for the constant true strain rate tests. Elastic strains were subtracted before the hardening ($d\sigma/d\epsilon^p$) was determined. The program used to numerically determine the hardening is included in Appendix B. Elastic constants for the Fe - 2% Si alloy are listed as a function of temperature in Table 4.3.

The hardening data was used to determine a functional form for the evolution equation for the internal variable. Section 4.0 indicated that given our chosen form for the rate equation, we may represent the evolution equation for the internal variable $s$ in terms of hardening and stress:

$$\frac{d\tilde{\sigma}}{d\tilde{\epsilon}^p} = ch\left(\tilde{\sigma}, \frac{\tilde{\sigma}}{c}, \theta\right) - \frac{c}{\dot{\epsilon}^p}\dot{r}\left(\frac{\tilde{\sigma}}{c}, \theta\right). \qquad 4.3.3$$

Since we have performed experiments to evaluate the rate equation and static recovery function, we may adjust the hardening data for the contribution of static recovery and evaluate the form of $h(\tilde{\sigma}, s, \theta)$.

*One important result of the recovery tests is that the static recovery function does not appreciably affect the hardening data. The integrated contribution of the recovery function to reducing the internal variable over a typical isothermal, constant true strain rate test is less than 1 percent of the instantaneous value of the internal variable. The static recovery function therefore may be ignored rather than added back to the hardening data, and the hardening data then represents in the absence of any contribution of static recovery:*

$$\frac{d\tilde{\sigma}}{d\tilde{\epsilon}^p} \approx ch\left(\tilde{\sigma}, \frac{\tilde{\sigma}}{c}, \theta\right) \qquad 4.3.4$$

The form of $h(\tilde{\sigma}, s, \theta)$ which we first investigated was the simple linear softening function proposed by Anand [1982]:

$$\frac{ds}{d\tilde{\epsilon}^p} = h_0\left(1 - \frac{s}{s^*}\right). \qquad 4.3.5$$

Here, $h_0$ represents a constant rate of athermal hardening which via mechanistic arguments is generally assumed to be of the order of one hundredth the shear modulus ($\mu/100$) [Kocks, 1966]. The ratio ($s/s^*$) may be considered to represent deformation dependent softening phenomena. The denominator $s^*$ may be interpreted as a saturation state associated with a given temperature, and stress or strain rate; We expect $s^*$ to be a function of the external variables $(\tilde{\sigma}, \dot{\tilde{\epsilon}}^p, \theta)$. The combined term $h_0(s/s^*)$ may alternatively be interpreted as the rate of dynamic softening. For isothermal, constant true strain rate tests where $\tilde{\sigma} = cs$, equation 4.3.5 may be expressed as:

$$\frac{d\tilde{\sigma}}{d\tilde{\epsilon}^p} = ch_0\left(1 - \frac{\tilde{\sigma}}{\tilde{\sigma}^*}\right), \qquad 4.3.6$$

where $\tilde{\sigma}^* = c\,s^*$ is the saturation or steady state stress. Equation 4.3.5 is attractive on practical grounds since it supposes two separate phenomena, hardening and dynamic softening, which interact linearly and for which models may be independently formulated and then summed. The constant $c$ represents the contribution of constant structure deformation kinetics, manifested here as a rate sensitivity of strain hardening. Equation 4.3.6 may be integrated directly to yield the Voce [1955] equation for stress/strain behavior:

$$\tilde{\sigma} = \tilde{\sigma}^* - (\tilde{\sigma}^* - \sigma_0) \exp\left(-\frac{ch_0}{\tilde{\sigma}^*}\tilde{\epsilon}^p\right), \qquad 4.3.7$$

where $\sigma_C = cs_0$ and $s_0$ is the initial value of $s$.

Examination of the hardening data, Figures 4.41 to 4.44, however, indicates that the softening is *not* linear; there is a substantial change in the softening rate as the steady state stress is approached. We chose to accomodate this change in the softening behavior via a modification to equation 4.3.5 through the introduction of an exponent $a$ to yield:

$$\frac{ds}{d\tilde{\epsilon}^p} = h_0\left(1 - \frac{s}{s^*}\right)^a, \qquad 4.3.8$$

or, for an isothermal, constant true strain rate test:

$$\frac{d\tilde{\sigma}}{d\tilde{\epsilon}^p} = ch_0\left(1 - \frac{\tilde{\sigma}}{\tilde{\sigma}^*}\right)^a. \qquad 4.3.9$$

Figure 4.45 indicates the behavior of the hardening version of equation 4.3.9 as the value of $a$ is varied. Equation 4.3.9 also retains the feature of a saturation stress, which is supported by the Fe - 2% Si data, where the stress appears to reach a constant value given isothermal, constant strain rate conditions. This feature does not necessarily extend to low ($\approx 0.3T_m$) temperatures where many materials do not appear to demonstrate a saturation stress, even for very large strains. [Hecker, 1981] Figure 4.46 indicates the correspondence between equation 4.3.9 and hardening data

for a given strain rate and a range of temperatures. A value of $a = 1.5$ was found to best represent the hardening curves for the Fe - 2% Si.

For low values of the internal variable $s$ ($s \ll s^*$), the value of $h_0$ may be interpreted as the rate of athermal hardening. The value of $h_0$ found for the Fe - 2% Si was 3498.0 MPa, which corresponds to a value of approximately $\mu/20$. This is greater than the hardening rate obtained and derived for State II hardening in single crystals which as stated previously is expected to be in the range of $\mu/100$ to $\mu/200$.

The integrated form of the equation 4.3.9 yields:

$$\tilde{\sigma} = \tilde{\sigma}^* - \left[(\tilde{\sigma}^* - \tilde{\sigma}_0)^{(1-a)} + (a-1)\left\{(ch_0)(\tilde{\sigma}^*)^{-a}\right\}\tilde{\epsilon}^p\right]^{\frac{1}{1-a}}. \qquad 4.3.10$$

where $\tilde{\sigma}_0 = cs_0$ and $s_0$ is the initial value of $s$.

This formulation also requires an expression for $s^*$, which may be interpreted as the saturation state. We propose a phenomenological form for $s^*(\theta, \tilde{\sigma}, s, \tilde{\epsilon})$ where

$$s^* = \tilde{s}\left[\frac{\dot{\tilde{\epsilon}}^p}{A}\exp\left(\frac{Q_{ds}}{R\theta}\right)\right]^n. \qquad 4.3.11$$

This form is motivated by requiring that the saturation state increases with strain rate, and is influenced by thermally activated processes represented by $Q_{ds}$, the activation energy associated with dynamic softening.

Once again, since we may represent $s^*$ by $\tilde{\sigma}^*/c$, we may plot $s^*$ versus strain rate in Figure 4.47 by dividing the saturation stress obtained during isothermal, constant true strain rate tests by the constant $c$ determined from the rate equation. The figure indicates that a power law relationship between strain rate and saturation state is justified. Figure 4.48 illustrates the correlation between the steady state data and a nonlinear least squares fit of equation 4.3.11 to the same data. Chapter 5 describes the routines and procedures used to fit the data to the material functions. The material constants obtained from the nonlinear least squares fit to 4.3.11 are:

$\tilde{s}$ = 36.3 MPa

$n$ = .06272

$Q_{ds}$ = 439.4 kJ/mole

The value of the activation energy associated with the steady state relation (493.4 kJ/mole) is almost twice that obtained for the rate equation (247.5 kJ/mole). The large value of 493.4 kJ/mole is an artifact of the form of equation 4.3.11. If we cast this equation in the form:

$$s^* = \tilde{s}\left[\frac{\dot{\epsilon}^p}{A}\right]^n \exp\left(\frac{Q_{ds}}{R\theta}\right), \qquad 4.3.12$$

then we obtain a value of $Q_{ds}$ = 27.6 kJ/mole with no change to the values of the other two material parameters.

Figure 4.49 demonstrates the relationship between steady state stress and the steady state value of the internal variable for different values of strain rate and temperature. An interesting feature of this plot is the linear relation between state and stress which reaches from the power law into the power law breakdown regime. One interpretation of this result is that power law breakdown is a consequence of the kinetics of the deformation process (incorporated through the parameter $c$) and is not due to any change in the basic processes governing the evolution of state. As a result power law breakdown should be represented by the rate equation in the manner provided by equation 4.1.3.

The final form of the dynamic term of the evolution equation was finally fixed to be:

$$h(\theta, s, \tilde{\sigma}) = h_0 \left|\left(1 - \frac{s}{s^*}\right)\right|^a \dot{\epsilon}^p \operatorname{sgn}\left(1 - \frac{s}{s^*}\right), \qquad 4.3.13$$

where $|x|$ signifies the absolute value and $\operatorname{sgn}(x)$ is the sign function defined below. The absolute value and sign function are necessary to accomodate strain softening.

The introduction of the exponent $a$ couples the hardening and dynamic softening terms, making the term indeterminate when $s^*$ is less than $s$. Such a situation is certainly possible in hot working processes where the strain rate decreases or the temperature increases at a material point. Such a change may cause the current value of $s$ to be greater than the asymptotic value represented by $s^*$ calculated under the new conditions. The sign function is defined as:

$$\text{sgn}(x) = \begin{cases} 1 & x \geq 0 \\ -1 & x < 0 \end{cases}$$

Chapter 6 contains the results from strain rate decrement tests which indicate the necessity of this form.

## 4.4 Summary of Constitutive Model

Once the different material functions were determined, they were combined into the the constitutive equations summarized below.

The rate equation:

$$\dot{\bar{\epsilon}}^p = A \exp\left(-\frac{Q}{R\theta}\right) \left[\sinh\left(\xi\frac{\tilde{\sigma}}{s}\right)\right]^{1/m}. \qquad 4.3$$

The evolution equation for the internal variable:

$$\dot{s} = h_0 \left|\left(1 - \frac{s}{s^*}\right)\right|^a \dot{\bar{\epsilon}}^p \operatorname{sgn}\left(1 - \frac{s}{s^*}\right) - B\mu \exp\left(-\frac{Q_r}{R\theta}\right) \left(\frac{s}{\mu(\theta)}\right)^p, \qquad 4.4.2$$

where

$$s^* = \tilde{s}\left[\frac{\dot{\bar{\epsilon}}^p}{A}\exp\left(\frac{Q_{ds}}{R\theta}\right)\right]^n. \qquad 4.3.11$$

The following chapter details the procedures used to determine the model parameters from a set of appropriate experimental data. The list of model parameters are: $A, Q, m, \xi, h_0, a, \tilde{s}, Q_{ds}, n, B, Q_r$, and $p$. Also, $\mu(\theta)$ is the elastic shear modulus used purely for purposes of normalizing the value of $s$. Its temperature dependence is listed in Table 4.3.

TABLE 4.1

Iron - 2% Silicon Jump Test Data

| Test Number | Temperature (Celsius) | Initial Strain Rate ($sec^{-1}$) | Final Strain Rate ($scc^{-1}$) | Stress before jump (MPa) | Stress after jump (MPa) |
|---|---|---|---|---|---|
| 1 | 700. | 2.00E-4 | 2.00E-4 | 74.0 | 74.0 |
| 2 | 700. | 2.00E-4 | 2.02E-3 | 74.0 | 90.5 |
| 3 | 700. | 2.00E-4 | 9.42E-3 | 74.0 | 102.3 |
| 4 | 700. | 2.00E-4 | 8.66E-2 | 74.0 | 131.0 |
| 5 | 700. | 2.00E-4 | 8.99E-1 | 74.0 | 182.0 |
| 6 | 800. | 2.20E-4 | 2.20E-4 | 30.0 | 30.0 |
| 7 | 800. | 2.20E-4 | 2.11E-3 | 30.0 | 41.6 |
| 8 | 800. | 2.20E-4 | 1.02E-2 | 30.0 | 49.5 |
| 9 | 800. | 2.20E-4 | 9.35E-2 | 30.0 | 65.4 |
| 10 | 800. | 2.20E-4 | .953E-0 | 30.0 | 78.3 |
| 11 | 900. | 1.90E-4 | 1.90E-4 | 12.0 | 12.0 |
| 12 | 900. | 1.90E-4 | 2.07E-3 | 12.0 | 20.0 |
| 13 | 900. | 1.90E-4 | 1.97E-2 | 12.0 | 28.0 |
| 14 | 900. | 1.90E-4 | 1.01E-1 | 12.0 | 35.0 |
| 15 | 900. | 1.90E-4 | 1.11E-0 | 12.0 | 47.0 |
| 16 | 1000. | 2.35E-4 | 2.35E-4 | 7.0 | 7.0 |
| 17 | 1000. | 2.35E-4 | 2.00E-3 | 7.0 | 10.6 |
| 18 | 1000. | 2.35E-4 | 1.00E-2 | 7.0 | 15.5 |
| 19 | 1000. | 2.35E-4 | 8.79E-2 | 7.0 | 21.6 |
| 20 | 1000. | 2.35E-4 | .899E-0 | 7.0 | 28.4 |

TABLE 4.2

Iron - 2% Silicon

Isothermal, Constant True Strain Rate Tests

| Test ID | Temperature (Celsius) | Strain Rate ($sec^{-1}$) | $\sigma^*$ (MPa) |
|---|---|---|---|
| 8508132 | 700 | 1.0 | 229.97 |
| 8511291 | 750 | 1.0 | 180.85 |
| 8506191 | 800 | 1.0 | 131.38 |
| 8511281 | 800 | 1.0 | 138.25 |
| 8506201 | 800 | .1 | 93.73 |
| 8504132 | 800 | .1 | 91.36 |
| 8054011 | 800 | .01 | 68.85 |
| 8503311 | 798 | .001 | 46.16 |
| 8511292 | 850 | 1.0 | 108.44 |
| 8504012 | 850 | .01 | 49.63 |
| 8506141 | 900 | 1.0 | 84.38 |
| 8502071 | 900 | .1 | 55.29 |
| 8501231 | 900 | .01 | 34.77 |
| 8504131 | 899 | .01 | 36.60 |
| 8501221 | 900 | .001 | 21.11 |
| 8412151 | 950 | .01 | 25.18 |
| 8511261 | 1000 | 1.0 | 57.57 |
| 8511301 | 1000 | 1.0 | 53.96 |
| 8503011 | 1000 | .316 | 44.71 |
| 8501081 | 1000 | .1 | 32.57 |
| 8502051 | 1000 | .0316 | 26.78 |
| 8501241 | 1000 | .01 | 19.77 |
| 8502061 | 1000 | .00316 | 15.76 |
| 8501121 | 1000 | .001 | 10.75 |
| 8511271 | 1100 | .502 | 34.11 |
| 8504041 | 1100 | .316 | 27.99 |
| 8504061 | 1100 | .316 | 28.12 |
| 8502081 | 1100 | .1 | 21.33 |
| 8504021 | 1100 | .01 | 12.24 |
| 8504121 | 1098 | .001 | 6.63 |
| 8508131 | 1200 | 1.0 | 25.66 |
| 8508091 | 1200 | .1 | 14.72 |

TABLE 4.3

Elastic Constants for Fe - 2% Si

| Temperature (Celsius) | $\mu$ (GPa) | E (GPa) | $\nu$ |
|---|---|---|---|
| 700 | 57 | 150 | .32 |
| 800 | 50 | 135 | .35 |
| 900 | 42 | 115 | .38 |
| 1000 | 37 | 105 | .41 |
| 1100 | 32 | 93 | .44 |
| 1200 | 30 | 87 | .47 |

Source: ASM Handbook, Volume 1, pg 641.

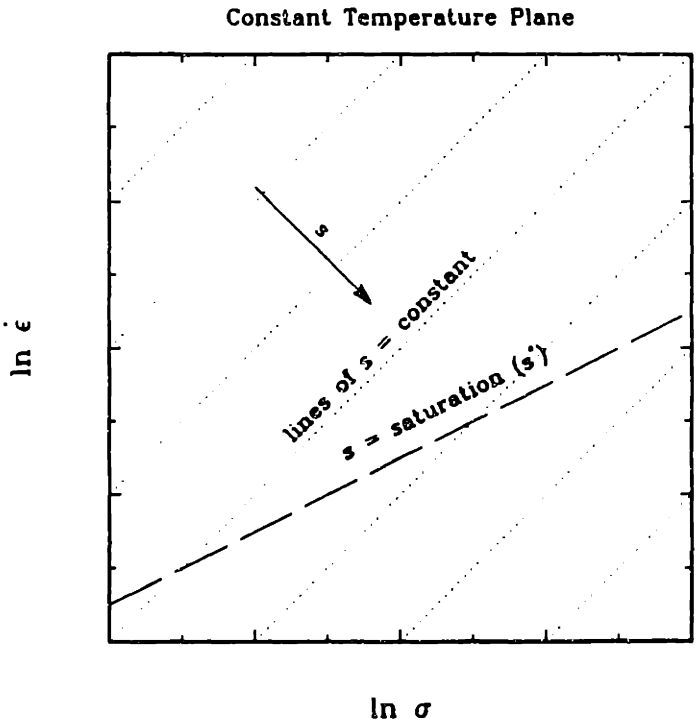


**Figure 4.1** *Lines of constant internal variable resulting from specification of values of stress, strain rate, and temperature (Lines are straight only for illustration.)*

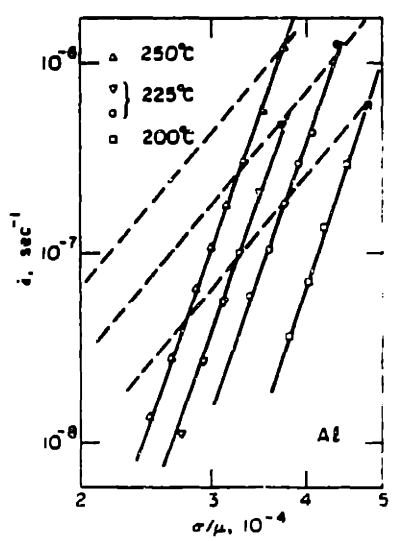


Stress dependence of the initial creep rate after various amounts of stress reduction at steady-state creep of Al. Solid marks indicate initial states. Dashed lines are the stress dependence of $\epsilon_s$ for each temperature (from [154]).

**Figure 4.2a** Constant structure data for aluminum.
*Reference [Mitra and McLean, 1967]*

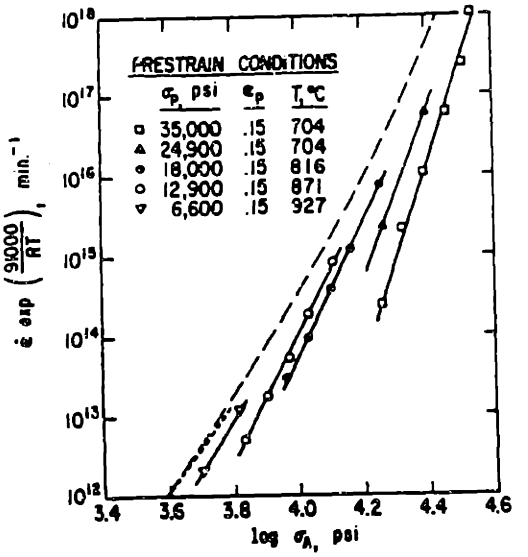


—Dependence of temperature-compensated creep rate on applied stress for specimens with different structures and internal stresses. Dashed and dotted curves—temperature compensated creep rate vs effective stress determined by two methods.

Figure 4.2b Constant structure data for 304 stainless. Reference [Cuddy, 1970]

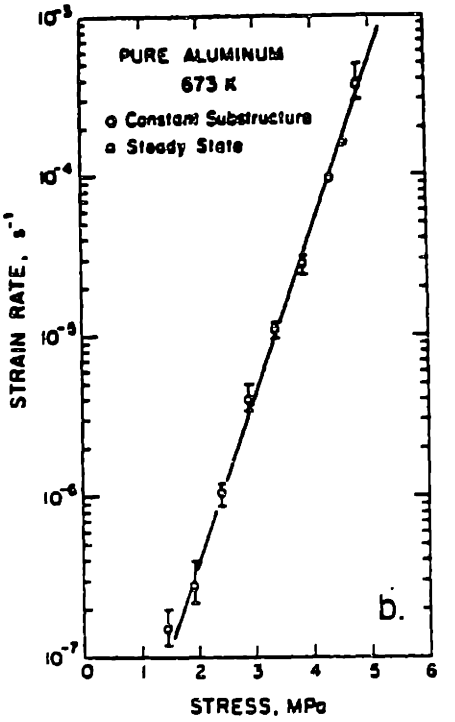


Figure 4.2c Constant structure data for aluminum. Reference [Gibeling and Nix, 1982]

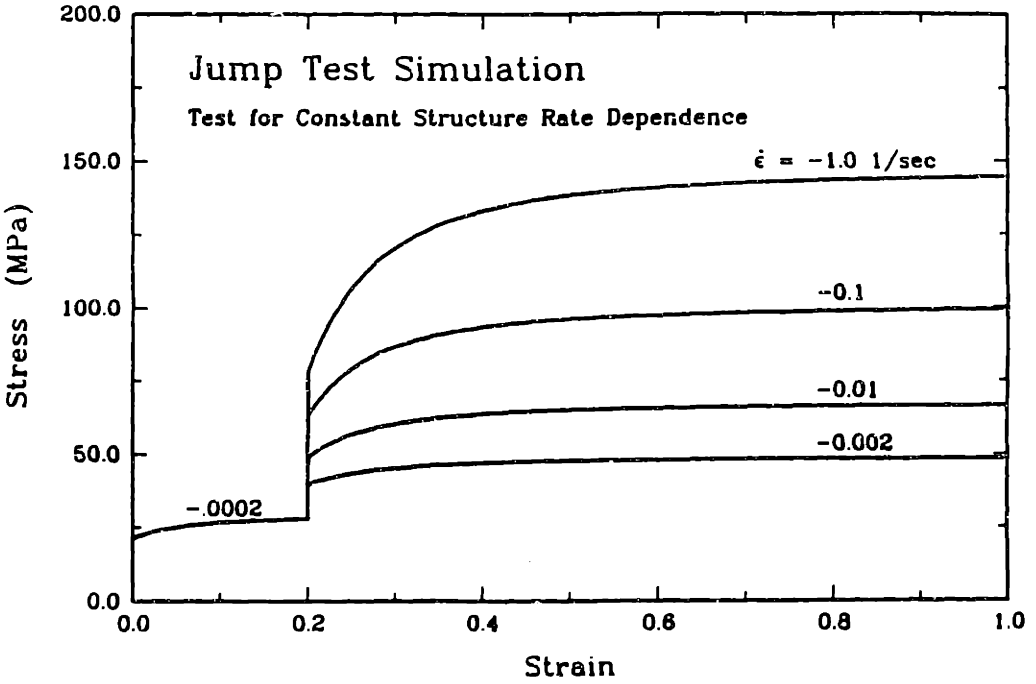


Figure 4.3 Schematic of series of strain rate jump tests where jumps occur at the same initial state.

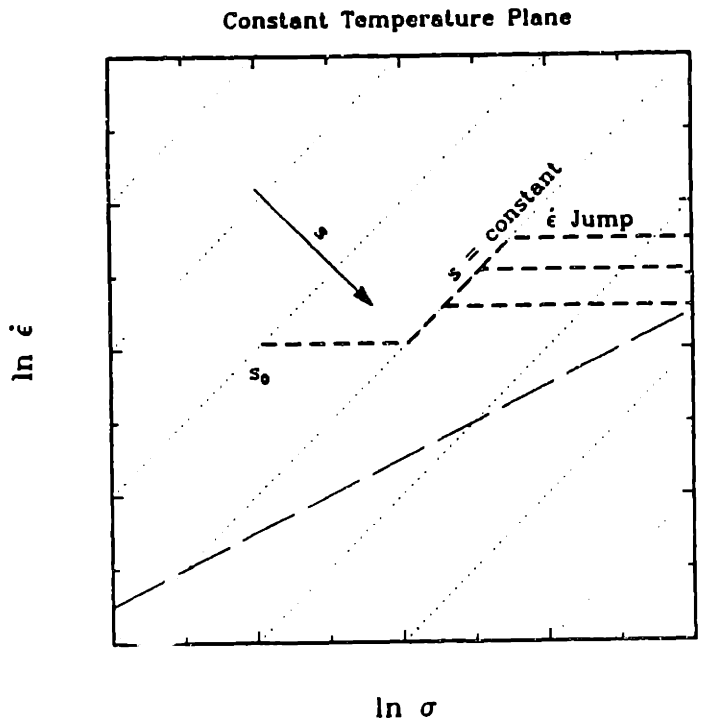


Figure 4.4 Constant state, strain rate jump tests illustrated in strain rate, stress and temperature space

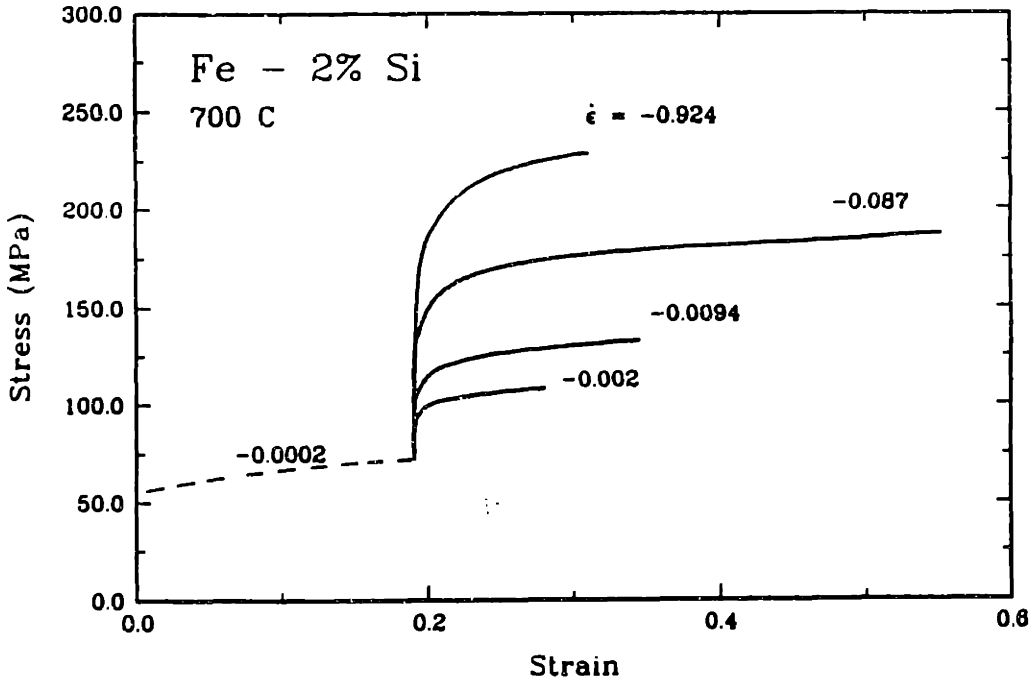


Figure 4.5 Strain rate jump tests with Fe – 2% Si to determine constant structure rate dependence.

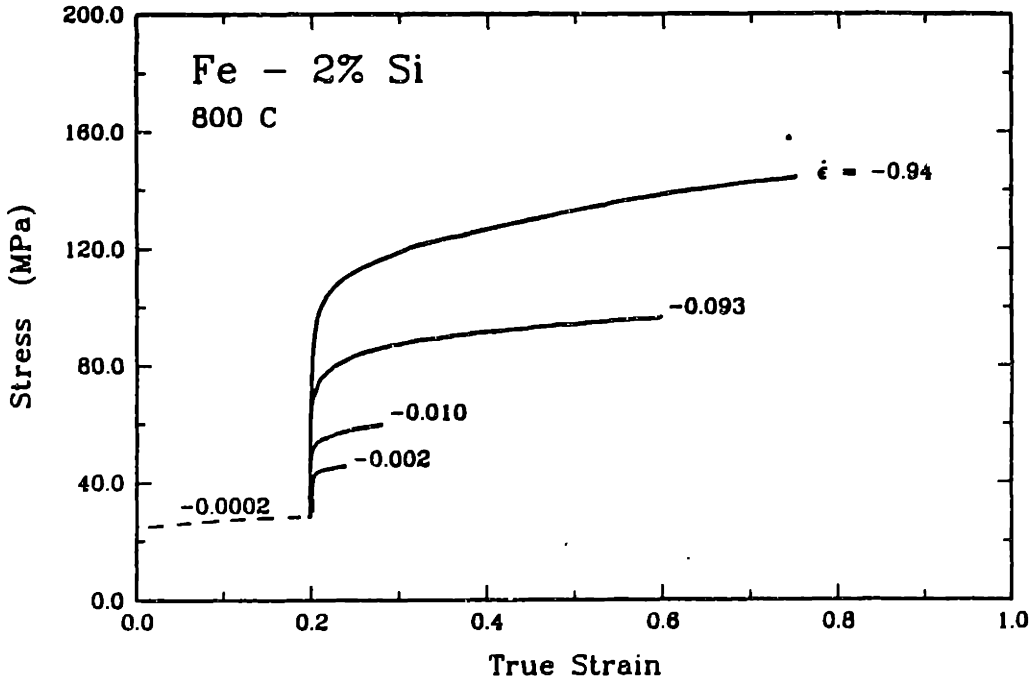


Figure 4.6 Strain rate jump tests with Fe – 2% Si to determine constant structure rate dependence.

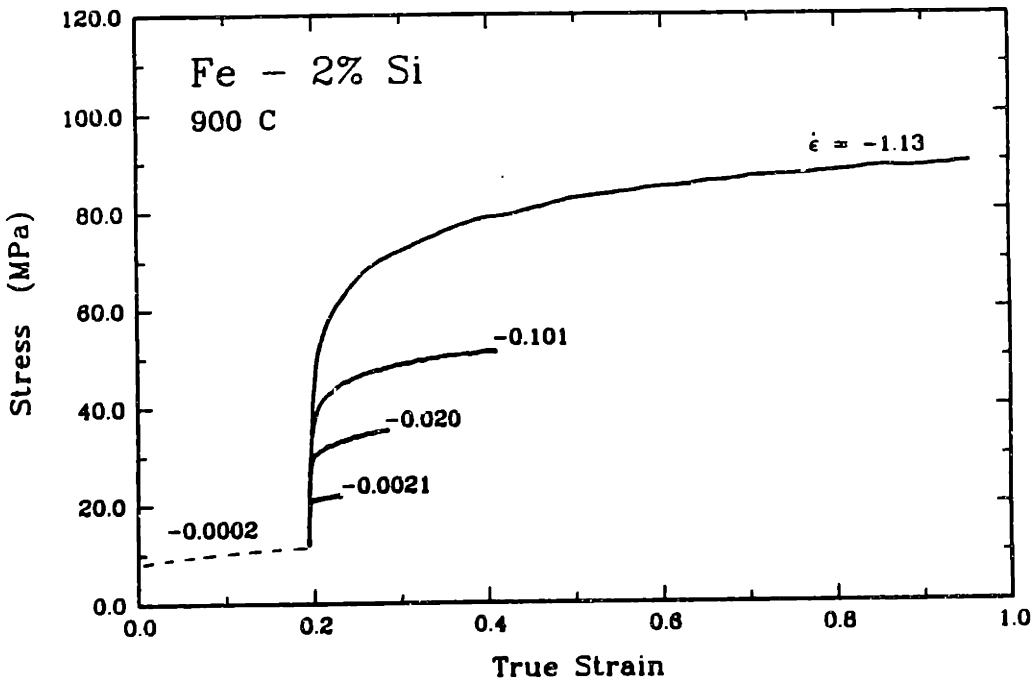


Figure 4.7 Strain rate jump tests with Fe – 2% Si to determine constant structure strain rate dependence.

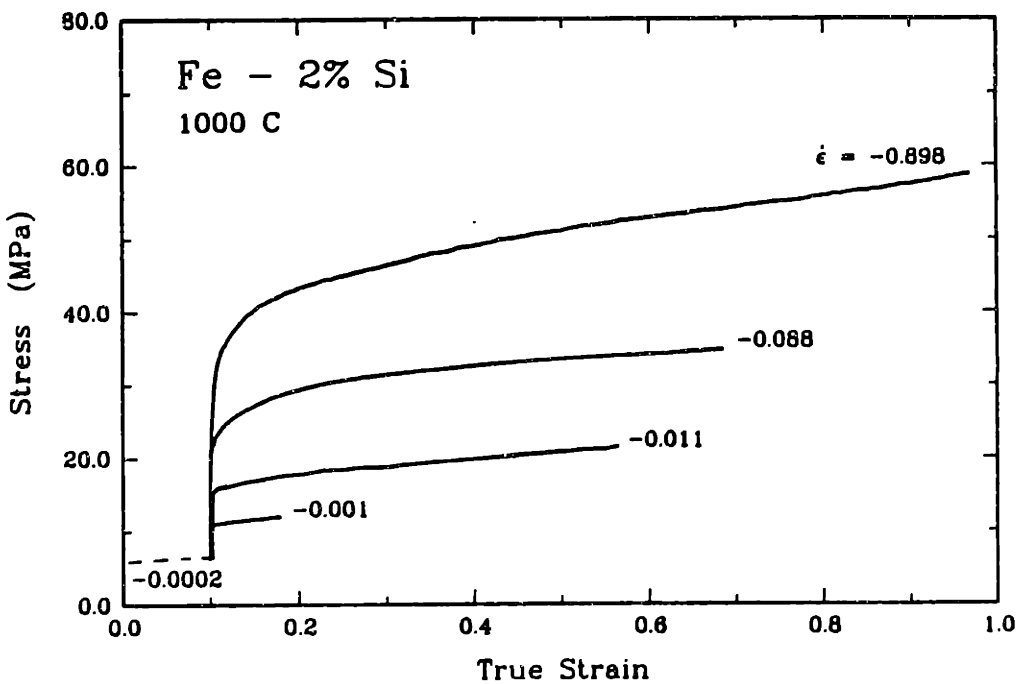


Figure 4.8 Strain rate jump tests with Fe – 2% Si to determine constant structure strain rate dependence

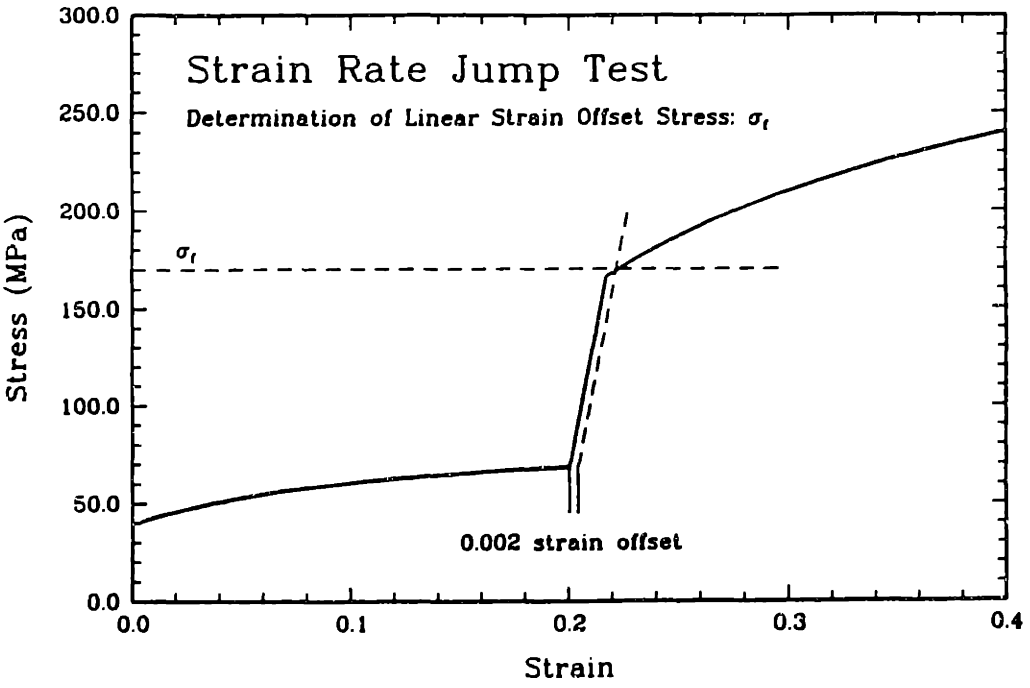


Figure 4.9 Schematic of strain rate jump test indicating 0.002 linear strain offset stress, $\sigma_f$.

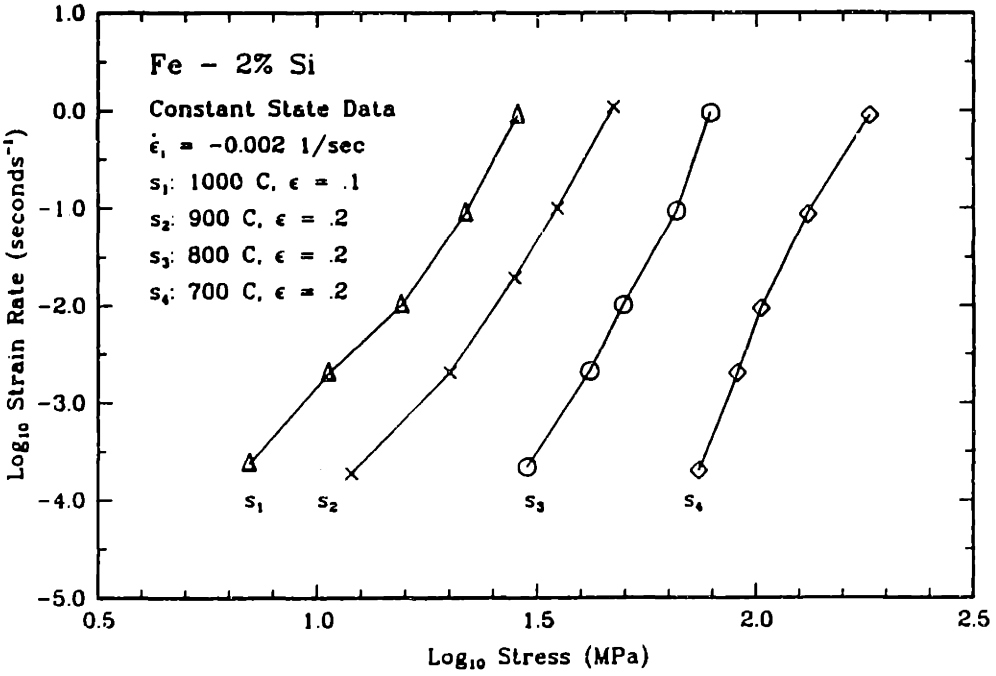


Figure 4.10 Stress/strain rate dependence of Fe - 2% Si at different constant states ($s_i$), determined from strain rate jump tests.

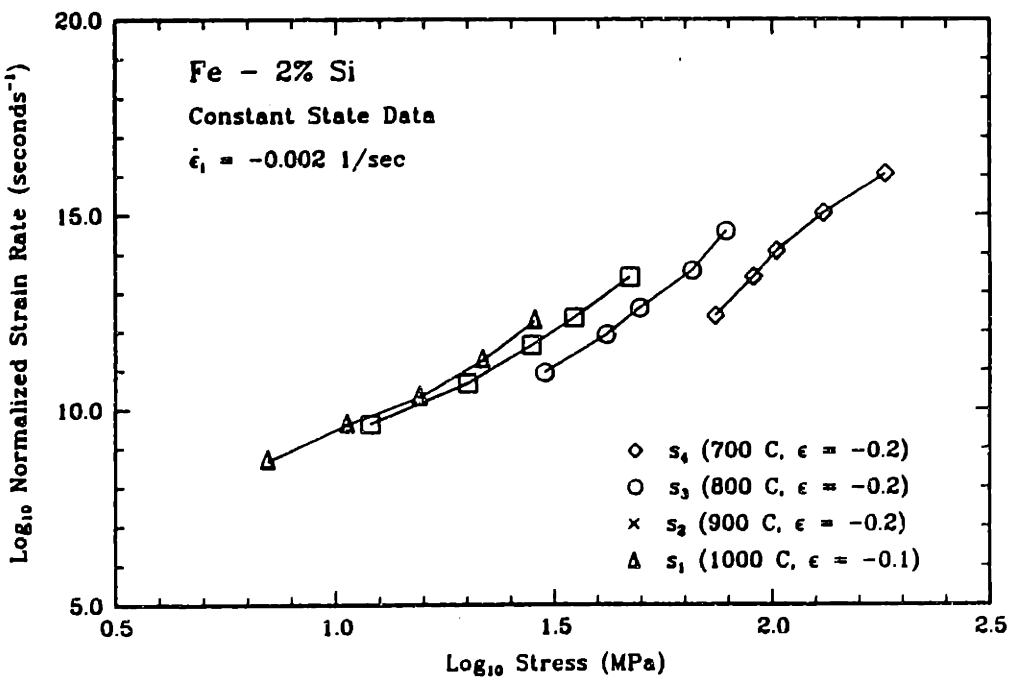


Figure 4.12 Stress/strain rate dependence of Fe – 2% Si at different constant states ($s_i$). The strain rate has been normalized by an Arrhenius term with constant activation energy of 251 kJ/mole.

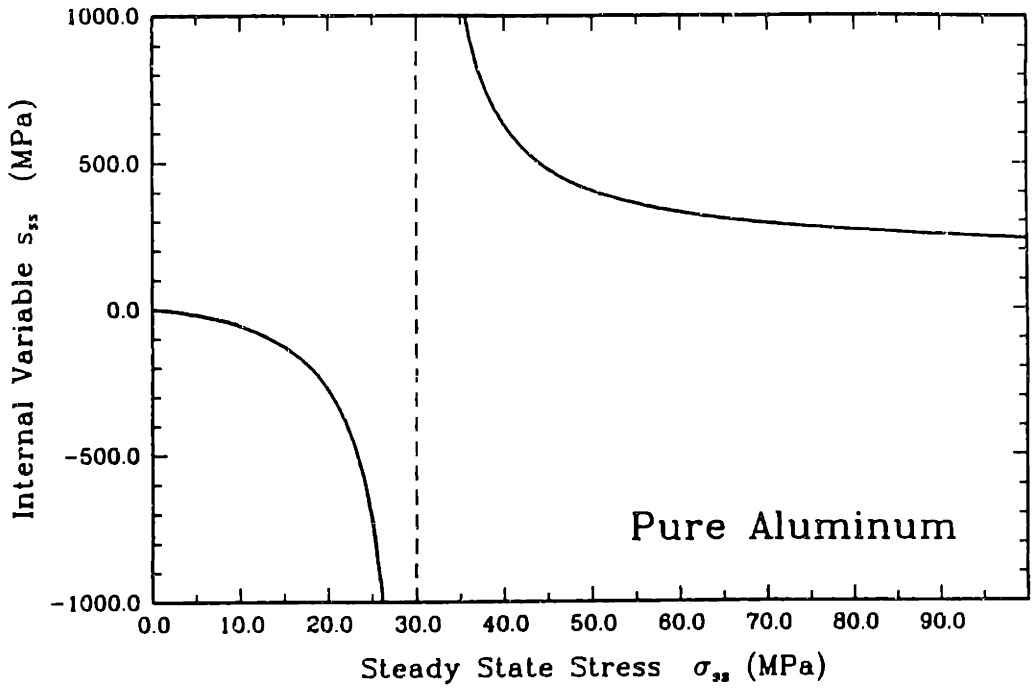


Figure 4.13 Relationship between steady state stress and the internal variable resulting from use of equation 4.1.1 as the rate equation.

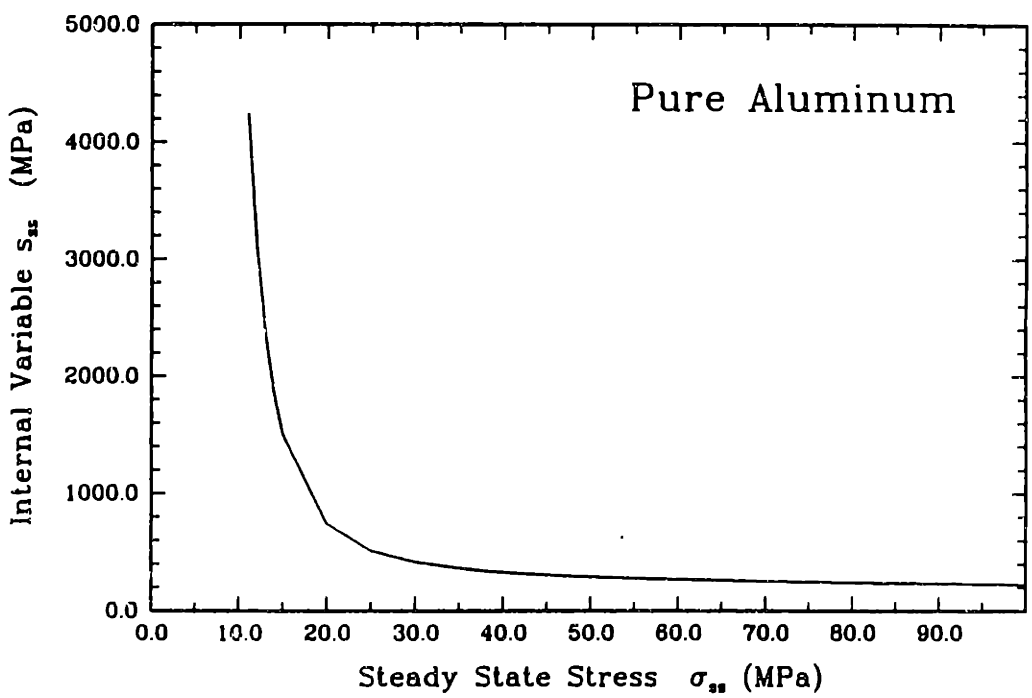


Figure 4.14 Relationship between steady state stress and the internal variable resulting from use of equation 4.1.2 as the rate equation.

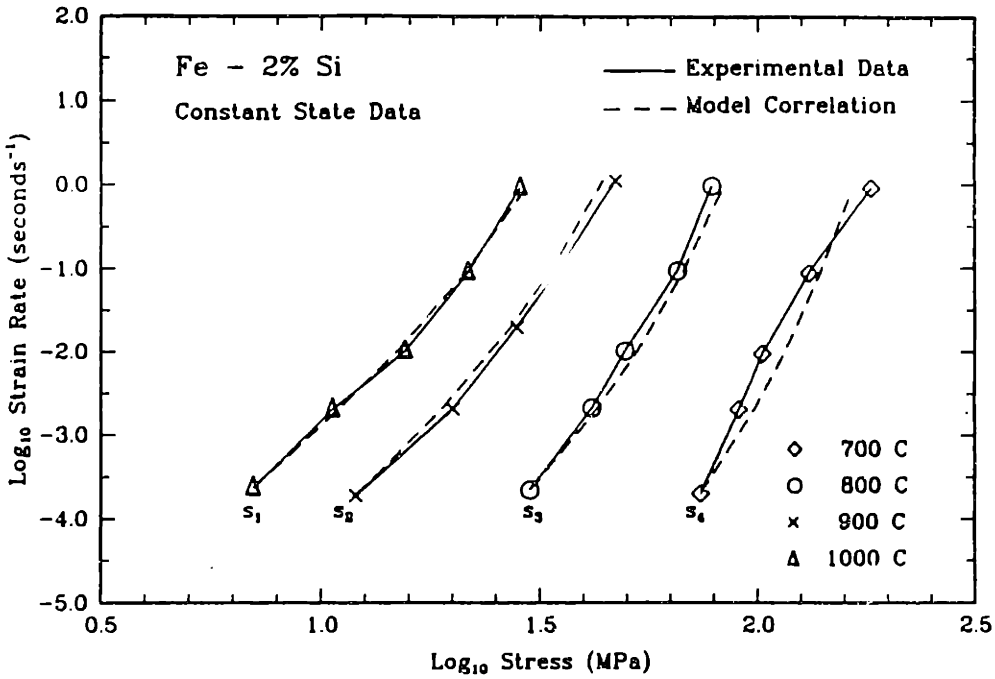


Figure 4.15 Correspondance between constant state data and fit of equation 4.1.3 to the same data.

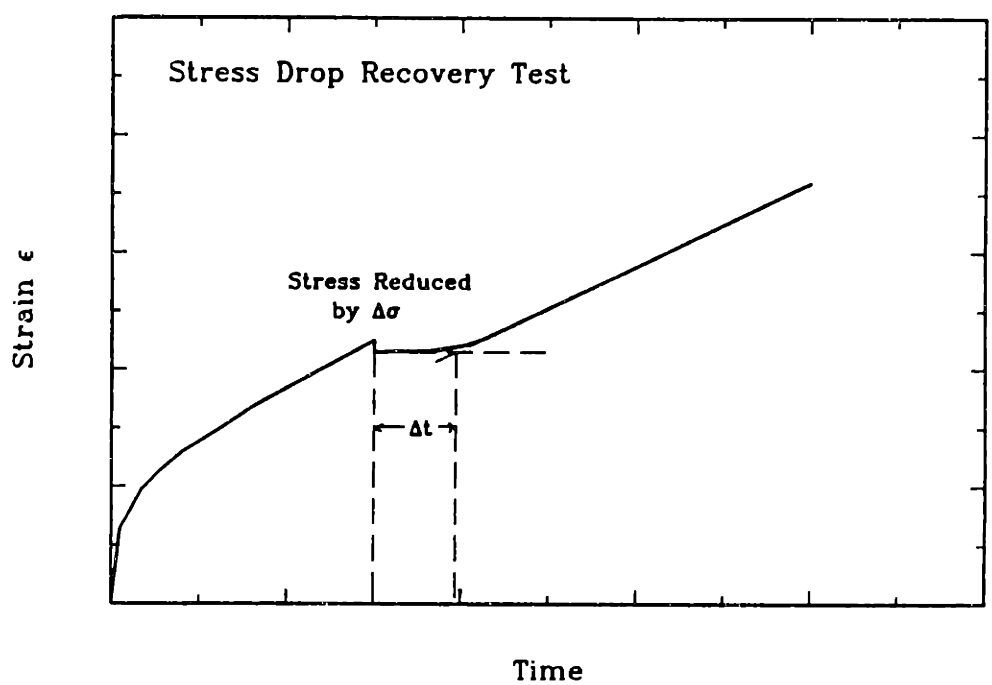


Figure 4.16 Schematic stress drop test illustrating parameters used by Mitra and McLean [1966] to evaluate recovery rate.

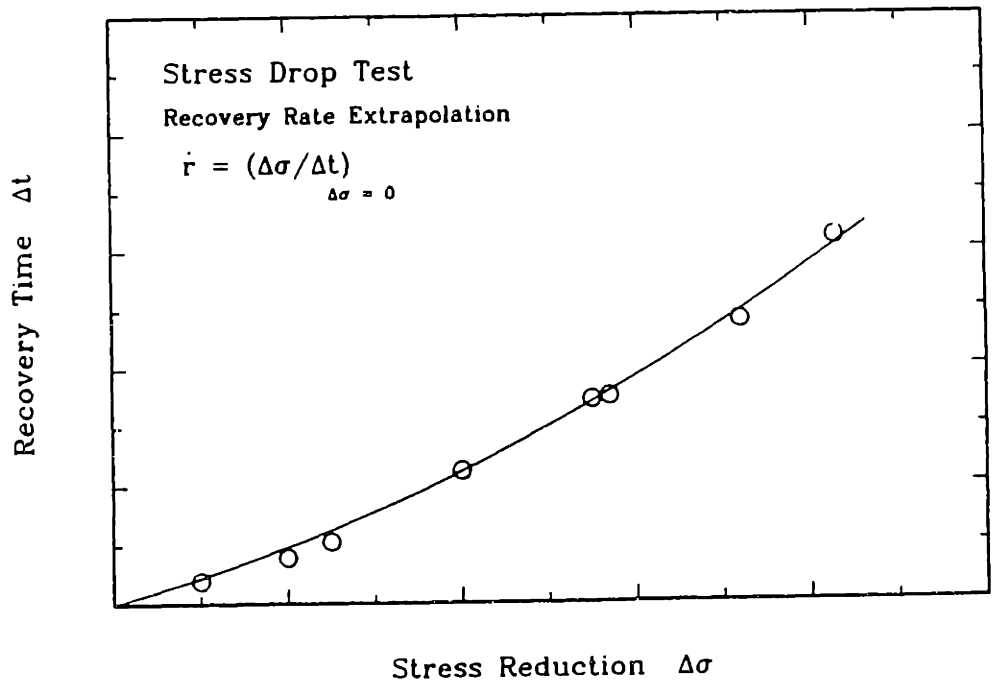


Figure 4.17 Illustration of back extrapolation of stress drop test to determine static recovery rate. Points indicated are for illustration only; they do not represent actual data.

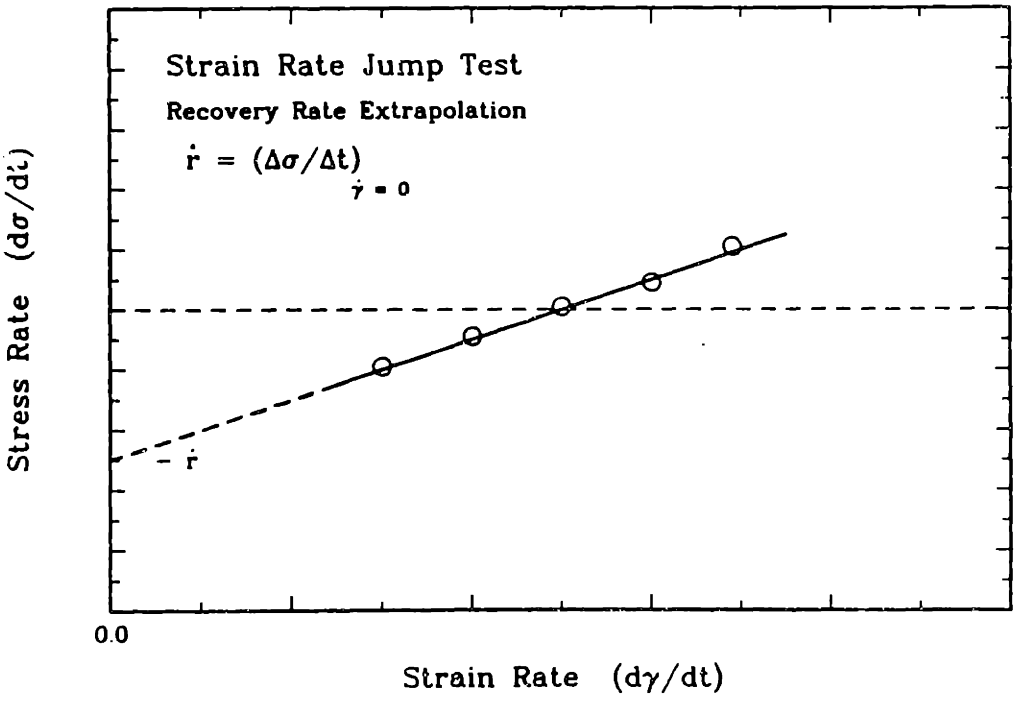


Figure 4.18 Illustration of static recovery rate measurement via back extrapolation of strain rate jump data. Proposed by Kocks [1977]. Points are for illustration only and do not represent test data.

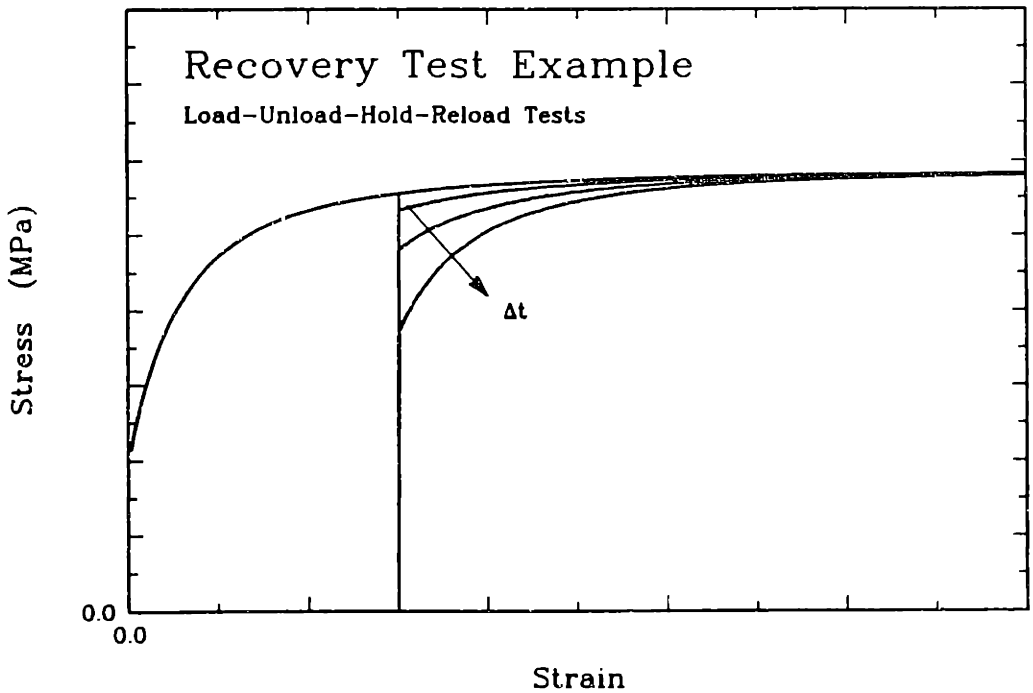


Figure 4.19 Schematic of load–unload–hold–reload test series used to evaluate rate of static recovery. Curves do not represent actual test data.

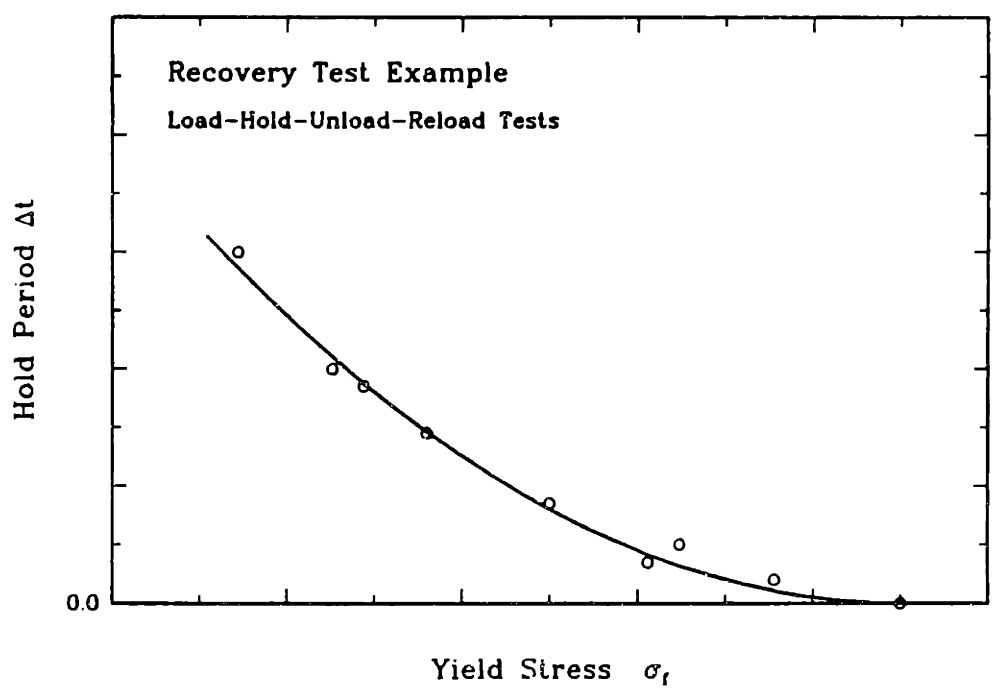


Figure 4.20 Hold period versus stress obtained immediately after reloading from hold period. Each point represents one hold period. Points are for illustration only and do not represent real data.

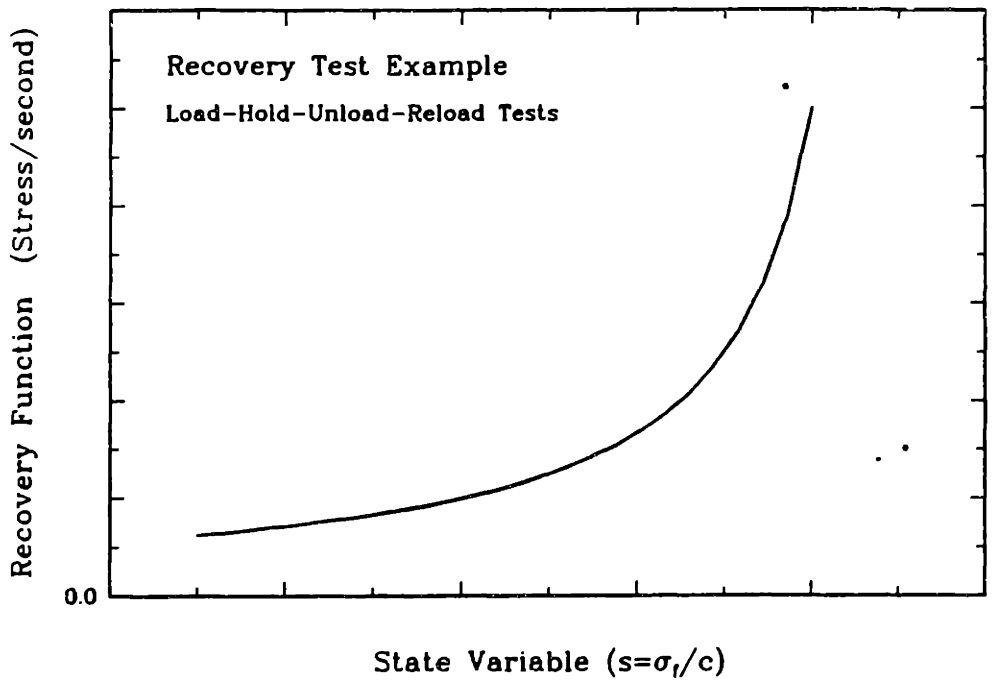


Figure 4.21 Schematic of load-unload-hold-reload data treated in manner suggested by equation 4.2.11. Curve is for illustration only; it does not represent actual test data.

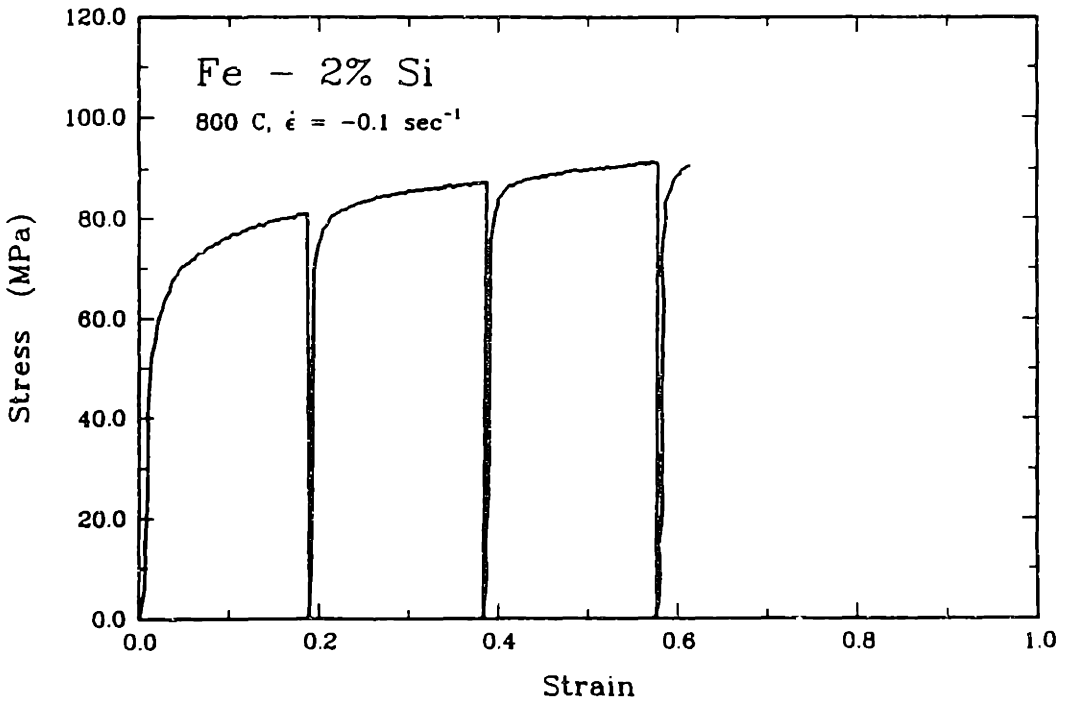


Figure 4.22 Multiple hold test data of Fe – 2% Si. Tests performed at 800 Celsius with 0.1 $sec^{-1}$ constant true strain rate. Duration of each hold period was 20 seconds.

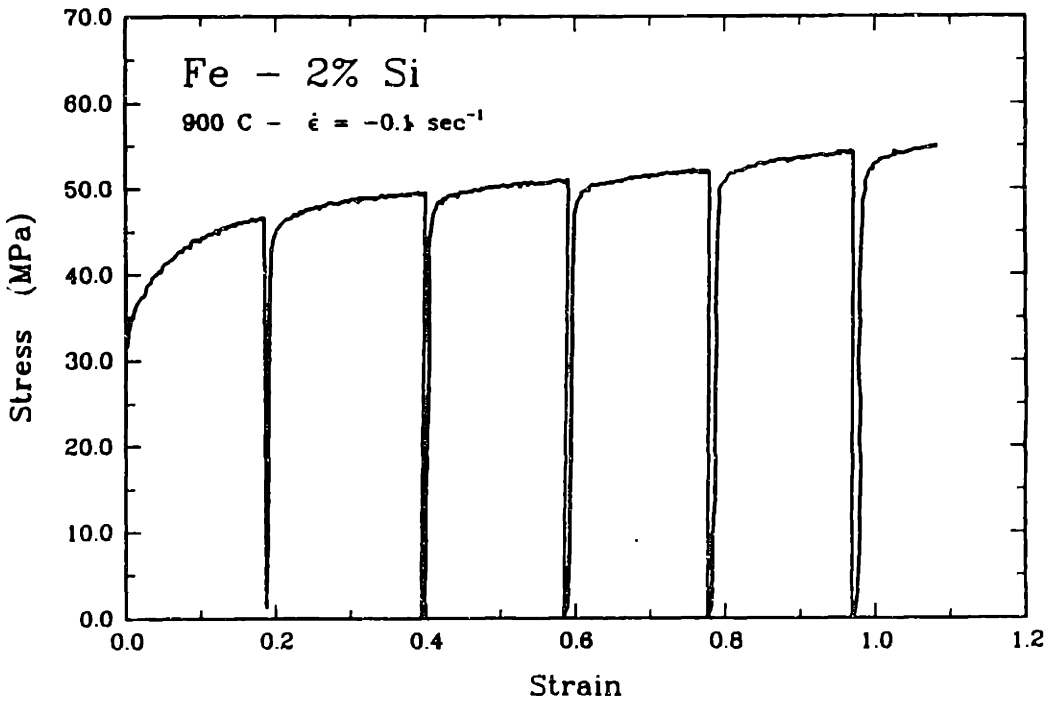


Figure 4.23 Multiple hold test data for Fe – 2% Si. Test performed at 900 Celsius with 0.1 $sec^{-1}$ constant true strain rate. Duration of each hold period was 20 seconds.

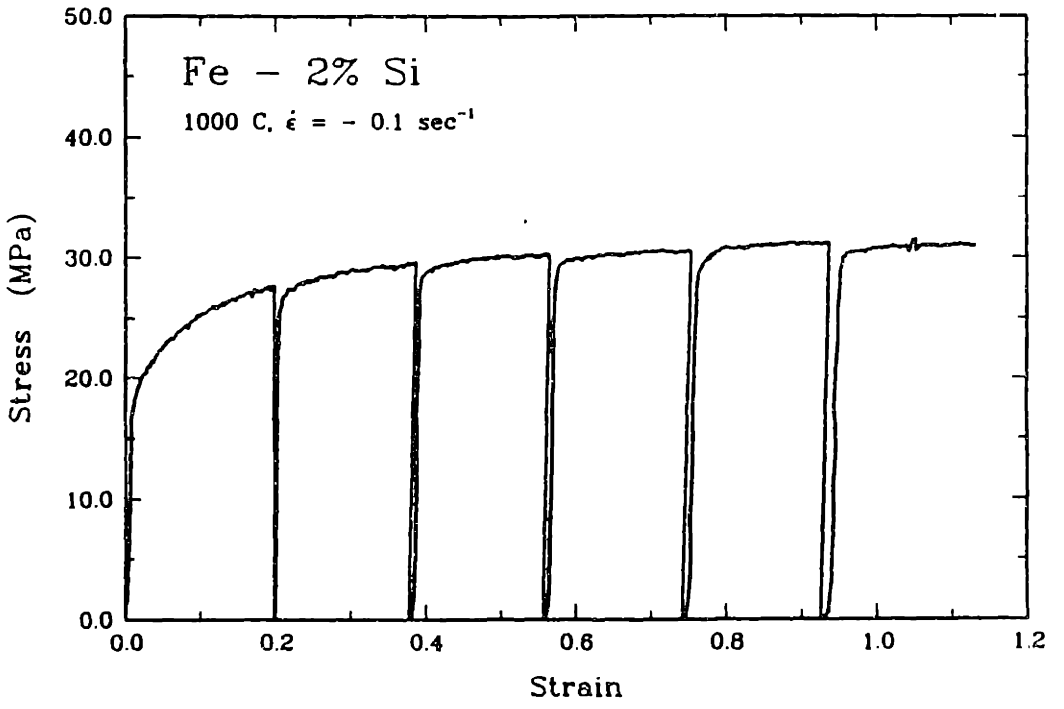


Figure 4.24 Multiple hold test data for Fe – 2% Si. Test performed at 1000 Celsius and 0.1 sec$^{-1}$ constant true strain rate. Duration of each hold period was 20 seconds.

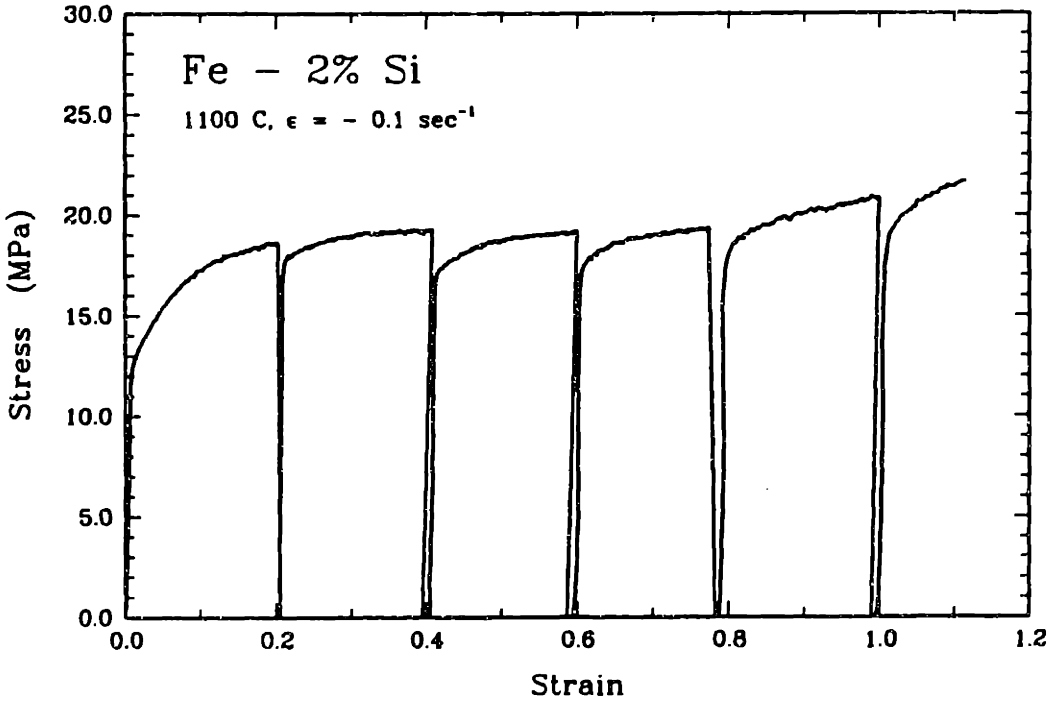


Figure 4.25 Multiple hold test data for Fe – 2% Si. Test performed at 1100 Celsius and 0.1 sec$^{-1}$ constant true strain rate. Duration of each hold period was 20 seconds.

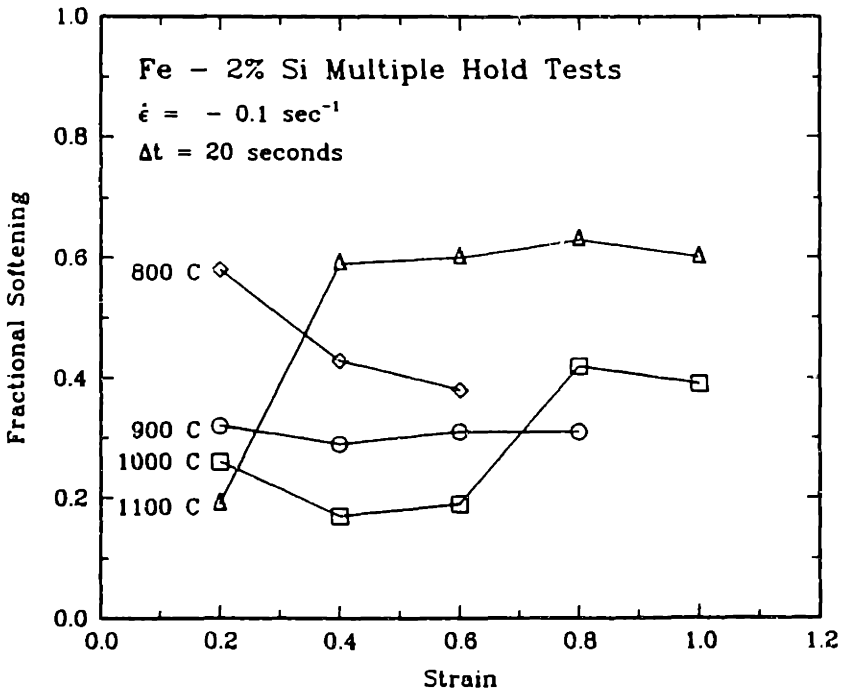


Figure 4.26 Fractional softening as a function of strain, determined from multiple hold tests on Fe – 2% Si.

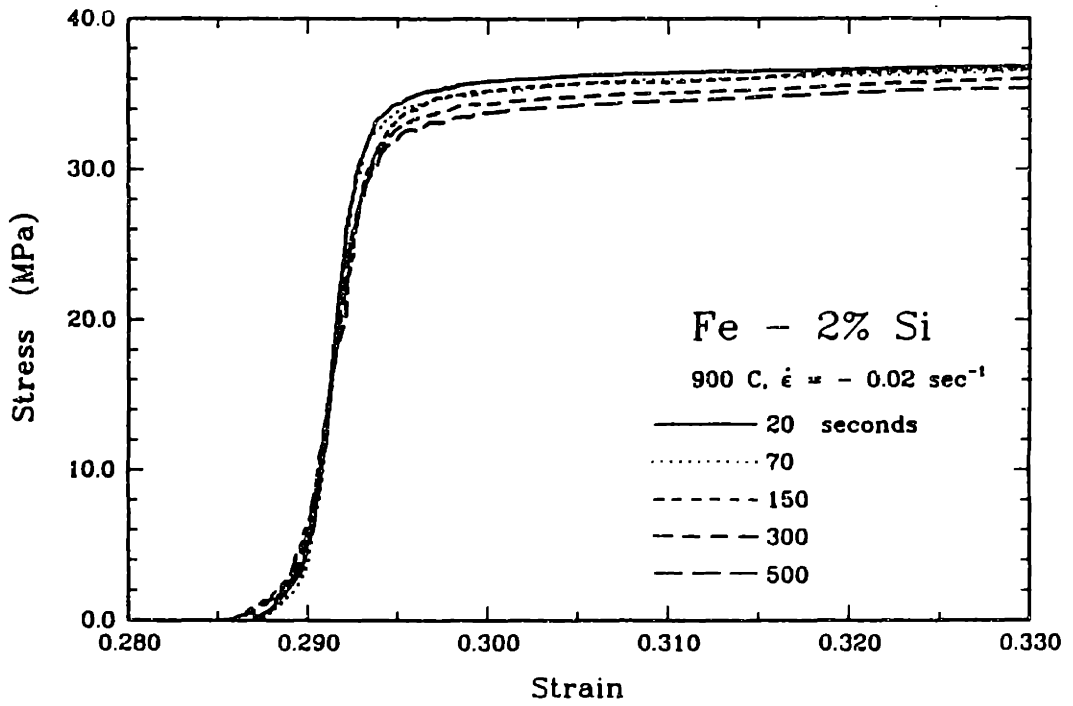


Figure 4.27 Load–unload–hold–reload tests on Fe – 2% Si. Data represents reload segment. Data has been shifted horizontally to superimpose elastic slopes.

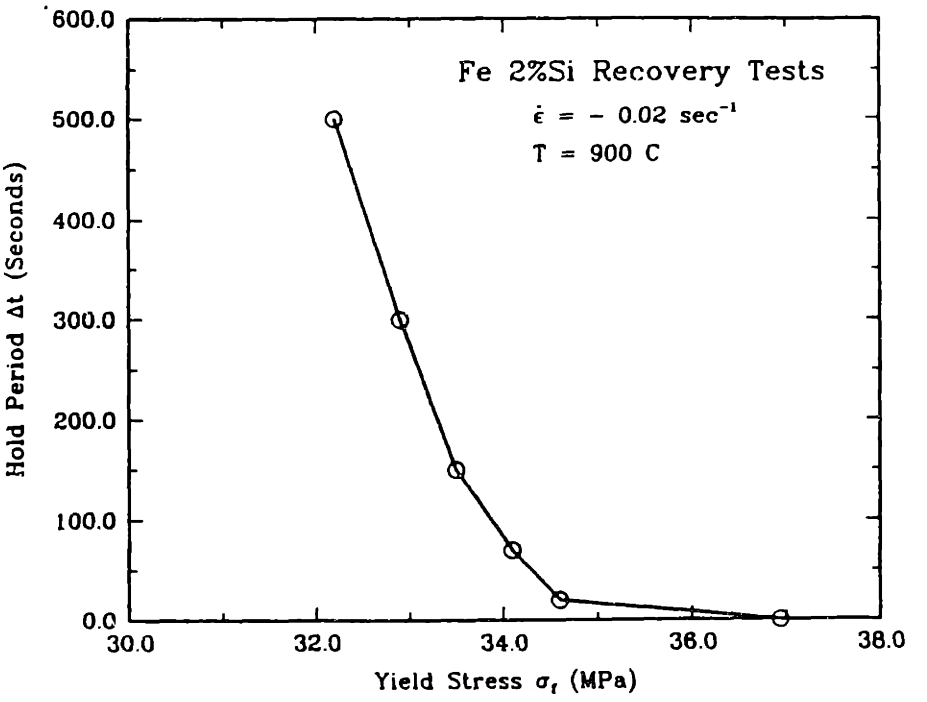


Figure 4.28 Hold period versus stress upon reloading for Fe - 2% Si. Tests performed at 900 degrees Celsius and at 0.02 sec$^{-1}$ constant true strain rate.

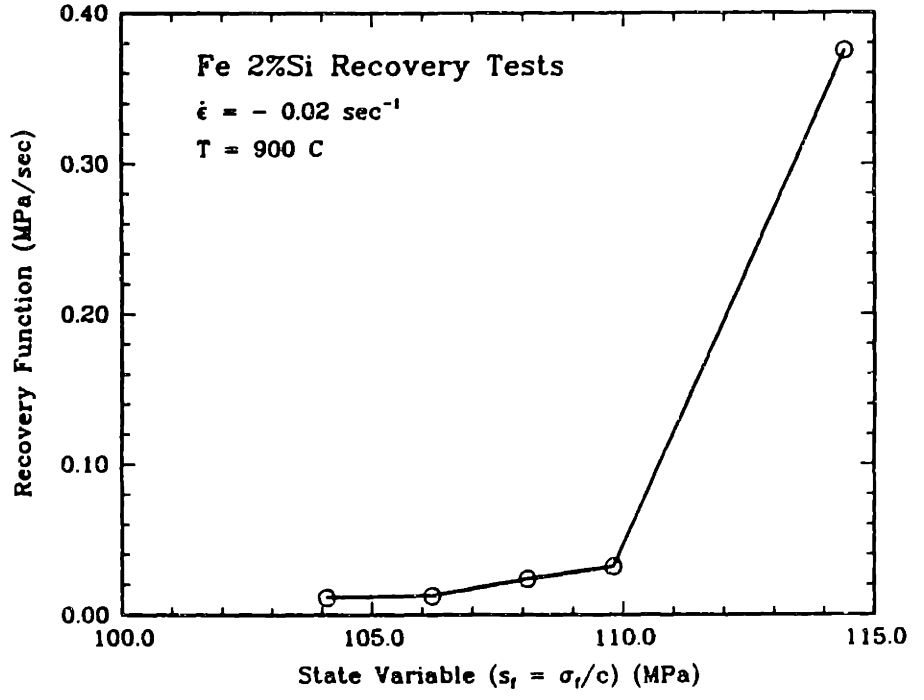


Figure 4.29 Recovery function dependence on state for Fe - 2% Si. Data obtained from Figure 4.28 according to equation 4.2.11.

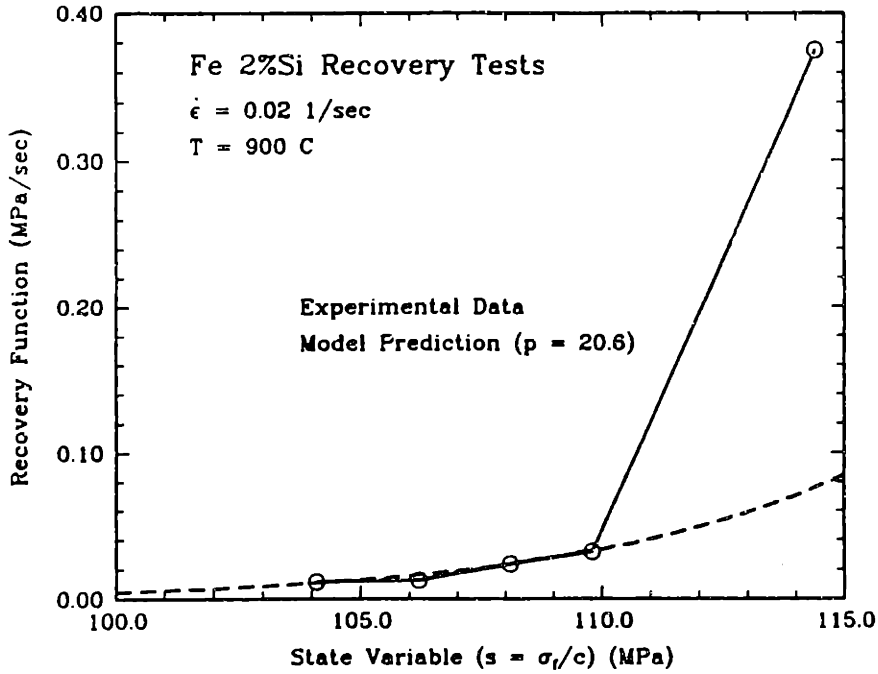


Figure 4.30 Fit of power law static recovery function to Fe – 2% Si recovery test data.

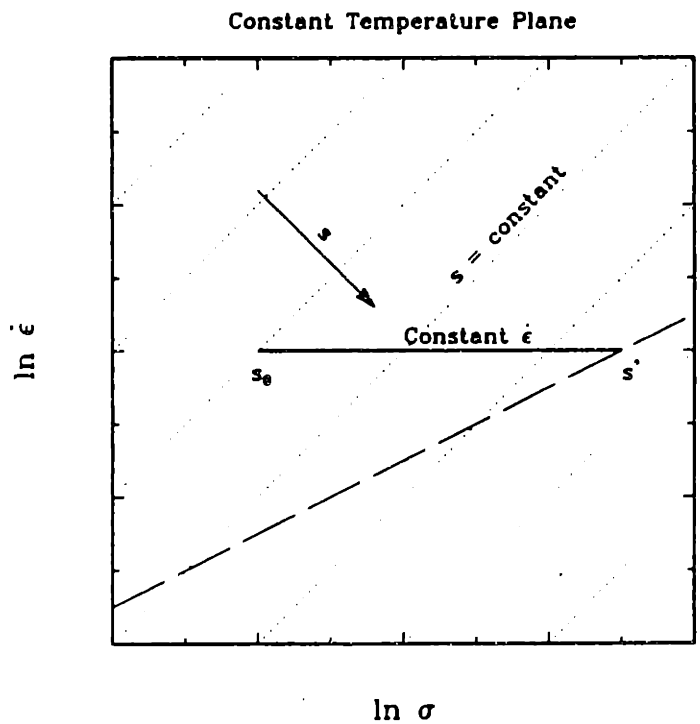


Figure 4.31 Schematic of isothermal, constant true strain test in stress, temperature, strain rate space. Material begins at state $s_0$ and reaches steady state value of $s^*$.

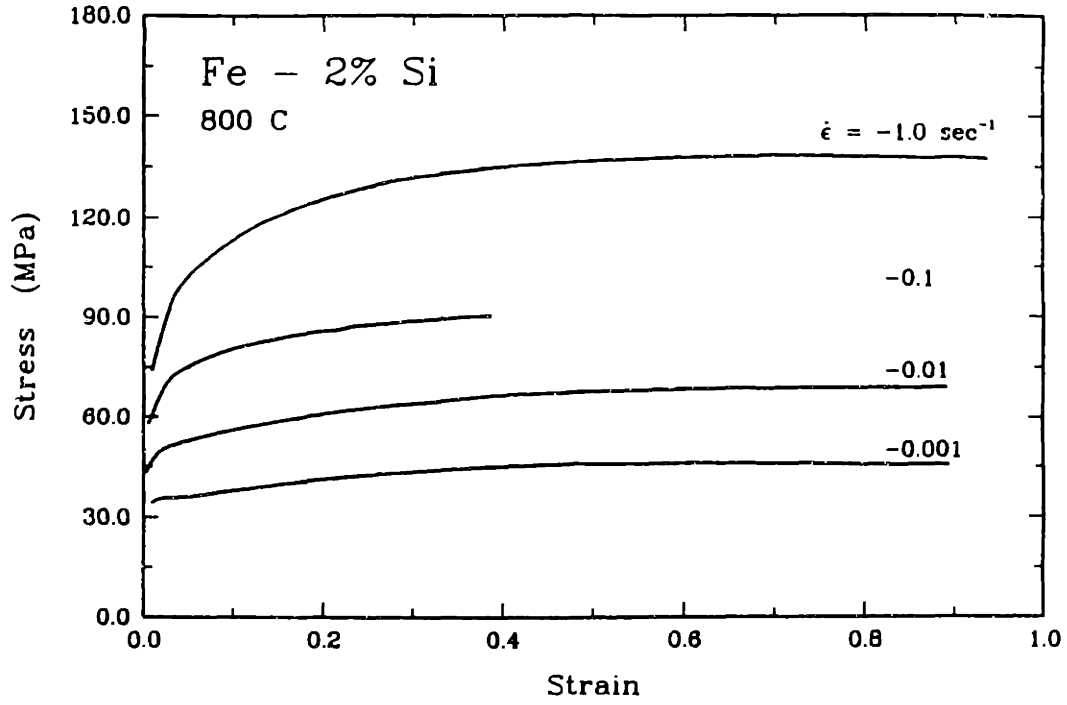


Figure 4.32 Isothermal, constant true strain rate tests on Fe – 2% Si at 800 degrees Celsius and different strain rates.

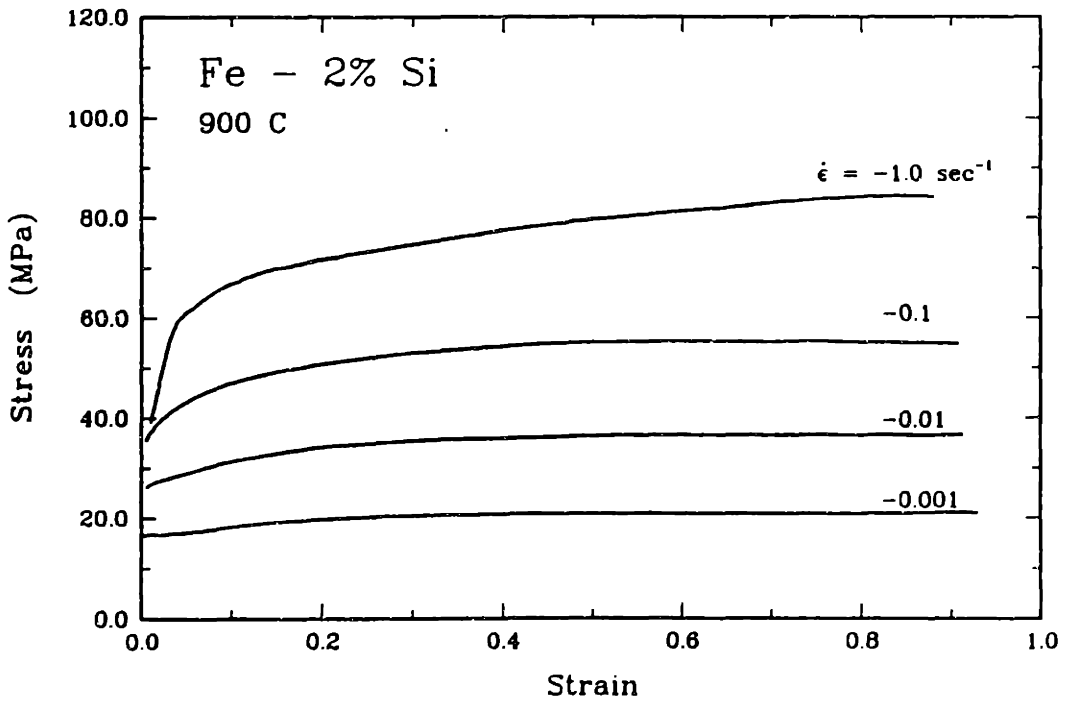


Figure 4.33 Isothermal, constant true strain rate tests on Fe – 2% Si at 900 degrees Celsius and different strain rate.

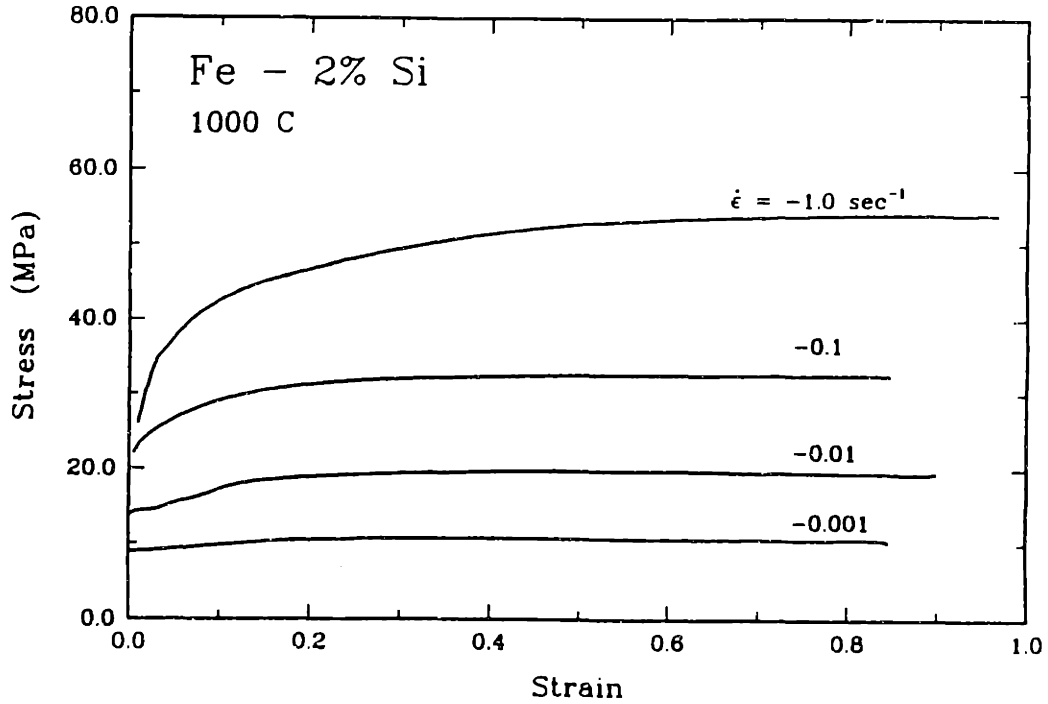


**Figure 4.34** Isothermal, constant true strain rate tests on Fe – 2% Si at 1000 degrees Celsius and different strain rates.

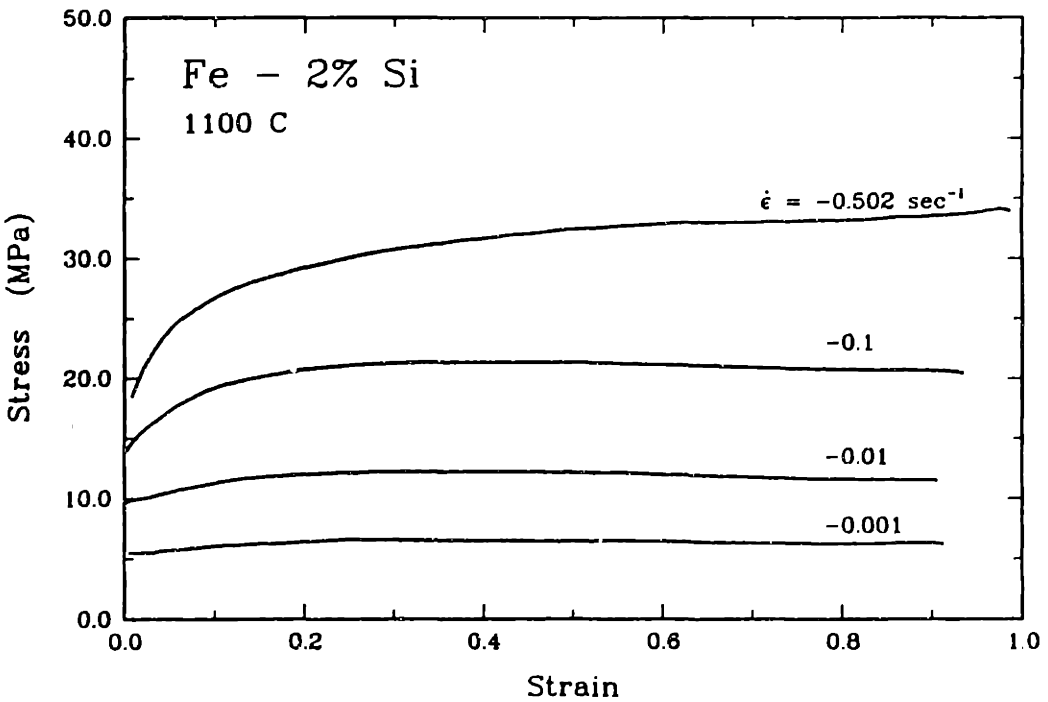


**Figure 4.35** Isothermal, constant true strain rate tests on Fe – 2% Si at 1100 Celsius and different strain rates.

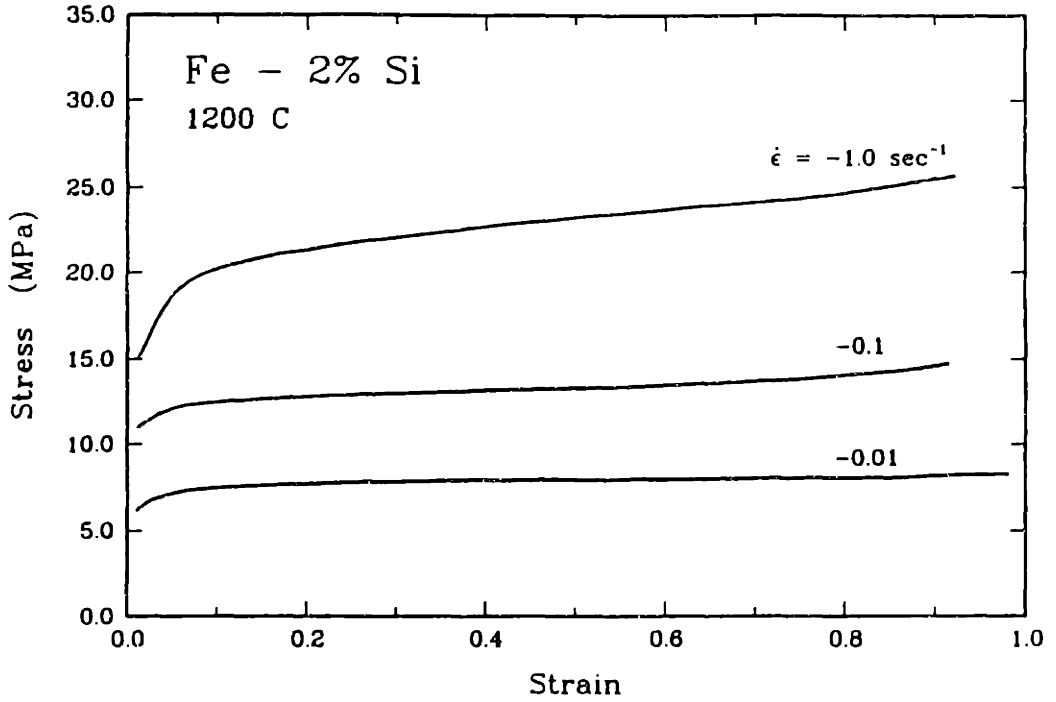


**Figure 4.36** Isothermal, constant true strain rate tests on Fe – 2% Si at 1200 degrees Celsius and different strain rates.

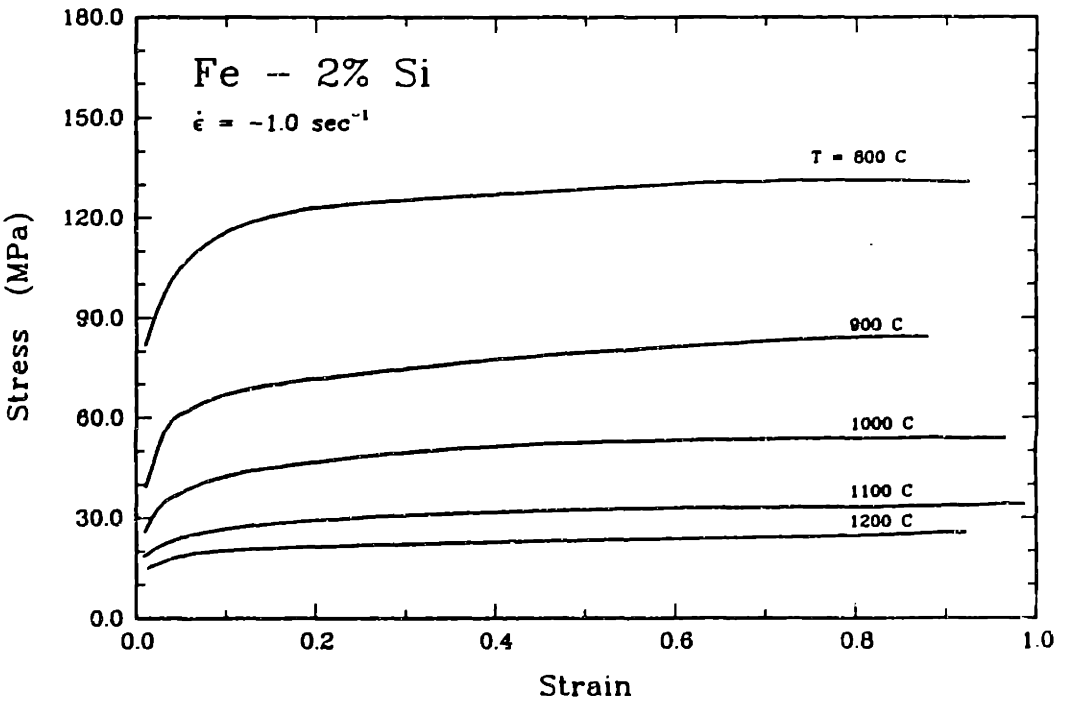


**Figure 4.37** Isothermal, constant true strain rate tests on Fe – 2% Si with strain rate of −1.0 sec$^{-1}$ and at different temperatures.

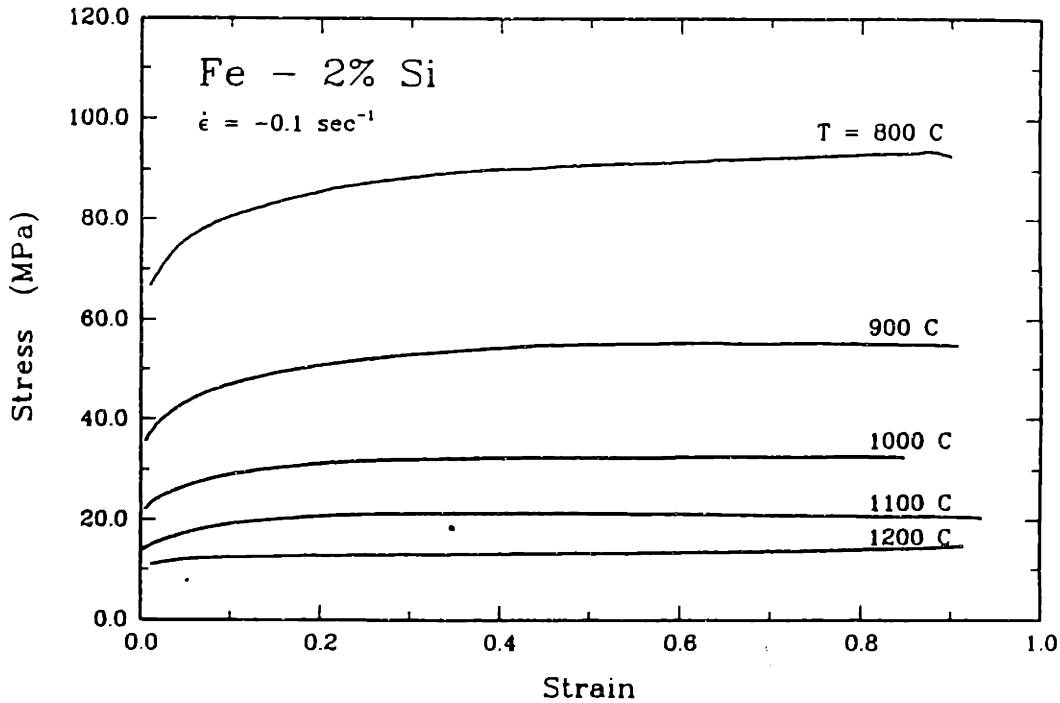


Figure 4.38 Isothermal, constant true strain rate tests on Fe – 2% Si with strain rate of -0.1 sec$^{-1}$ and at different temperatures.

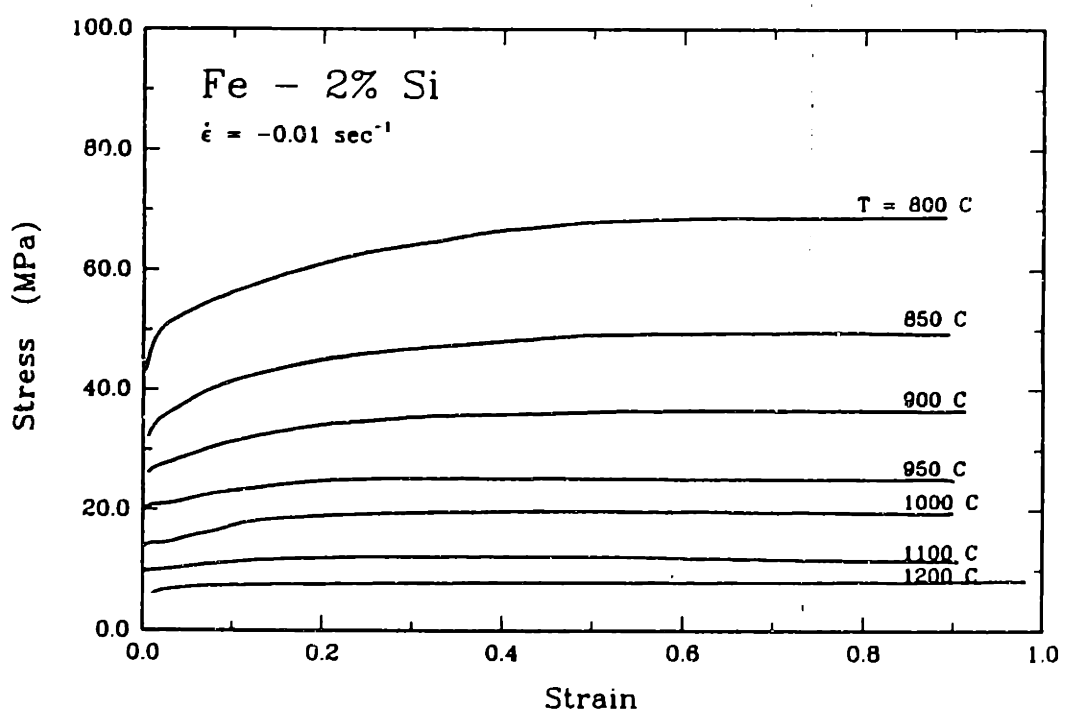


Figure 4.39 Isothermal, constant true strain rate tests on Fe – 2% Si with strain rate of -0.01 sec$^{-1}$ and at different temperatures.

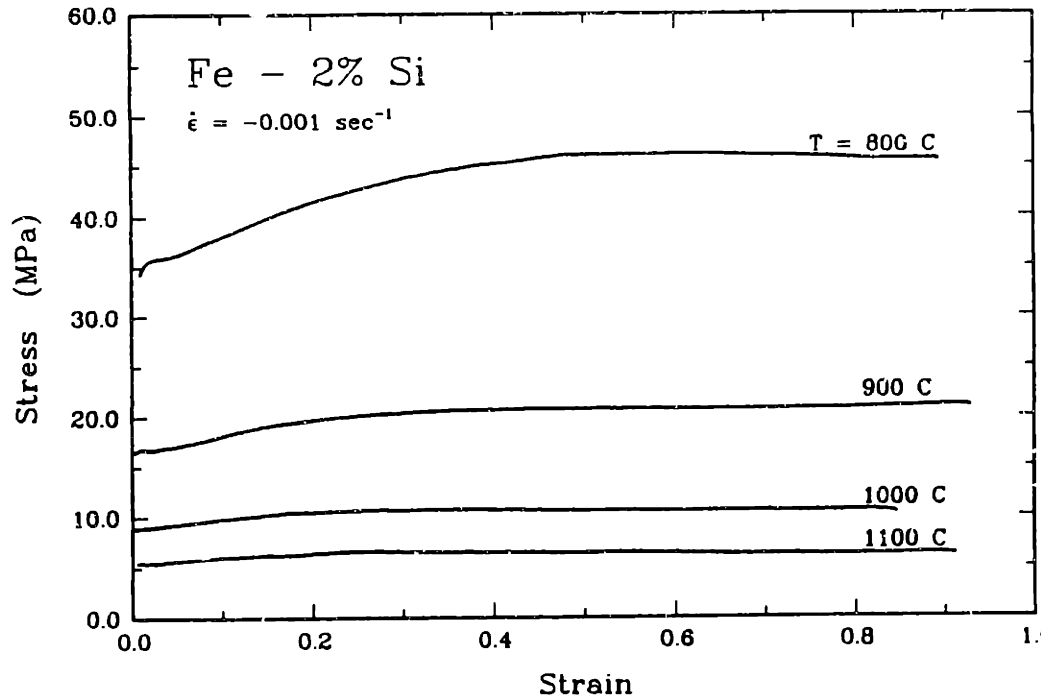


**Figure 4.40** Isothermal, constant true strain rate tests on Fe – 2% Si with strain rate of −0.001 sec $^{-1}$ and at different temperatures.

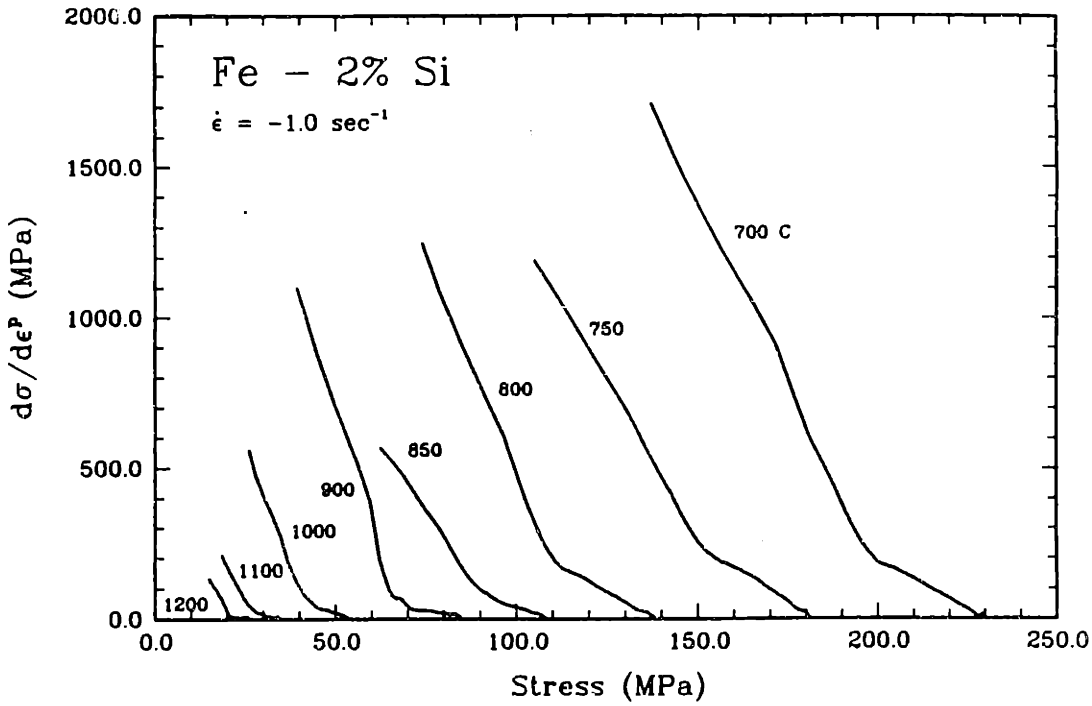


**Figure 4.41** Plastic hardening data ($d\sigma/d\epsilon^P$) derived from isothermal, constant true strain rate tests on Fe – 2% Si. Strain rate of -1.0 sec$^{-1}$.

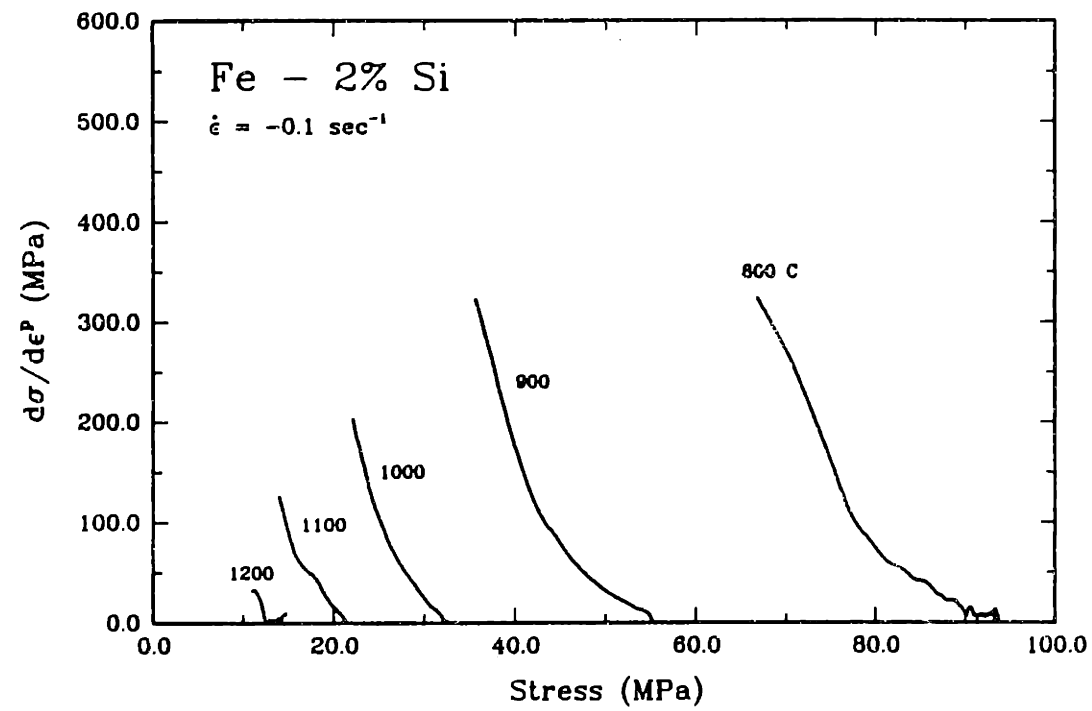


**Figure 4.42** Plastic hardening data ($d\sigma/d\epsilon^P$) derived from isothermal, constant true strain rate tests on Fe – 2% Si. Strain rate of -0.1 sec$^{-1}$.

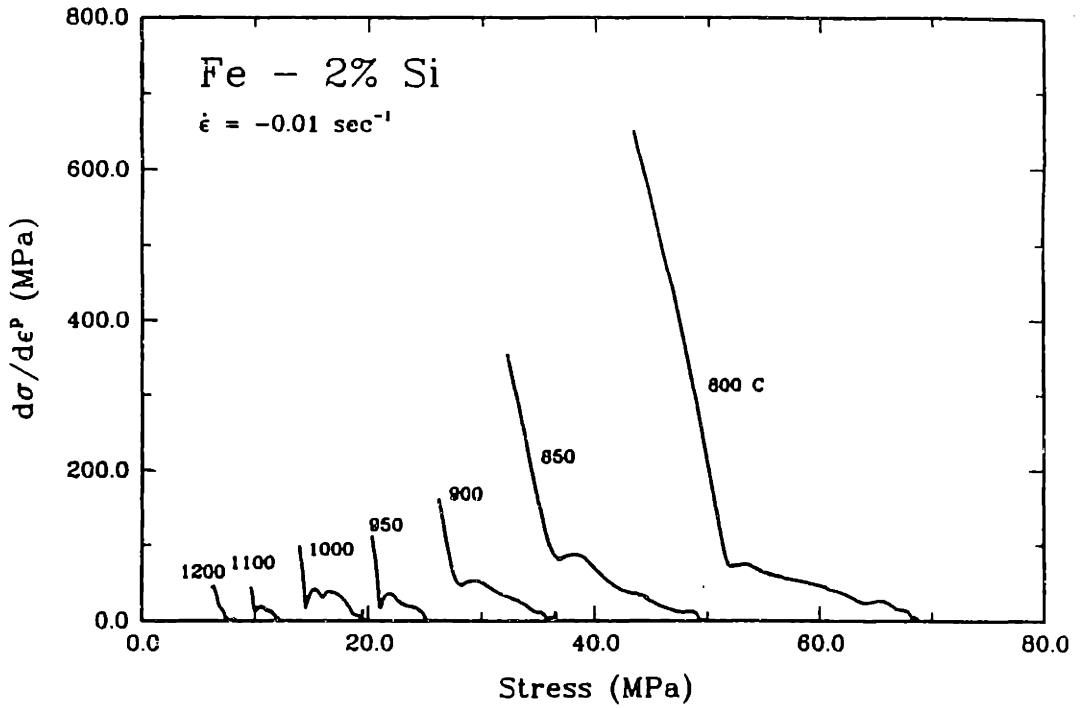


**Figure 4.43** Plastic hardening data ($d\sigma/d\epsilon^p$) derived from isothermal, constant true strain rate tests on Fe – 2% Si. Strain rate of $-0.01$ sec$^{-1}$.

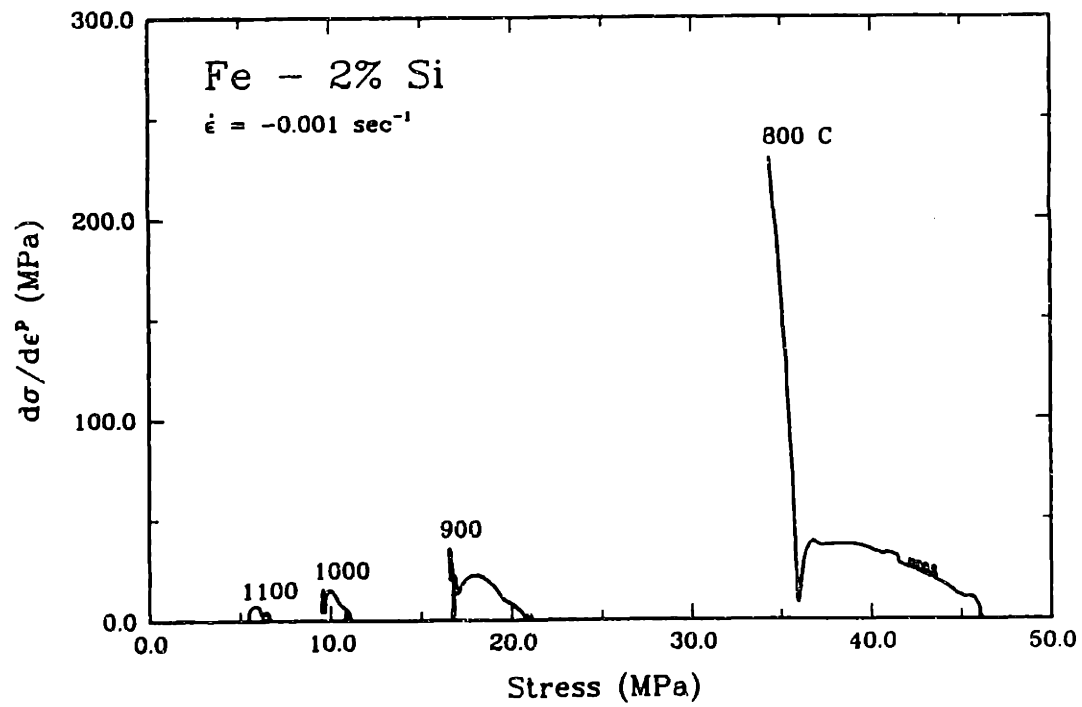


**Figure 4.44** Plastic hardening data ($d\sigma/d\epsilon^p$) derived from isothermal, constant true strain rate tests on Fe – 2% Si. Strain rate of $-0.001$ sec$^{-1}$.

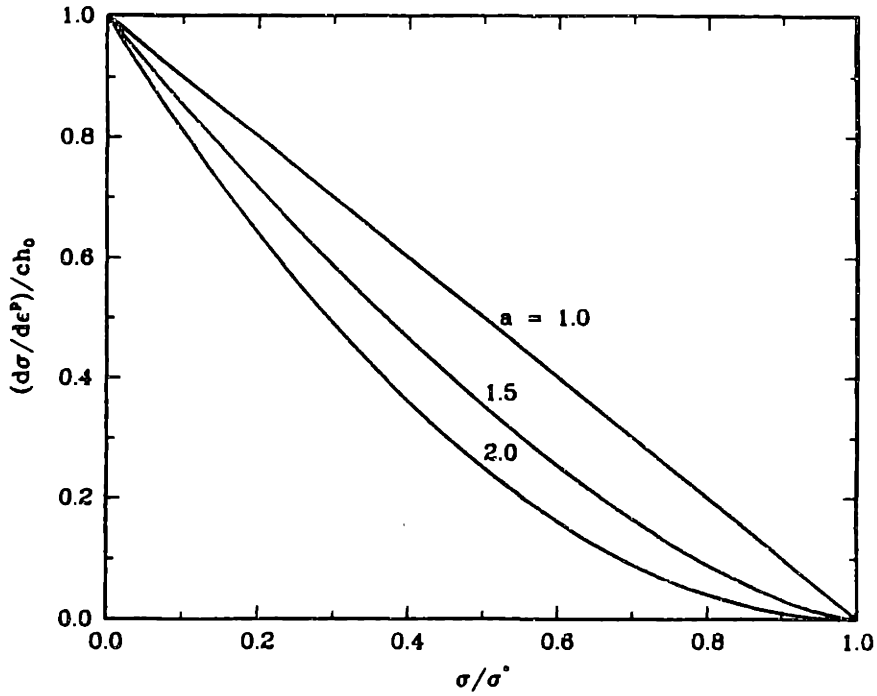


Figure 4.45 Variation in equation 4.3.9 as the value of exponent a is varied.

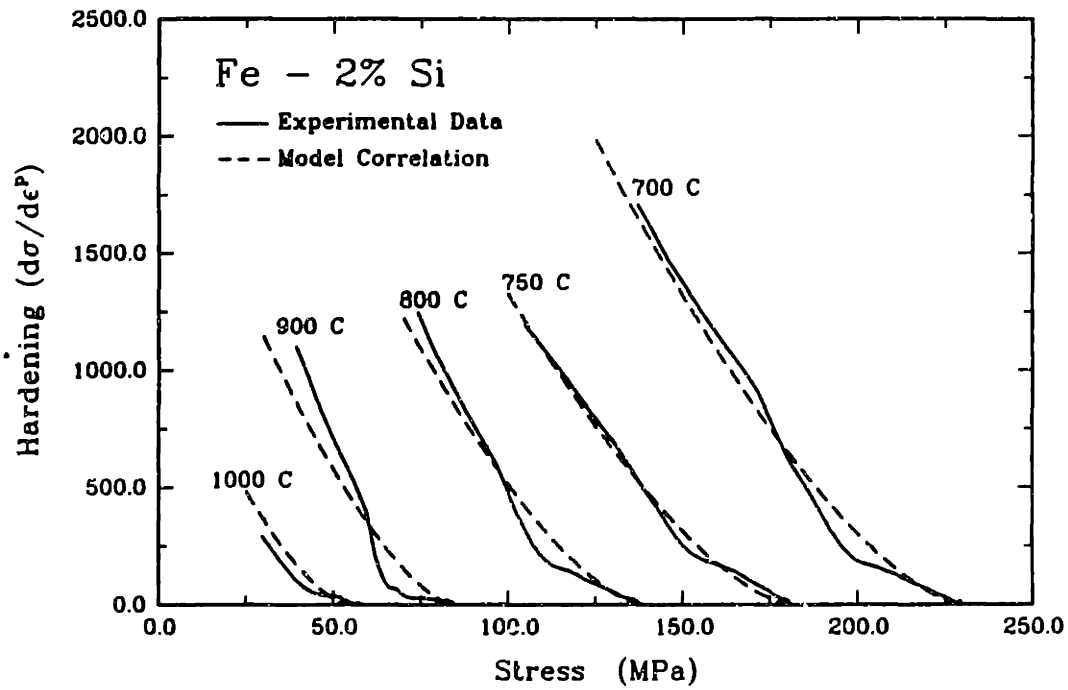


Figure 4.46 Correspondance between hardening data and equation 4.3.9 for a value of a=1.5.

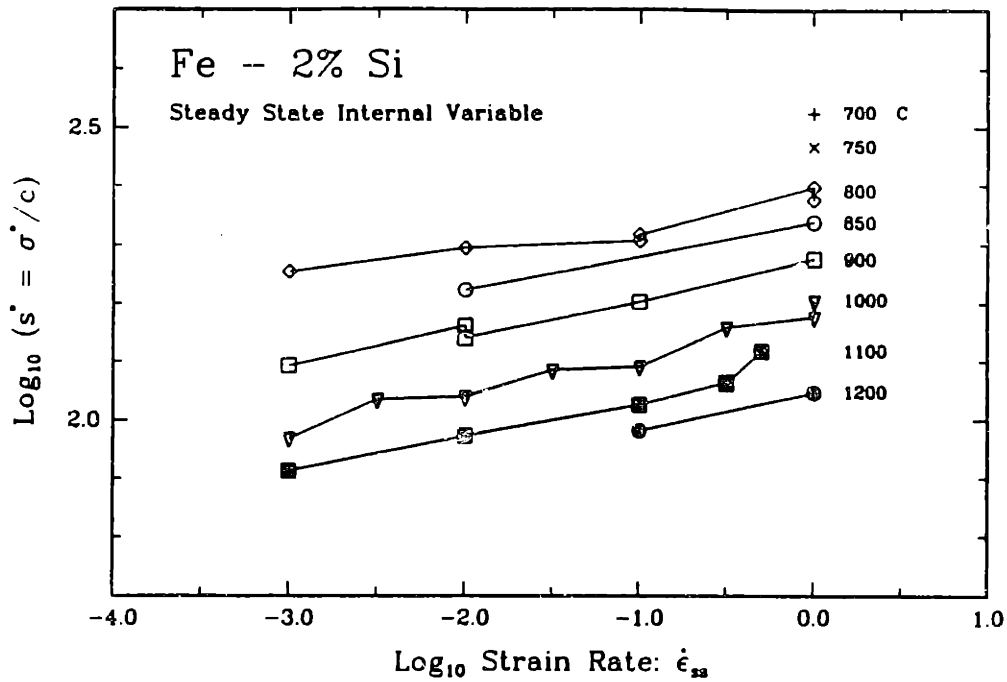


Figure 4.47 Saturation value of internal variable derived via $s^* = \sigma^*/c$ versus strain rate for Fe – 2% Si. Data obtained from isothermal, constant true strain rate tests.

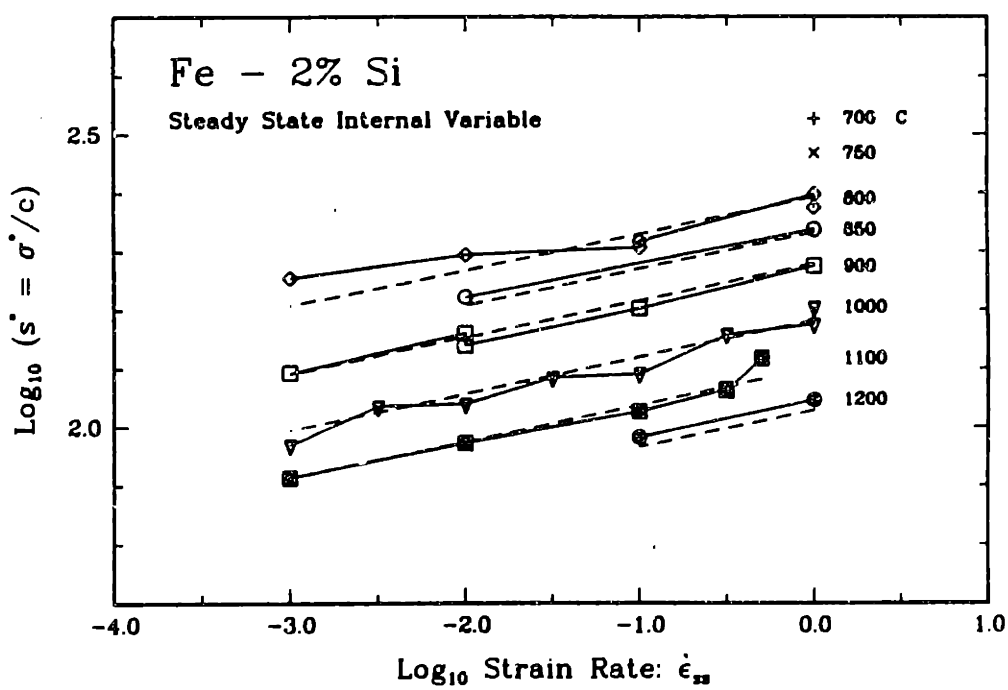


Figure 4.48 Fit of equation 4.3.11 for saturation of internal variable data for Fe – 2% Si. Data obtained from isothermal, constant true strain rate tests.

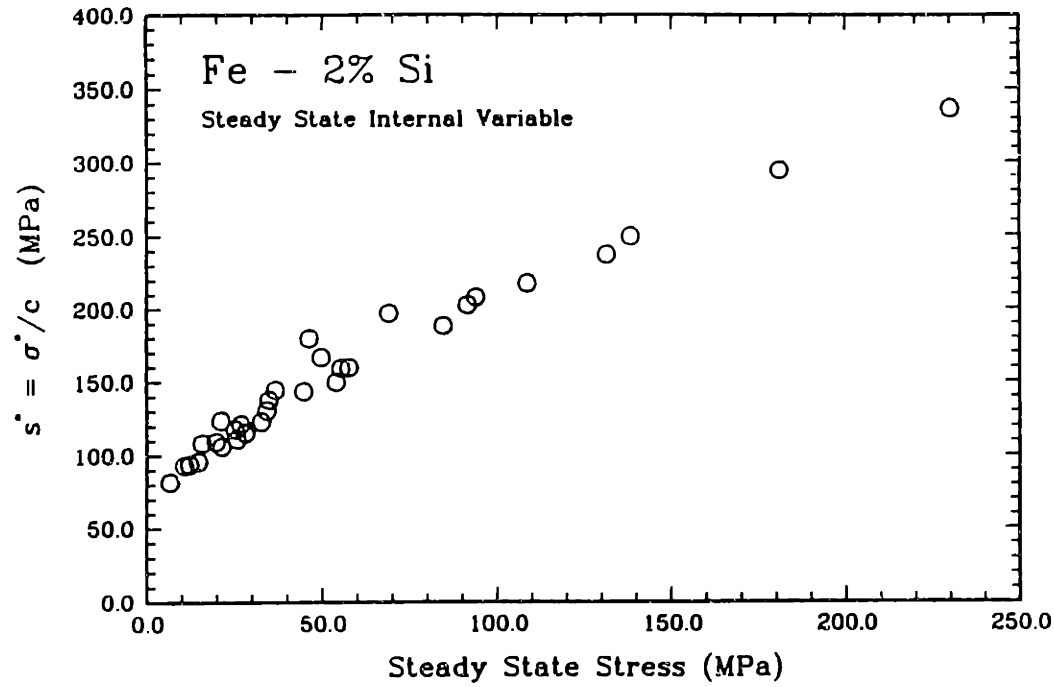


Figure .4.49 Saturation value of internal variable versus saturation stress for Fe – 2% Si. Data obtained from isothermal, constant true strain rate tests.

# Chapter 5

# Determination of Material Parameters

Fitting of the parameters associated with our constitutive model follows the progression of testing described in the previous two chapters. Parameters associated with each material response function are determined from the tests used to characterize that particular aspect of material behavior. The rate equation parameters are therefore determined from the jump test data, static recovery function parameters are determined from the load-unload-hold-reload data, and the dynamic hardening and recovery function is determined from the isothermal, constant true strain rate tests.

The fitting procedure exploits extensively the proportionality between stress and the internal variable resulting from the consequences of an isothermal, constant true strain rate test. At a fixed temperature and a fixed compressive strain rate, equation 4.1.3 implies:

$$s = |\sigma|/c, \tag{5.1}$$

where $c$ is a constant defined by

$$c \equiv \frac{1}{\xi} \sinh^{-1}\left[\left\{\frac{|\dot{\epsilon}^p|}{A}\exp\left(\frac{Q}{R\theta}\right)\right\}^m\right]. \tag{5.2}$$

This relationship permits the substitution of $(\sigma/c)$ for the internal variable $s$ while determining model parameters. Since the internal variable $s$ represents some generalized resistance to plastic deformation it is difficult, if not practically impossible, to measure a value of $s$ directly. Ideally we would like to have some macroscopic or microscopic quantity which we may correlate with $s$. Some possibilities for such measures are discussed in Chapter Six. In the absence of a directly measureable quantity, equation 5.1 permits the determination of model parameters without directly knowing the value of the internal variable.

The following procedure provides a deterministic method for evaluating the material parameters associated with the constitutive model presented in Chapter Four. The stress after a change in strain rate, whether it be associated with a strain rate jump or a recovery test reloading, is determined in our data as the stress corresponding to a 0.2% offset from the strain at the change in strain rate.

1. Determination of rate equation parameters: $A, Q$ and $m$.

   The strain rate jump tests provide constant state data for different states at different temperatures. If we normalize the stresses after each jump by the stress before each jump, then the rate equation eliminates the contribution of the internal variable since the test before and after the jump is both isothermal and at a constant true strain rate:

$$\frac{\sigma_f}{\sigma_i} = \frac{c_f s}{c_i s}, \tag{5.3}$$

   or,

$$\frac{\sigma_f}{\sigma_i} = \frac{\sinh^{-1}\left[\left\{\frac{\dot{\epsilon}_f}{A}\exp\left(\frac{Q}{R\theta}\right)\right\}^m\right]}{\sinh^{-1}\left[\left\{\frac{\dot{\epsilon}_i}{A}\exp\left(\frac{Q}{R\theta}\right)\right\}^m\right]}, \tag{5.4}$$

   where

   $\sigma_f$ = stress immediately after jump,

$\sigma_i$ = stress immediately before jump,

$\dot{\epsilon}_f$ = strain rate after jump,

$\dot{\epsilon}_i$ = strain rate before jump, and

$\theta$ = test temperature.

Equation 5.4 is fit to the jump test data $(\sigma_f, \sigma_i, \dot{\epsilon}_f, \dot{\epsilon}_i, \theta)$ for each temperature through a nonlinear least squares fit to provide the parameters $m$ and the combined term

$$\left\{ \frac{\exp\left(\frac{Q}{R\theta}\right)}{A} \right\}^m$$

as a function of temperature. The pre-exponential $A$ and the activation energy $Q$ are then determined via a second nonlinear least squares fit of the temperature to the above term. The constant $m$ is taken as the average value across all temperatures. Nonlinear fitting throughout this procedure was performed with an IMSL numerical subroutine ZXSSQ which provides for minimization of a nonlinear objective function on the basis of a least squares residue. The programs used in the fitting, ISOCON and its associated subroutine FITISO, are listed in Appendix C.

The three constants $(A, Q, m)$ could be determined simultaneously via a three parameter least squares fit, but it was found that the two step procedure produced a better correlation with the data.

Figure 5.1 indicates the correlation between the jump test data and the rate equation prediction using parameters determined via the above process.

It should be stated that the procedure described in this step does not produce an unambiguous value for the activation energy, $Q$. Strain rate jump

tests directly measure the functional relation between stress and strain rate. Temperature jump tests are necessary if one wishes to measure the activation energy directly. We are able to determine an activation energy here since the rate equation cast in the form of equation 5.4 retains a variation with temperature. A different rate equation may very well not permit the determination of an activation energy from strain rate jump test data. Practically, very little error is introduced to the model if one chooses to use the same value of activation energy for both $Q$ and $Q_{ds}$.

2. Determination of state/stress scaling factor: $\xi$

   As was indicated in Section 4.3.1 the parameter $\xi$ is a dimensionless scaling factor included in the rate equation to enforce our requirement that the value of the internal variable $s$ always be greater than the value of the equivalent tensile stress $\tilde{\sigma}$. Motivated by an interpretation of $s$ to represent some athermal measure of deformation resistance, this corresponds to requiring the proportionality constant $c$ to be less than one, where $\tilde{\sigma} = cs$ for isothermal, constant true strain rate conditions. The parameter does not improve the predictive capability of the model; it may be set equal to one with no adverse effect. A reasonable value of $\xi$ may therefore be calculated by requiring:

$$\xi > \sinh^{-1}\left[\left\{\frac{\dot{\bar{\epsilon}}^p}{A}\exp\left(\frac{Q}{R\theta}\right)\right\}^m\right],$$

   where the strain rate and temperature are the highest and lowest values of their applicable ranges, respectively.

3. Determination of static recovery term parameters: $B, Q_r$ and $p$.

   The static recovery function parameters were determined via a nonlinear least squares fit of equation 4.2.13 to the recovery data analyzed in the manner

described in Section 3.3, where 4.2.13 is:

$$\frac{-d\Delta t}{d(\sigma_f/c)} = \exp\left(\frac{Q_r}{R\theta}\right)\ \frac{\mu^p}{\mu B}\ \left(\frac{\sigma_f}{c}\right)^{-p}. \qquad 4.2.13$$

Here, $c$ is the stress/internal variable constant defined by 5.2. We assumed here that $Q_r$ equals the activation energy for self-diffusion of alpha iron, 300 kJ/mole. [Frost & Ashby, 1982] We provide two justifications for this assumption. One, static recovery has been observed to be associated with non-conservative climb of dislocations, [Takeuchi and Argon, 1976] the relevant activation energy then is that of self-diffusion. Two, we checked this assumption via the following test. We performed two load-unload-hold-reload tests at the same value of $c$ but at different temperatures (and consequently different strain rates). The strain rates needed to produce the same value of $c$ may be determined from the rate equation with the parameters determined in Step 1. If we design the tests to obtain the same values of stress just before unloading ($\sigma_i$) and immediately after reloading ($\sigma_f$) then, according to our model, the value of the internal variable is the same both at the beginning and at the end of the hold period for both tests. If these conditions are met, then for the two tests at the two temperatures according to 3.3.17:

$$\exp\left(-\frac{Q_r}{R\theta_1}\right)\Delta t_1 = \exp\left(-\frac{Q_r}{R\theta_2}\right)\Delta t_2. \qquad 3.3.17$$

Tests were performed according to the above procedure, varying the hold times until the same value of $\sigma_f$ was obtained. The two tests used for the measurement of $Q_r$ possessed the following experimental parameters:

| Test | Temperature (Celsius) | Strain rate (1/sec) | Hold strain | $\sigma_i$ (MPa) | $\sigma_f$ (MPa) | $\Delta t$ (sec) |
|---|---|---|---|---|---|---|
| 1 | 800. | .00506 | .10 | 46.7 | 40.7 | 352. |
| 2 | 900. | .1 | .20 | 46.5 | 40.8 | 20. |

Equation 3.3.17 using the values from the above table produces a value of $Q_r = 300.2$ kJ/mole, in excellent agreement with our assumed value for self-diffusion.

The recovery data used to fit 3.3.16 is plotted in Figure 4.29, and listed below in Table 5.1. Fitting was accomplished via a nonlinear least squares fit similar to that used in Step 1. The programs used for the fitting, STATCON and FITREC, are similarly listed in Appendix C.

**Table 5.1**

Recovery Test Data

900 Celsius - 0.02 1/sec

| $\Delta t$ (seconds) | $\sigma_f$ (MPa) | $(-d\Delta t)/d(\sigma_f/c)$ (seconds/MPa) |
|---|---|---|
| 20 | 34.6 | 2.67 |
| 70 | 34.1 | 31.25 |
| 150 | 33.5 | 42.19 |
| 300 | 32.9 | 78.74 |
| 500 | 32.2 | 86.96 |

The correlation between the recovery data and the recovery function prediction is plotted in Figure 5.2. Notice that the state exponent in this case exceeds 20, significantly greater than the exponent of 4 proposed by Argon [Prinz and Argon, 1984] and Nix [Nix and Gibeling, 1985]. The point corresponding to the shortest hold period was ignored in the curve fitting. We associated the rapid initial stress decrease accompanying short hold times with very small scale rearrangement or anelastic effects. One consequence of including this effect would be to increase the value of the exponent $p$ to magnitudes of 50 to 100. We therefore chose to ignore this effect with the consequence of representing longer time recovery effects with greater accuracy than short time

effects.

It should be noted that one may evaluate the static recovery function using offset stresses measured at a larger strain offset than the 0.002 strain offset used above. This was done with the Fe - 2% Si data using a 0.02 strain offset. The value of the exponent $p$ resulting from the analysis exceeded thirty. Selection of a different strain offset therefore did not reduce the relatively high magnitude of the state variable exponent.

4. Determination of the Saturation Stress $\sigma^*$.

   The value of the saturation stress $\sigma^*$ is determined for each test from the steady state value reached in the $(\sigma, \epsilon^p)$ data[1].

5. Determination of $a, ch_0$, and $\sigma_0$.

   The combined constant $ch_0$ and the parameter $a$ for each test are determined by a least squares fit of the hardening $(\sigma, d\sigma/d\epsilon^p)$ data according to equation 4.20, restated here:

$$\frac{d\sigma}{d\epsilon^p} = ch_0 \left(1 - \frac{\sigma}{\sigma^*}\right)^a .$$

   After the values of $a$ and $ch_0$ are obtained the value of $\sigma_0$ is obtained by a least square fit of the constant strain rate $(\sigma, \epsilon^p)$ data to equation 4.21 for fixed values of $a$ and $ch_0$. Alternatively, $ch_0, a$, and $\sigma_0$ may be determined by a similar least squares fit of the $(\sigma, \epsilon^p)$ data to the integrated stress-strain relation of equation 4.21. We believe that the first approach is more physically motivated, but the second should work well, especially when it is difficult because of lack of sufficient data points or noisy data to differentiate numerically the $(\sigma, \epsilon^p)$ data. Normally there is variation in the values of $a$ determined from

[1] If a steady state is not reached in the experiments, then $\sigma^*$ is estimated by extrapolating the $\sigma$ versus $d\sigma/d\epsilon^p$ data to $d\sigma/d\epsilon^p = 0$.

different tests. The value of $a$ is therefore determined as the average of the values determined from each individual test. After the value of $a$ is fixed, the least squares fit of equation 4.20 is performed to determine the final value of $ch_0$. For the 2% silicon iron the value of $a = 1.5$ describes our experimental data well. Accordingly, for this material we fix $a = 1.5$. The range of data used to determine $ch_0$ and $\sigma_0$ corresponds to $\epsilon^p > 1\%$ because there are various uncertainties associated with measuring small strains in compression by our test techniques. Figure 4.46 illustrates the correspondence between the hardening data and equation 4.20 using $a = 1.5$. The program used in this step, QNON, is listed in Appendix C.

6. Determination of $h_0$.

   The value of $h_0$ is then obtained as the simple average:

$$h_0 = \frac{\sum_{i=1}^{q} \left( [ch_0]_i / c_i \right)}{q}, \tag{5.1}$$

   where $[ch_0]_i$ is the value of $ch_0$ determined in step 5 for test $i$, $c_i$ is the corresponding value of $c$ defined in 5.2, and $q$ is the number of tests. The value of $h_0$ was determined to be 3498.0 MPa.

7. Determination of $\tilde{s}, n,$ and $Q_{ds}$.

   The values of $\tilde{s}, n$ and the activation energy $Q_{ds}$ are then determined by a non-linear least squares fit to equation 4.22 cast in terms of stress:

$$\sigma^* = c\tilde{s} \left[ \frac{\dot{\epsilon}}{A} \exp\left( \frac{Q_{ds}}{R\theta} \right) \right]^n .$$

   The programs used for this fit are named SATCONS and its associated subroutine FITSAT. They are included in Appendix C.

   Note: Although there is no physically justified reason for doing so, one may set $Q_{ds}$ equal to the value of $Q$ determined for the rate equation without

introducing a significant amount of error in the predictive capability of the model. The different values of activation energy in the two equations reflect a difference in the physical mechanisms governing that particular aspect of the material response. The model, however, does not appear to be extremely sensitive to averaging these two values of activation energy.

8. Determination of $s_0$.

   The value of $s_0$ for each test, the initial value of the deformation resistance $s$, is then determined by dividing the value of $\sigma_0$ determined in step 5 by the corresponding value of $c$ defined in equation 5.2. Table 5.2 provides the average $s_0$ values for each test temperature, determined via the procedure described above.

The material parameters for the 2% silicon iron obtained by the method outlined above are listed in Table 5.1. The value of the activation energy $Q = 247.5$ kJ/mole is within the range 237 to 251 kJ/mole for the activation energy for lattice self-diffusion in ferrite (see, for example Ashby and Frost [1982]). We note that for a similar silicon steel, Uvira and Jonas [1968] have previously obtained a value of $Q = 333.6$ kJ/mole. As discussed in Chapter 4, however, there is no reason to expect the activation energy associated with the rate equation to be equal to either that of self-diffusion or that obtained from a fit to steady state data.

## 5.1 Minimum number of tests

One reasonable question associated with the determination of material parameters is: What is the minimum number of tests that need be performed to provide sufficient data to follow the above procedure? Certainly one need not perform as many tests as are presented in this thesis.

If we ignore the static recovery function, it is possible to determine all of the constants from a series of strain rate jump tests like those presented in Section 4.1. The jump segments provide constant structure data for determining the parameters associated with the strain rate equation. We may determine the parameters associated with the saturation state equation if we perform the tests such that the stress reaches a constant value before the jump and then allow the stress to reach a new steady state after the jump. Finally, the hardening segments of the curves before and after each jump provides the parameters for the evolution equation for the internal variable.

It is possible (although certainly not recommended) to determine all of the material parameters from six (6) strain rate jump tests, divided into two sets of three jump tests with each set performed at a different temperature. This set of tests represents the minimum number required to uniquely determine each material parameter, once again assuming that we have neglected static recovery. Obviously, more tests are required to provide confidence in the quality of the correlation between material and model, with appropriate tests spanning the range of strain rates, stresses, and temperatures to be represented by the model.

TABLE 5.2

Initial Values of Internal Variable $s$

| Temperature Celsius | $s_0$ MPa |
|---|---|
| 700 | 134.2 |
| 750 | 121.1 |
| 800 | 102.7 |
| 850 | 89.6 |
| 900 | 74.6 |
| 950 | 79.1 |
| 1000 | 66.1 |
| 1100 | 58.4 |
| 1200 | 60.1 |

TABLE 5.3

Material Parameters for 2% Silicon Iron

| Material Parameter | Value |
|---|---|
| $A$ | $1.26 \times 10^8$ sec$^{-1}$ |
| $Q$ | 247.5 kJ/mole |
| $\xi$ | 5.00 |
| $m$ | 0.22793 |
| $\tilde{s}$ | 36.3 MPa |
| $Q_{ds}$ | 439.4 kJ/mole |
| $n$ | 0.06272 |
| $h_0$ | 3498.0 MPa |
| $a$ | 1.5 |
| $B$ | $1.08 \times 10^{60}$ (MPa/sec) |
| $Q_r$ | 300.0 kJ/mole |
| $p$ | 20.6 |

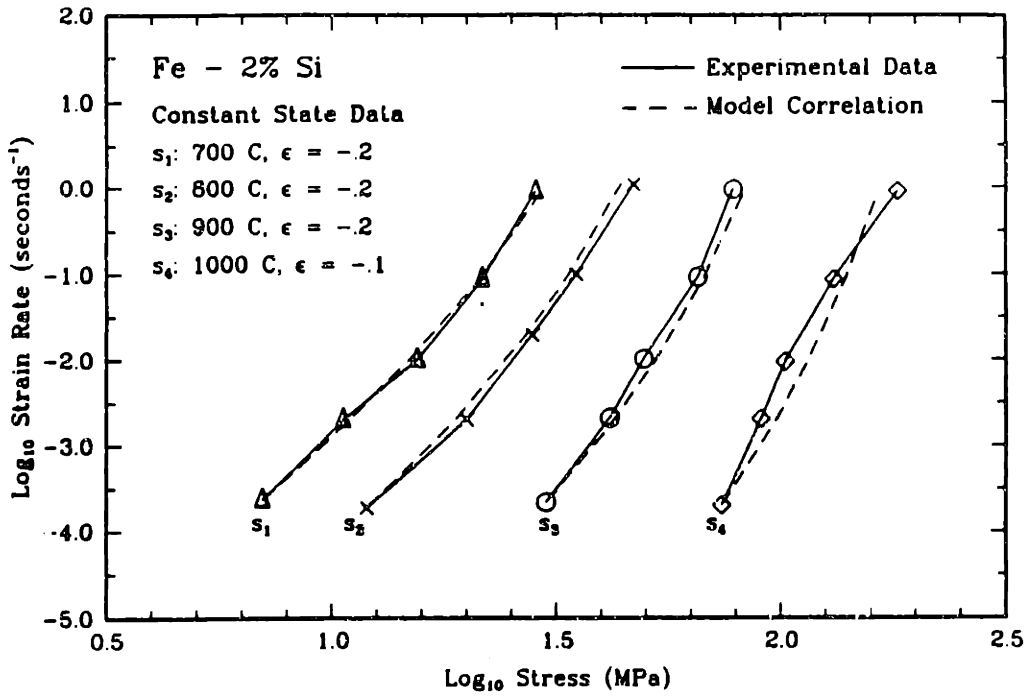


Figure 5.1 Correspondence between constant state data and fit of equation 4.1.3 to the same data.

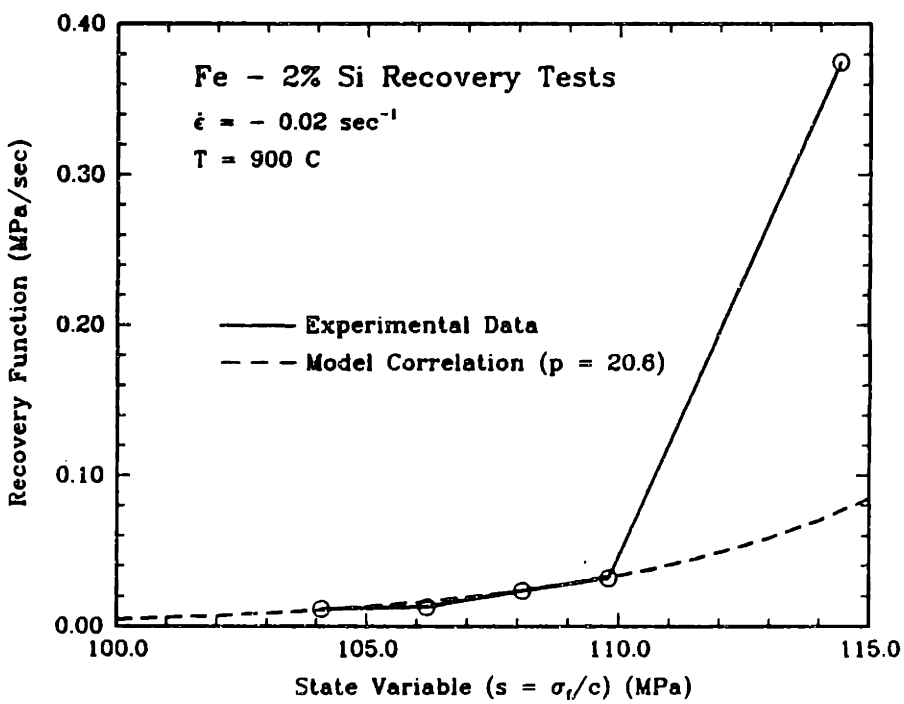


Figure 5.2 Fit of power law static recovery function to Fe – 2% Si recovery test data.

# Chapter 6

# Evaluation and Validation of Constitutive Model

No consistent criteria have been established for the evaluation of different constitutive models; most comparisons to date consist of checking whether models represent basic qualitative aspects of material behavior. Nevertheless, the evaluation and validation of a model involves several considerations independent of the physical system it supposedly represents. These considerations include:

1. At the very least, the model should represent the physical data upon which the model is based and from which the material parameters of the model are determined.

2. Comparison between the predictions from the model and the physical system should encompass the variable space to be modelled. Given a set of external and internal variables, the model should represent the physical system throughout all permutations of those variables. If the model parameters have been evaluated using data from a subset of the variable space, validation should include not only that subset but as much of the variable space as possible. Validation should therefore examine the predictive capability of the model at reasonable points, including the limits, of the variable space.

3. Item one above supposes that all of the relevant variables are measurable. Unfortunately in our case there is no direct correlation of the internal variable $s$ to a physical quantity. One consideration therefore in our investigation is whether we may find some some means of correlating $s$ to some physical measurement which we may then take to represent $s$.

The tests which follow provide initial validation of the model with consideration of the above issues.

Five sets of tests follow. First, the model is correlated with the original material tests, and the correlation is found to be excellent. Second, a load control test is compared with a prediction from the constitutive model. Data obtained from the load controlled experiments was not used in the evalutation of the material parameters for the model. Third, strain rates jump tests where the strain rate is increased twice during one test is compared with the predicted model response. Fourth, a strain rate decrement test is used to confirm the presence of strain softening. Fifth, a specimen is proposed and tested to investigate both the ability to predict a variation in state subject to an inhomogenous deformation and to investigate different macroscopic measurements which may be correlated with the internal variable.

## 6.1 Numerical Integration of Constitutive Equations

The simulations presented in this chapter were produced via one of two integration procedures, both of which are represented by programs listed in Appendix D. The first program, ISOINT, uses an IMSL numerical subroutine to evaluate all tests where the true strain rate is constant. Given a constant true strain rate and isothermal conditions, integration of the constitutive model reduces to integration

of the evolution equation for the internal variable. Although the coupled system of equations is relatively "stiff", the evolution equation for $s$ is not. Therefore the IMSL subroutine DVERK which employs a fifth order Runge-Kutta algorithm for non-stiff systems of differential equations was employed. A typical simulation required less than 5 seconds of CPU time on a Data General MV4000.

Simulations of experiments involving other boundary conditions were performed using the finite element program ABAQUS. The constitutive equations obtained in this investigation have been incorporated by Anand et al. [1985] as a material model via a user-material interface in ABAQUS developed by Hibbitt, Karlsson, and Sorensen, Inc. of Providence, Rhode Island. The coupled differential constitutive equations are numerically very stiff and require special computational schemes for efficient integration in time. Anand et al. use an implicit time-integration procedure with automatic time stepping. Using this time-integration procedure in ABAQUS we may evaluate material response in arbitrary three dimensional loading conditions. A simulation of an isothermal, constant true strain rate test using ABAQUS requires approximately 10 minutes of CPU time as opposed to the 5 seconds required by ISOINT.

## 6.2 Simulation of Original Experiments

Figures 6.1 through 6.14 present isothermal, constant true strain rate test, recovery test, and jump test simulations with the original experimental data. All simulations were produced using ISOINT. The initial values of the internal variable, $s_0$, used in these simulations varied with temperature and are included in Table 5.2. The correlation between the model and the experimental data is excellent. The only large discrepancy between the model and the experiments occurs with the 700 degree

Celsius, strain rate jump tests (Figure 6.10). This is not unanticipated since the jump test data was not well represented by the rate equation at that temperature.

## 6.3 Load Boundary Condition Test

Since the *independent* variables in the major portion of the experiments were strain rate and temperature, it is important to investigate the predictive capability of the constitutive model when they are *dependent* variables. Experiments which permit such comparison include load or stress controlled tests and temperature variation tests.

A simple isothermal, load controlled compression experiment was selected where the load was increased linearly at a rate of 2000 Newtons per second up to 20,000 Newtons, held for 10 seconds, and then decreased linearly to zero load, illustrated in Figure 6.15. Displacement was recorded versus time, the true strain and stress calculated, and the strain rate determined from the strain versus time data. Total accumulated compressive strain in this test exceeded -0.9. Figure 6.16 illustrates the agreement between the experimental strain rate and predicted strain rate versus time. The ABAQUS input data for the simulation is included in Appendix E.

Although the initial loading segment of the test produces the worst agreement between the model and the data, it is also the most severe test of the model, since the model is being asked to follow a rate of change in one of the state variables. The constant load segment, where the applied stress varies more slowly, is duplicated very well by the model.

## 6.4 Strain Rate Decrement and Double Jump Tests

Figures 6.17 to 6.19 show variations in the strain rate jump tests, where the strain rate is in the first case increased twice and in the second case decreased once. The model represents the double jump test data very well, duplicating both hardening and instantaneous strain rate dependence.

Although the constitutive model predicts the final steady state stress in the strain rate decrement test, the model predicts a transition to that stress after the strain rate decrement which is much different from the actual data. The experimental data changes abruptly to the new value of steady state stress. This behavior was unexpected. It is not clear whether this represents true material behavior or is some experimental artifact. Similar data obtained with identical tests on 1100 aluminum [Kim et al., 1986] demonstrated a material response like that predicted by the constitutive model. It is possible that the abrupt transition is a characteristic of the analog function generator or the servohydraulic, although preliminary examinations of the hardware failed to detect any abnormalities. It would be useful to perform the same tests on some other metals using different hardware to determine whether this result is reproducible.

The steady state stress reached after the strain rate decrement corresponds to be the steady state value for a monotonic test at the final strain rate and temperature. The $sgn(-)$ function adopted in the evolution equation for the internal variable simulates strain softening, permitting the model to predict the new saturation state.

## 6.5 State Gradient Specimen and Testing

One assumption of an internal variable constitutive model is that the value of the internal variable provides some measure of the mechanical state of the material.

The aim of this particular test was to determine the correlation between the value of the internal variable predicted by the constitutive model and the variation in deformation resistance within an inhomogeneously deformed test specimen. A simple conical compression specimen geometry was selected to produce a gradient of deformation along the vertical axis. Figure 6.20 shows a typical gradient specimen before and after testing.

A typical test sequence consisted of compressing the specimen at elevated temperature, immediately quenching, and then machining a series of small cylindrical compression specimens from the center axis of the deformed specimen. The yield stress obtained from a compression test on each compression specimen provides a measure of the deformation resistance in the region of the gradient specimen from which the compression specimen was machined. Microhardness tests were also performed along the center section of the compressed specimen to evaluate whether microhardness could be correlated with the internal variable.

Since we have evaluated the internal variable $s$ by measuring a 0.2% yield stress, and since the yield stress is temperature dependent, ideally we would perform these compression experiments at the original gradient test temperature. This is operationally difficult to do since the specimen requires a finite amount of time to heat to test temperature, and recovery processes may erase the variation in deformation-induced microstructure between specimens. We may perform these yield tests at room temperature, but then we are faced with the dilemma of relating the room temperature yield stress, where the high temperature value of $c$ may not be applicable, to the deformation resistance.

A set of initial tests were performed using Fe - 2% Si gradient specimens. The specimens were heated using an induction coil and then cooled with a helium gas quench immediately after compression. Room temperature yield tests using com-

pression specimens taken from the axis of the quenched specimens *produced no discernable variation in yield stress as a function of axial position in the gradient specimen.* It was uncertain whether the lack of variation was due to inadequate quench rates, insufficient grains per compression specimen cross-section, or the true absence of a variation in state.

We then decided to perform an identical set of tests using 1100 aluminum in place of the Fe - 2% Si. The use of aluminum permitted large gradient specimens, faster quench rates, and easier machining and testing of the yield stress compression specimens. A set of parallel experiments following the methods applied to the Fe - 2% Si have been performed by Kwon Hee Kim [Kim et al. 1986] to determine the material parameters for 1100 aluminum for the model developed in this investigation. The aluminum could be tested in an air atmosphere using a radiant lamp, clamshell furnace which permitted heating rates more than two orders of magnitude greater than was possible using the vacuum furnace. The radiant furnace also permitted a water quench which also increased quenching rates. Aluminum thus permitted both the possibility of a more reliable retention of high temperature microstructure and the potential of performing the yield tests at elevated temperatures. Figure 6.21 shows the aluminum gradient specimen dimensions.

The gradient specimen compression test was simulated using ABAQUS and the user material subroutine described in Section 6.2. Appendix E contains the ABAQUS input file describing the finite element model. Figure 6.22 illustrates the displacements resulting from a simulation of a test on the 1100 aluminum at 300 degrees Celsius and at a compression rate of 1 millimeter per second. Figure 6.23 provides a contours of constant value of the internal variable for this same test. Values provides in the contour table are in terms of equivalent shear stress and must be multiplied by $\sqrt{3}$ to obtain equivalent tensile values.

Tests were performed with the aluminum gradient specimen at both room temperature and at 300 degrees Celsius. The room temperature test was performed to provide a large variation in state to compare with the higher temperature test results. The elevated temperature specimen reached 300 degrees from room temperature in approximately 500 seconds and was quenched from 300 degrees Celsius to room temperature in less than 10 seconds. After compression, both specimens were sectioned along their axis of symmetry. Figures 6.24 and 6.25 show the variation in microhardness along the longitudinal axis of both specimens. Each data point in the figures represents the average of 8 to 10 readings at each position. Although some variation is evident in the room temperature specimen, there was no detectable variation in microhardness in the quenched specimen.

Compression specimens (approximately 7.0 mm in diameter by 7.0 mm in length) were machined coaxial with the axis of the compressed gradient specimens as indicated in Figures 6.26 and 6.27. These figures indicate the variation in yield stress measured *at room temperature* from the compression specimens obtained from both the room temperature and 300 degree Celsius gradient specimens. Figure 6.28 shows the actual stress-strain data for the five compression specimens machined from the 300 degree gradient specimen. Figure 6.27 also shows the variation in the value of the internal variable $s$ predicted by the ABAQUS simulation, *where the values of $s$ have been multiplied by a constant (.830) such that the model prediction and the measured yield stress coincide for the rightmost data point.* The model prediction appears to represent qualitatively the variation in yield stress along the length of the specimen very well, duplicating not only the magnitude of variation in stress but also the axial position of that variation.

It should be noted that the constitutive model cannot be extrapolated to room temperature given material constants which were determined from tests at higher

homologous temperatures. The constitutive model does not predict the room temperature yield stress variation from the quenched gradient specimen, a calculation which may be done by multiplying the predicted value of $s$ by the proportionality constant $c$ obtained by inserting room temperature parameters into equation 5.2. Such a calculation overestimates the actual yield stress by approximately a factor of 2.

Nevertheless, the predicted variation in the internal variable appears to indicate the relative variation in plastic deformation resistance very well.

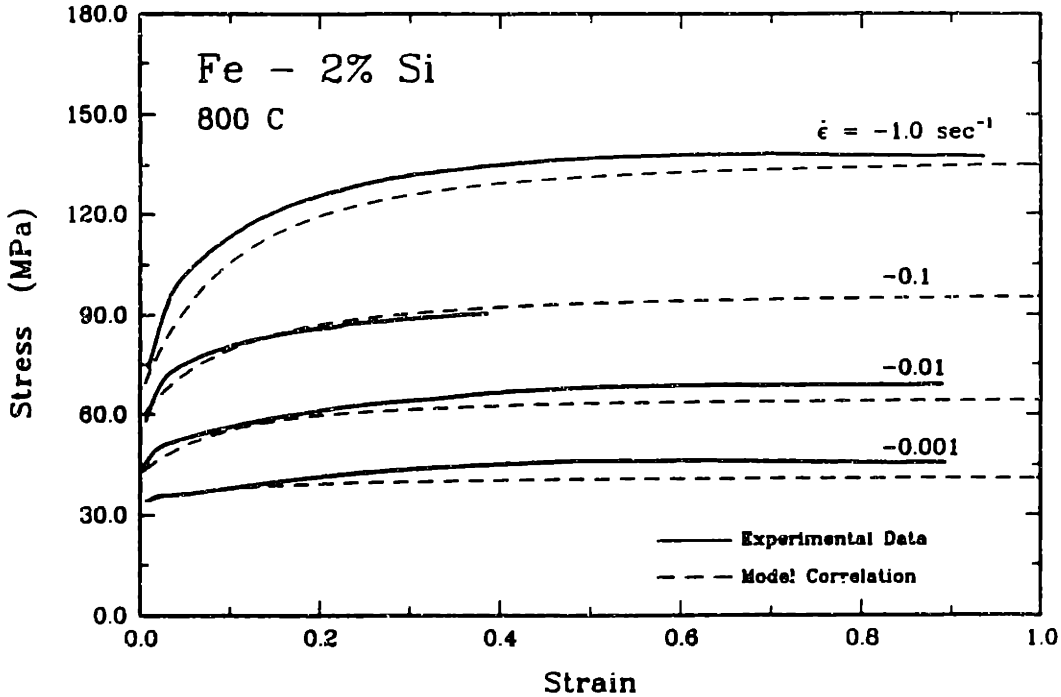


**Figure 6.1** Correlation of constitutive model with isothermal, constant true strain rate tests on Fe – 2% Si at 800 degrees Celsius.

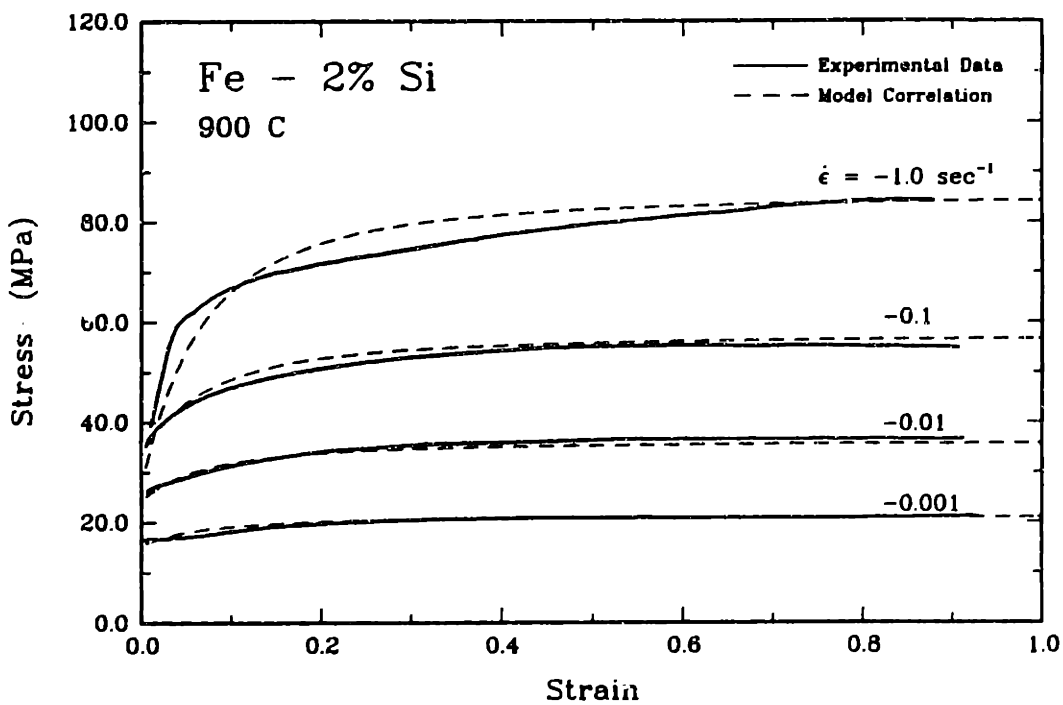


**Figure 6.2** Correlation of constitutive model with isothermal, constant true strain rate tests on Fe – 2% Si at 900 degrees Celsius.

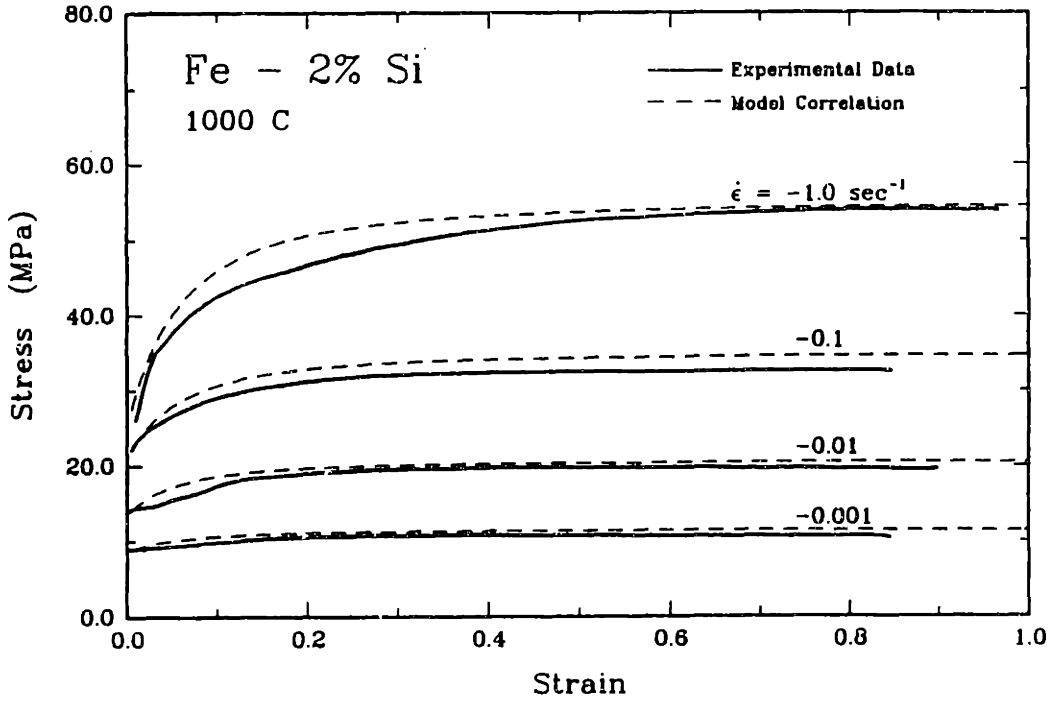


Figure 6.3 Correlation of constitutive model with isothermal, constant true strain rate tests on Fe – 2% Si at 1000 degrees Celsius.

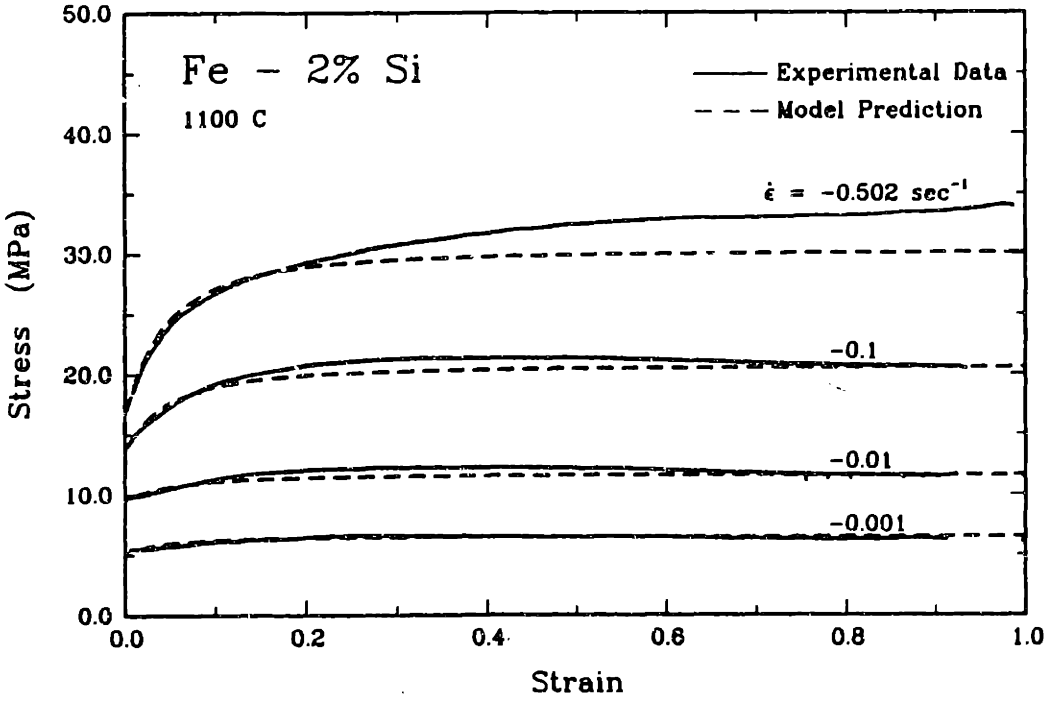


Figure 6.4 Correlation of constitutive model with isothermal, constant true strain rate tests on Fe – 2% Si at 1100 degrees Celsius.

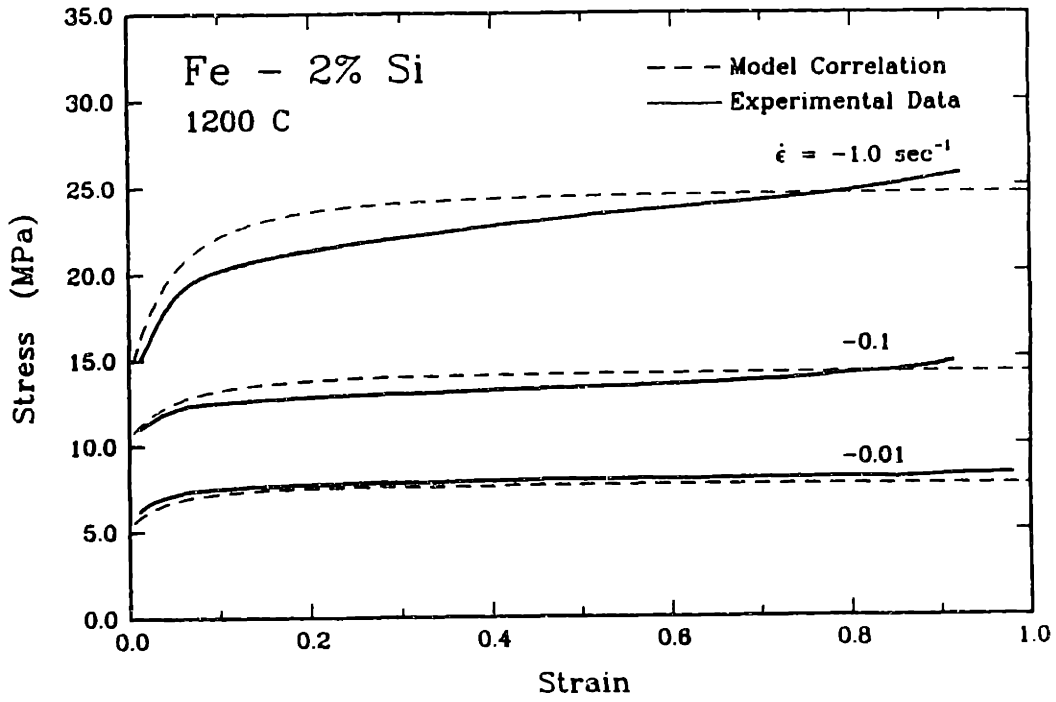


**Figure 6.5** Correlation of constitutive model with isothermal, constant true strain rate tests on Fe – 2% Si at 1200 degrees Celsius.

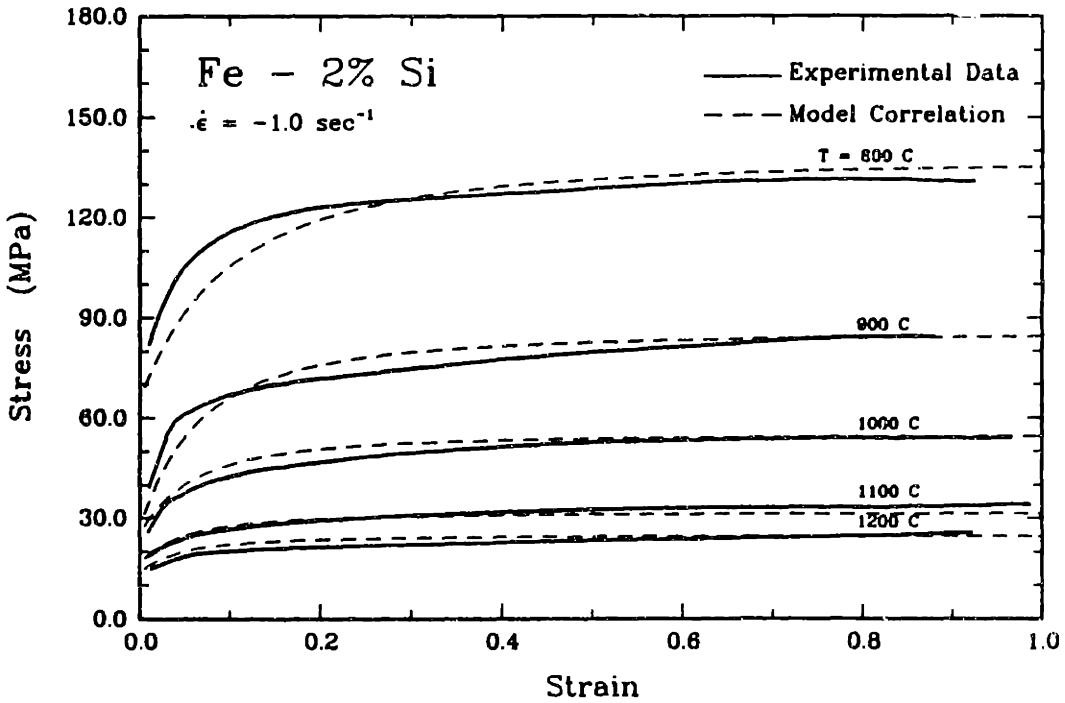


**Figure 6.6** Correlation of constitutive model with isothermal, constant true strain rate tests on Fe – 2% Si with strain rate of −1.0 sec$^{-1}$.

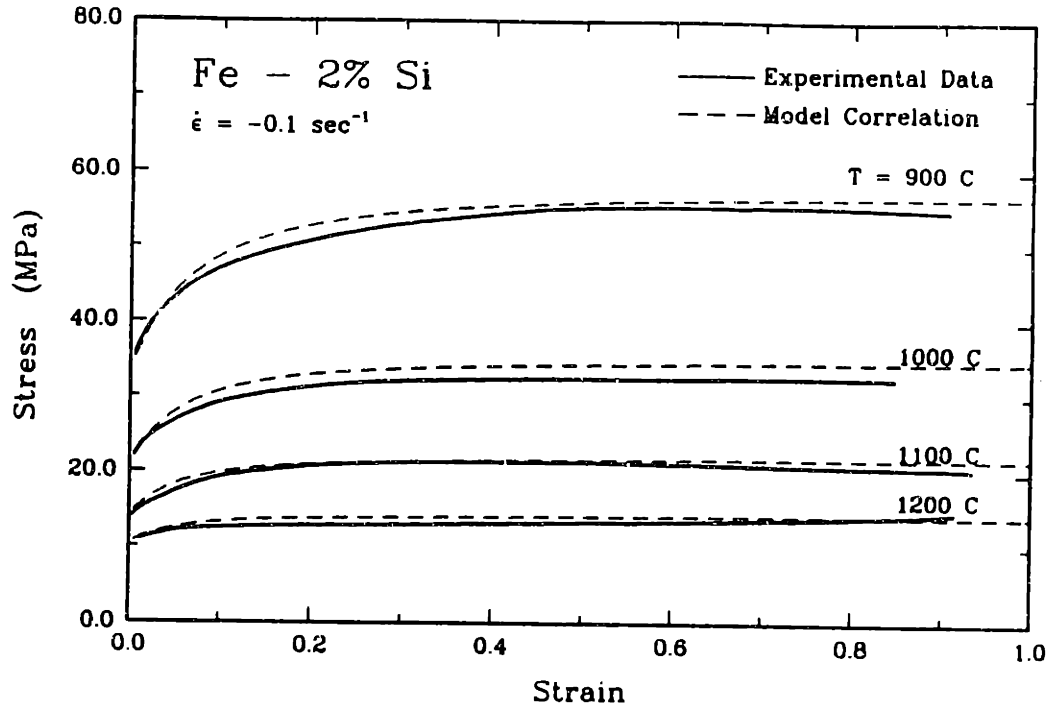


**Figure 6.7** Correlation of constitutive model with isothermal, constant true strain rate tests on Fe – 2% Si with strain rate of $-0.1\ sec^{-1}$.

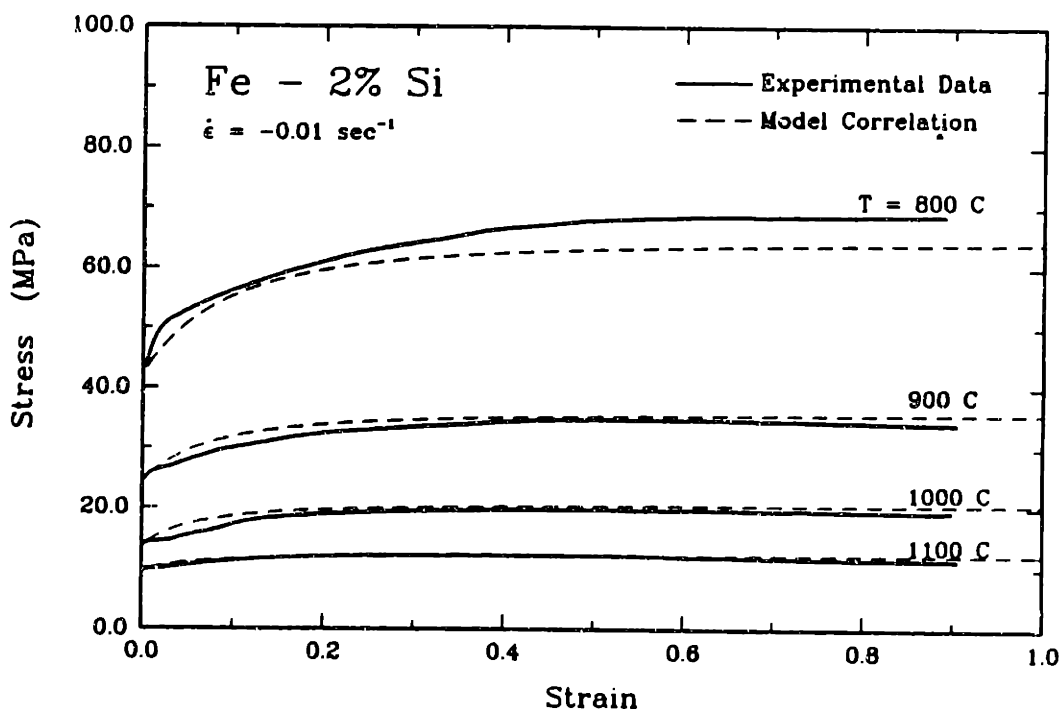


**Figure 6.8** Correlation of constitutive model with isothermal, constant true strain rate tests on Fe – 2% Si with strain rate of $-0.01\ sec^{-1}$.

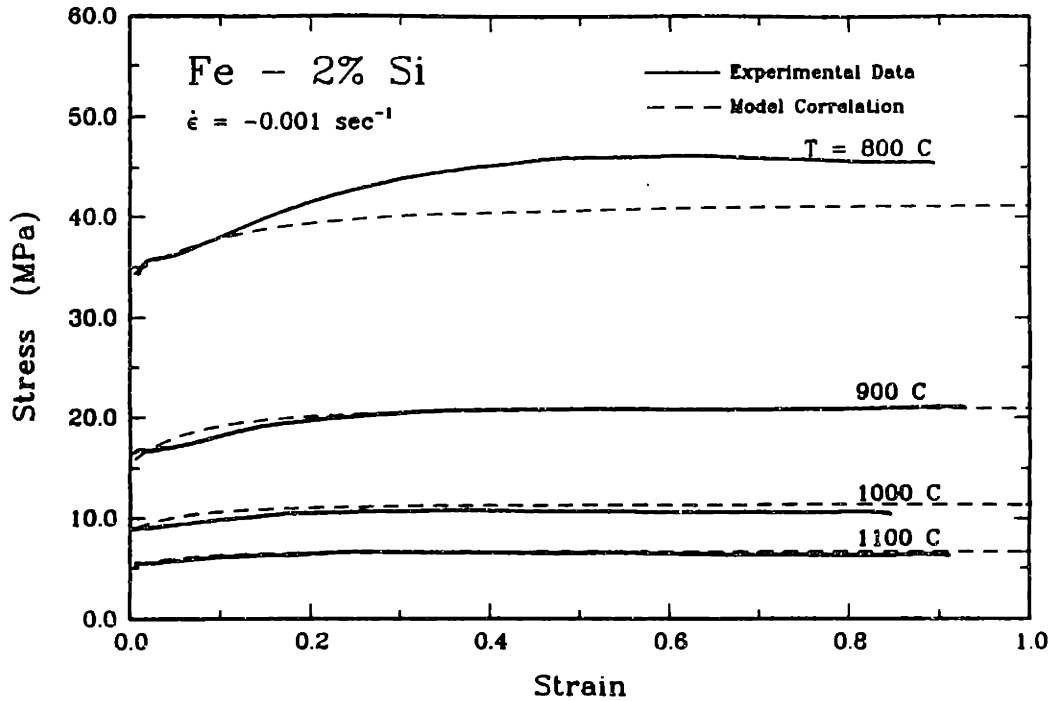


**Figure 6.9** Correlation of constitutive model with isothermal, constant true strain rate tests on Fe – 2% Si with strain rate of $-0.001\ sec^{-1}$.

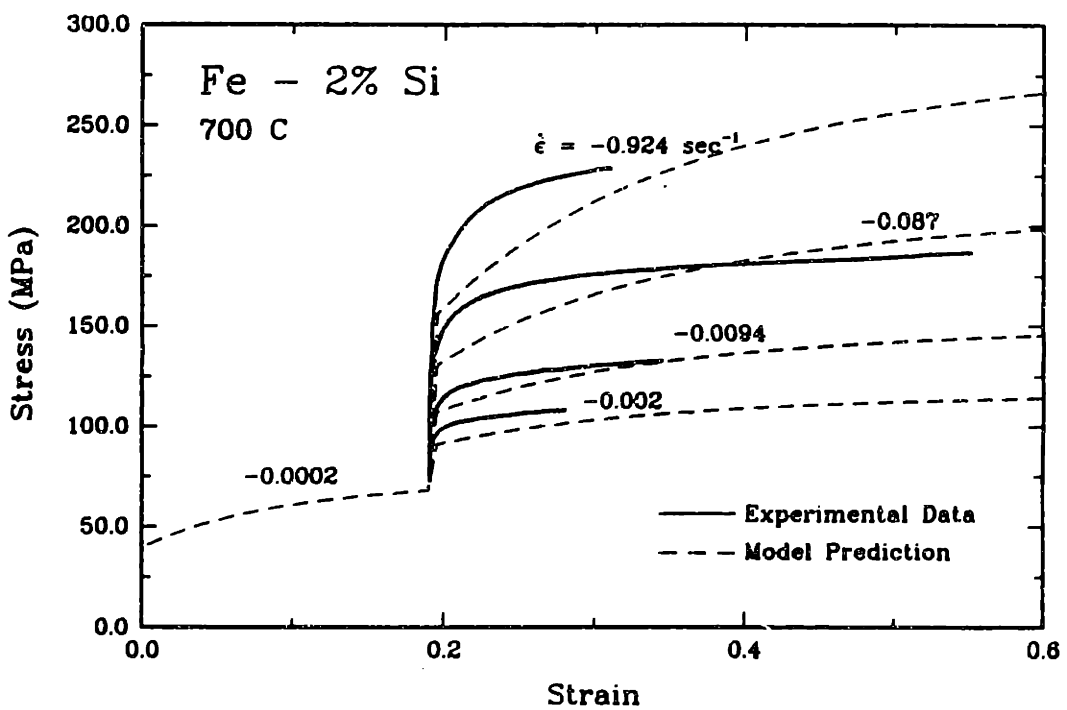


**Figure 6.10** Correlation of constitutive model with strain rate jump tests on Fe – 2% Si at 700 degrees Celsius.

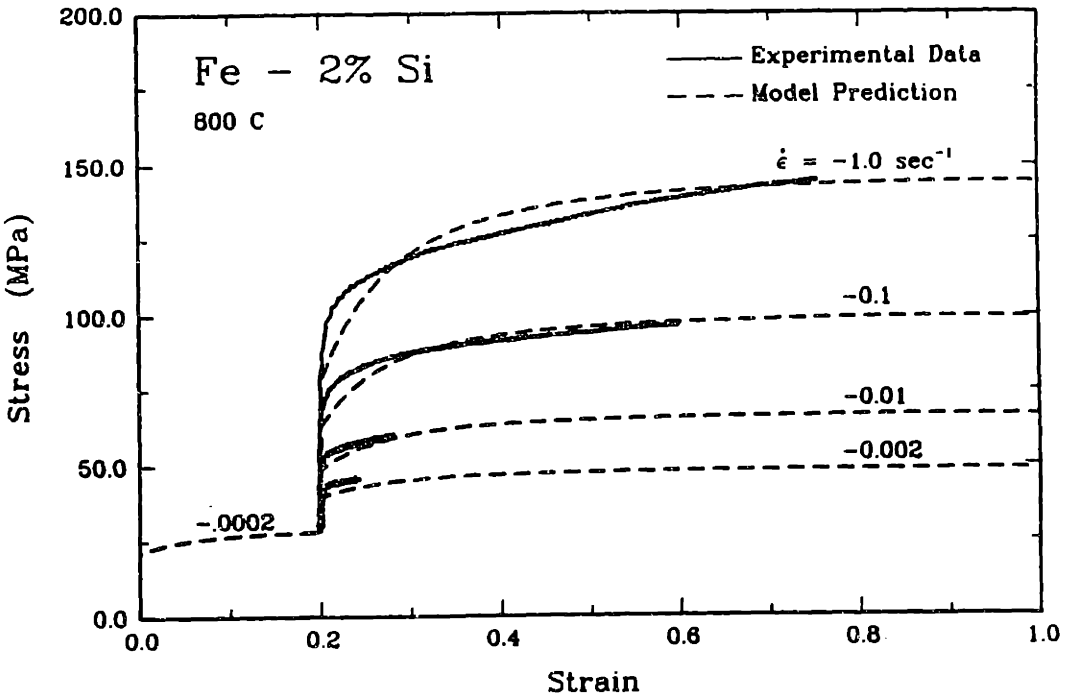


Figure 6.11 Correlation of constitutive model with strain rate jump tests on Fe – 2% Si at 800 degrees Celsius.

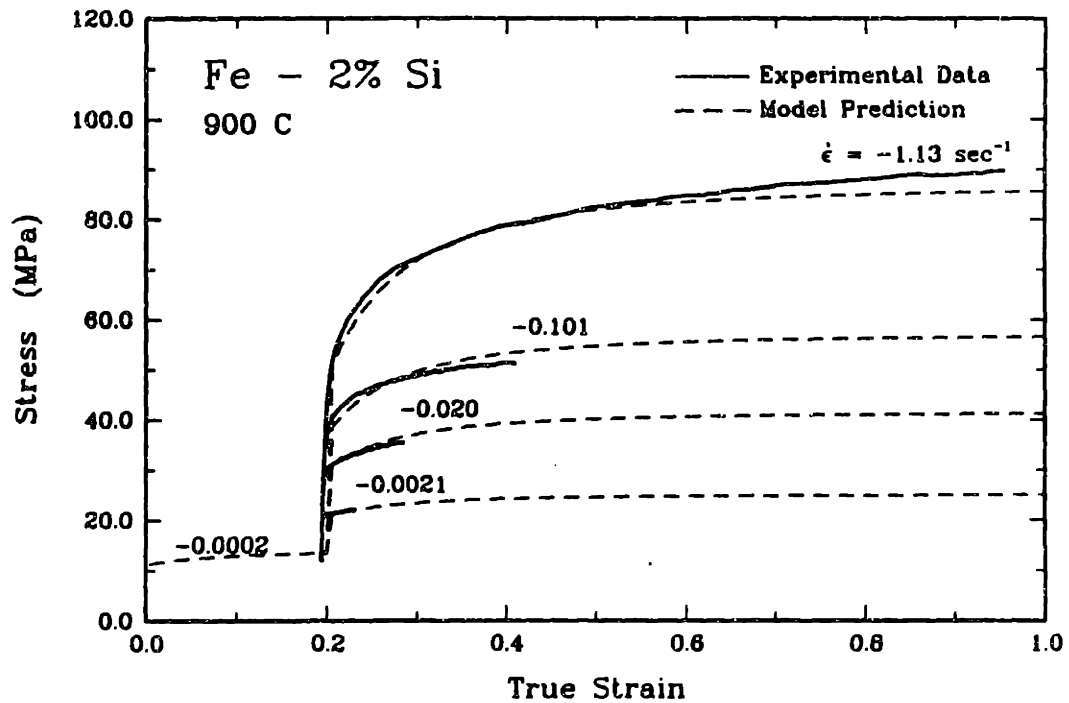


Figure 6.12 Correlation of constitutive model with strain rate jump tests on Fe – 2% Si at 900 degrees Celsius.

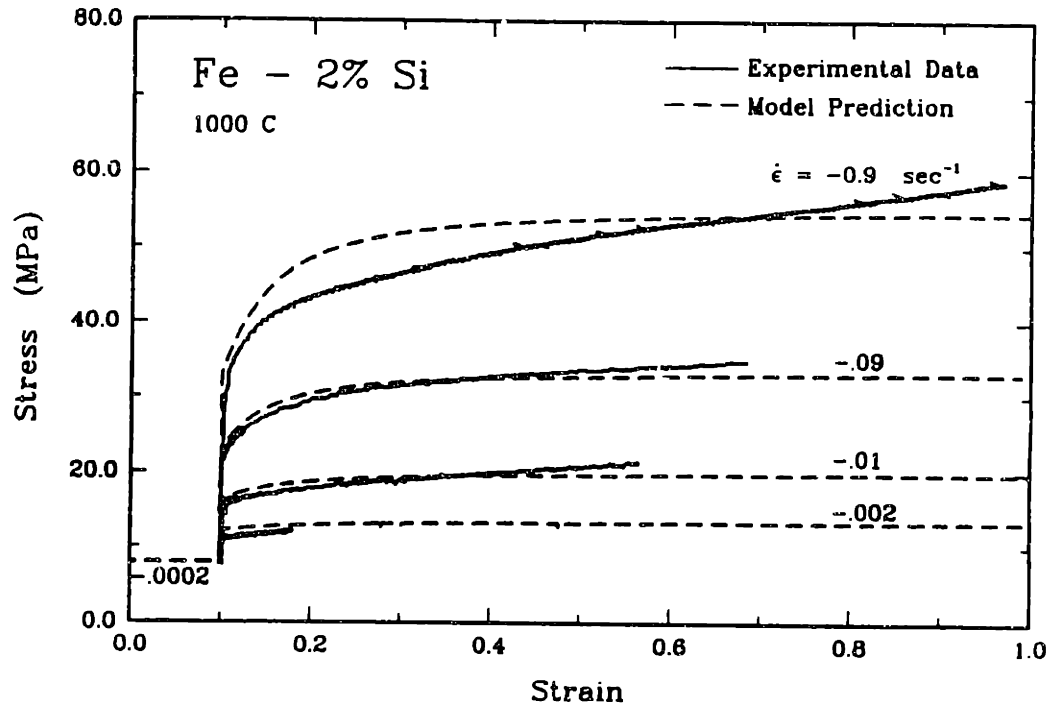


**Figure 6.13** Correlation of constitutive model with strain rate jump test on Fe – 2% Si at 1000 degrees Celsius.

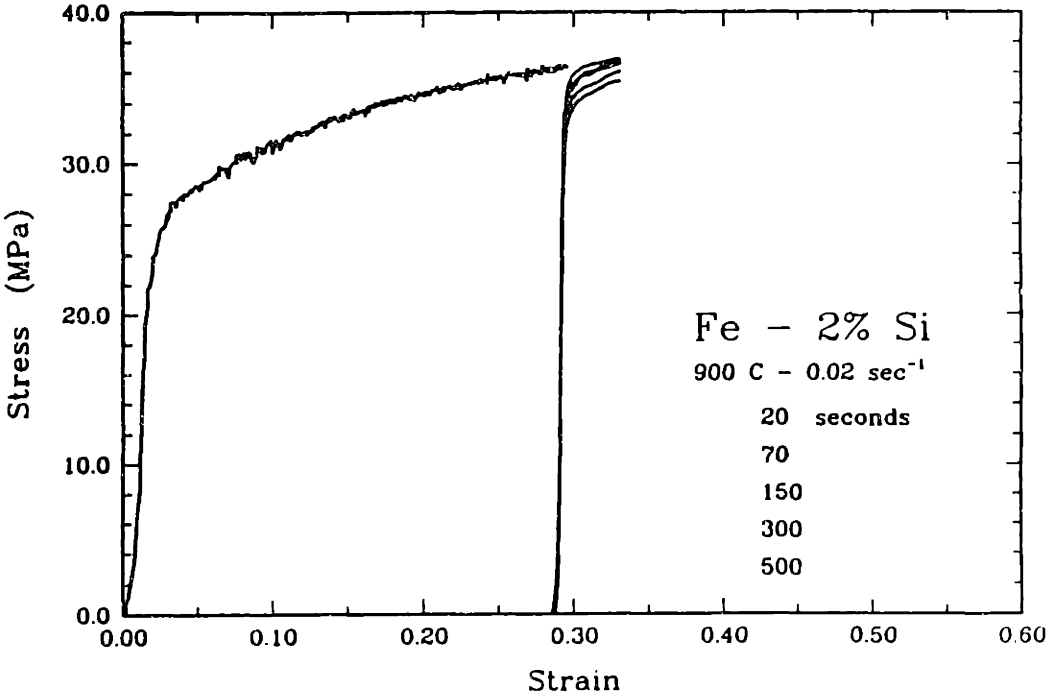


Figure 6.14a Load-unload-hold-reload tests on Fe - 2% Si

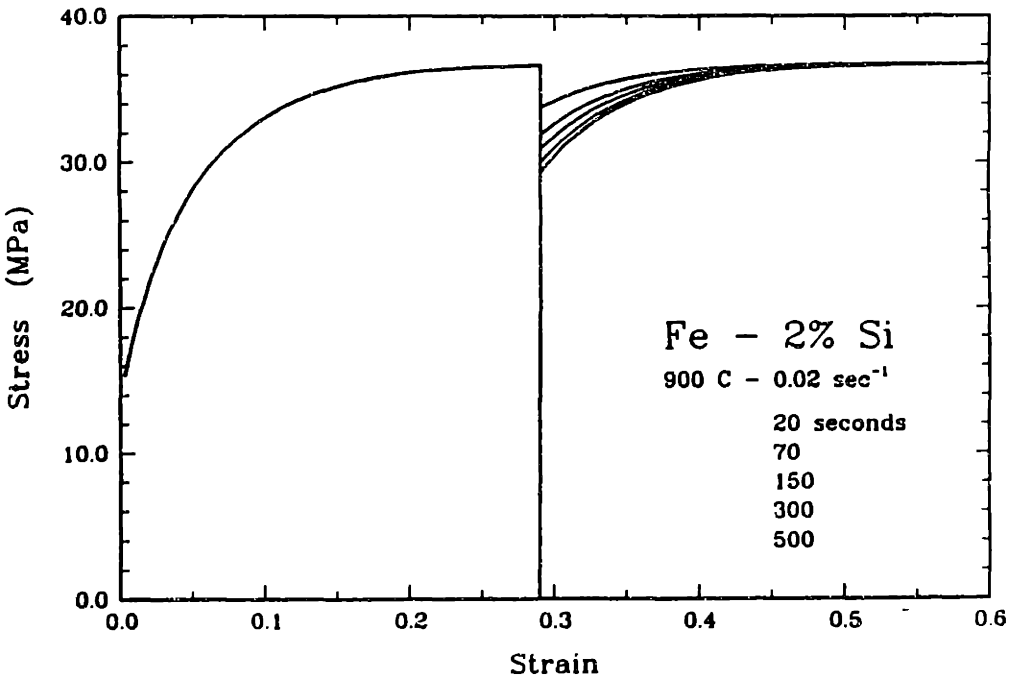


Figure 6.14b Simulation of load-unload-hold-reload tests on Fe - 2% Si.

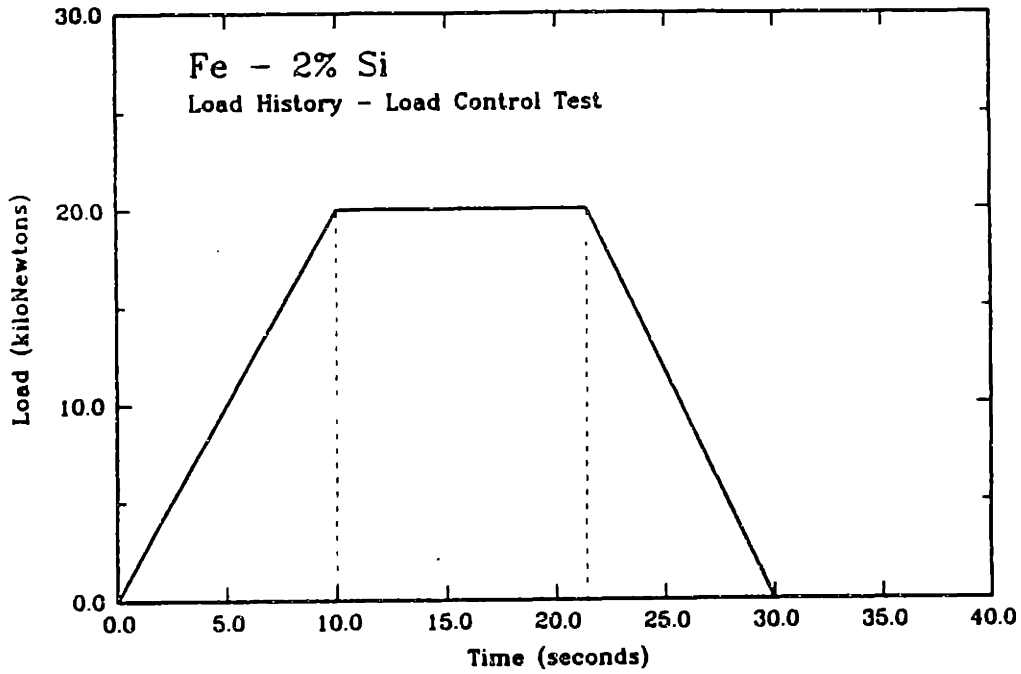


Figure 6.15 Load history used on load boundary condition test of constitutive model.

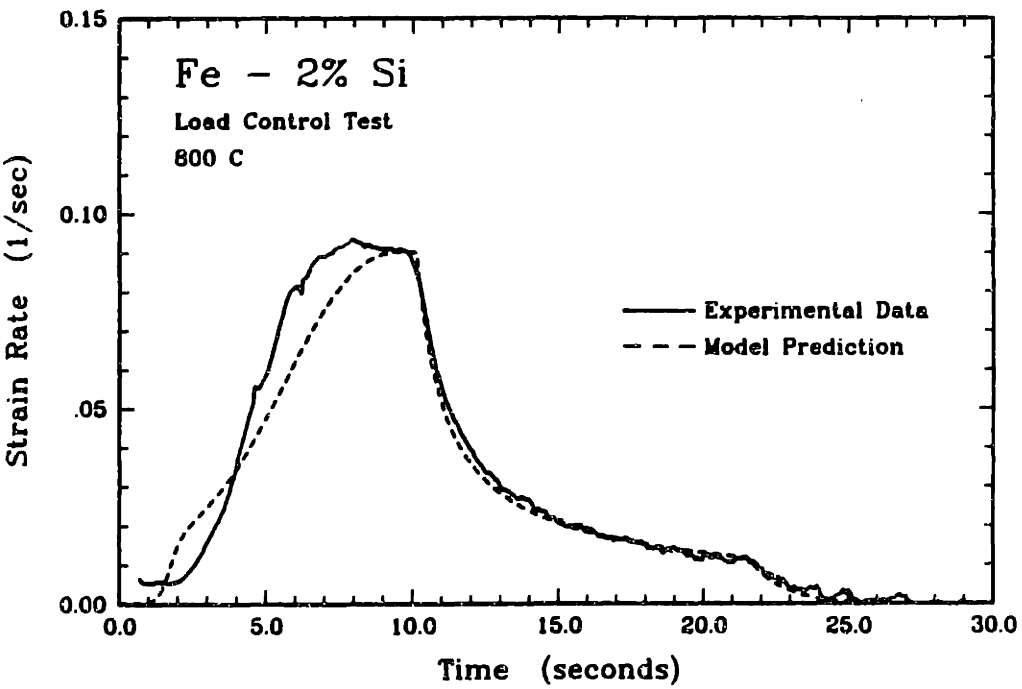


Figure 6.16 Predicted and actual strain rates measured during load boundary condition test on Fe – 2% Si compression specimen.

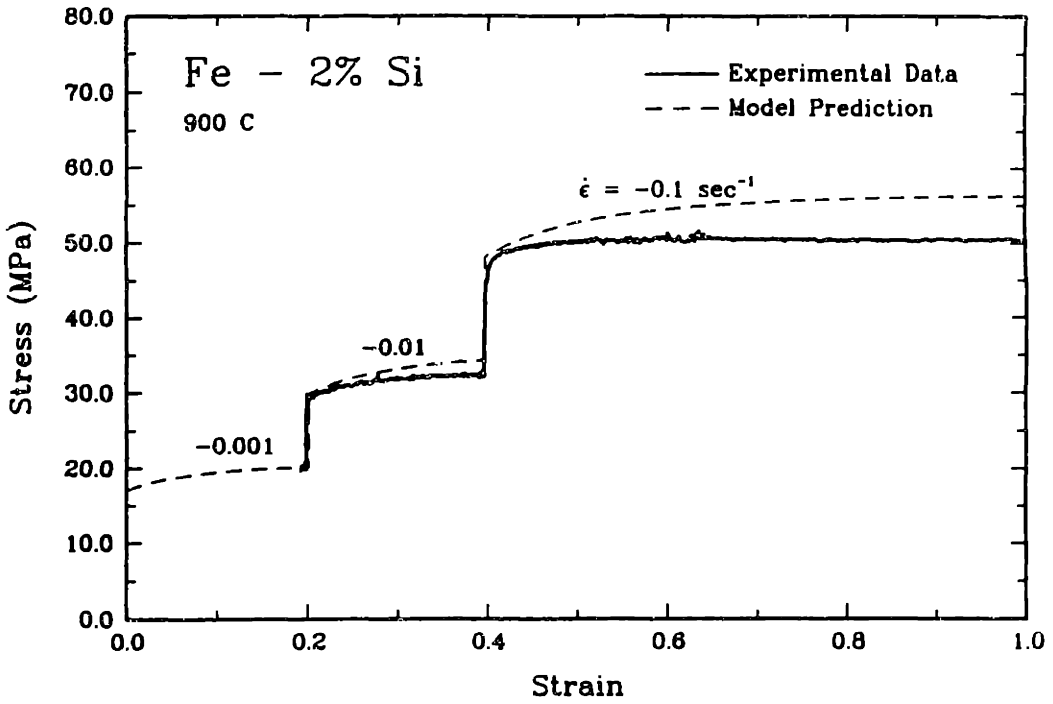


**Figure 6.17** Predicted and actual stress response for double strain rate jump test on Fe – 2% Si.

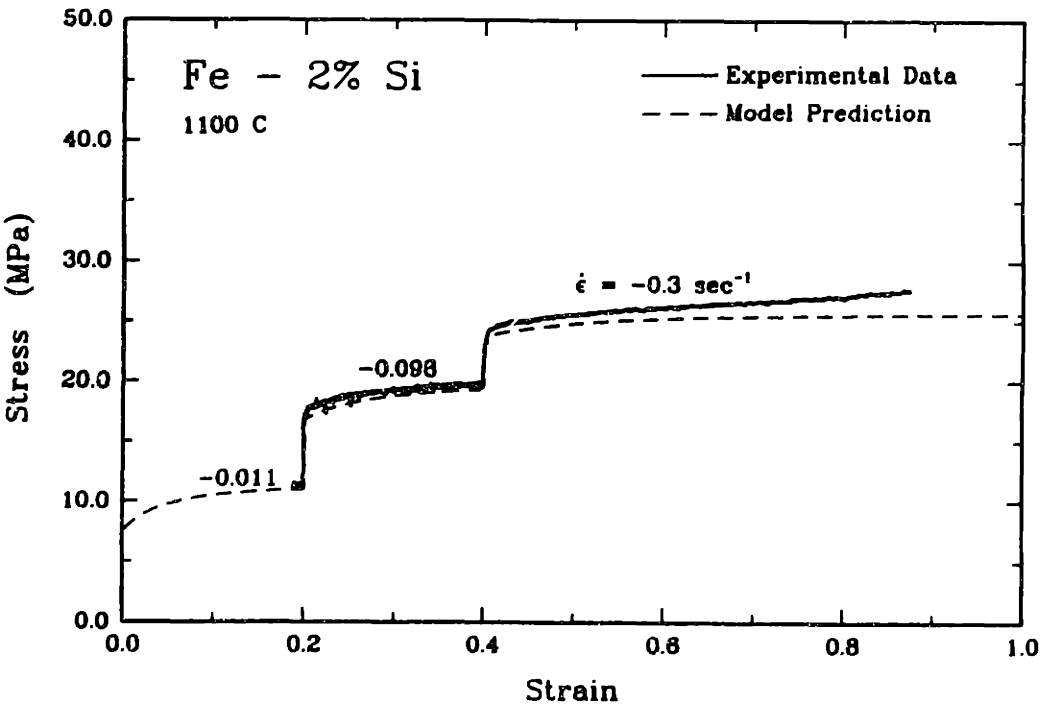


**Figure 6.18** Predicted and actual stress response for double strain rate jump test on Fe – 2% Si

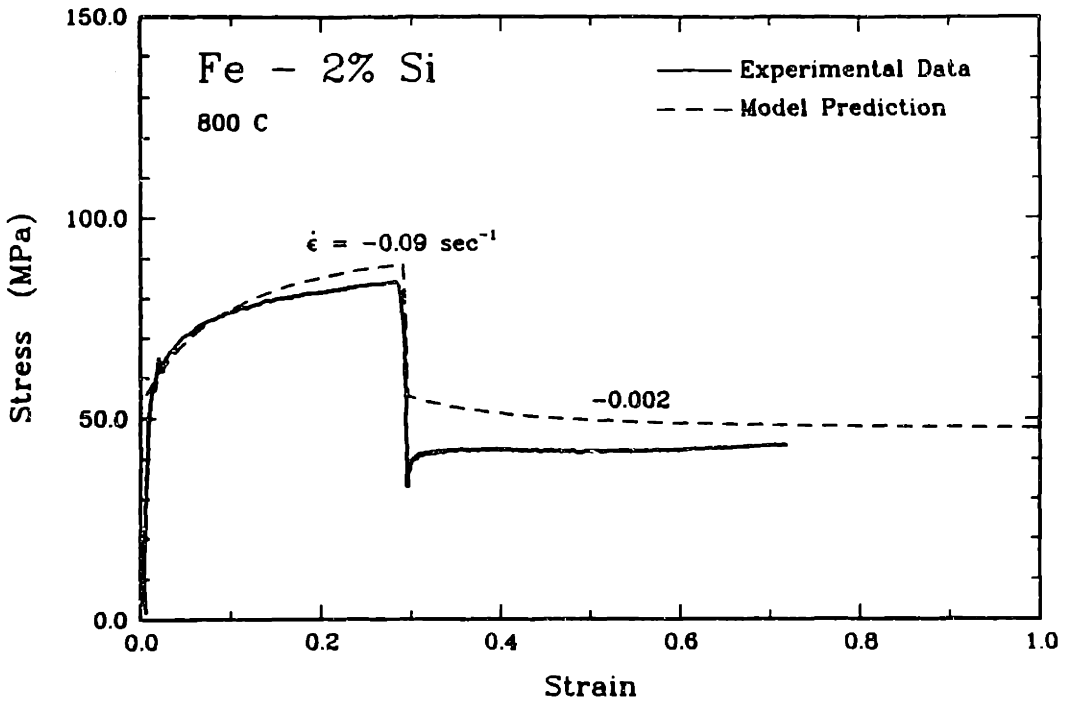


**Figure 6.19** Strain rate decrement test on Fe – 2% Si. Notice that data does not demonstrate strain softening after decrement in strain rate.

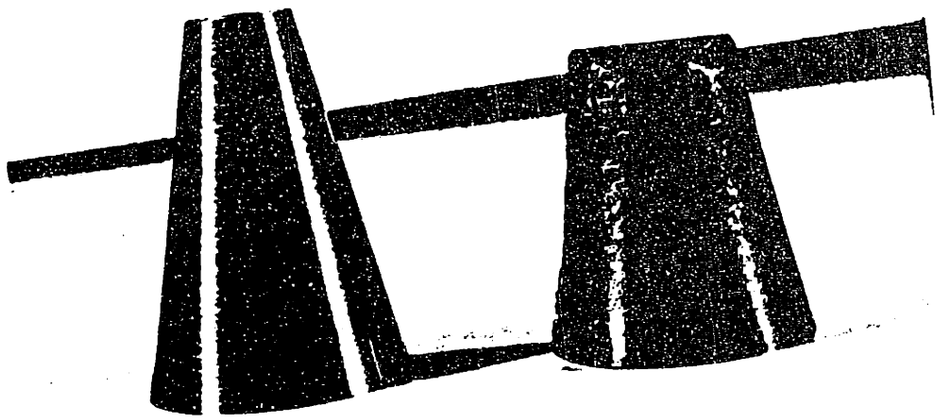

Figure 6.20 State gradient specimen before and after testing.

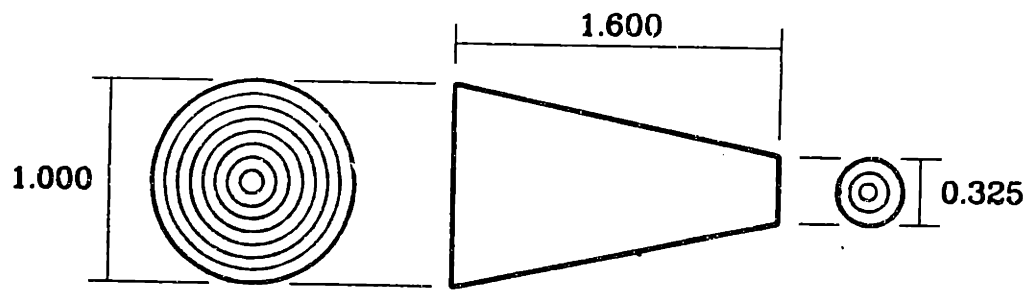


Groove spacing: 0.030
Groove depth : 0.005

Figure 6.21 Dimensions of 1100 Al state gradient specimen. (All dimensions in inches.)

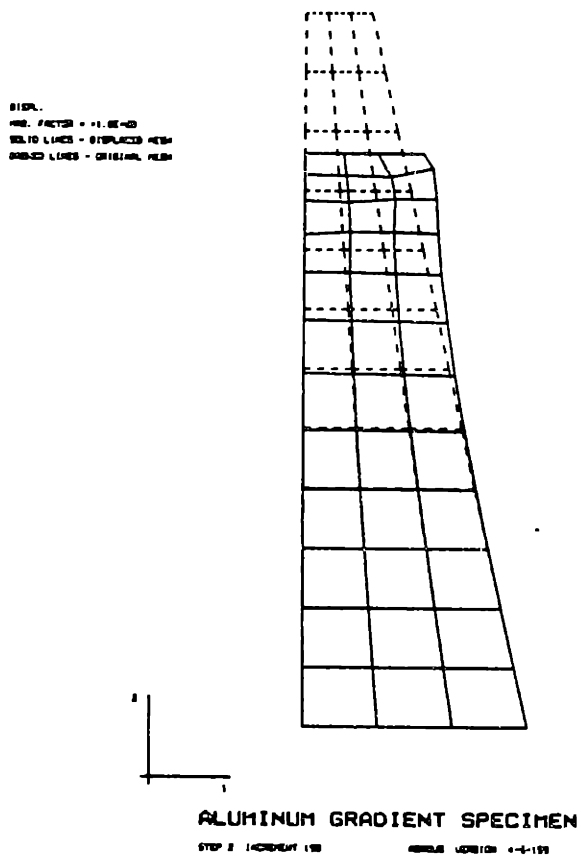


**Figure 6.22 ABAQUS finite element mesh of aluminum state gradient specimen. Figure includes original mesh geometry and shape at end of test simulation.**

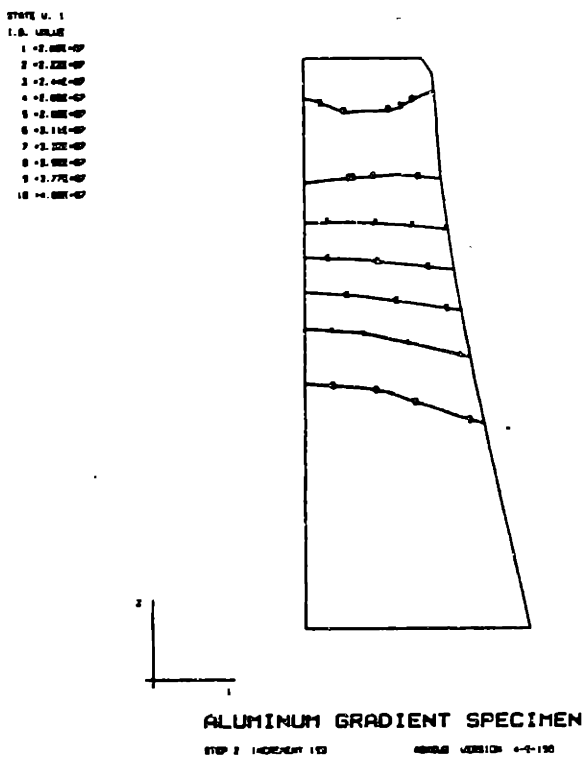


**Figure 6.23 Contours of constant internal variable values from ABAQUS simulation of 1100 aluminum state gradient test. Values indicated in contour table are in terms of equivalent shear stress.**

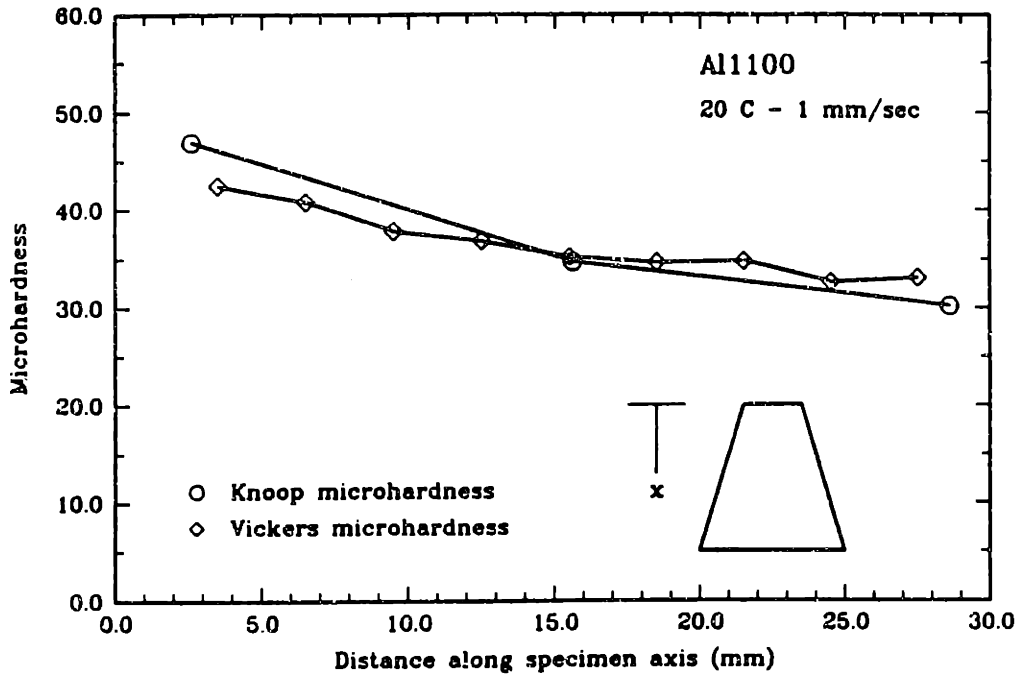


Figure 6.24 Variation in microhardness along central axis of 1100 aluminum gradient specimen. Specimen compressed at room temperature.

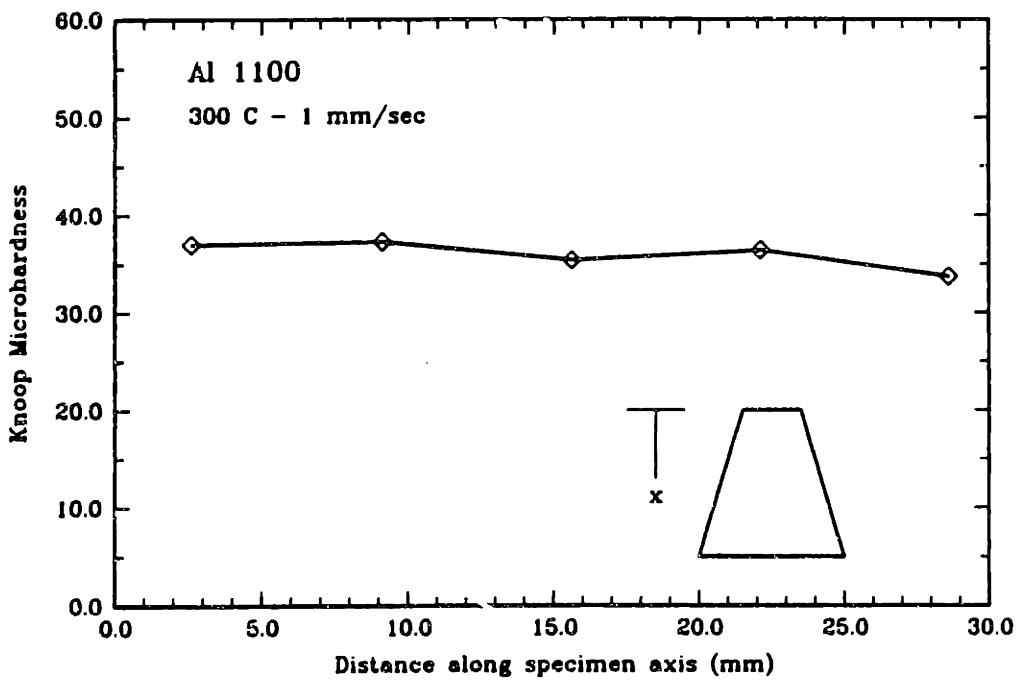


Figure 6.25 Variation in microhardness along central axis of 1100 aluminum gradient specimen. Specimen tested at 300 degrees Celsius and quenched.

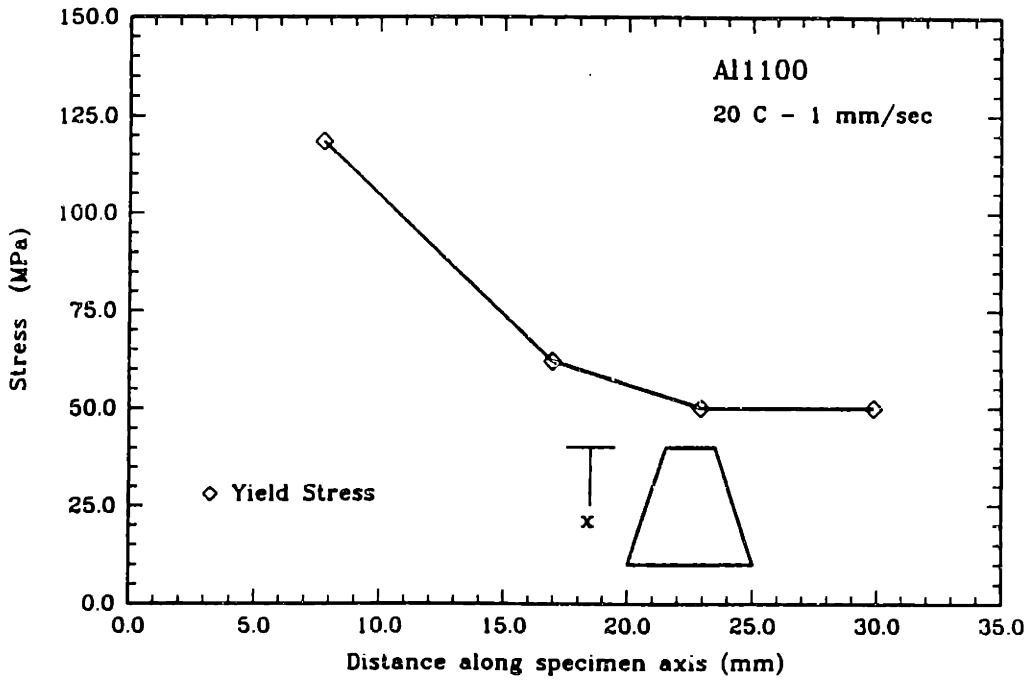


Figure 6.26 Variation in room temperature yield stress along axis of 1100 aluminum gradient specimen. Specimen compressed at room temperature.

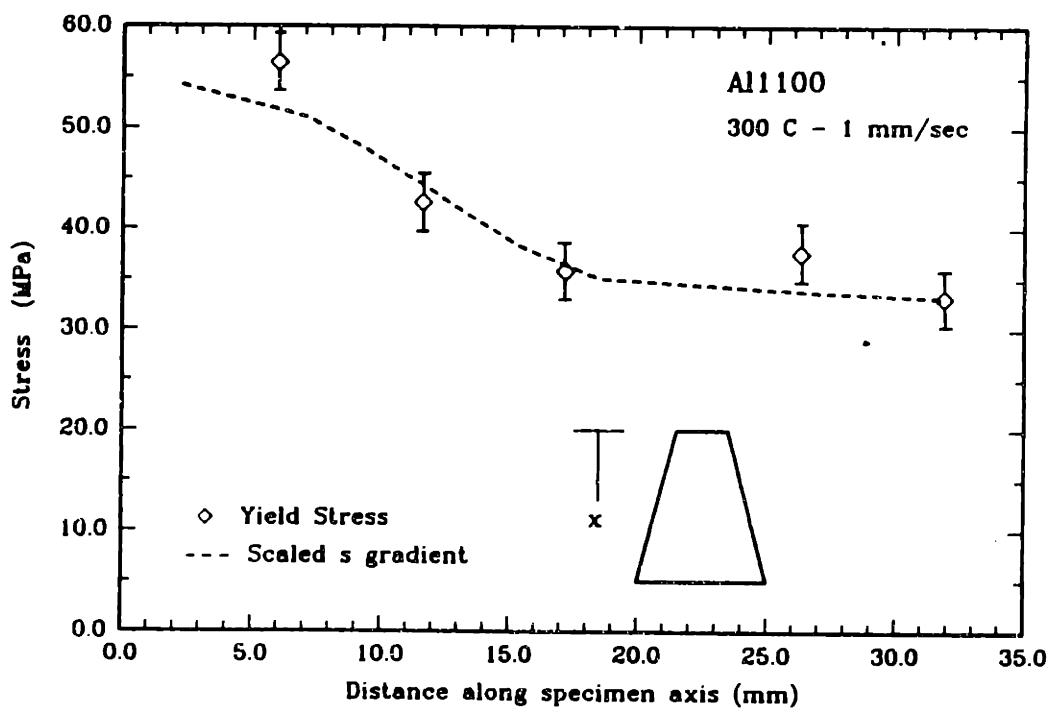


Figure 6.27 Variation in room temperature yield stress along axis of 1100 aluminum gradient specimen. Specimen compressed at 300 degrees Celsius and then quenched.

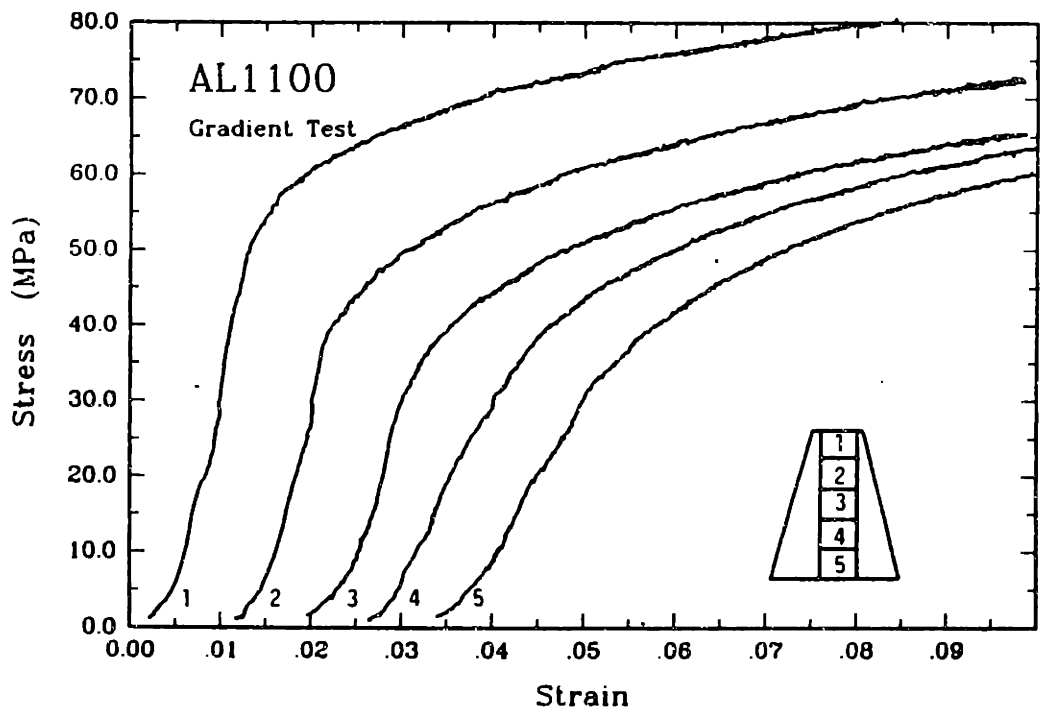


**Figure 6.28** Stress/strain data from compression specimens machined from quenched 1100 aluminum gradient specimen. (Data shifted for comparison.)

# Chapter 7

# Conclusion and Discussion

The success of this constitutive model in representing rate dependent metal deformation supports the notion of the sufficiency of a scalar internal variable model for hot working. Such a result is of significant practical importance. Depending on the forms of the material functions, a single scalar model is most likely easier to fit to test data than multiple variable models. A single scalar model also provides a potential reduction in computational requirements both by simplifying the updating of material states from a tightly coupled, stiff set of nonlinear differential equations and by reducing the number of variable values stored at each integration point in a large finite element model.

The constitutive model developed in this thesis is now being used both to model other metals and to simulate hot working processes. The model, as indicated in Chapter 6, has been applied to a face-centered cubic metal, 1100 aluminum [Kim, et al., 1986]. The correlation between the model and the 1100 aluminum data appears to be better than the correlations presented in this thesis for the iron - 2% silicon alloy. This model employing 1100 aluminum material parameters has been used in ABAQUS finite element simulations of closed die forging operations. The finite element predictions of load histories and material flow agrees well with actual forging tests.

A limitation of this model derives from the fact that anisotropic material behavior has been ignored, with the consequence that errors may develop with large deformations. Small scale anisotropy associated with reversed loading, Bauchinger-type phenomena was reasonably assumed to saturate after a few percent strain, and large scale effects due to the development of texture were ignored primarily because of the current lack of simple techniques for modelling the evolution of crystalline orientation. The fact that the assumption of isotropy was enforced in this investigation through the use of monotonic tests on identically-oriented specimens does not mean however that the texture development in the Fe - 2% Si alloy is insignificant. It would be reasonable in further investigations to investigate the accuracy of the constitutive model as a function of variation of material orientation after large deformations.

The model presented here has been developed for single phase metals under large deformations where the dominant deformation processes are assumed to be thermally activated. Materials which may possess a strong athermal component of deformation resistance, such as precipitation or dispersion strengthened metals therefore may not be well represented.

Several conclusions may be drawn about constitutive models for hot working given the research presented herein:

1. The dependence of strain rate upon stress at a given constant structure is not well represented by a power law, much less by that power law exponent which correlates the steady state stress to the steady state strain rate. Furthermore, given a single internal variable model for creep, where the dependence of strain rate upon stress and state is expressed in the form:

$$\dot{\epsilon} = f(\theta)\left(\frac{\sigma}{s}\right)^n, \qquad 7.1$$

the exponent $n$ should not be the steady state stress exponent. If we expect the steady state value of the internal variable $s$ to increase with stress, $n$ must be greater than the values of 3 to 5 normally associated with creep.

2. If power law breakdown is the result of a change in deformation mechanism, that mechanism is associated with the constant structure kinetics and not with a change in the character of the microstructure. Power law breakdown therefore should be represented in the deformation rate equation.

3. It may be possible to neglect static recovery, i.e., recovery in the absence of load, in simulating many hot working processes. The static recovery rate measured in this investigation did not affect the material response over the range of strain rates and temperatures tested. This restriction applies only to recovery processes; recrystallization if present will most likely effect the material response.

Similarly, some conclusions may be made concerning mechanistically inspired deformation models:

1. Athermal hardening rates measured from this investigation are greater than the theoretical value of $\mu/100$ derived for single crystal deformation. There seems to be no reason to assume *a priori* this value for polycrystalline deformation.

2. There is similarly no reason to assume as do some investigators [Lee and Zaverl, Miller] that the activation energy determined from steady data data should be used to represent temperature dependence in a deformation rate equation where structure is incorporated through internal variables. Activation energies measured from jump test data are different from that obtained from steady state data. The activation energy determined in this investigation from the steady state stress strain rate data for the Fe - 2% Si was 312 kJ/mole, while that determined from the jump test data was 245 kJ/mole.

Internal variable models which postulate separate rate equations for deformation and microstructure evolution requires material data which is generally not available.

The fundamental consideration is that one should perform experiments to characterize each material function unambiguously. Constant structure tests such as the jump tests described in this thesis are essential if one wishes to evaluate or fit the deformation equation to data which represent only deformation kinetics. Similarly, tests designed such that deformation kinetics may either be neglected, as in the load-unload-hold-reload tests, or compensated for in some phenomenological way (e.g. using the constant $c$ in this model) provide data representative of the evolution of structure.

Such testing addresses important questions concerning appropriate material functions. One obvious case in point is the characterization of deformation rate equations like those discussed in Section 4.1.1. Strain rate, stress, and temperature jump tests provide the capability of directly evaluating deformation kinetics. Such techniques are certainly applicable to fundamental investigations on single crystals as well as polycrystalline engineering alloys. It is likely that such experimentation will become more common as internal variable formulations gain acceptance. Such experimentation in conjunction with increased understanding of the processes controlling the evolution of structure may provide, in time, more consensus on the form of constitutive models for high temperature deformation.

## REFERENCES


1. ALEXOPOULOS, P, KEUSSEYAN, R. L., WIRE, G. L., and LI, C. Y., "Experimental Investigation of Nonelastic Deformation Emphasizing Transient Phenomena by Using a State Variable Approach", Mechanical Testing for Deformation Model Development, ASTM STP 765, 1982, pp. 148-184.

2. ANAND, L., "Constitutive Equations for Rate-Dependent Deformation of Metals at Elevated Temperatures," Journal of Engineering Materials and Technology, **104**, January, 1982, pp. 12-17.

3. ANAND, L., "Constitutive Equations for Hot-Working of Metals", International Journal of Plasticity, **1**, 1985, pp. 213-231.

4. ARGON, A., "Physical Basis of Constitutive Equations for Inelastic Deformation," Constitutive Equations in Plasticity, MIT Press, 1975, pp. 1-22.

5. Compression Tests of Metallic Materials at Elevated Temperatures with Conventional or Rapid Heating Rates and Strain Rates, ASTM Standard E 209-65, **3.01**, pp. 389-397.

6. BAILEY, R. W., "Note on the Softening of Strain Hardened Metals and Its Relation to Creep", The Journal of the Institute of Metals, **25-1**, 1926, pp. 27-43.

7. BERGSTROM, Y., "A Dislocation Model for the Stress-Strain Behaviour of Polycrystalline $\alpha$-Fe with Special Emphasis on the Variation of the Densities of Mobile and Immobile Dislocations", Materials Science and Engineering, **5**, 1969/70, pp. 193-200.

8. BERGSTROM, Y. and HALLEN, H., "An Improved Dislocation Model for the Stress-Strain Behaviour of Polycrystalline $\alpha$-Fe", Materials Science and Engineering, **55**, 1982, pp. 49-61.

9. BODNER, S. R., "Constitutive Equations for Elastic-Viscoplastic Strain Hardening Materials", Journal of Applied Mechanics, June 1975, pp. 385-389.

10. BODNER, S. R., "A Hardness Law for Inelastic Deformation", International Journal of Engineering Science, **16**, 1978, pp. 221-230.

11. BODNER, S. R., "Uniaxial Cyclic Loading of Elastic-Viscoplastic Materials", Journal of Applied Mechanics, December, 1979, **46**, pp. 805-810.

12. CERNOCKY, E. P. and KREMPL, E., "A Non-Linear Uniaxial Integral Constitutive Equation Incorporating Rate Effects, Creep and Relaxation", International Journal of Non-Linear Mechanics, **14**, 1979, pp. 183-203.

13. CERNOCKY, E. P. and KREMPL, E., "A Theory of Thermoviscoplasticity Based on Infinitesimal Total Strain," International Journal of Solids and Structures, **16**, 1980, pp. 723-741.

14. CERNOCKY, E. P. and KREMPL, E., "A Theory of Viscoplasticity Based on Infinitesimal Total Strain," Acta Mechanica, **36**, 1980, pp. 263-289.

15. CERNOCKY, E. P., "An Examination of Four Viscoplastic Constitutive Theories in Uniaxial Monotonic Loading," International Journal of Solids and Structures, **18-11**, 1982, pp. 989-1005.

16. CERNOCKY, E. P., "Comparison of the Unloading and Reversed Loading Behavior of Three Viscoplastic Constitutive Theories", International Journal of Non-Linear Mechanics, **17-4**, 1982, pp. 255-266.

17. CERNOCKY, E. P. and KREMPL, E., "Evaluation of a Uniaxial Nonlinear, Second-Order Differential Overstress Model for Rate-Dependence, Creep and Relaxation", International Journal of Solids and Structures, **19-9**, 1983, pp. 753-766.

18. CHABOCHE, J. L.,Bulletin de L'Academie des Sciences, Serie des Sciences Techniques, **25-1**, 1977, p. 33.

19. CHAIT, R. and PAPIRNO, R., Compression Testing of Homogeneous Materials and Composites, ASTM STP 808, 1983.

20. CHAN, K. S., LINDHOLM, U. S., BODNER, S. R., and WALKER, K. P., "A Survey of Unified Constitutive Theories", Nonlinear Constitutive Relations for High Temperature Application - 1984, NASA Conference Publication 2369, 1985, pp. 1-23.

21. COTTRELL, A. H. and AYTEKIN, V., J. Institute of Metals, **77**, 1950, p. 381.

22. CUDDY, L. J., "Internal Stresses and Structures Developed During Creep", Metallurgical Transactions, **1**, February, 1970. pp. 395-401.

23. ESTRIN, Y. and MECKING, H., "A Unified Phenomenological Description of Work Hardening and Creep Based on One-Parameter Models", Acta Metallurgica, **32-1**, 1984, pp. 57-70.

24. GAROFALO, F., "An Empirical Relation Defining the Stress Dependence of Minimum Creep Rate in Metals", Transactions of the AIME, **227**, April, 1963, pp. 351-355.

25. GIBELING, J. C., and NIX, W. D., "Anomalous and Constant Substructure Creep Transients in Pure Aluminum," International Conference on the Strength of Metals and Alloys, ICSMA 6, Pergamon Press, 1982, pp. 613-618.

26. GIBELING, J. C., HOLBROOK, J. H., and NIX, W. D., "A Critical Analysis of the Determination of Deformation Mechanisms by Strain Rate Change Tests", Acta Metallurgica, **32-9**, 1984, pp. 1287-1295.

27. GITTUS, J. H., "A model of Creep Embodying Dislocations whose Movements Produce Work Hardening and Recovery", Philosophical Magazine, 1970.

28. GURTIN, M. E., An Introduction to Continuum Mechanics, Academic Press, New York.

29. HALLEN, H., "A Theory of Dynamic Recovery in F.C.C. Metals", Materials Science and Engineering, **72**, 1985, pp. 119-123.

30. HART, E. W., "A Phenomenological Theory for Plastic Deformation of Polycrystalline Metals", Acta Metallurgica, **18**, 1970, pp. 599-610.

31. HART, E. W. and SOLOMON, H. D., "Load Relaxation Studies of Polycrystalline High Purity Aluminum", Acta Metallurgica, **21-3**, March, 1973, pp. 295-307.

32. HART, E. W., "Constitutive Relations for the Nonelastic Deformation of Metals", Journal of Engineering Materials and Technology, July, 1976, pp. 193-202.

33. HART, E. W., "Load Relaxation Testing and Material Constitutive Relations", Stress Relaxation Testing, ASTM STP 676, 1979, pp. 983-991.

34. HECKER, S. S., STOUT, M. G., and EASH, D. T., "Experiments on Plastic Deformation at Finite Strains", Plasticity of Metals at Finite Strain: Theory, Experiment and Computation, E. H. Lee and R. L. Mallett, ed., Proceeding of Research Workshop held at Stanford University, June 29 - July 1, 1981, pp. 162-205.

35. HSU, T. C., "A Study of the Compression Test for Ductile Materials", Materials Research and Standards, **9-12**, 1969, pp. 20-23.

36. HU, Transactions of the Metallurgical Society of the AIME, **230**, 1964, p 230.

37. IMMARIGEON, J. P., Laboratory Technical Report LTR-ST-786, National Aero. Est., Canada, 1975.

38. IMSL Library, IMSL Inc., NBC Building, 7500 Bellaire Boulevard, Houston, Texas, 770036-5085, 1984 version.

39. JONAS, J. J., SELLARS, C. M., and TEGART, W. J. McG., "Strength and Structure under Hot Working Conditions", Metallurgical Reviews, Review **130**, The Metals and Metallurgy Trust, 1969.

40. JONAS, J. J., "The Back Stress in High Temperature Deformation," Acta Metallurgica, **17**, April, 1969, pp. 397-405.

41. KIM, K. H., LUSH, A. M., and ANAND, L. "Constitutive Equations and Computational Procedures for Hot Working of Metals", Proceedings of 13th Conference on Production Research and Technology, November 18-21, 1986, pp. 231-241.

42. KLEPACZKO, J., "Strain Rate History Effects for Polycrystalline Aluminum and Theory of Intersections", Journal Mechanics and Physics of Solids, **16**, 1968, pp. 255-266.

43. KLEPACZKO, J., FRANTZ, R. A., and DUFFY, J., "History Effects in Polycrystalline FCC Metals Subjected to Rapid Changes in Strain Rate and Temperature," Rozprawy Inzynierskie, Engineering Transactions, **25-1**, 1977, pp. 3-22.

44. KLEPACZKO, J. and DUFFY, J., "History Effects in Polycrystalline BCC metals and steel subjected to rapid changes in strain rate and temperature", Reference incomplete, 1982, pp. 419-436.

45. KLEPACZKO, J. and DUFFY, J., "Strain Rate History Effects in Body-Centered-Cubic Metals", Mechanical Testing for Deformation Model Development, ASTM STP 765, 1982, pp. 251-268.

46. KLEPACZKO, J. and CHIEM, C. Y., "On Rate Sensitivity of FCC Metals, Instantaneous Rate Sensitivity, and Rate Sensitivity of Strain Hardening", Journal Mechanics and Physics of Solids, **34-1**, 1986, pp. 29-54.

47. KOCKS, U. F., "A Statistical Theory of Flow Stress and Workhardening", The Philosophical Magazine, **8**, June, 1966, pp. 541-566.

48. KOCKS, U. F., ARGON, A. S., and ASHBY, M. F., "Thermodynamics and Kinetics of Slip", Progress in Materials Science **19**, Pergamon, 1975.

49. KOCKS, U. F., "Recovery Glide Theory of Creep", Proceedings, ASM Symposium, Rate Processes in Plastic Deformation of Materials, Ed. J.C.M. Li, 1975, pp. 356-383.

50. KOCKS, U. F., "Laws for Work-Hardening and Low-Temperature Creep", Journal of Engineering Materials and Technology, January, 1976, pp. 76-85.

51. KOCKS, U. F., "Strain Hardening and Strain Rate Hardening", Mechanical Testing for Deformation Model Development, ASTM STP 765, 1982, pp. 121-138.

52. KREMPL, E., McMAHON, J. J., and YAO, D., "Viscoplasticity Based on Overstress with a Differential Growth Law for the Equilibrium Stress," 2nd Symposium on Nonlinear Constitutive Relations for High Temperature Applications, NASA Conference Publication 2369, 1985, pp. 25-50.

53. KUHLMANN-WILSDORF, D., "Theory of Workhardening 1934-1984", Metallurgical Transactions A, **16A**, December, 1985, pp. 2091-2108.

54. LEE, D, and ZAVERL, F., "A Generalized Strain Rate Dependent Constitutive Equation for Anisotropic Metals", Acta Metallurgica, **26**, 1978, pp. 1771-1780.

55. LEE, D. and ZAVERL, F., "Further Development of Generalized Constitutive Relations for Metal Deformation", Metallurgical Transactions, **11A**, June, 1980, pp. 983-991.

56. LEE, D. and ZAVERL, F., "Development of Constitutive Equations for Nuclear Reactor Core Materials", Journal of Nuclear Materials, **88**, 1980, pp. 104-110.

57. LEE, E. H., "Elastic-Plastic Deformations at Finite Strains", Journal of Applied Mechanics, **36**, p. 1.

58. LI, C. Y., "State Variable Theories for Nonelastic Deformation", Metallurgical Treatises, AIME, ed. John Tien etal., AIME, 1981, pp. 469-486.

59. LI, J. C. M., Notes on Garofalo paper in same volume, Transactions of the AIME, **227**, December, 1963, pp. 1474-1477.

60. LOWE, T. C, and MILLER, A. K., "A Materials Model for Strain Softening with Applications in Modelling Strain Localization," 4th International Conference on Mechanical Behavior of Materials, Stockholm, August, 1983.

61. LUTON, M. J., PETKOVIC, R. A., and JONAS, J. J., "Kinetics of Recovery and Recrystallization in Polycrystalline Copper", Acta Metallurgica, 1980, **28**, pp. 729-741.

62. LYTTON, J. L., BARRETT, C. R., and SHERBY, O. D., "Substructure Formation During High-Temperature Creep of (110)[001]-Oriented Polycrystalline Fe – 3.1 % Si." Transactions of the Metallurgical Society of the AIME, **233**, July, 1965, pp. 1399-1408.

63. McCLINTOCK, F. A., and ARGON, A. S., "Mechanical Behavior of Materials", Addison-Wesley, 1966.

64. McQUEEN, H. J., "The Experimental Roots of Thermomechanical Treatments for Aluminum Alloys", Thermomechanical Processing of Aluminum Alloys, Edited by James G. Morris, AIME, 1979.

65. McQUEEN, H. J., "Review of Simulations of Multistage Hot-Forming of Steels", Canadian Metallurgical Quarterly, **21**, 1982, pp. 445.

66. McQUEEN, H. J. and JONAS, J. J., "Recent Advances in Hot Working: Fundamental Dynamic Softening Mechanisms", Journal of Applied Metalworking, **3-3**, July, 1984, pp. 233-241.

67. McQUEEN, H. J. and JONAS, J. J., "Role of the Dynamic and Static Softening Mechanisms in Multistage Hot Working," Journal of Applied Metalworking, **3-4**, January, 1985, pp. 410-420.

68. MECKING, H. and KIRCH, F., "Recovery and Recrystallization During Deformation", Recrystallization of Metallic Materials, F. Haessner, ed., 1970, pp. 257-288.

69. MECKING, H. and KOCKS, U. F., "Kinetics of Flow and Strain Hardening", Acta Metallurgica, **29**, 1981, pp. 1675-1685.

70. MECKING, H., NICKLAS, B., ZARUBOVA, N., and KOCKS, U. F., "A Universal Temperature Scale for Plastic Flow", Acta Metallurgica, **34-3**, 1986, pp. 527-535.

71. MIHRAM, G. A., Simulation, Statistical Foundations and Methodology, Academic Press, 1972.

72. MILLER, A. K., "An Inelastic Constitutive Model for Monotonic, Cyclic, and Creep Deformation: Part I - Equations, Development, and Analytical Procedures, and Part II Application to Type 304 Stainless Steel," Journal of Engineering Materials and Technology, **98-2**, 1976, pp. 97-113.

73. MILLER. A. K. and SHERBY, O. D., "A Simplified Phenomenological Model for Non-elastic Deformation: Prediction of Pure Aluminum Behavior and Incorporation of Solute Strengthening Effects," Acta Metallurgica, **26**, 1978, pp. 289-304.

74. MILLER, A. K., "Unified Constitutive Equations for Time-Dependent Plasticity," Plasticity of Metals at Finite Strain, E.H. Lee and R.L. Mallett, ed. Stanford University Div. of Applied Mechanics, 1982, pp. 130-160.

75. MITRA, S. K. and McLEAN, D., "Work Hardening and Recovery in Creep," Proc. Royal Society A, **295**, 1966, p. 288.

76. MITRA, S. K. and McLean, D., Journal of Metallurgical Science, **1**, 1967, p. 192.

77. NIEDENZU, K. and DAWSON, J. W., "Boron-Nitrogen Compounds", Springer-Verlag, 1965.

78. NIX, W. D., GIBELING, J. C., and HUGHES, D. A., "Time-Dependent Deformation of Metals", Metallurgical Transactions A, **16A**, December, 1985, pp. 2215-2226.

79. OROWAN, E., Proceedings Royal Society of London, **52**, 1940.

80. OROWAN, E., "The Creep of Metals", Journal West Scotland Iron and Steel Institute, **54**, 1946-47, pp. 45-96.

81. PETKOVIC, R. A., LUTON, M. J., and JONAS, J. J., "Recovery and Recrystallization of Polycrystalline Copper After Hot Working", Acta Metallurgica, **27**, 1979, pp. 1633-1648.

82. PRINZ, F. B. and ARGON, A. S., "The Evolution of Plastic Resistance in Large Strain Plastic Flow of Single Phase Subgrain Forming Metals", Acta Metallurgica, **32-7**, 1984, pp. 1021-1028.

83. RHODE, R. W. and NORDSTROM, T. V., Scripta Metallurgica, **7**, 1973, p. 1227.

84. RICE, J. R., "On the Structure of Stress-Strain Relations for Time-Dependent Plastic Deformation of Metals", Journal of Applied Mechanics, September, 1970, pp. 728-737.

85. RICE, J. R., "Continuum Mechanics and Thermodynamics of Plasticity in Relation to Microscale Deformation Mechanisms", Constitutive Equations in Plasticity, M.I.T. Press, 1975, pp. 22-79.

86. RUINA, A., "Slip Instability and State Variable Friction Laws", Journal of Geophysical Research, **88-B12**, December 10, 1983, pp. 10359-10370.

87. RYAN, N. D., McQUEEN, H. J., and JONAS, J. J., "The Deformation Behavior of Types 304, 316, and 317 Austenitic Stainless Steels During Hot Torsion", Canadian Metals Quarterly, **22-3**, 1983, pp. 369-378.

88. SANKAR, J., HAWKINS, D., and McQUEEN, H. J., "Behavior of Low-Carbon and HSLA Steels During Torsion-Simulated Continuous and Interrupted Hot-Rolling Practice", Metals Technology, September, 1979, pp. 325-331.

89. SCHMIDT, C. G. and MILLER, A. K., "A Unified Phenomenological Model for Non-Elastic Deformation of Type 316 Stainless Steel, Part I: Derivation of the Model and Part II, Fitting and Predictive Capabilities," Res Mechanica, **3**, 1981, pp. 109-129 and 175-193.

90. SELLARS, C. M. and Tegart, W. J. McG., "Hot Workability", International Metallurgical Reviews, 1972, **17**, pp. 1-24.

91. SELLARS, C. M., "Recrystallization of Metals During Hot Deformation", Phil. Transactions of the Royal Society of London, A-288, 1978, pp. 147-158.

92. SELLARS, C. M. and WHITEMAN, J. A., "Recrystallization and Grain Growth in Hot Rolling", Metal Science, March-April, 1979, pp. 187-194.

93. SEMIATIN, S. L. and LAHOTI, G. D., "The Forging of Metals," Scientific American, **245-2**, August, 1981, pp. 98-106.

94. SHANNON, R. E., Systems Simulation, the Art and Science, Prentice Hall, 1975.

95. SHERBY, O. D., LYTTON, J. L., and DORN, J. E., "Activation Energies for Creep of High Purity Aluminum", Acta Metallurgica, **5**, April, 1957, pp. 219-227.

96. SHERBY, O. D. and BURKE, P. M., "Mechanical Behavior of Crystalline Solids at Elevated Temperature", Progress in Materials Science **13**, Pergamon, 1968.

97. SHERBY, O. D. and YOUNG, C, "Some Factors Influencing the Strain Rate-Temperature Dependence of the Flow Stress in Polycrystalline Solids", Rate Processes in Plastic Deformation of Materials, Proceedings of the John E. Dorn Symposium, ASM, J. C. M. Li and A. K. Mukherjee, ed., pp. 497-541.

98. SHERBY, O. D., KLUNDT, R. H., and MILLER., A. K., "Flow Stress, Subgrain Size, and Subgrain Stability at Elevated Temperature", Metallurgical Transactions A, **8A**, June 1977, pp. 843-850.

99. STOUFFER, D. C. and BODNER, S. R., "A Constitutive Model for the Deformation Induced Anisotropic Plastic Flow of Metals", International Journal of Engineering Science, **17**, 1979, pp. 757-764.

100. SWEARENGEN, J. C., ROHDE, R. W., and HICKS, D. L., "Mechanical State Relations for Inelastic Deformation of Iron: the Choice of Variables", Acta Metallurgica, **24**, 1976, pp. 969-975.

101. SWEARENGEN, J. C., LOWER, T. C., and LIPKIN, J., "Constitutive Equations for Rate-Dependent Plasticity", Annual Review of Materials Science, 1985, pp. 249-270.

102. TAKEUCHI, S. and ARGON, A. S., "Steady State Creep of Single Phase Crystalline Matter at High Temperature", Journal of Materials Science, **11**, 1976, pp. 1542-1566.

103. THOMSEN, E. G., YANG, C. T., KOBAYASHI, S., "Mechanics of Plastic Deformation in Metal Processing,", Macmillan Company, 1965.

104. UVIRA, J. L. and JONAS, J. J., "Hot Compression of Armco Iron and Silicon Steel", Transactions of the Metallurgical Society of the AIME, **242**, August, 1968, pp. 1619-1626.

105. VALANIS, K. C., "A Theory of Viscoplasticity Without a Yield Surface", Archives of Mechanics, **23-4**, 1971, pp. 517-551.

106. WANG, C. C., "A New Representation Theorem for Isotropic Functions", Archives of Rational Mechanics & Analysis, **36**, p. 166 and 198.

107. WONG, W. A. and JONAS, J. J., "Aluminum Extrusion as a Thermally Activated Process", Transactions of the AIME, **242**, November 1968, pp. 2271-2280.

108. YOSHINAGA, H., HORITA, Z., and KURISHITA, H., "Determination of High-Temperature Deformation Mechanism in Crystalline Materials by the Strain-Rate Change Test", Acta Metallurgica, **29**, 1981, pp. 1815-1824.

109. YOUNG, C. M. and SHERBY, O. D., "Subgrain Formation and Subgrain-Boundary Strengthening in Iron-Based Materials", Journal of the Iron and Steel Institute, September, 1973, pp. 640-647.

110. ZENER, C. and HOLLOMAN, J. H., "Effect of Strain Rate Upon Plastic Flow of Steel", Journal of Applied Physics, **15**, January, 1944, pp. 22-32.

## LIST OF FIGURES

Figure 4.19 Load-unload-hold-reload test series schematic used to evaluate rate of static recovery.

Figure 4.20 Hold period versus stress obtained immediately after reloading from hold period. Each point represents one hold period. Points are for illustration only; they do not represent data.

Figure 4.21 Schematic of load-unload-hold-reload data treated in manner suggested by equation 4.2.11. Curve is for illustration only; it does not represent actual test data.

Figure 4.22 Multiple hold test data for Fe - 2% Si. Test performed at 800 degrees Celsius with 0.1 constant true strain rate. Hold period all all cases was 20 seconds.

Figure 4.23 Multiple hold test data for Fe - 2% Si. Test performed at 900 degrees Celsius with 0.1 constant true strain rate. Hold period all all cases was 20 seconds.

Figure 4.24 Multiple hold test data for Fe - 2% Si. Test performed at 1000 degrees Celsius with 0.1 constant true strain rate. Hold period all all cases was 20 seconds.

Figure 4.25 Multiple hold test data for Fe - 2% Si. Test performed at 1100 degrees Celsius with 0.1 constant true strain rate. Hold period all all cases was 20 seconds.

Figure 4.26 Fractional softening as function of strain, determined from multiple hold tests on Fe - 2% Si.

Figure 4.27 Load-unload-hold-reload tests on Fe - 2% Si. Data indicated represent reload segment. Data has been shifted horizontally to superimpose elastic slopes.

Figure 4.28 Hold period versus stress upon reloading for Fe – 2% Si. Tests performed at 900 degrees Celsius and at 0.02 1/sec constant true strain rate.

Figure 4.29 Recovery function dependence on state for Fe – 2% Si. Data obtained by treatment of Figure 4.28 according to equation 4.2.11.

Figure 4.30 Fit of power law, static recovery function to Fe – 2% Si recovery test data.

Figure 4.31 Schematic of isothermal, constant true strain rate test in stress, temperature, strain rate space. Material begins at state $s_0$ and reaches a steady state value of $s^*$.

## LIST OF TABLES

# APPENDIX A

## Summaries of Constitutive Models

## CONSTITUTIVE MODEL SUMMARY

1. **Authors:** S.R. Bodner, Y. Partom, D.C. Stouffer

2. **Papers:**


1. D. C. Stouffer and S. R. Bodner, "A Constitutive Model for the Deformation Induced Anisotropic Plastic Flow of Metals," International Journal of Engineering Science, Vol. 17, 1979, pp. 757-764.
2. S. R. Bodner, "Uniaxial Cyclic Loading of Elastic-Viscoplastic Materials," Journal of Applied Mechanics, December, 1979, Vol. 46, pp. 805-801.
3. S. R. Bodner, "A Hardness Law for Inelastic Deformation," International Journal of Engineering Science, Vol. 16, 1978, pp. 221-230.
4. S. R. Bodner, "Constitutive Equations for Elastic-Viscoplastic Strain-Hardening Materials," Journal of Applied Mechanics, June, 1975, pp. 385-389.


3. **Constitutive Model:**

$$D_{ij} = D^e_{ij} + D^p_{ij} \tag{1}$$

where

$$L_{ij} = D_{ij} + W_{ij} \tag{2}$$

$$D^p_2 = (1/2) D^p_{ij} D^p_{ij} \tag{3}$$

$$J_2 = (1/2)\sigma'_{ij}\sigma'_{ij} \tag{4}$$

Rate equation

$$D^p_{ij} = D_0 \exp\left[-\frac{1}{2}\left(\frac{Z^2_{klmn}}{J_2}\right)^n\right]\frac{\sigma'_{ij}}{\sqrt{J_2}} \tag{5}$$

Evolution equations (ambiguous)

$$Z_{ijkl} = Z_{0_{ijkl}} + e_{ijkl}\int_0^t q\dot{z}(\tau)d\tau + e_{ijkl}\frac{D_{mn}}{D^p_2}\int_0^t (1-q)\dot{z}(\tau)\frac{D_{mn}}{D^p_2}d\tau \tag{6}$$

$$\dot{z} = m(z_1 - z_0)\exp[-mW^p]\dot{W}^p = m(z_1 - z_0)\sigma_{ij}D^p_{ij} \tag{7}$$

Secondary equations

$$e_{ij} = \text{basis of} \quad Z_{0_{ijkl}} \tag{8}$$

Isotropic case:

$$D^p_{ij} = D_0 \exp\left[-\frac{1}{2}\left(\frac{z^2}{J_2}\right)^n\right]\frac{\sigma'_{ij}}{\sqrt{J_2}} \tag{9}$$

Material Constants:

| Constant | Name |
|---|---|
| $D_0$ | preexponential multiplier |
| n | |
| $Z_1$ | saturation value of Z |
| m | |

Internal Variables:

| Symbol | Name |
|---|---|
| $W^P$ | plastic work |
| Z | Fourth order anisotropy tensor |

## 4. Experiments:

1. Type: Constant strain rate, jump, relaxation, unload/reload
   Material: Titanium RMI-40
   Source: Reference 4
   Temperature: room temp
   Strain rates: $1.6 \times 10^{-6}$ to $3.2 \times 10^{-3}$
2. Type: Cyclic
   Material: Titanium, Copper, Aluminum
   Source: Reference 2
   Temperature: room temperature
   Strain rates: $2 \times 10^{-4}$ to $2 \times 10^{-2}$

## 5. Material constant determination:

1. Not indicated.

## 6. Mechanisms mentionned: none

## 8. Summary:

1. All tests at room temperature, no thermal effects.
2. Plastic work is an internal variable.
4. No recovery.

## CONSTITUTIVE MODEL SUMMARY

**1. Authors:** E. P. Cernocky and E. Krempl

**2. Papers:**


1. E. P. Cernocky and E. Krempl, "Evaluation of a Uniaxial Nonlinear, Second-Order Differential Overstress Model for Rate-Dependence, Creep and Relaxation", International Journal of Solids and Structures, 19-9, 1983, pp. 753-766.
2. E. P. Cernocky and E. Krempl, "A Non-Linear Uniaxial Integral Constitutive Equation Incorporating Rate Effects, Creep and Relaxation", International Journal of Non-Linear Mechanics, 14, 1979, pp. 183-203.
3. E. P. Cernocky and E. Krempl, "A Theory of Thermoviscoplasticity Based on Infinitesimal Total Strain," International Journal of Solids and Structures, 16, 1980, pp. 723-741.
4. E. P. Cernocky and K. Krempl, "A Theory of Viscoplasticity Based on Infinitesimal Total Strain," Acta Mechanica, 36, 1980, pp. 263-289.
5. E. P. Cernocky, "An Examination of Four Viscoplastic Constitutive Theories in Uniaxial Monotonic Loading," International Journal of Solids and Structures, 18-11, 1982, pp. 989-1005.
6. E. P. Cernocky, "Comparison of the Unloading and Reversed Loading Behavior of Three Viscoplastic Constitutive Theories", International Journal of Non-Linear Mechanics, 17-4, 1982, pp. 255-266.


**3. Constitutive Model:**

Stress/strain rate/temperature relationship

$$\sigma_{ij} = m[\sigma_{ij}, \epsilon_{ij}, \theta]\dot{\psi}_{ij} - k[\sigma_{ij}, \epsilon_{ij}, \theta]\dot{\sigma}_{ij} + G_{ij}[\epsilon_{ij}, \theta] \tag{1}$$

where

$$\psi_{ij} = \frac{\nu\epsilon_{nn}}{(1+\nu)(1-2\nu)}\delta_{ij} + \frac{\epsilon_{ij}}{(1+\nu)} - \frac{\alpha}{(1-2\nu)}(\theta-\theta_0)\delta_{ij} \tag{2}$$

and the overstress magnitude is defined as:

$$\Gamma = \{(\sigma_{ij} - G_{ij}[\ \ ])(\sigma_{ij} - G_{ij}[\ \ ])\}^{1/2}. \tag{3}$$

Also,

$$\frac{m[\Gamma]}{k[\Gamma]} = E[\theta], \tag{4}$$

$G_{ij}$ are called the equilibrium stress/strain curves, and is represented by:

$$G_{ij}[\epsilon_{ij}, \theta] = \psi_{ij}\frac{g(\varphi, \theta)}{\varphi}, \tag{5}$$

where $\varphi$ is an effective strain defined by:

$$\varphi = \left( \frac{1.5 e_{ij} e_{ij}}{(1+\nu)^2} \right)^{1/2}, \tag{6}$$

and $e_{ij}$ is the deviatoric strain tensor. $g(\varphi, \theta)$ has the appearance of a uniaxial stress-strain curve. $\theta$ is absolute temperature.

**Conservation of Energy:**

$$\rho \hat{C}[\theta] \dot{\theta} = \sigma_{ij} \dot{\epsilon}_{ij} - \frac{d}{dt} \left[ \frac{1+\nu}{2E} \sigma_{ij} \sigma_{ij} - \frac{\nu}{2E} {\sigma_{kk}}^2 + \alpha \theta \sigma_{kk} \right] - q_{i,i} + \rho R. \tag{7}$$

Material Constants:

| Constant | Name |
|---|---|
| $\nu, E$ | elastic constants |

Internal Variables:

| Symbol | Name |
|---|---|
| $\epsilon_{ij}$ | total strain |

## 4. Experiments:

1. Type: Uniaxial, monotonic loading
   Material: 304 stainless steel
   Source: E. Krempl, "An Experimental Study of Room Temperature Sensitivity, Creep, and Relaxation of AISI type 304 Stainless Steel., Journal Mechanics and Physics of Solids, **27**, 1979, pp. 363-375.

## 5. Material constant determination:

1. Described in Reference 5 above.

## 6. Mechanisms mentionned:

1. None, phenomenological

## 8. Summary:

1. Strain as internal variable
2. Phenomenological, no mechanistic modelling.

3. "Overstress" formulation, predicts a limiting stress/strain curve for infinitely slow strain rates.
4. No explicit evaluation of temperature dependence.

# CONSTITUTIVE MODEL SUMMARY

**1. Authors:** J.H. Gittus

**2. Papers:**

1. J.H. Gittus, "A Model of Creep Embodying Dislocations whose Movements Produce Work Hardening and Recovery",

**3. Constitutive Model:**

Rate equation

$$\dot{\epsilon} = b\rho v \tag{1}$$

Evolution equations

$$\frac{d\rho}{dt}\frac{1}{\rho_0} = -\dot{\epsilon}_o \left(\frac{\rho}{\rho_0} - \frac{\rho_\infty}{\rho_0}\right)\left(\alpha\frac{\rho}{\rho_o} + \beta\right) + \gamma\left(1 - \frac{\rho}{\rho_o}\right) \tag{2}$$

Material Constants:

| Constant | Name |
|---|---|
| $\rho$ | mobile dislocation density |
| $\rho_0$ | beginning (maximum) mobile dislocation density |
| $\rho_\infty$ | dislocation density asymptote |
| $\dot{\epsilon}_0$ | initial strain rate |
| $\alpha, \beta$ | weight parameters for density reduction rate |
| $\gamma$ | parameter for dislocation remobilization rate |

Internal Variables:

| Symbol | Name |
|---|---|
| $\rho$ | mobile dislocation density |

**4. Experiments:**

1. Type: Tension
   Material: Nickel
   Source: Mitra and McLean

**5. Material constant determination:**

1. Not given.

**6. Mechanisms mentionned:**

1. Work hardening and recovery.

3. Composite cell structure permitting internal stress.

**8. Summary:**

1. Inspired by Bailey-Orowan model.
2. Evoluation based on mobile dislocation structure.
4. Softening based on "remobilization" of trapped mobile dislocations.

## CONSTITUTIVE MODEL SUMMARY

**1. Authors:** E.W. Hart

**2. Papers:**


1. E. W. Hart, "Load Relaxation Testing and Material Constitutive Relations," Stress Relaxation Testing, ASTM STP 676, 1979, pp. 983-991.
2. E. W. Hart, "Constitutive Relations for the Nonelastic Deformation of Metals," Journal of Engineering Materials and Technology, July, 1976, pp. 193-202.
3. E. W. Hart, "A Phenomenological Theory for Plastic Deformation of Polycrystalline Metals," Acta Metallurgica, Vol. 18, 1970, pp. 599-610.
4. E. W. Hart, and H. D. Solomon,"Load Relaxation Studies of Polycrystalline High Purity Aluminum," Acta Metallurgica, Vol. 21, No. 3, March 1973, pp. 295-307.


**3. Constitutive Model:**

$$\dot{\mathbf{E}} = \dot{\mathbf{A}} + \dot{\mathbf{B}} \tag{1}$$

$$\mathbf{T} = \mathbf{T}_a + \mathbf{T}_f \tag{2}$$

**Rate equation**

$$\dot{\mathbf{E}} = \frac{\dot{\epsilon}}{\sigma_f}\mathbf{T}_f \tag{3}$$

$$\dot{\epsilon} = \dot{a}^*(T)\left(\frac{\sigma_f}{M}\right)^M \tag{4}$$

**Evolution equations**

$$\mathbf{A} = \left(\frac{a}{\sigma_a}\right)\mathbf{T}_a \tag{5}$$

$$\frac{d(\ln \sigma^*)}{dt} = \Gamma(\sigma^*, \sigma_a)\dot{\beta} - \mathcal{R}(\sigma^*, T) \tag{6}$$

**Secondary equations**

$$a = (\mathbf{A}\cdot\mathbf{A})^{1/2}$$

$$\beta = (\mathbf{B}\cdot\mathbf{B})^{1/2}$$

$$\sigma_a = (\mathbf{T}_a\cdot\mathbf{T}_a)^{1/2}$$

$$\sigma_f = (\mathbf{T}_f\cdot\mathbf{T}_f)^{1/2}$$

$$\sigma_a = Ma \tag{7}$$

$$\dot{\mathbf{B}} = \left(\frac{\dot{\beta}}{\sigma_a}\right)\mathbf{T}_a \tag{8}$$

$$\ln\left(\frac{\sigma^*}{\sigma_a}\right) = \left(\frac{\dot{\epsilon}^*}{\dot{\beta}}\right)^\lambda \tag{9}$$

$$\dot{\epsilon}^* = \left(\frac{\sigma^*}{G}\right)^m f \exp\left(\frac{-Q}{RT}\right) \tag{10}$$

Isotropic case:

Material Constants:

| Constant | Name |
|---|---|
| M | anisotropic stress scaling factor |
| M | glide activation energy |
| m | stress sensitivity exponent |
| $\lambda$ | |
| $f$ | pre-exponential |
| Q | activation energy |
| G | shear modulus |
| R | gas constant |

Internal Variables:

| Symbol | Name |
|---|---|
| $\sigma^*$ | scalar, isotropic hardness, units stress |
| A | tensor, anisotropy, units strain rate |

**4. Experiments:**

1. **Type:** Stress relaxation
   **Material:** 1100 Aluminum
   **Source:** General Electric research lab, reference 4
   **Temperature:** unknown
   **Strain rates:** unknown
2. **Type:** Stress relaxation
   **Material:** Niobium
   **Source:** Yamada Li, Acta Met.,Vol.22, Feb. 1974, pp. 249-253
   **Temperature:** unknown
   **Strain rates:**

**5. Material constant determination:**

1. Not clearly indicated, stress relaxation data used.

**6. Mechanisms mentionned:**

**8. Summary:**

1. Power law breakdown not accomodated.
2. One of few investigators including anelastic effects.

3. No implicit recovery modelling.
4. Offers a model for grain boundary sliding.
5. Includes discussion of crystal anisotropy.
6. Isotropic variable does not occur explicitly in rate equation.

## CONSTITUTIVE MODEL SUMMARY

1. **Authors:** D. Lee and F. Zaverl, Jr.

2. **Papers:**


1. "Further Development of Generalized Constitutive Relations for Metal Deformation," Metallurgical Transactions, Vol. 11A, June, 1980, pp. 983-991.
2. "Development of Constitutive Equations for Nuclear Reactor Core Materials," Journal of Nuclear Materials, Vol. 88, 1980, pp. 104-110.
3. "A Generalized Strain Rate Dependent Constitutive Equation for Anisotropic Metals," Acta Metallurgica, Vol. 26, 1978, pp. 1771-1780.


3. **Constitutive Model:**

$$\dot{\epsilon}_{ij} = \frac{3}{2}\frac{\dot{\bar{\epsilon}}}{\bar{\sigma}}\frac{\partial f}{\partial \sigma_{ij}} = \dot{\lambda}\frac{\partial f}{\partial \sigma_{ij}} \tag{1}$$

$$3f = M_{ijkl}\left(\sigma_{ij} - \alpha_{ij}\right)\left(\sigma_{kl} - \alpha_{kl}\right) - k^2 = tr\mathbf{M}\left(\mathbf{T} - \mathbf{B}\right) \otimes \left(\mathbf{T} - \mathbf{B}\right) \tag{2}$$

$$\bar{\sigma} = \left[M_{ijkl}(\sigma_{ij} - \alpha_{ij})(\sigma_{kl} - \alpha_{kl}\right]^{1/2} \tag{3}$$

Rate equation

$$\dot{\bar{\epsilon}} = \dot{\epsilon_o}\left(\frac{\bar{\sigma}}{\tau}\right)^m \left\{exp\left[-\frac{B}{kT}\left[1 - \left(\frac{\bar{\sigma}}{\tau}\right)^p\right]\right] + exp\left(-\frac{D}{kT}\right)\right\} \tag{4}$$

Evolution equations

$$\dot{M}_{ijkl} = q(M^e_{ijkl} - M_{ijkl})\dot{\lambda} \tag{5}$$

$$\dot{\alpha}_{ij} = q(\alpha^e_{ij} - \alpha_{ij})\dot{\lambda} \tag{6}$$

$$\dot{k} = q(k^e - k)\dot{\lambda} \tag{7}$$

Secondary equations

$$\dot{\alpha}^e_{ij} = c\dot{\sigma}'_{ij} - g\sigma'_{ij}\dot{\lambda} \tag{8}$$

$$\dot{k}^e = h\dot{\lambda} \tag{9}$$

Isotropic case:

$$3f = M_{ijkl}(\sigma_{ij}\sigma_{kl}) - k^2 \tag{10}$$

$$\frac{\partial f}{\partial \sigma_{ij}} = \frac{2}{3}M_{ijkl}\sigma_{kl} \tag{11}$$

$$\dot{k} = q(k^e - k)\dot{\lambda} \tag{12}$$

$$k^e = h\frac{3}{2}\frac{\dot{\bar{\epsilon}}}{\bar{\sigma}} \tag{13}$$

Material Constants:

| Constant | Name |
|---|---|
| m | pre-exponential exponent |
| B | glide activation energy |
| D | diffusion activation energy |
| $\dot{\epsilon_0}$ | pre-exponential |
| q | |
| h | k variable hardening |
| c | $\alpha$ variable stress rate dependence |
| g | $\alpha$ variable stress dependence |

Internal Variables:

| Symbol | Name |
|---|---|
| k | effective flow strength |
| $a_i$ | back stress |
| $M_{ij}$ | anisotropy tensor |

**4. Experiments:**

1. Type: Tension,compression, monotonic and cyclic
   Material: Zircaloy-2 sheet, 304 stainless
   Source: General Electric research labs, GE nuclear
   Temperature: 25-450 C (Zircaloy-2)
   25-650 C (304 stainless)
   Strain rates: $2.78 \times 10^{-}4$ 1/sec
2. Type: Stress relaxation
   Material: same as above
   Source: same as above
   Temperature: same as above
   Strain rates: loaded at $2.1 \times 10^{-2}$ cm per second

**5. Material constant determination:**

1. Rate equation from load relaxation assuming constant structure.
2. Internal variable values from monotonic tension and compression.

**6. Mechanisms mentionned:** none

**8. Summary:**

1. Plastic potential = yield function.

2. Rate equation includes diffusion and glide processes.
3. Principle axes of anisotropy coincide with principle axes of stress.
4. No implicit recovery modelling.
5. Relatively low honologous temperatures and strain rates.

## CONSTITUTIVE MODEL SUMMARY

**1. Authors:** Alan K. Miller

**2. Papers:**


1. A. K. Miller, "An Inelastic Constitutive Model for Monotonic, Cyclic, and Creep Deformation: Part I - Equations, Development, and Analytical Procedures, and Part II Application to Type 304 Stainless Steel," Journal of Engineering Materials and Technology, Vol. 98, No. 2, pp. 97-113, 1976.
2. A. K. Miller, "Unified Constitutive Equations for Time-Dependent Plasticity," Plasticity of Metals at Finite Strain, E.H. Lee and R.L. Mallett, ed. Stanford University Div. of Applied Mechanics, 1982, pp. 130-160.
3. A. K. Miller and O. D. Sherby, "A Simplified Phenomenological Model for Non-elastic Deformation: Prediction of Pure Aluminum Behavior and Incorporation of Solute Strengthening Effects," Acta Metallurgica, 26, pp. 289-304, 1978.
4. C. G. Schmidt and A. K. Miller, "A Unified Phenomenological Model for Non-Elastic Deformation of Type 316 Stainless Steel, Part I: Derivation of the Model and Part II, Fitting and Predictive Capabilities," Res Mechanica, 3, pp. 109-129 and 175-193, 1981.
5. T.C. Lowe and A.K. Miller, "A Materials Model for Strain Softening with Applications in Modelling Strain Localization," 4th International Conference on Mechanical Behavior of Materials, Stockholm, August, 1983.
6. O.D. Sherby, R.H. Klundt, and A.K. Miller, "Flow stress, subgrain size and subgrain stability at elevated temperatures," Met. Trans., 8A, 1977, pp. 843-860.


**3. Constitutive Model:**

Rate equation

$$\dot{\epsilon} = B\theta' \left\{ \sinh \left[ \left( \frac{\left| \frac{\sigma}{E} - R \right|}{\sqrt{[F_{sol,1} + F_{def}(1 + F_{sol,2})]}} \right)^{1.5} \right] \right\}^n \operatorname{sgn}\left( \frac{\sigma}{E} - R \right) \tag{1}$$

$$\theta' = \exp\left( \frac{-Q_{1d}}{kT} \right) + f \exp\left( \frac{-Q_{2d}}{kT} \right) \tag{2}$$

Evolution equations

$$\dot{R} = H_1 \exp\left( -H_3 R \operatorname{sgn}\left( \frac{\sigma}{E} - R \right) \right) \left[ \dot{\epsilon} - B\theta' \sinh\left( A_1 |R| \right)^n \operatorname{sgn}(R) \right] \tag{3}$$

$$\dot{F}_{def} = H_2 \left( C_2 + |R|^{1.5} - \left( \frac{A_2}{A_1} \right)^{1/1.5} F_{def} \right) |\dot{\epsilon}| - H_2 B C_2 \theta' \left\{ \sinh\left( A_2 F_{def}^{1.5} \right) \right\}^n \tag{4}$$

Secondary equations

$$F_{sol,1} = F_{sol,10} + \sum_{i=1}^{3} M_i \left\{ \exp\left[ - \left( \frac{\log\left(|\dot{\epsilon}|/\theta'_{sol,1}\right) - J_i}{B_i} \right)^2 \right] \right\} \tag{5}$$

$$\theta'_{sol,1} = \exp\left(\frac{-Q_{sol,1}}{kT}\right) \tag{6}$$

$$\begin{aligned} F_{sol,2} = & F_{sol,20} + \sum_{i=1}^{2} N_i \left\{ \exp\left[ - \left( \frac{\log\left(|\dot{\epsilon}|/\theta'_{sol,2}\right) - K_i}{C_i} \right)^2 \right] \right\} \\ & + F_{sol,30} + O_i \left\{ \exp\left[ - \left( \frac{\log\left(|\dot{\epsilon}|\right) - L_i}{D_i} \right)^2 \right] \right\} \end{aligned} \tag{7}$$

$$\theta'_{sol,2} = \exp\left(\frac{-Q_{sol,2}}{kT}\right) \tag{8}$$

Isotropic case:

Material Constants:

| Constant | Name |
|---|---|
| $A_1$ | |
| $A_2$ | |
| B | |
| $B_i$ | |
| $C_i$ | |
| $C_2$ | |
| $D_i$ | |
| $E$ | |
| $F_{sol,1}$ | solute friction stress, non-interaction |
| $F_{sol,2}$ | solute friction stress, interacting with $F_{def}$ |
| $F_{sol,10}$ | |
| $F_{sol,20}$ | |
| $F_{sol,30}$ | |
| $H_1$ | |
| $H_2$ | |
| $H_3$ | |
| $J_i$ | |
| $K_i$ | |
| $L_i$ | |
| $M_i$ | |
| $N_i$ | |
| $n$ | |
| $O_i$ | |
| $Q_{cd}$ | |

$Q_{ld}$
$Q_{sol,1}$
$Q_{sol,2}$

Internal Variables:

| Symbol | Name |
|---|---|
| $F_{def}$ | scalar, isotropic hardening |
| R | tensor, rest stress, anisotropic hardening |

## 4. Experiments:

1. Type: Creep, Constant strain rate, Stress drop, Cyclic
   Material: 316 Stainless Steel
   Source: see paper 4, large compilation
   Temperature: 538 to 816 Celsius
   Strain rates:

## 5. Material constant determination:

1. $Q_{ld}$ and $Q_{cd}$ from diffusion data.
2. $f$ assumed constant.
3. Steady state data used fit rate equation.
4. $F_{sol,1}$ behavior determined from yield stress behavior of annealed material.
5. $F_{sol,2}$, $H_2$, $C_2$, $A_2$ behavior determined simultaneously from low temperature data (no recovery) and steady state data.
6. $H_1$, $H_2$, $A_1$ determined from cyclic stress-strain data and stress drop tests.

## 6. Mechanisms mentionned:

1. Hardening
2. Recovery
3. Bauschinger effect
4. Solute induced variation in flow stress
5. Solute effect on hardening, activation energy

## 8. Summary:

1. Rate equation based on sinh function proposed by Sherby.
2. Solute strengthening variables not history dependent, but temperature and rate dependent. $F_{sol,2}$ interacts with scalar $F_{def}$ to produce instantaneous change in state upon jump in strain rate or temperature.

3. Applied to uniaxial deformation only.

## CONSTITUTIVE MODEL SUMMARY

**1. Authors:** W.D. Nix, J.C. Gibeling

**2. Papers:**

1. W.D. Nix, J.C. Gibeling, and D.A. Hughes, "Time-Dependent Deformation of Metals", Metallurgical Transactions A, **16A**, December, 1985, pp. 2215-2226.
2. W.D. Nix and J.C. Gibeling, "Mechanisms of Time-Dependent Flow and Fracture of Metals", Proceedings of the 1985 ASM Symposium on Flow and Fracture at Elevated Temperatures, October 1-2, 1983.

**3. Constitutive Model:**

Rate equation:

$$\dot{\gamma}_{c,w} = \dot{\gamma}_0 \left\{ \exp\left(-\frac{\Delta F}{kT}\right) \right\} \left\{ \exp\left(\frac{\Delta F}{kT} \frac{\tau_{c,w}}{\hat{\tau}_{c,w}}\right) - 1 \right\} \tag{1}$$

Evolution equations:

$$\frac{d\hat{\tau}_c}{d\gamma_c} = \frac{\mu}{200} - 10\frac{b}{w}\nu_0 \frac{\mu}{\dot{\gamma}_c} \left[\exp\left(-\frac{W_{ce}}{kT}\right)\right] \left[\exp\left(\frac{\tau_c b \alpha W_{ce}}{\mu kT}\right) - 1\right] \tag{2}$$

$$\frac{d\hat{\tau}_w}{d\gamma_c} = \frac{b\mu^2}{L_w \hat{\tau}_w} - \frac{1}{2}\mu \left(\frac{\hat{\tau}_w}{\mu}\right)^3 \frac{\mu b}{kT} D_l \frac{1}{\dot{\gamma}_c} \tag{3}$$

Rate compatibility:

$$\dot{\gamma} = \dot{\gamma}_c + \frac{\dot{\tau}_c}{\mu} = \dot{\gamma}_w + \frac{\dot{\tau}_w}{\mu} \tag{4}$$

Equilibrium:

$$\tau = \frac{L_c}{L_c + L_w}\tau_c + \frac{L_w}{L_c + L_w}\tau_w \tag{5}$$

Material Constants:

| Constant | Name |
|---|---|
| $\Delta F$ | activation energy |
| $\dot{\gamma}_0$ | premultiplier |
| $\mu$ | shear modulus |
| $w$ | cross-slip site spacing |
| $\nu_0$ | cross-slip attempt frequency |
| $W_{ce}$ | activation enthalpy for cross-slip |
| $\alpha$ | cross-slip adjustment parameter |
| $L_w$ | cell wall width |
| $D_l$ | lattice diffusivity |

Internal Variables:

| Symbol | Name |
|---|---|
| $\hat{r}_c$ | cell interior structure |
| $\hat{r}_w$ | cell wall structure |

**4. Experiments:**

1. Type: Torsion
   Material: Ni-Co
   Source: Reference 1
   Temperature: 295, 573 K
   Strain rates: $1.0 \times 10^{-3}$

**5. Material constant determination:**

1. No fitting to experimental data

**6. Mechanisms mentionned:**

1. Athermal hardening, static recovery via diffusion, dynamic recovery via cross-slip.
2. Mechanically activated dislocation motion.
3. Composite cell structure permitting internal stress.

**8. Summary:**

1. Mechanistically inspired.
2. Static and dynamic recovery modelled.
4. Two internal variables, cellular structure.
4. Permits continued hardening without saturation, although saturation at high temperatures may occur.
5. Thermally activated cross-slip included.
6. Steady state behavior result only of lattice diffusion.

## CONSTITUTIVE MODEL SUMMARY

1. **Authors:** F.B. Prinz, A. S. Argon

2. **Papers:**

   1. F. B. Prinz and A. S. Argon, "The Evolution of Plastic Resistance in Large Strain Plastic Flow of Single Phase Subgrain Forming Metals", Acta Metallurgica, 32-7, 1984, pp. 1021-1028.

3. **Constitutive Model:**

Rate equation

$$\dot{\gamma} = b\rho_1 v_0 \exp\left(-\frac{F_j}{kT}\right) x \exp\left[\frac{2\mathcal{E}\delta}{kT}\left(s - \frac{\sqrt{3/2}}{2\pi}x^{1/2}\right)^{2/3}\right] \tag{1}$$

with

$$s = (\sigma/\tau_{01}) - 0.85\mu b\rho^{1/2}$$

$$x = \left(\frac{24\pi^2}{(2\mathcal{E}\delta/kT)^2}\right) s^{2/3}$$

Evolution equations

$$\frac{d\rho_1}{d\gamma} = \left(\frac{2\pi\alpha}{bK^2}\right)\rho_1{}^{1/2} - \frac{L_a}{K^2 b}\rho_1 \tag{2}$$

$$\frac{d\rho_2}{d\gamma} = \sqrt{2/3}\left(\frac{a}{h}\frac{1}{b}\right) x^{1/2}\rho_1{}^{1/2} - \frac{2}{\dot{\gamma}}K_i\rho_2{}^i \tag{3}$$

Equilibrium:

$$\tau = \tau_1 + \tau_2\left(\frac{a-c}{a}\right) \tag{5}$$

Material Constants:

| Constant | Name |
|---|---|
| $v_0$ | attempt frequency |
| $F_j$ | jog energy for forest dislocation intersection process |
| $\mu$ | shear modulus |
| $\mathcal{E}$ | dislocation line tension |
| $\delta$ | width of forest tree |
| $\tau_{01}$ | Orowan stress, $\mu b\sqrt{\rho_1}$ |
| $\alpha$ | approximately 0.5 |
| $K$ | spacing factor for impenetrable regions |
| $L_a$ | dislocation length eliminated per dynamic recovery event |
| $h$ | cell wall thickness |
| $a$ | mean cell wall spacing |

Internal Variables:

| Symbol | Name |
|---|---|
| $\rho_1$ | cell interior dislocation density |
| $\rho_2$ | cell wall dislocation density |

## 4. Experiments:

1. Type: Uniaxial
   Material: Aluminum (Al - 6%Ni)
   Source: D. J. Lloyd, et.al., Scritpa Metall.,11, 1977, p. 297
   Temperature: 300 K
   Strain rates: $1.0 \times 10^{-4}$

## 6. Mechanisms mentionned:

1. Athermal hardening, static recovery via diffusion, dynamic recovery via cross-slip.
2. Mechanically activated dislocation motion.
3. Composite cell structure permitting internal stress.

## 8. Summary:

1. Mechanistically inspired.
2. Static and dynamic recovery modelled.
4. Two internal variables, cellular structure.
5 Steady state stress occurs.
6. Dynamic recovery not thermally activated.
7. Rate of accumulation of dislocations in cell wall derived from analysis of mobile dislocation population.

# APPENDIX B

## Data Acquisition and Reduction Programs

```
10 '*************************************************************************
20 '*                                                                       *
30 '*           SAMPL2.BAS - DATA ACQUISITION USING CHANNELS 0 AND 1        *
40 '*  Stuart Brown                                    Rev. 1.00   2-28-86   *
50 '*************************************************************************
60 '
70 '--------------- STEP 1 ----------------------------------------
80 'Load DASH16.BIN by loading at 92K (Hex 1700) outside basic workspace
90  CLEAR, 49152!
100 DEF SEG = 0
110 SG = 256 * PEEK(&H511) + PEEK(&H510)
120 SG = SG + 49152!/16
130 DEF SEG = SG
140 BLOAD "DASH16.BIN", 0          'Load it
150 DIM DIO%(8),A%(20001)           'Initialize data arrays
160 DIO%(0) = &H300 'DASH-16 board base address
170 DIO%(1) = 2      'Selected interrupt level for DASH-16
180 DIO%(2) = 3      'Selected DMA level for DASH-16
190 DASH16 = 0       'Declare & initialize other CALL parameters
200 FLAG% = 0
210 MD% = 0          'Select Mode 0 - initialize driver
220 CALL DASH16 (MD%, DIO%(0),FLAG%)    'do it
230 IF FLAG%<>0 THEN PRINT "INITIALIZATION ERROR":STOP  'any error?
240 '
250 '--------------- STEP 2 ----------------------------------------
260 '
270 'Set up multiplexer scanning limits for channels 0 to 1
280 '
290 MD%=1            'Mode 1 - set scan limits
300 DIO%(0)=1
310 DIO%(1)=2
320 CALL DASH16 (MD%, DIO%(0),FLAG%)
330 IF FLAG%<>0 THEN PRINT "Error in scan limits # ";FLAG% : STOP
340 '
350 '--------------- STEP 3 ----------------------------------------
360 'Prompt for sampling rate
370 '
380 INPUT "Enter sampling rate in Hertz (up to 1000, even number) : ",SAMRT%
390 INPUT "Enter number of desired samples (maximum 10,000)       : ",NSAM%
400 SAMDUR  = NSAM%/SAMRT%
410 PRINT
420 PRINT "Duration of sampling period is:  ",SAMDUR," seconds."
430 PRINT
440 MD% = 17
450 DIO%(0) = 2 : DIO%(1) = 250000!/SAMRT%
460 CALL DASH16 (MD%, DIO%(0),FLAG%)
470 IF FLAG%<>0 THEN PRINT"Error in scan rate set up # ";FLAG% : STOP
480 '
490 '--------------- STEP 4 ----------------------------------------
500 PRINT "Press any key to start data collection"
510 B$ = INKEY$
520 IF B$="" THEN 510
530 'Do NSAM% conversions into array A%(*) using mode 4
540 DIO%(0) = NSAM%*2        'Number of conversions
550 DIO%(1) = VARPTR(A%(0))   'Array locator
560 DIO%(2) = 1               'Trigger source - programmable timer
570 MD%=4
580 CALL DASH16 (MD%, DIO%(0),FLAG%)
590 IF FLAG%<>0 THEN PRINT "Error in mode 4 # ";FLAG% : STOP
600 PRINT "Data acquisition done"
610 PRINT "Hit any key to continue"
```

```
620 B$ = INKEY$
630 IF B$="" THEN 620
640 '
650 '--------------- STEP 5 ----------------------------------------
660 'Review even 100th data point voltage and store in integer form
670 '
680 FOR I% =0 TO NSAM%*2 STEP 200
690 A1 = A%(I%)/204.7 : A2 = A%(I%+1)/204.7
700 J%=I%/2
710 PRINT J%,A1,A2
720 NEXT I%
730 INPUT "Input first data point to be saved  : ",FSTPT%
740 INPUT "Input last data point to be saved   : ",LSTPT%
750 INPUT "Input name of file to hold data     : ",INFILE$
760 OPEN INFILE$ FOR OUTPUT AS #2
770 FOR J% = FSTPT% TO LSTPT%
780 I% = J% * 2
790 PRINT #2,J%;A%(I%);A%(I%+1)
800 NEXT J%
810 CLOSE #2
820 END
```

## Data Reduction of Raw Load/Deflection Data

The following procedure used to obtain smooth true stress versus true strain data, and hardening data from load/deflection data resulting from uniaxial compression or tension tests. It uses four programs, TRUECON, JUMPPT, POLYS, and HARDEN, to generate a generic data file which may then serve as a relatively "clean" set of uniaxial test data. The purpose of this procedure is to provide data cleansed of any test machine or data acquisition idiosyncrasies, providing a standard format available for subsequent analysis.

The procedure described herein assumes the following format for the raw data obtained from constant true strain rate tests:

| | | |
|---|---|---|
| First row: | Number of data points(integer) | |
| | Test ID (integer) | |
| | Temperature in Celsius | |
| | Strain rate | |
| Subsequent rows: | Data arranged in columns | |
| | Column | Contents |
| | 1 | Sample number |
| | 2 | Displacement in A/D integer units |
| | 3 | Load in A/D integer units |

Entries on the same row are separated by commas or spaces. The programs treat the data as free-formatted. The programs are structured such that the output of a particularly program serves as the input of the next program in sequence. Each program produces an output file which consists of the input file plus additional columns of data which result from the analysis of that program. A copy of each relevant program is attached to the end of this appendix.

## B.1 Converting to True Stress/True Strain Data: TRUECON

The program TRUECON uses the raw data file to produce a file with the follow structure in free-formatted form.

| | |
|---|---|
| First row: | Same as raw data file |
| Subsequent rows: | Data arranged in columns |
| Column | Contents |
| 1 | Sample number |
| 2 | Load in Newtons |
| 3 | Displacement in mm |
| 4 | True stress in MPa |
| 5 | True strain |

TRUECON requests the following input:

1. Specimen area in square millimeters.
2. Temperature in degrees Celsius.
3. Coefficient of thermal expansion.
4. Compliance of test machine in kiloNewtons/mm.
5. Starting actuator displacement (zero load point).
6. File name containing input data.
7. File name to contain output data.

## B.2 Smoothing of True Stress/Strain Data: (JUMPPT and POLYS)

Programs JUMPPT and POLYS serve to smooth the true stress data produced by program TRUECON. JUMPPT smoothes the strain data and calculates the strain rate. POLYS smoothes the stress data. Both strain and stress are smoothed versus sample number (which may be considered equivalent to time). The programs smooth by fitting a cubic polynomial to segments of the stress/strain data, and uses the value predicted by the cubic at the center of the segment to be the smoothed value at that point. The segment is called a "bin" and is moved point by point along the set of data, producing a smoothed value at the center point of the bin. The user specifies 1/2 the number of data points in the bin. The bin size should never

be less than 10 and frequently may have to be larger to obtain adequate smoothing. The 1/2 bin size is therefore always 5 or greater.

JUMPPT, POLYS and the next program HARDEN use double precision IMSL subroutines to perform their relative tasks. The correct IMSL library obviously must then be specified when linking either of these two programs.

JUMPPT requests the following input:

1. Name of input data file (TRUECON output).
2. First sample number in first range of data where strain rate is to be determined.
3. Last sample number is first range of data where strain rate is to be determined.
4. First sample number in second range of data where strain rate is to be determined.
5. Last sample number in second range of data where strain rate is to be determined. (Two ranges are specified so that strain rates before and after a strain rate jump may be determined if desired.)
6. Data sampling interval in seconds.
7. Name of output data file.
8. First sample number in range for strain smoothing.
9. Last sample number in range for strain smoothing.
10. 1/2 bin size for smoothing.

JUMPPT produces the following output file:

| | |
|---|---|
| First row: | Same as raw data file |
| Subsequent rows: | Data arranged in columns |
| Column | Contents |
| 1 | Sample number |
| 2 | Load in Newtons |
| 3 | Displacement in mm |
| 4 | True stress in MPa |
| 5 | True strain (smoothed) |
| 6-8 | Null data |
| 9 | Strain rate |

POLYS requests the following input:

1. Name of input file (JUMPPT output).
2. 1/2 smoothing bin size.
3. First sample number in range for stress smoothing.
4. Last sample number in range for stress smoothing.
5. Name of output file.

POLYS produces the following output file:

| | |
|---|---|
| First row: | Same as raw data file |
| Subsequent rows: | Data arranged in columns |

| Column | Contents |
|---|---|
| 1 | Sample number |
| 2 | Load in Newtons |
| 3 | Displacement in mm |
| 4 | True stress in MPa |
| 5 | True strain (smoothed) |
| 6 | True stress (smoothed) |
| 7-8 | Null |
| 9 | Strain rate |

The user should plot the smoothed and unsmoothed data after each smoothing operation to confirm that the smoothing does not distort the actual data.

## B.3 Plastic Hardening Determination: (HARDEN)

The next step required is to determine the rate of hardening, i.e., the rate of change of stress with strain, for each constant true strain rate test. This is accomplished with program HARDEN. HARDEN produces a new data file of the original data from POLYS with two new columns:

1. Column 7: Plastic hardening
2. Column 8: Plastic strain

HARDEN requests the following input:

1. File name of input data (POLYS output).
2. First sample in range of data for hardening calculation.
3. Last sample in range of data for hardening calculation.
4. 1/2 smoothing bin size.
5. File name to contain output data.
6. Young's modulus in GPA at test temperature. (Used to calculate plastic strain.

HARDEN calculates the hardening, or slope of the stress versus plastic strain curve, by selecting a bin of data (like POLYS) fitting a cubic polynomial to the data in the bin, then using the derivative of the polynomial at the center point of the bin to be the hardening rate at that point. The bin moves through the data, sequentially fitting the data to the polynomial and taking the derivative at the center point. The size of the bin, in data points, is specified by the user each time HARDEN is run. A good range seems to be between 5 and 10, although this depends on the smoothness of the data being analyzed. The bin size may have to be increased if there are many data points $> 100$ which are closely packed or if the data is particularly noisy.

To summarize, HARDEN produces the following output file:

| | |
|---|---|
| First row: | Same as raw data file |
| Subsequent rows: | Data arranged in columns |
| Column | Contents |
| 1 | Sample number |
| 2 | Load in Newtons |
| 3 | Displacement in mm |
| 4 | True stress in MPa |
| 5 | True strain (smoothed) |
| 6 | True stress (smoothed) |
| 7 | Plastic strain |
| 8 | Plastic hardening |
| 9 | Strain rate |

Once again, it is a good idea to plot the hardening (column 8) versus stress to confirm that HARDEN produced reasonable results. It is also a good idea to try several different bin sizes to examine the variation in predicted hardening.

```
C
C       TRUECON
C
C
C               CONVERTS LOAD VERSUS DISPLACEMENT DATA FILES
C               INTO TRUE STRESS VERSUS TRUE STRAIN DATA FILES.
C
C               DATA IS READ FROM FORTRAN DATA FILE SPECIFIED BY
C               ASSIGN FOR025 [INFILE] STATEMENT. DATA IS OUTPUT
C               TO FOR026 [OUTFILE]. THE INPUT FILE
C               FORMAT IS:
C                               NUM             NUMBER OF DATA POINTS
C                               ARRAY           SAMPLE,LOAD,DISPLACEMENT
C
C               VARIABLES:
C
C                               AREA            SPECIMEN AREA IN MM**2
C                               TEMP            TEST TEMPERATURE IN CELSIUS
C                               ALPHA           COEF OF THERMAL EXPANSION
C                               COMP            TEST MACHINE COMPLIANCE
C                               DISP            STARTING DISPLACEMENT
C                               LI              INITIAL SPECIMEN LENGTH
C                               LS              SPECIMEN LENGTH ADJUSTED
C                                                 FOR TEMPERATURE
C                               LOADCF          CONVERSION FACTOR FOR LOAD,
C                                                 (NEWTONS/VOLT)
C                               DISPCF          CONVERSION FACTOR FOR DISPLACE-
C                                                 MENT (MM/VOLT)
C                               NTESTID         IDENTIFICATION NUMBER FOR
C                                                 TEST (INTEGER)
C                               TEMPT           TEST TEMPERATURE IN CELSIUS
C                               RATE            TEST STRAIN RATE
C                               NX              NUMBER OF DATA POINTS
C                               INFILE          INPUT FILE NAME
C                               OUTFILE         OUTPUT FILE NAME
C                               ARRAY(I,J)      DATA FILE
C                               SIZE            TEMPERATURE SCALING FACTOR
C                                                 FOR SPECIMEN DIMENSIONS
C
C               STUART BROWN  1-3-84
C
C       INITIALIZE DATA
C
      REAL ARRAY2(2000,5),ARRAY(1,3)
C
      REAL AREA,TEMP,ALPHA,COMP,DISP,LI,LS,TEMPT,RATE,SIZE,LOADCF
      REAL DISPCF
      CHARACTER*20 INFILE,OUTFILE
C
C     READ DATA AND CONVERT TO TRUE STRESS AND STRAIN
C
4     FORMAT(A20)
5     FORMAT (F10.5)
      PRINT *,"INPUT SPECIMEN AREA IN MM*MM          "
      READ (*,5) AREA
      PRINT *,"INPUT TEMP IN DEGREES CELSIUS         "
      READ (*,5) TEMP
      PRINT *,"INPUT COEF THERMAL EXPANSION * 10^6 "
      READ (*,5) ALPHA
      PRINT *,"INPUT COMPLIANCE IN KN/MM             "
      READ (*,5) COMP
      PRINT *,"INPUT STARTING DISPLACEMENT           "
      READ (*,5) DISP
      PRINT *,"INPUT STARTING LENGTH IN MM           "
```

```
      READ (*,5) LI
      PRINT *,"INPUT RAW DATA FILE NAME                "
      READ (*,4) INFILE
      PRINT *,"INPUT LOAD CONVERSION FACTOR (NEWTONS/VOLT)   "
      READ (*,5) LOADCF
      PRINT *,"INPUT DISP CONVERSION FACTOR (MM/VOLT)        "
      READ (*,5) DISPCF
      PRINT *,"INPUT OUTPUT FILE NAME                  "
      READ (*,4) OUTFILE
      OPEN (25,FILE=INFILE,STATUS='OLD'
     1      ,RECFM='DS')
      READ (25,*) NUM,TESTID,TEMPT,RATE
      DO 10 I = 1,NUM
C
         READ (25,*) ARRAY(1,1),ARRAY(1,3),ARRAY(1,2)
         SIZE = 1. + (TEMP-20.) * ALPHA * 1.E-06
         LS = LI * SIZE
         SS = ARRAY(1,3)
         ARRAY(1,3) = DISPCF * ARRAY(1,2) / 204.7
         ARRAY(1,2) = LOADCF * SS  / 204.7
         ENG = (ARRAY(1,3) - ARRAY(1,2)/(COMP*1000) - DISP)/LS
         ARRAY2(I,5) = -ALOG(1.+ ENG)
         ARRAY2(I,4) = -ARRAY(1,2) * (1. + ENG)/(AREA*SIZE**2)
         ARRAY2(I,1) =  ARRAY(1,1)
         ARRAY2(I,3) = ARRAY(1,3)
         ARRAY2(I,2) = ARRAY(1,2)
C
10    CONTINUE
C
C     STORE TRUE STRESS AND STRAIN DATA
C
      OPEN (26,FILE=OUTFILE,STATUS='NEW',
     1      RECFM='DS')
      WRITE (26,*) NUM,NTESTID,TEMPT,RATE
      DO 20 I=1,NUM
C
         WRITE (26,*) (ARRAY2(I,J),J=1,5)
C
20    CONTINUE
      CLOSE (UNIT=25)
      CLOSE (UNIT=26)
      STOP
      END
```

```
C
C     JUMPPT
C
C          STU BROWN  2-16-86
C
C          DETERMINES SMOOTHED STRAIN AND INTERSECTION STRAIN
C
C          VARIABLES
C
C               ARRAYT(1200,9)
C                              1       SAMPLE NUMBER
C                              2       LOAD
C                              3       DISPLACEMENT
C                              4       TRUE STRESS
C                              5       TRUE STRAIN
C                              6       SMOOTHED STRESS
C                              7       PLASTIC STRAIN
C                              8       HARDENING
C                              9       STRAIN RATE
C
      DOUBLE PRECISION LPT1,LPT2,UPT1,UPT2,ARRAYT(1200,9),SAMRATE
      DOUBLE PRECISION ARRAY1(1200,2),ARRAY2(1200,2),JUMPPT
      DOUBLE PRECISION ALBAP(3),DES(5),ANOVA(14),STAT(9),PRED(1,7)
      CHARACTER*20 INFILE,OUTFILE,ANSWER
C
C                                                    SMOOTHING VARIABLES
C
      DOUBLE PRECISION SPT1,SPT2,WORK(2,1200),X(100),Y(100),RSQ,P(200)
      DOUBLE PRECISION T(16),C(6),S(6),A(3),B(3),Z(4)
      REAL RATE(1200),STRAIN(1200),STRAINL(1200)
5     FORMAT(15A)
C
      PRINT *,"PROGRAM JUMPPT"
      PRINT *,"ENTER NAME OF INPUT DATA FILE       "
      READ (*,5) INFILE
      PRINT *,"STRAIN RATE DETERMINATION SECTION   "
      PRINT *,"INPUT FIRST POINT FOR LOWER RANGE   "
      READ (*,*) LPT1
      PRINT *,"INPUT SECOND POINT FOR LOWER RANGE  "
      READ (*,*) LPT2
      PRINT *,"INPUT FIRST POINT FOR UPPER RANGE   "
      READ (*,*) UPT1
      PRINT *,"INPUT SECOND POINT FOR UPPER RANGE  "
      READ (*,*) UPT2
      PRINT *,"INPUT DATA SAMPLING INTERVAL  (SEC) "
      READ (*,*) SAMRATE
C
C                                                    READ DATA
C
      NPT1 = 0
      NPT2 = 0
      OPEN(24,FILE=INFILE,RECFM='DS')
      OPEN(12,FILE='ERROR.LS')
      READ (24,*) NPT
      DO 10 I = 1, NPT
C
          READ(24,*) (ARRAYT(I,J),J=1,5)
          ARRAYT(I,6) = 0.
          ARRAYT(I,7) = 0.
          ARRAYT(I,8) = 0.
          ARRAYT(I,9) = 0.
          IF ((ARRAYT(I,1).GE.LPT1).AND.(ARRAYT(I,1).LE.LPT2)) THEN
C
```

```
                NPT1 = NPT1 + 1
                ARRAY1(NPT1,1) = ARRAYT(I,1)
                ARRAY1(NPT1,2) = ARRAYT(I,5)
C
          ELSE IF ((ARRAYT(I,1).GE.UPT1).AND.(ARRAYT(I,1).LE.UPT2))
     1    THEN
                NPT2 = NPT2 + 1
                ARRAY2(NPT2,1) = ARRAYT(I,1)
                ARRAY2(NPT2,2) = ARRAYT(I,5)
C
            END IF
C
10      CONTINUE
        CLOSE(24)
C
C                                                  PERFORM LINEAR REGRESSION
C
        IX = 1200
        IMOD = 0
        IPRED = 0
        ALBAP(1) = .05
        ALBAP(2) = .05
        IP = 1
        NN = 0
C
        CALL RLONE(ARRAY1,IX,NPT1,IMOD,IPRED,ALBAP,DES,ANOVA,STAT,
     1             PRED,IP,NN,IER)
        PRINT *,"REGRESSION COEF FOR LOWER RANGE =  ",(STAT(1)/SAMRATE)
        A1  = STAT(1)
        B1 = STAT(5)
        PRINT *,"IER (ERROR PARAMETER)           =  ",IER
C
        IX = 1200
        IMOD = 0
        IPRED = 0
        ALBAP(1) = .05
        ALBAP(2) = .05
        IP = 1
        NN = 0
        CALL RLONE(ARRAY2,IX,NPT2,IMOD,IPRED,ALBAP,DES,ANOVA,STAT,
     2             PRED,IP,NN,IER)
        PRINT *;"REGRESSION COEF FOR UPPER RANGE =  ",(STAT(1)/SAMRATE)
        A2 = STAT(1)
        B2 = STAT(5)
        PRINT *,"IER (ERROR PARAMETER)           =  ",IER
C
C                                                 CALCULATE INTERSECTION
C
C
C                                                  BEGIN SMOOTHING SECTION
C
        PRINT *,"  "
        PRINT *,"SMOOTH STRAIN AND DETERMINE STRAIN RATE? (Y OR N)"
        READ (*,5) ANSWER
        IF (ANSWER.EQ.'N') GO TO 500
        PRINT *,"ENTER NAME OF OUTPUT FILE      "
        READ (*,5) OUTFILE
        OPEN(25,FILE=OUTFILE,RECFM='DS')
        PRINT *,"ENTER INITIAL SAMPLE NUMBER  "
        READ (*,*)  SPT1
        PRINT *,"ENTER FINAL SAMPLE NUMBER    "
        READ (*,*)  SPT2
        PRINT *,"ENTER 1/2 BIN SIZE           "
```

```
      READ (*,*) NBIN
C
C                                                    SELECT DATA ARRAY
C
      NBEG = NPT
      NSAM = 0
      DO 15 I = 1,NPT
C
          IF ((ARRAYT(I,1).GE.SPT1).AND.(ARRAYT(I,1).LE.SPT2)) THEN
C
                NSAM = NSAM + 1
                ARRAY2(NSAM,1) = ARRAYT(I,1)
                ARRAY2(NSAM,2) = ARRAYT(I,5)
C
          NBEG = MIN(NBEG,I)
          END IF
15        CONTINUE
C                                                    SET UP WORK ARRAY
C
      DO 20 I = 1,NBIN
C
          WORK(1,I) = ARRAYT(NBEG-NBIN+I-1,1)
          WORK(2,I) = ARRAYT(NBEG-NBIN+I-1,5)
          WORK(2,NBIN+NSAM+I) = 2*ARRAY2(NSAM,2)-ARRAY2(NSAM-I,2)
          WORK(1,NBIN+NSAM+I) = 2*ARRAY2(NSAM,1)-ARRAY2(NSAM-I,1)
20        CONTINUE
C
      DO 30 I = 1,NSAM
C
          WORK(1,NBIN+I) = ARRAY2(I,1)
          WORK(2,NBIN+I) = ARRAY2(I,2)
30        CONTINUE
      OPEN(27,FILE='ZOUT',RECFM='DS')
      DO 33 I = 1,NSAM+2*NBIN
          WRITE(27,*) WORK(1,I),WORK(2,I)
33        CONTINUE
C
C                                                          CURVE FIT
C
      RSQ = 99.99D0
      MD = 3
      N = 2*NBIN + 1
      DO 50 I = 1,NSAM
      WRITE(27,*) I
C
         DO 40 J = 1,N
C
            X(J) = WORK(1,I+J-1)
            Y(J) = WORK(2,I+J-1)
            WRITE(27,*) X(J),Y(J)
40          CONTINUE
C
         DO 45 K = 1,6
C
             C(K) = 0.0
45           CONTINUE
C
         CALL RLFOTH(X,Y,N,RSQ,MD,ID,P,C,S,A,B,IER)
         CALL RLDOPM(C,ID,A,B,T)
         STRAIN(I) = SNGL(C(1) + C(2)*ARRAY2(I,1) +
     1                C(3)*ARRAY2(I,1)**2 + C(4)*ARRAY2(I,1)**3)
         RATE(I)   = SNGL((C(2) + 2*C(3)*ARRAY2(I,1) +
     1                3*C(4)*ARRAY2(I,1)**2)/SAMRATE)
```

```
            STRAINL(I)= SNGL(STAT(1)*ARRAY2(I,1)+STAT(5))
50          CONTINUE
      CLOSE(27)
C
C                                                          OUTPUT RESULTS
C
        WRITE(25,*) NPT
        DO 60 I= 1,NPT
C
          IF((ARRAYT(I,1).LT.SPT1).OR.(ARRAYT(I,1).GT.SPT2))  THEN
C
               WRITE(25,*) (ARRAYT(I,J),J=1,9)
C
          ELSE
C
               WRITE(25,*) (ARRAYT(I,J),J=1,4),STRAIN(I-NBEG+1),
     1            STRAINL(I-NBEG+1),(ARRAYT(I,J),J=7,8),RATE(I-NBEG+1)
          END IF
C
C
60        CONTINUE
          CLOSE(25)
500       STOP
          END
```

```
C       POLYS
C
C
C                 DATA SMOOTHING PROGRAM FOR STRESS/STRAIN CURVES
C
C                 STUART BROWN 5-29-85/MOD MEHRDAD HAGHI 7-16-85
C
C                 VARIABLES
C
C                      NX                NUMBER OF DATA POINTS
C                      ADATA(I,NX)       ORIGINAL DATA ARRAY
C                       ROW 1              SAMPLE NUMBER
C                       ROW 2              LOAD
C                       ROW 3              DISPLACEMENT
C                       ROW 4              TRUE STRESS
C                       ROW 5              TRUE STRAIN
C                       ROW 6              SMOOTHED STRESS
C                       ROW 7              PLASTIC STRAIN
C                       ROW 8              HARDENING
C                       ROW 9              STRAIN RATE
C                      NPT               1/2 SMOOTHING FRAME SIZE
C                      WORK(2,NX)        WORK ARRAY FOR SMOOTHING
C                      X(I)              X AXIS WORK ARRAY
C                      Y(I)              SMOOTHED VARIABLE WORK ARRAY
C                      P(I)              WORK VECTOR
C                      C(6)              REGRESSION COEFFICIENTS
C                      S(6)              SCALING COEFFICIENTS
C                      A(3)                "          "
C                      B(3)                "          "
C
C
C                 I/O ASSIGNMENTS
C
C                      FOR025  INPUT FILE, PER ADATA(I,NX) ABOVE
C
C                      FOR026  OUTPUT FILE, PER ADATA(I,NX) ABOVE
C
      PROGRAM POLYS
C
C                                                          INITIALIZE DATA
C
      REAL ADATA(9,2000),WORK(2,2000),SSTRESS(2000),ZERO
      CHARACTER*20 INFILE,OUTFILE
      DOUBLE PRECISION P(100),T(16),X(50),Y(50),C(6),S(6),A(3),B(3),
     1                 Z(4),RSQ
      RSQ = 99.99D0
      MD = 2
5     FORMAT(15A)
C
C                                                          READ DATA
C
      PRINT *,"WHAT IS INPUT FILENAME?     "
      READ (*,5) INFILE
      PRINT *,"INPUT 1/2 BIN SIZE          "
      READ (*,*) NPT
      PRINT *,"WHAT IS INITIAL SAMPLE NUMBER?  "
      READ (*,*) NSAM1
      PRINT *,"WHAT IS FINAL SAMPLE NUMBER?  "
      READ (*,*) NSAM2
      PRINT *,"WHAT IS OUTPUT FILENAME?    "
      READ (*,5) OUTFILE
      OPEN (12,FILE="ERROR.LS")
      OPEN (25,FILE=INFILE,RECFM='DS')
      READ (25,*) NX
```

```
      NSAM = 0
      DO 10 I = 1,NX
C
         READ (25,*) (ADATA(J,I),J=1,9)
         IF ((ADATA(1,I).GE.NSAM1).AND.(ADATA(1,I).LE.NSAM2)) THEN
             NSAM = NSAM + 1
             END IF
         IF (ADATA(1,I).EQ.NSAM1) NBEG=I
C
C
C
10    CONTINUE
      CLOSE (UNIT=25)
C
C
C                                                          SETUP WORK ARRAY
C
      NEND = NBEG + NSAM - 1
      DO 20 I = 1,NPT
C
          WORK(1,I) = 2*ADATA(1,NBEG)-ADATA(1,NBEG+NPT-I+1)
          WORK(2,I) = 2*ADATA(4,NBEG)-ADATA(4,NBEG+NPT-I+1)
          WORK(2,NSAM+NPT+I) = 2*ADATA(4,NEND)-ADATA(4,NEND-I)
          WORK(1,NSAM+NPT+I) = 2*ADATA(1,NEND)-ADATA(1,NEND-I)
20        CONTINUE
C
      DO 30 I = 1,NSAM
C
          WORK(1,I+NPT) = ADATA(1,I+NBEG-1)
          WORK(2,I+NPT) = ADATA(4,I+NBEG-1)
30        CONTINUE
C
C
C                                                          CURVE FIT
C
      N = 2*NPT + 1
      DO 50 I = 1,NSAM
C
          DO 40 J = 1, 2*NPT+1
C
              X(J) = DBLE(WORK(1,I+J-1))
              Y(J) = DBLE(WORK(2,I+J-1))
40            CONTINUE
C
          CALL RLPOTH(X,Y,N,RSQ,MD,ID,P,C,S,A,B,IER)
          CALL RLDOPM(C,ID,A,B,T)
          SSTRESS(I) = SNGL(C(1)+C(2)*ADATA(1,I+NBEG-1)
     1              +C(3)*ADATA(1,I+NBEG-1)**2)
50        CONTINUE
C
C
C                                                          OUTPUT RESULTS
C
      OPEN (26,FILE=OUTFILE)
      WRITE (26,*) NX
      ZERO = 0.0
      DO 60 I = 1,NX
C
          IF ((ADATA(1,I).LT.NSAM1).OR.(ADATA(1,I).GT.NSAM2)) THEN
C
              WRITE (26,*) (ADATA(J,I),J=1,5),ZERO,(ADATA(K,I),K=7,9)
C
              ELSE
```

```
C
              WRITE (26,*) (ADATA(J,I),J=1,5),SSTRESS(I-NBEG+1),
     1                     (ADATA(K,I),K=7,9)
              END IF
C
60         CONTINUE
C
       CLOSE (26)
       STOP
       END
```

```
C       HARDEN
C
C               HARDENING PROGRAM FOR JUMP TESTS
C
C               STUART BROWN 7-18-86
C
C               VARIABLES
C
C                   NX                  NUMBER OF DATA POINTS
C                   ADATA(I,NX)         ORIGINAL DATA ARRAY
C                    ROW 1                SAMPLE NUMBER
C                    ROW 2                LOAD
C                    ROW 3                DISPLACEMENT
C                    ROW 4                STRESS
C                    ROW 5                STRAIN
C                    ROW 6                SMOOTHED STRESS
C                    ROW 7                PLASTIC STRAIN
C                    ROW 8                HARDENING
C                    ROW 9                STRAIN RATE
C                   NPT                 1/2 SMOOTHING FRAME SIZE
C                   WORK(2,NX)          WORK ARRAY FOR SMOOTHING
C                   X(I)                X AXIS WORK ARRAY
C                   Y(I)                SMOOTHED VARIABLE WORK ARRAY
C                   P(I)                WORK VECTOR
C                   C(6)                REGRESSION COEFFICIENTS
C                   S(6)                SCALING COEFFICIENTS
C                   A(3)                  "          "
C                   B(3)                  "          "
C
C
C               I/O ASSIGNMENTS
C
C                   FOR025  INPUT FILE, PER ADATA(I,NX) ABOVE
C
C                   FOR026  OUTPUT FILE, PER ADATA(I,NX) ABOVE
C
      PROGRAM POLYS
C
C                                                       INITIALIZE DATA
C
      REAL ADATA(9,2000),WORK(2,2000),HARDEN(2000),ZERO,E
      CHARACTER*20 INFILE,OUTFILE
      DOUBLE PRECISION P(100),T(16),X(50),Y(50),C(6),S(6),A(3),B(3),
     1                 Z(4),RSQ
      RSQ = 99.99D0
      MD = 2
5     FORMAT(15A)
C
C                                                       READ DATA
C
      PRINT *,"WHAT IS INPUT FILENAME?          "
      READ (*,5) INFILE
      PRINT *,"WHAT IS INITIAL SAMPLE NUMBER?   "
      READ (*,*) NSAM1
      PRINT *,"WHAT IS FINAL SAMPLE NUMBER?     "
      READ (*,*) NSAM2
      PRINT *,"ENTER 1/2 BIN SIZE               "
      READ (*,*) NPT
      PRINT *,"WHAT IS OUTPUT FILENAME?         "
      READ (*,5) OUTFILE
      PRINT *,"ENTER YOUNG'S MODULUS IN GPA     "
      READ (*,*) E
      OPEN (12,FILE="ERROR.LS")
```

```
      OPEN (26,FILE='ZOUT',RECFM='DS')
      OPEN (25,FILE=INFILE,RECFM='DS')
      READ (25,*) NX
      NSAM = 0
      DO 10 I = 1,NX
C
         READ (25,*) (ADATA(J,I),J=1,9)
         ADATA(7,I) = ADATA(5,I) - ADATA(6,I)/(E*1000.)
         IF ((ADATA(1,I).GE.NSAM1).AND.(ADATA(1,I).LE.NSAM2)) THEN
             NSAM = NSAM + 1
             END IF
         IF (ADATA(1,I).EQ.NSAM1) NBEG=I
C
C
C
10    CONTINUE
      CLOSE (UNIT=25)
C
C
C                                                          SETUP WORK ARRAY
C
      NEND = NBEG + NSAM - 1
      DO 20 I = 1,NPT
C
          WORK(1,I) = ADATA(7,NBEG+I-NPT-1)
          IF (WORK(1,I).LT.WORK(1,I-1))  WORK(1,I)=WORK(1,I-1)+.000001
          WORK(2,I) = ADATA(6,NBEG+I-NPT-1)
          WORK(2,NSAM+NPT+I) = 2*ADATA(6,NEND)-ADATA(6,NEND-I)
          WORK(1,NSAM+NPT+I) = 2*ADATA(7,NEND)-ADATA(7,NEND-I)
20        CONTINUE
C
      DO 30 I = 1,NSAM
C
          WORK(1,I+NPT) = ADATA(7,I+NBEG-1)
          IF (WORK(1,I+NPT).LT.WORK(1,I+NPT-1))  WORK(1,I+NPT) =
     1          WORK(1,I+NPT-1)+.000001
          WORK(2,I+NPT) = ADATA(6,I+NBEG-1)
30        CONTINUE
      DO 31 J = 1,NSAM+2*NPT
          WRITE(26,*) WORK(1,J),WORK(2,J)
31        CONTINUE
      CLOSE(26)
C
C
C                                                          CURVE FIT
C
      N = 2*NPT + 1
      DO 50 I = 1,NSAM
C
          DO 40 J = 1, 2*NPT+1
C
              X(J) = DBLE(WORK(1,I+J-1))
              Y(J) = DBLE(WORK(2,I+J-1))
40            CONTINUE
C
          CALL RLPOTH(X,Y,N,RSQ,MD,ID,P,C,S,A,B,IER)
          CALL RLDOPM(C,ID,A,B,T)
          HARDEN(I) = SNGL(C(2)+2*C(3)*ADATA(7,I+NBEG-1))
50        CONTINUE
C
C
C                                                          OUTPUT RESULTS
C
```

```
      OPEN (26,FILE=OUTFILE)
      WRITE (26,*) NX
      ZERO = 0.0
      DO 60 I = 1,NX
C
          IF ((ADATA(1,I).LT.NSAM1).OR.(ADATA(1,I).GT.NSAM2)) THEN
C
              WRITE (26,*) (ADATA(J,I),J=1,7),ZERO,ADATA(9,I)
C
              ELSE
C
          WRITE (26,*) (ADATA(J,I),J=1,7),HARDEN(I-NBEG+1),ADATA(9,I)
C
              END IF
C
60        CONTINUE
C
      CLOSE (26)
      STOP
      END
```

# APPENDIX C

## Material Parameter Determination Programs

```
C
C     QNON
C
C           FIT OF HARDENING DATA BETWEEN SPECIFIED VALUES OF
C           STRESS
C
C           STUART BROWN 8-13-85
C
C           VARIABLES
C
C               NX                  NUMBER OF DATA POINTS
C               ADATA(NX,7)         DATA ARRAY
C                 ROW 5               SMOOTHED STRESS
C                     6               HARDENING
C                     7               PLASTIC STRAIN
C               STRESS(NX)          SMOOTHED STRESS
C               STRAIN(NX)          PLASTIC STRAIN
C               SL                  LOWER STRESS DATA LIMIT FOR FIT
C               SU                  UPPER STRESS DATA LIMIT FOR FIT
C               Q,QD                EXPONENT IN HARDENING LAW
C               CH0                 C * H0
C               SIGS,SIGSD          SIGMA STAR
C               S0                  SIGMA ZERO
C               S0CALC              SIGMA ZERO FROM FIRST DATA POINT
C
      PROGRAM QNON
      EXTERNAL FITQ1,FITQ2
C
      REAL ADATA(450,7),MAXSTRAIN
      DOUBLE PRECISION Q,CH0,SIGS
      DOUBLE PRECISION X(2),F(450),XJAC(450,2),XJTJ(3),XY(450,2)
     1     ,WORK(918),PARM(4),STRAIN(450),STRESS(450),HARDEN(450)
      DOUBLE PRECISION EPS,DELTA,SSQ,SU,SL,STSSUM,S0CALC
      COMMON STRAIN,STRESS,XY,SIGS,Q,CH0
      CHARACTER*20 FNAME,PNAME
7     FORMAT(20A)
C
C                                                   INITIALIZE DATA
C
C                                                   ZXSSQ PARAMETERS
C
      N = 1
      M = 1
      NSIG = 6
      EPS = 0.0D0
      DELTA = 0.0D0
      MAXFN = 5000
      IOPT = 1
      IXJAC = 450
      N1 = 1
C
C                                                   READ STRESS RANGE
C
      PRINT 10
10    FORMAT (' INPUT LOWER STRESS LIMIT FOR FIT      ')
      READ *,SL
      WRITE (6,20)
20    FORMAT (' INPUT UPPER STRESS LIMIT FOR FIT      ')
      READ *,SU
C
C                                                   READ DATA AND SET UP
C                                                   ZXSSQ FIT
C
```

```
      PRINT *,"NAME OF DATA FILE                    "
      READ(*,7) FNAME
      OPEN (25,FILE=FNAME,RECFM='DS')
      READ(25,*) NX
      PRINT *,"READING DATA"
      DO 30 I = 1,NX
C
           READ(25,*) (ADATA(I,J),J=1,7)
           STRESS(I) = DBLE(ADATA(I,5))
           STRAIN(I) = DBLE(ADATA(I,7))
           HARDEN(I) = DBLE(ADATA(I,6))
           IF (STRESS(I).GT.SIGS) THEN
C
               SIGS = STRESS(I)
               MAXSTRAIN = STRAIN(I)
               END IF
C
30         CONTINUE
C
C                                                    SELECT DATA FOR FIT
C
      DO 33 I = 1,NX
C
           IF ((STRESS(I).GT.SL).AND.(STRESS(I).LT.SU).AND.
     1          (STRAIN(I).LT.MAXSTRAIN)) THEN
C
               XY(N1,1) = STRESS(I)
               XY(N1,2) = HARDEN(I)
               N1 = N1 + 1
               END IF
C
33         CONTINUE
C
      N1 = N1 - 1
      CLOSE (UNIT=25)
      PRINT *,"FINISHED READING DATA"
C
C                                                    CALCULATE SIGS AND
C                                                    TRANSFORM DATA
C
      SIGS = SIGS + 1.0D-3
C
C                                                    HARDENING FIT
C
      WRITE (6,35)
35    FORMAT (' INPUT ESTIMATE OF CH0          ')
      READ *,X(1)
      WRITE (6,36)
36    FORMAT (' INPUT ESTIMATE OF Q            ')
      READ *,Q
      PRINT *,"STARTING FIRST ZXSSQ"
      CALL ZXSSQ(FITQ1,N1,M,NSIG,EPS,DELTA,MAXFN,IOPT,PARM,X,
     1           SSQ,F,XJAC,IXJAC,XJTJ,WORK,INFER,IER)
      PRINT *,"ZXSSQ FINISHED"
      CH0 = X(1)
      WRITE(6,40) Q
40    FORMAT (' Q =     ',D10.5)
      WRITE(6,50) SIGS
50    FORMAT (' SIGS =  ',D10.5)
      WRITE(6,55) CH0
55    FORMAT (' CH0 =   ',D10.5)
      WRITE(6,60) IER
60    FORMAT (' IER =   ',I5)
```

```
C
C                                                       SET UP PLOT FILE
C                                                       OF DATA VERSUS
C                                                       FIT CURVE
C
      PRINT *,"NAME OF HARDENING PLOT FILE          "
      READ (*,7) PNAME
      OPEN(UNIT=24,FILE=PNAME)
      WRITE(24,*) NX
      DO 100 I = 1,NX
C
         HARD = REAL(CH0*(1.D0 - (STRESS(I)/SIGS))**Q)
         STRESSR = REAL(STRESS(I))
         WRITE (24,*) STRESSR,ADATA(I,6),HARD
100      CONTINUE
C
      CLOSE(24)
C
C                                                       SET UP FOR FIT FOR S0
C
      PRINT *,"INPUT ESTIMATE OF SIGMA ZERO      "
      READ (*,*) X(1)
      PRINT *,"ZXSSQ STARTING"
      CALL ZXSSQ(FITQ2,NX,N,NSIG,EPS,DELTA,MAXFN,IOPT,PARM,X,
     1           SSQ,F,XJAC,IXJAC,XJTJ,WORK,INFER,IER)
      PRINT *,"ZXSSQ FINISHED"
      WRITE(6,75) INFER,IER
75    FORMAT (' INFER =  ',I7,'   IER = ',I5)
      WRITE(6,80) X(1)
80    FORMAT (' S0 =      ',D10.5)
      S0CALC=SIGS-(SIGS-DBLE(ADATA(1,1)))
     1           *DEXP(DBLE(ADATA(1,3))*CH0/SIGS)
      WRITE(6,90) S0CALC
90    FORMAT (' S0CALC = ',D10.5)
C
C                                                       SET UP PLOT FILE
C                                                       OF DATA VERSUS
C                                                       FIT CURVE
C
      PRINT *,"NAME OF STRESS/STRAIN PLOT FILE        "
      READ (*,7) PNAME
      OPEN(UNIT=25,FILE=PNAME)
      WRITE(25,*) NX
      DO 120 I = 1,NX
C
         STRESSC = REAL(SIGS-((SIGS-X(1))**(1-Q)+
     1             (Q-1)*CH0*STRAIN(I)/(SIGS**Q))**(1/(1-Q)))
         STRAINR = REAL(STRAIN(I))
         STRESSR = REAL(STRESS(I))
         WRITE (25,*) STRAINR,STRESSR,STRESSC
120      CONTINUE
C
      CLOSE(25)
      STOP
      END
```

```
C
C     FITQ1
C
C          EVALUATION SUBROUTINE FOR QNON
C
C          STUART BROWN   8-14-85
C
      SUBROUTINE FITQ1(X,NX,N,F)
      DOUBLE PRECISION X(2),F(450),STRESS(450),STRAIN(450),SIGS,Q
     1                 ,XY(450,2),CH0
      COMMON STRAIN,STRESS,XY,SIGS,Q,CH0
C
      PRINT *,X
C
      DO 10 I=1,NX
C
          F(I) = XY(I,2) - X(1)*((1.D0-(XY(I,1)/SIGS))**Q)
C
10        CONTINUE
      RETURN
      END
```

```
C
C     FITQ2
C
C          EVALUATION SUBROUTINE FOR QNON
C
C          STUART BROWN   8-14-85
C
      SUBROUTINE FITQ2(X,NX,N,F)
      DOUBLE PRECISION X(2),F(450),STRESS(450),STRAIN(450),SIGS,Q
     1                 ,XY(450,2),CH0
      COMMON STRAIN,STRESS,XY,SIGS,Q,CH0
C
      PRINT *,X
C
      DO 10 I=1,NX
C
          F(I) = STRESS(I) - SIGS + ((SIGS-X(1))**(1-Q)
     1             + (Q-1)*CH0*STRAIN(I)/(SIGS**Q))**(1/(1-Q))
C
10        CONTINUE
      RETURN
      END
```

```
C
C     ISOCON
C
C           DETERMINES MATERIAL CONSTANTS FOR CONSTANT
C           STATE DATA USING NONLINEAR, LEAST SQUARES, IMSL ROUTINE
C           ZXSSQ. (DOUBLE PRECISION VERSION)
C
C           STUART BROWN  4-4-86
C
C           VARIABLES
C
C              DATA(NX,6)          DATA FILE
C                COLUMN 1              TEST ID NUMBER
C                       2              TEMPERATURE
C                       3              INITIAL STRAIN RATE
C                       4              FINAL STRAIN RATE
C                       5              FINAL STRESS
C                       6              INITIAL STRESS
C              TEMP(25)            TEMPERATURE (KELVIN)
C              RATEI(25)           INITIAL STRAIN RATE
C              RATEF(25)           FINAL STRAIN RATE
C              CURVE(25)           ID NUMBERS OF CURVES
C              STRESSF(25)         STRESS IMMEDIATELY AFTER JUMP
C              STRESSI(25)         STRESS IMMEDIATELY BEFORE JUMP
C              X(3)                EQUATION PARAMETERS
C              F(25)               RESIDUE FROM FIT
C              N                   NUMBER OF PARAMETERS
C              NSIG                SIGNIFICANT DIGITS REQUIRED FOR
C                                      PARAMETERS
C
C           FILE ASSIGNMENTS
C
C              FOR025              INPUT FILE
C
C           SUBROUTINES
C
C              FITISO              USED IN ZXSSQ
C              ZXSSQ               FITTING ROUTINE
C
      PROGRAM ISOCON
C                                        INITIALIZE DATA
C
      EXTERNAL FITISO
      DOUBLE PRECISION X(5),F(99),XJAC(99,5),XJTJ(15),RATEI(99)
     1     ,WORK(238),PARM(4),RATEF(99),STRESSF(99),TEMP(99),CURVE(99)
     2     ,STRESSI(99)
      REAL DATA(99,6)
      DOUBLE PRECISION EPS,DELTA,SSQ,Q,A,STXI,MP
      CHARACTER*20 INFILE
      COMMON RATEI,RATEF,TEMP,STRESSF,Q,A,STXI,MP,STRESSI
      N = 2
      NSIG = 8
      EPS = 0.0D0
      DELTA = 0.0D0
      MAXFN = 5000
      IOPT = 0
      IXJAC = 99
C
C                                          READ DATA
C
6     FORMAT(20A)
      PRINT *,"ENTER NAME OF DATA FILE:    "
      READ (*,6) INFILE
```

```
      OPEN (25,FILE=INFILE,RECFM='DS')
      OPEN (12,FILE='ERROR.LS')
      READ(25,*) NX
      DO 10 I = 1,NX
C
          READ(25,*) (DATA(I,J),J=1,6)
          RATEI(I) = DBLE(DATA(I,3))
          STRESSF(I) = DBLE(DATA(I,5))
          STRESSI(I) = DBLE(DATA(I,6))
          TEMP(I) = DBLE(DATA(I,2)) + 273.14D+0
          RATEF(I) = DBLE(DATA(I,4))
10        CONTINUE
C
      CLOSE (UNIT=25)
C
C                                                ESTIMATE CONSTANTS
C
      PRINT *,"INPUT ESTIMATE OF A-Q TERM          :  "
      READ (*,*) X(1)
      PRINT *,"INPUT ESTIMATE OF M                 :  "
      READ (*,*) X(2)
C
C                                                PERFORM FIT
C
      CALL ZXSSQ(FITISO,NX,N,NSIG,EPS,DELTA,MAXFN,IOPT,PARM,X,
     1           SSQ,F,XJAC,IXJAC,XJTJ,WORK,INFER,IER)
      WRITE (*,70) INFER,IER
70    FORMAT (' INFER = ',I7,'       IER = ',I5)
      WRITE (*,80) X(1)
80    FORMAT (' A/Q = ',D12.5)
      WRITE (*,81) X(2)
81    FORMAT (' M   = ',D12.5)
      PRINT *,(F(J),J=1,NX)
      STOP
      END
```

```
C
C     FITISO
C
C         EVALUATION SUBROUTINE FOR ISOCON
C
C         STUART BROWN   4-4-86
C
      SUBROUTINE FITISO(X,NX,N,F)
      DOUBLE PRECISION X(5),F(99),RATEI(99),STRESSF(99),TEMP(99)
      DOUBLE PRECISION ZI,ZF,ARGNUMER,ARGDENOM,Q,A,STXI,MP,RATEF(99),A1
      DOUBLE PRECISION STRESSI(99),ARG1,ARG2
      COMMON RATEI,RATEF,TEMP,STRESSF,Q,A,STXI,MP,STRESSI
C
      PRINT *,X(1),X(2)
C
      DO 10 I = 1,NX
C
        ARGNUMER = X(1) * RATEF(I)**X(2)
        ARGDENOM = X(1) * RATEI(I)**X(2)
        ARG1 = DLOG( ARGNUMER + DSQRT( 1.0D0 + ARGNUMER*ARGNUMER ))
        ARG2 = DLOG( ARGDENOM + DSQRT( 1.0D0 + ARGDENOM*ARGDENOM ))
        F(I) = (STRESSF(I)/STRESSI(I)) - (ARG1/ARG2)
10      CONTINUE
C
      RETURN
      END
```

```
C
C     SATCONS
C
C           DETERMINES TWO  MATERIAL CONSTANTS FOR SATURATION
C           STRESS DATA USING NONLINEAR, LEAST SQUARES, IMSL ROUTINE
C           ZXSSQ. (DOUBLE PRECISION VERSION)
C
C           STUART BROWN  11-22-86
C
C           VARIABLES
C
C              DATA(NX,6)          DATA FILE
C                COLUMN 1              TEST ID NUMBER
C                       2              TEMPERATURE
C                       3              STRAIN RATE
C                       4              C * H0
C                       5              SIGMA STAR
C                       6              SIGMA ZERO
C              TEMP(25)            TEMPERATURE (KELVIN)
C              RATE(25)            TEST STRAIN RATES
C              SIGSTAR(25)         TEST SIGMA STARS
C              CURVE(25)           ID NUMBERS OF CURVES
C              CHO(25)             C * H0 VALUES
C              X(3)                EQUATION PARAMETERS
C              F(25)               RESIDUE FROM FIT
C              N                   NUMBER OF PARAMETERS
C              NSIG                SIGNIFICANT DIGITS REQUIRED FOR
C                                      PARAMETERS
C
C           FILE ASSIGNMENTS
C
C              FOR025              INPUT FILE
C
C           SUBROUTINES
C
C              FITSAT              USED IN ZXSSQ
C              ZXSSQ               FITTING ROUTINE
C
      PROGRAM SATCONS
C                                          INITIALIZE DATA
C
      EXTERNAL FITSAT
      DOUBLE PRECISION X(3),F(99),XJAC(99,3),XJTJ(10)
     1     ,WORK(219),PARM(4),RATE(99),SIGSTAR(99),TEMP(99),CHO(99)
      REAL DATA(99,6)
      DOUBLE PRECISION EPS,DELTA,SSQ,Q,XI,PM,A
      CHARACTER*20 INFILE
      COMMON RATE,SIGSTAR,TEMP,CHO,Q,XI,PM,A
      N = 3
      NSIG = 6
      EPS = 0.0D0
      DELTA = 0.0D0
      MAXFN = 5000
      IOPT = 0
      IXJAC = 99
C
C                                            READ DATA
C
6     FORMAT(20A)
      PRINT *,"ENTER NAME OF DATA FILE:    "
      READ (*,6) INFILE
      OPEN (25,FILE=INFILE,RECFM='DS')
      OPEN (12,FILE='ERROR.LS')
```

```
      READ(25,*) NX
      DO 10 I = 1,NX
C
          READ(25,*) (DATA(I,J),J=1,6)
          RATE(I) = DBLE(DATA(I,3))
          SIGSTAR(I) = DBLE(DATA(I,5))
          TEMP(I) = DBLE(DATA(I,2)) + 273.14D+0
          CHO(I) = DBLE(DATA(I,4))
10        CONTINUE
C
      CLOSE (UNIT=25)
C
C                                                  ESTIMATE CONSTANTS
C
      PRINT *,"INPUT ESTIMATE OF STILDA:          :  "
      READ (*,*) X(1)
      PRINT *,"INPUT ESTIMATE OF N                :  "
      READ (*,*) X(2)
      PRINT *,"INPUT ESTIMATE OF QDS              :  "
      READ (*,*) X(3)
      PRINT *,"INPUT VALUE OF XI                     "
      READ (*,*) XI
      PRINT *,"INPUT VALUE OF A                      "
      READ (*,*) A
      PRINT *,"INPUT VALUE OF M                      "
      READ (*,*) PM
      PRINT *,"INPUT VALUE OF Q                      "
      READ (*,*) Q
C
C                                                  PERFORM FIT
C
      CALL ZXSSQ(FITSAT,NX,N,NSIG,EPS,DELTA,MAXFN,IOPT,PARM,X,
     1           SSQ,F,XJAC,IXJAC,XJTJ,WORK,INFER,IER)
      WRITE (*,70) INFER,IER
70    FORMAT (' INFER = ',I7,'      IER = ',I5)
      WRITE (*,80) (X(I),I=1,3)
80    FORMAT (' STILDA  = ',D12.5,/' N        = ',D12.4,
     1       /' QDS     = ',D12.5)
      PRINT *,(F(J),J=1,NX)
      STOP
      END
```

```
C
C     FITSAT
C
C         EVALUATION SUBROUTINE FOR SATCONS
C
C         STUART BROWN   11-22-86
C
      SUBROUTINE FITSAT(X,NX,N,F)
      DOUBLE PRECISION X(3),F(99),RATE(99),SIGSTAR(99),TEMP(99),CHO(99)
      DOUBLE PRECISION Q,XI,PM,A,ARG,C
      COMMON RATE,SIGSTAR,TEMP,CHO,Q,XI,PM,A
C
      PRINT *,X(1),X(2)
C
      DO 10 I = 1,NX
C
        ARG = ((RATE(I)/A)*DEXP(Q/(8.314D-3*TEMP(I))))**PM
        C = (1/XI)*DLOG(ARG + DSQRT(1+ARG*ARG))
        F(I) = DLOG(SIGSTAR(I)) - DLOG(C*X(1)*((RATE(I)/A)*
     1          DEXP(X(3)/(8.314D-3*TEMP(I))))**X(2))
10      CONTINUE
C
      RETURN
      END
```

```
C
C     HOCALC
C
C           DETERMINES H0 AND INITIAL STATE VALUES USING MATERIAL
C           CONSTANTS DETERMINED FROM SATCONS, AND ZERCON PROGRAMS.
C
C           STUART BROWN  12-13-85
C
C           VARIABLES
C
C              DATA(NX,6)          DATA FILE
C                COLUMN 1               TEST ID NUMBER
C                       2               TEMPERATURE
C                       3               STRAIN RATE
C                       4               C * H0
C                       5               SIGMA STAR
C                       6               SIGMA ZERO
C              TEMP(99)            TEMPERATURE (KELVIN)
C              RATE(99)            TEST STRAIN RATES
C              SIGSTAR(99)         TEST SIGMA STARS
C              CURVE(99)           ID NUMBERS OF CURVES
C              CH0(99)             C * H0 VALUES
C
C           FILE ASSIGNMENTS
C
C              FOR025              INPUT FILE
C              FOR026              OUTPUT FILE
C
C
      PROGRAM H0CALC
C                                                INITIALIZE DATA
C
      REAL RATE(99),SIGSTAR(99),TEMP(99),CH0(99),SIGZERO(99)
      REAL DATA(99,6),X,C(99),S0(99),H0(99)
      REAL ALPHA,A,Q,M,H0AVE,H0SUM
      CHARACTER*20 INFILE,OUTFILE
C
C                                                   INPUT CONSTANTS
C
      PRINT *,"INPUT VALUE OF A       :  "
      READ (*,*) A
      PRINT *,"INPUT VALUE OF ALPHA   :  "
      READ (*,*) ALPHA
      PRINT *,"INPUT VALUE OF Q       :  "
      READ (*,*) Q
      PRINT *,"INPUT VALUE OF M       :  "
      READ (*,*) M
C
C                                                 READ DATA
C
6     FORMAT(20A)
      PRINT *,"ENTER NAME OF INPUT DATA FILE:   "
      READ (*,6) INFILE
      OPEN (25,FILE=INFILE,RECFM='DS')
      PRINT *,"ENTER NAME OF OUTPUT DATA FILE:  "
      READ (*,6) OUTFILE
      OPEN (26,FILE=OUTFILE,RECFM='DS')
      READ(25,*) NX
      WRITE(26,*) NX
C
      H0SUM = 0.
C
      DO 10 I = 1,NX
```

```
C
          READ(25,*) (DATA(I,J),J=1,6)
          RATE(I) = DATA(I,3)
          SIGSTAR(I) = DATA(I,5)
          TEMP(I) = DATA(I,2) + 273.14E+0
          CH0(I) = DATA(I,4)
          SIGZERO(I) = DATA(I,6)
          X = (RATE(I)*EXP(Q/8.314E-3/TEMP(I))/A)**M
          C(I) = (1/ALPHA)*ALOG(X+SQRT(1+X*X))
          S0(I) = SIGZERO(I)/C(I)
          H0(I) = CH0(I)/C(I)
          H0SUM = H0(I) + H0SUM
          WRITE (26,9) (DATA(I,J),J=1,6),S0(I),C(I),H0(I)
9             FORMAT(2F9.0,F6.3,4F10.4,F9.5,F9.0)
C
10        CONTINUE
C
      CLOSE (UNIT=26)
      CLOSE (UNIT=25)
C
C                                                    PERFORM FIT
C
      H0AVE = H0SUM/NX
      WRITE (*,70) H0AVE
70    FORMAT (' H0 =  ',F9.3)
      STOP
      END
```

# APPENDIX D

## Constitutive Model Integration Routines

```
C
C       ISOINT
C
C       INTEGRATION OF ISOTHERMAL, CONSTANT RATE TESTS
C
C       STUART BROWN   10-29-86
C
C
C               VARIABLE        DESCRIPTION
C
C               CP      STRESS/STATE PROPORTIONALITY
C               THOLD           HOLD TIME
C               EMOD            YOUNG'S MODULUS IN MPA
C               TDUR            DURATION OF TEST
C               RATE            STRAIN RATE
C               N               NUMBER OF EQUATIONS
C               IND             SUBROUTINE OPTION FLAG
C               TOL             LOCAL CONVERGENCE TOLERANCE
C               NW
C               X               TIME
C               Y(1)            VALUE OF STATE VARIABLE
C               C(21)
C               IER
C               W(1,9)
C
      PROGRAM ISOINT
      EXTERNAL EVOL
      REAL STRESS,STRAIN,THOLD,W(1,9),C(24),Y(1)
      CHARACTER*20 OUTFILE,INFILE
      COMMON RATE, H0, SSTAR, P, A, S0, B, QR, SMOD
5     FORMAT(A)
C
      PRINT *,"ENTER INPUT  FILENAME     "
      READ (*,5) INFILE
      PRINT *,"ENTER OUTPUT FILENAME     "
      READ (*,5) OUTFILE
C
C                                              READ DATAFILE
C
      OPEN(24,FILE=INFILE,RECFM='DS',STATUS='OLD')
      READ (24,*)  RATE1          ! STRAIN RATE ONE
      READ (24,*)  RATE2          ! STRAIN RATE TWO
      READ (24,*)  SJUMP          ! JUMP STRAIN
      READ (24,*)  TEMP           ! TEMPERATURE IN CELSIUS
      READ (24,*)  SFIN           ! FINAL VALUE OF STRAIN
      READ (24,*)  NSTEPLD1       ! # STEPS IN LOADING PERIOD 1
      READ (24,*)  NSTEPLD2       ! # STEPS IN LOADING PERIOD 2
      READ (24,*)  Y(1)           ! INITIAL VALUE OF S (MPA)
      READ (24,*)  EMOD           ! YOUNGS MODULUS (MPA)
      READ (24,*)  SMOD           ! SHEAR MODULUS (MPA)
      READ (24,*)  XI             ! STRESS/STATE SCALING
      READ (24,*)  Q              ! RATE ACTIVATION ENERGY
      READ (24,*)  EM             ! RATE EXPONENT
      READ (24,*)  AP             ! PREEXPONENTIAL
      READ (24,*)  H0             ! ATHERMAL HARDENING RATE
      READ (24,*)  A              ! EXPONENT IN HARDENING LAW
      READ (24,*)  STILDE         ! SATURATION SCALING
      READ (24,*)  EN             ! SATURATION EXPONENT
      READ (24,*)  QDS            ! SATURATION ACTIVATION ENERGY
      READ (24,*)  B              ! STATIC REC PREMULTIPLIER
      READ (24,*)  QR             ! RECOVERY ACTIVATION ENERGY
      READ (24,*)  P              ! RECOVERY TERM EXPONENT
      CLOSE (24)
```

```
C
C
      S0 = Y(1)
      ARG = ((RATE1/AP)*EXP(Q/((TEMP+273.16)*8.314E-3)))**EM
      CP  = (1./XI)*ALOG(ARG+SQRT(1.+ARG*ARG))
      SSTAR=STILDE*((RATE1/AP)*EXP(QDS/((TEMP+273.16)*8.314E-3)))**EN
      TINT1 = SJUMP/RATE1
      TINT2 = (SFIN-SJUMP)/RATE2
      TLD1  = TINT1/NSTEPLD1
      TLD2  = TINT2/NSTEPLD2
      OPEN(UNIT=25,FILE=OUTFILE)
      WRITE (25,*) NSTEPLD1 + NSTEPLD2
C
C                                  INITIAL LOADING INTEGRATION LOOP
C
      X = 0.0
      RATE = RATE1
      DO 100 I = 1, NSTEPLD1
C
            N = 1
            TEND = X + TLD1
            IND = 1
            NW = 1
            TOL = .0010
            CALL DVERK(N,EVOL,X,Y,TEND,TOL,IND,C,NW,W,IER)
            STRESS = CP*Y(1)
            STRAIN = ( STRESS / EMOD ) +( X * RATE1 )
            WRITE(25,*)  STRAIN,STRESS,TEND,Y(1)
C
            IF ((IND.LT.0).OR.(IER.GT.0.)) THEN
C
                  PRINT *,"IND = ",IND," AND IER = ",IER
                  GO TO 400
C
                  END IF
C
100   CONTINUE
C
      X = 0.0
      RATE = RATE2
      ARG = ((RATE2/AP)*EXP(Q/((TEMP+273.16)*8.314E-3)))**EM
      CP  = (1./XI)*ALOG(ARG+SQRT(1.+ARG*ARG))
      SSTAR=STILDE*((RATE2/AP)*EXP(QDS/((TEMP+273.16)*8.314E-3)))**EN
      DO 200 I = 1, NSTEPLD2
C
            N = 1
            TEND = X + TLD2
            IND = 1
            NW = 1
            TOL = .0010
            CALL DVERK(N,EVOL,X,Y,TEND,TOL,IND,C,NW,W,IER)
            STRESS = CP*Y(1)
            STRAIN = ( STRESS / EMOD ) +( X * RATE2) + SJUMP
            WRITE(25,*)  STRAIN,STRESS,TEND+TINT1,Y(1)
C
            IF ((IND.LT.0).OR.(IER.GT.0.)) THEN
C
                  PRINT *,"IND = ",IND," AND IER = ",IER
                  GO TO 400
C
                  END IF
C
200   CONTINUE
```

```
C
400     CLOSE(25)
        STOP
        END
C
C
C       EVOL
C
C               EVALUATION SUBROUTINE FOR ISOINT
C
C               STUART BROWN  10-28-86
C
        SUBROUTINE EVOL(N,X,Y,YPRIME)
C
        REAL Y(N),YPRIME(N),THOLD
        COMMON RATE,H0,SSTAR,P,A,S0,B,QR,SMOD
C
          YPRIME(1) = H0 * ((1-(Y(1)/SSTAR))**A) * RATE  -
     1     (B*(Y(1)/SMOD)**P)*SMOD*EXP(-QR/((TEMP+273.16)*8.314E-3))
C
C
        RETURN
        END
```

```
C
C       RECINT
C
C       INTEGRATION OF RECOVERY TESTS
C
C       STUART BROWN   10-29-86
C
C
C               VARIABLE        DESCRIPTION
C
C               CP      STRESS/STATE PROPORTIONALITY
C               THOLD           HOLD TIME
C               EMOD            YOUNG'S MODULUS IN MPA
C               TDUR            DURATION OF TEST
C               RATE            STRAIN RATE
C               N               NUMBER OF EQUATIONS
C               IND             SUBROUTINE OPTION FLAG
C               TOL             LOCAL CONVERGENCE TOLERANCE
C               NW
C               X               TIME
C               Y(1)            VALUE OF STATE VARIABLE
C               C(21)
C               IER
C               W(1,9)
C
        PROGRAM RECINT
        EXTERNAL EVOL
        REAL STRESS,STRAIN,THOLD,W(1,9),C(24),Y(1)
        CHARACTER*20 OUTFILE,INFILE
        COMMON THOLD, RATE, H0, SSTAR, B, EMU, TEMP, QR, P, THB, A, S0
5       FORMAT(A)
C
        PRINT *,"ENTER INPUT  FILENAME     "
        READ (*,5) INFILE
        PRINT *,"ENTER OUTPUT FILENAME     "
        READ (*,5) OUTFILE
C
C                                                   READ DATAFILE
C
        OPEN(24,FILE=INFILE,RECFM='DS',STATUS='OLD')
        READ (24,*)  RATE                 ! STRAIN RATE
        READ (24,*)  SHOLD                ! HOLD STRAIN
        READ (24,*)  THOLD                ! TIME HELD FOR RECOVERY
        READ (24,*)  SFIN                 ! FINAL VALUE OF STRAIN
        READ (24,*)  NSTEPLD1             ! # STEPS IN LOADING PERIOD
        READ (24,*)  NSTEPHD              ! # STEPS IN HOLD PERIOD
        READ (24,*)  NSTEPLD2             ! # STEPS IN RELOADING PERIOD
        READ (24,*)  Y(1)                 ! INITIAL VALUE OF S (MPA)
        READ (24,*)  EMOD                 ! YOUNGS MODULUS (MPA)
        READ (24,*)  CP                   ! STATE/STRESS PROPORTIONALITY
        READ (24,*)  H0                   ! ATHERMAL HARDENING RATE
        READ (24,*)  A                    ! EXPONENT IN HARDENING LAW
        READ (24,*)  SSTAR                ! SATURATION VALUE OF S
        READ (24,*)  B                    ! PREMULTIPLIER IN RECOVERY TERM
        READ (24,*)  EMU                  ! SHEAR MODULUS IN GPA
        READ (24,*)  QR                   ! RECOVERY ACTIVATION ENERGY
        READ (24,*)  TEMP                 ! TEMPERATURE IN KELVIN
        READ (24,*)  P                    ! RECOVERY TERM EXPONENT
        CLOSE (24)
C
C
        S0 = Y(1)
        THB = SHOLD/RATE
```

```
      TLD1I = THB/NSTEPLD1
      TLD2 = (SFIN-SHOLD)/RATE
      TLD2I = TLD2/NSTEPLD2
      THDI  = THOLD/NSTEPHD
      OPEN(UNIT=25,FILE=OUTFILE)
      WRITE (25,*) NSTEPLD1+NSTEPHD+NSTEPLD2+1
C
C                                  INITIAL LOADING INTEGRATION LOOP
C
      X = 0.0
      DO 100 I = 1, NSTEPLD1
C
            N = 1
            TEND = X + TLD1I
            IND = 1
            NW = 1
            TOL = .0010
            CALL DVERK(N,EVOL,X,Y,TEND,TOL,IND,C,NW,W,IER)
            STRESS = CP*Y(1)
            STRAIN = ( STRESS / EMOD ) +( X * RATE )
            WRITE(25,*)  STRAIN,STRESS,TEND,Y(1)
C
            IF ((IND.LT.0).OR.(IER.GT.0.)) THEN
C
                  PRINT *,"IND = ",IND," AND IER = ",IER
                  GO TO 400
C
                  END IF
C
100   CONTINUE
C
C                                        HOLD INTEGRATION LOOP
C
      DO 200 I = 1, NSTEPHD
C
            N = 1
            TEND = X + THDI
            IND = 1
            NW = 1
            TOL = .001
            CALL DVERK(N,EVOL,X,Y,TEND,TOL,IND,C,NW,W,IER)
            STRESS = 0.0
            STRAIN = THB * RATE
            WRITE(25,*)  STRAIN,STRESS,TEND,Y(1)
C
            IF ((IND.LT.0).OR.(IER.GT.0.)) THEN
C
                  PRINT *,"IND = ",IND," AND IER = ",IER
                  GO TO 400
C
                  END IF
C
200   CONTINUE
C
C                                                RELOADING INTEGRATION
C
C
      STRESS = CP * Y(1)
      STRAIN = (STRESS/EMOD) + (X-THOLD)*RATE
      WRITE (25,*) STRAIN,STRESS,X,Y(1)
C
      DO 300 I = 1, NSTEPLD2
C
```

```
                N = 1
                TEND = X + TLD2I
                IND = 1
                NW = 1
                TOL = .001
                CALL DVERK(N,EVOL,X,Y,TEND,TOL,IND,C,NW,W,IER)
                STRESS = CP * Y(1)
                STRAIN = ( STRESS / EMOD ) + (X-THOLD) * RATE
                WRITE(25,*)  STRAIN,STRESS,TEND,Y(1)
C
                IF ((IND.LT.0).OR.(IER.GT.0.)) THEN
C
                        PRINT *,"IND = ",IND," AND IER = ",IER
                        GO TO 400
C
                        END IF
C
300     CONTINUE
400     CLOSE(25)
        STOP
        END
C
C
C       EVOL
C
C               EVALUATION SUBROUTINE FOR RECINT
C
C               STUART BROWN  10-28-86
C
        SUBROUTINE EVOL(N,X,Y,YPRIME)
C
        REAL Y(N),YPRIME(N),THOLD
        COMMON THOLD,RATE,H0,SSTAR,B,EMU,TEMP,QR,P,THB,A,S0
C
        IF ((X.LT.THB).OR.(X.GE.(THB+THOLD)))  THEN
C
                YPRIME(1) = H0 * ((1-(Y(1)/SSTAR))**A) * RATE
     1           - B*EXP(-QR/8.314E-3/TEMP)*EMU * (Y(1)/EMU)**P
C
                ELSE
                YPRIME(1)= -B*EXP(-QR/8.314E-3/TEMP)*EMU*(Y(1)/EMU)**P
C
                END IF
C
        RETURN
        END
```

```
      SUBROUTINE UMAT(STRESS,STATEV,DDSDDE,SSE,SPD,SCD,STRAN,DSTRAN,
     1  TIME,DTIME,TEMP,DTEMP,PREDEF,DPRED,MATERL,NDI,NSHR,NTENS,
     2  NSTATV,PROPS,NPROPS,COORDS)
C**********************************************************************
C  Isotropic Thermo-Elasto-Viscoplasticity with pressure sensitive
C  plastic flow and plastic dilatancy.
C**********************************************************************
C  This UMAT version interfaces with the *VISCO procedure in ABAQUS.
C  Automatic timestep control is done using the CEMAX parameter. The
C  timestep is decreased if CEMAX exceeds CETOL.
C**********************************************************************
C  This UMAT version is not for use in plane stress or any other cases
C  where more strain terms than stress terms are used.
C**********************************************************************
C State Variables:
C   STATEV(1) = S       (plastic flow resistance,tensile,suggested
C                        units are N/m2)
C   STATEV(2) = TH      (temperature,suggested units are Deg.K)
C Two more are for debugging and plotting purposes.
C   STATEV(3) = F       (plastic shear strain rate)
C   STATEV(4) = time integral of F   (plastic shear strain)
C**********************************************************************
C Contents of PROPS vector in this version:
C J   PROPS(J)
C--- ----------
C 1   PLSLMT -- limit on equiv. plastic tensile strain increment
C 2   PHI -- degree of implicitness (ranges from 0 to 1)
C 3   OMEGA -- fraction of plastic work going into adiabatic heating
C 4   S0 -- initial value for internal variable S
C 5   T0 -- initial value for temperature
C 6   AMU -- shear modulus
C 7   AKAPPA -- bulk modulus
C 8   ALPHA -- thermal expansion coefficient
C 9   RHO -- density
C 10  C -- specific heat
C 11  A -- pre-exponential factor in plastic shear strain rate
C 12  Q/R -- activation energy divided by universal gas constant
C 13  XP -- exponent in eqn for F (1./strain rate sensitivity)
C 14  PALPHA -- pressure sensitivity parameter
C 15  H0 -- pre-multiplier in hardening rate equation
C 16  SB -- pre-multiplier for saturation value of S
C 17  AN -- exponent in equation for saturation value of S
C 18  B -- pre-multiplier for rate of static restoration
C 19  SA -- annealed value of S
C 20  P -- exponent in equation for RDOT
C The above list of properties is specific to the functions chosen for
C modeling one particular material. For other materials a different list
C may be desirable. For example, additional properties would be needed
C to define functions of temperature for the elastic constants and for
C the annealed value of internal variable S.
C**********************************************************************
C See subroutines UMPROP, GAMDOT, and SDOT for suggested units for
C the above properties.
C**********************************************************************
C The values input for S0,A,H0,SB,B,SA should correspond to tensile
C test data. These values are converted to equivalent shear values
C within the subroutines.
C**********************************************************************
C The parameter PHI controls the degree of implicitness of the
C integration procedure.
C    PHI=0.0   ---- explicit
C    PHI=1.0   ---- fully implicit
C Suggested value of PHI: equal to or greater than 0.50
```

```
C*****************************************************************
C The parameter OMEGA controls whether the problem is isothermal or
C adiabatic.
C     OMEGA=0.0  ---- isothermal
C     OMEGA=1.0  ---- adiabatic
C Suggested value for fast deformations is 0.9
C*****************************************************************
      IMPLICIT REAL*8(A-H,O-Z)
C*****************************************************************
C Common blocks CERROR and CONSTS appear here exactly as they exist in
C ABAQUS version 4-5-159. They will generally be different for other
C ABAQUS versions.
C*****************************************************************
      COMMON/CERROR/RESMAX(30),JNREMX(30),ERRMAX(2),CETOL,CSLIM,
     1  CEMAX,PCTOL,TLIMIT,PSUBIN,RESMIN,DUMAX(30),JNDUMX(30),ERRPRE,
     2  UDELSS,PTOL,AMTOL,DMKET,DMRETL,SIGTOL,DSIGMX,UTOL,UMAX,U4MAX,
     3  VMAX,V4MAX,AMAX,A4MAX,TMAX,EPPMAX,PMAX,R4MAX,NGOPEN,NGCLOS,
     4  ROTTOL,ROTFAC,JRIKND,NINCCS,RIKUB,RIKUMX,RIKMU,RIKLAM,RIKDLA,
     5  RIKRO,RIKOLD,RIKLMX,QMAX,DUMAXP,STRRAT,PCUT,RIKDLO
C*****************************************************************
      COMMON/CONSTS/PI,SIN60,COS60,KCROS2(3),KCROS3(3),ZERO,LZERO,LONE,
     1  ONE,TWO,HALF,ABIG,ASMALL,BCBIG,LOCSHR(2,3),THIRD,PRECIS,BLANK
C*****************************************************************
      DIMENSION STRESS(NTENS),STATEV(NSTATV),DDSDDE(NTENS,NTENS),
     1  STRAN(NTENS),DSTRAN(NTENS),PREDEF(1),DPRED(1),PROPS(NPROPS),
     2  COORDS(3)
C*****************************************************************
      SQART3=TWO*SIN60
      NDIP1=NDI+1
      PHIDT=PROPS(2)*DTIME
C*****************************************************************
C Initialize the state variables, if necessary.
C*****************************************************************
      IF (STATEV(1).LE.ZERO) THEN
      STATEV(1)=PROPS(4)/SQART3
      STATEV(2)=PROPS(5)
      STATEV(4)=ZERO
      END IF
C*****************************************************************
C Set the state variables.
C*****************************************************************
      S=STATEV(1)
      TH=STATEV(2)
C*****************************************************************
C The parameter TAUTOL is the minimum value allowed for TAUB. This
C avoids difficulties that could arise when dividing by TAUB. The value
C used corresponds to a stress level at which F is considered
C negligible, while 1./TAUTOL**2 can still be evaluated.
C*****************************************************************
      TAUTOL=S*1.D-6
C*****************************************************************
C Subroutine UMPROP determines AMU,AKAPPA,ALPHA,RHO,and C based upon
C the temperature TH, using data supplied in PROPS. For the present
C case, the properties are assumed constant and input directly in PROPS.
C In other cases, additional data constants defining functions of TH for
C each property may be input.
C*****************************************************************
      CALL UMPROP (AMU,AKAPPA,ALPHA,RHO,C,TH,PROPS,NPROPS)
C*****************************************************************
C Pressure PB and equivalent shear stress TAUB
C*****************************************************************
      CALL SINV (STRESS,SINV1,SINV2)
      TAUB=DMAX1(SINV2/SQART3,TAUTOL)
```

```
      PB=-SINV1
C*****************************************************************
C Subroutine SBETA determines the value of the plastic dilatancy
C factor BETA. Presently set to zero.
C*****************************************************************
      CALL SBETA (TAUB,PB,TH,S,BETA)
C*****************************************************************
      IF (PROPS(3).GT.ZERO) THEN
      CON1=PROPS(3)*(TAUB-BETA*PB)/(RHO*C)
      ELSE
      CON1=ZERO
      END IF
C*****************************************************************
C Subroutine GAMDOT determines the equivalent plastic shear strain rate
C F and its derivatives PDA,PDB,PDC,PDD with respect to TAUB,PB,TH,and
C S, respectively. To make the subsequent calculations more convenient,
C PDB,PDC, and PDD are returned as:
C          RATIOB =  PDB/PDA
C          RATIOC =  PDC/PDA
C          RATIOD =  PDD/PDA
C CON2 is returned for use in subroutine SDOT.
C*****************************************************************
      CALL GAMDOT (TAUB,PB,TH,S,PROPS,NPROPS,SQART3,
     1             F1,PDA,RATIOB,RATIOC,RATIOD,CON2)
      AMUB=AMU*TAUB/(TAUB+AMU*PHIDT*F1)
C*****************************************************************
C Subroutine SDOT determines the hardening rate H and the sta ic
C restoration rate RDOT. SA, the annealed value of S at this
C temperature, is also returned.
C*****************************************************************
      CALL SDOT(TAUB,PB,TH,S,AMU,CON2,PROPS,NPROPS,SQART3,F1,H,RDOT,SA)
      DR=RDOT*DTIME
C*****************************************************************
      G=AMU-(RATIOB*AKAPPA*BETA+RATIOC*CON1+RATIOD*H)
      V=PHIDT*PDA*G
      V1=F1*DTIME/(ONE+V)
      V2=PHIDT*PDA/(ONE+V)
C*****************************************************************
C Trace of strain increment -- DVOL
C*****************************************************************
      DVOL=ZERO
      DO 10 K1=1,NDI
   10 DVOL=DVOL+DSTRAN(K1)
C*****************************************************************
C Convert stress to deviatoric stress.
C*****************************************************************
      DO 20 K1=1,NDI
   20 STRESS(K1)=STRESS(K1)+PB
C*****************************************************************
C Deviatoric stress times strain increment -- SDSI
C*****************************************************************
      SDSI=ZERO
      DO 30 K1=1,NTENS
   30 SDSI=SDSI+STRESS(K1)*DSTRAN(K1)
C*****************************************************************
C Effective plastic shear strain increment.
C*****************************************************************
      DGAMPB=V1+V2*(AMU*SDSI/TAUB-AKAPPA*RATIOB*DVOL)
C*****************************************************************
C Increments DS and DTH.
C*****************************************************************
      DS=H*DGAMPB-DR
      DTH=CON1*DGAMPB
```

```
C**********************************************************************
C Constants for Jacobian and stress increment.
C**********************************************************************
      V3=TWO*AMUB
      V11=AKAPPA-TWO*THIRD*AMUB
      V4=V11*DVOL
      V5=AKAPPA*ALPHA*DTH/THIRD
      V6=AKAPPA*BETA*DGAMPB
      V7=V4-V5-V6
      V8=AMU*DGAMPB/TAUB-(AMU-AMUB)*SDSI/TAUB**2
      V9=AMUB
      V12=(V2*AMU**2+AMUB-AMU)/TAUB**2
      V13=-V2*AKAPPA*RATIOB*AMU/TAUB
      V14=V2*AKAPPA*(AMU/TAUB)*(BETA+CON1*ALPHA/THIRD)
      V15=-V2*AKAPPA**2*RATIOB*(BETA+CON1*ALPHA/THIRD)
      V16=V11-V15
C**********************************************************************
C Calculate the Jacobian, which is nonsymmetric unless V13=V14. This
C is generally true only if OMEGA=0, BETA=0, and PDB=0. Otherwise,
C ABAQUS will use only the symmetric part of the Jacobian unless an
C unsymmetric Jacobian has been called for on the title card.
C Note that STRESS used here is the deviatoric stress.
C**********************************************************************
      DO 40 K1=1,NTENS
      DO 40 K2=1,NTENS
   40 DDSDDE(K1,K2)=-V12*STRESS(K1)*STRESS(K2)
      DO 50 K1=1,NDI
      DO 50 K2=1,NTENS
      DDSDDE(K1,K2)=DDSDDE(K1,K2)-V14*STRESS(K2)
   50 DDSDDE(K2,K1)=DDSDDE(K2,K1)-V13*STRESS(K2)
      DO 60 K1=1,NDI
      DDSDDE(K1,K1)=DDSDDE(K1,K1)+V3
      DO 60 K2=1,NDI
   60 DDSDDE(K1,K2)=DDSDDE(K1,K2)+V16
      IF (NSHR.GT.0) THEN
      DO 70 K1=NDIP1,NTENS
   70 DDSDDE(K1,K1)=DDSDDE(K1,K1)+V9
      END IF
C**********************************************************************
C Calculate complete STRESS at the end of the increment using the
C deviatoric stress at the beginning of the increment.
C**********************************************************************
      DO 80 K1=1,NDI
   80 STRESS(K1)=(ONE-V8)*STRESS(K1)+V3*DSTRAN(K1)+V7-PB
      IF (NSHR.GT.0) THEN
      DO 90 K1=NDIP1,NTENS
   90 STRESS(K1)=(ONE-V8)*STRESS(K1)+V9*DSTRAN(K1)
      END IF
C**********************************************************************
C Update the state variables.
C**********************************************************************
      CALL SINV (STRESS,SINV1,SINV2)
      TAUB=DMAX1(SINV2/SQART3,TAUTOL)
      PB=-SINV1
      TH=TH+DTH
      S=S+DS
      IF (S.LT.SA) S=SA
      CALL GAMDOT (TAUB,PB,TH,S,PROPS,NPROPS,SQART3,
     1             F2,PDA,RATIOB,RATIOC,RATIOD,CON2)
      STATEV(1)=S
      STATEV(2)=TH
      STATEV(3)=F2
      STATEV(4)=STATEV(4)+DGAMPB
```

```
C**********************************************************************
C Comparison of the plastic strain rates before and after the time
C increment. To be used by the automatic integration scheme of ABAQUS.
C Note that the factor SQART3 is used to convert shear strain to
C tensile strain.
C**********************************************************************
      DIFF=DTIME*DABS(F1-F2)/SQART3
      CEMAX=DMAX1(CEMAX,DIFF)
C**********************************************************************
C Check magnitude of plastic strain increment against a reference level.
C This allows the automatic timestep control in ABAQUS to limit the size
C of the plastic strain increment using the variable CEMAX.
C**********************************************************************
      PLSLMT=PROPS(1)*SQART3
      IF (PLSLMT.GT.ZERO) THEN
      PLSCHK=(DGAMPB/PLSLMT)*CETOL
      CEMAX=DMAX1(CEMAX,PLSCHK)
      END IF
      RETURN
      END
C**********************************************************************

C**********************************************************************
      SUBROUTINE UMPROP (AMU,AKAPPA,ALPHA,RHO,C,TH,PROPS,NPROPS)
C**********************************************************************
C Determine the following constants for the material:
C AMU ---- shear modulus (suggested units: N/m2)
C AKAPPA - bulk modulus (suggested units: N/m2)
C ALPHA -- thermal expansion coefficient (suggested units: 1/Deg.K)
C RHO ---- mass density (suggested units: kg/m3)
C C ------ specific heat (suggested units: Joules/kg/Deg.K)
C In general, these properties are functions of temperature, but in
C the present case they are input directly, assuming no temperature
C dependence. Additional entries in PROPS could be used to define them
C as functions of temperature.
C**********************************************************************
      IMPLICIT REAL*8(A-H,O-Z)
C**********************************************************************
      DIMENSION PROPS(NPROPS)
C**********************************************************************
      AMU=PROPS(6)
      AKAPPA=PROPS(7)
      ALPHA=PROPS(8)
      RHO=PROPS(9)
      C=PROPS(10)
C**********************************************************************
      RETURN
      END
C**********************************************************************

C**********************************************************************
      SUBROUTINE SBETA (TAUB,PB,TH,S,BETA)
C**********************************************************************
C Subroutine SBETA determines the plastic dilatancy factor.
C**********************************************************************
      IMPLICIT REAL*8(A-H,O-Z)
C**********************************************************************
      BETA=0.0D+0
C**********************************************************************
      RETURN
      END
C**********************************************************************
```

```
C*********************************************************************
      SUBROUTINE GAMDOT (TAUB,PB,TH,S,PROPS,NPROPS,SQART3,
     1                   F,PDA,RATIOB,RATIOC,RATIOD,CON2)
C*********************************************************************
C Subroutine GAMDOT determines the equivalent plastic shear strain rate
C and its derivatives PDA,PDB,PDC,PDD with respect to TAUB,PB,TH,and S,
C respectively. Note that the following derivative terms are returned:
C             RATIOB = PDB/PDA
C             RATIOC = PDC/PDA
C             RATIOD = PDD/PDA
C*********************************************************************
      IMPLICIT REAL*8(A-H,O-Z)
C*********************************************************************
      COMMON/CONSTS/PI,SIN60,COS60,KCROS2(3),KCROS3(3),ZERO,LZERO,LONE,
     1  ONE,TWO,HALF,ABIG,ASMALL,BCBIG,LOCSHR(2,3),THIRD,PRECIS,BLANK
C*********************************************************************
      DIMENSION PROPS(NPROPS)
C*********************************************************************
C Material parameters defining the equivalent plastic shear strain rate
C PROPS(11)=A --- pre-exponential factor
C   suggested units are: 1./sec
C PROPS(12)=Q/R --- activation energy divided by universal gas constant
C   suggested units for Q are: kJ/mol
C   suggested units for R are: 8.314D-3 kJ/mol/Deg.K
C PROPS(13)=1./AM -- 1./strain rate sensitivity
C PROPS(14)=PALPHA -- pressure sensitivity parameter
C   suggested units are: 1/(N/m2)
C Note:   PALPHA=2*(DMU/DPB)/MU0 ,  with
C             MU0 -- shear modulus at zero pressure
C             DMU/DPB -- pressure dependency of shear modulus
C*********************************************************************
      AL = 3.250D0
      CON2=SQART3*PROPS(11)*DEXP(-PROPS(12)/TH)
C*********************************************************************
      F=CON2*(DSINH(TAUB*AL/(S*(ONE+PROPS(14)*PB))))**PROPS(13)
C*********************************************************************
C Note that a tolerance was set on the minimum value of TAUB allowed,
C to avoid calculational difficulties.
C*********************************************************************
      SP = S*(ONE+PROPS(14)*PB)
      PDA=F*PROPS(13)*DCOSH(TAUB*AL/SP)*AL/DSINH(TAUB*AL/SP)/SP
      RATIOB=0.0
      RATIOC=PROPS(12)*S*DTANH(TAUB*AL/S)/(AL*PROPS(13)*TH**2)
      RATIOD=-TAUB/S
C*********************************************************************
      RETURN
      END
C*********************************************************************

C*********************************************************************
      SUBROUTINE SDOT (TAUB,PB,TH,S,AMU,CON2,PROPS,NPROPS,SQART3,F,
     1                 H,RDOT,SA)
C*********************************************************************
C This subroutine determines the hardening rate H and the static
C restoration rate RDOT.
C*********************************************************************
      IMPLICIT REAL*8(A-H,O-Z)
C*********************************************************************
      COMMON/CONSTS/PI,SIN60,COS60,KCROS2(3),KCROS3(3),ZERO,LZERO,LONE,
     1  ONE,TWO,HALF,ABIG,ASMALL,BCBIG,LOCSHR(2,3),THIRD,PRECIS,BLANK
C*********************************************************************
      DIMENSION PROPS(NPROPS)
C*********************************************************************
```

```
C Material parameters determining the rate of hardening:
C PROPS(15)=H0 -- pre-multiplier in hardening rate equation
C   suggested units: N/m2
C PROPS(16)=SB -- pre-multiplier for saturation value of S
C   suggested units: N/m2
C PROPS(17)=AN -- exponent in eqn. for saturation value of S
C PROPS(18)=B --- pre-multiplier for rate of static restoration
C   suggested units: N/m2
C PROPS(19)=SA -- annealed value of S.
C   suggested units: N/m2
C PROPS(20)=P --- exponent of ((S/SA)-1.) in RDOT
C The following constant was calculated in GAMDOT.
C          CON2 = A*DEXP( -Q/(R*TH) )
C Note that H0,SB,B, and SA should be from tensile test data because
C a conversion to pure shear data is done in this subroutine.
C*************************************************************************
C First calculate H.
C*************************************************************************
      SS=(PROPS(16)/SQART3)*(F/CON2)**PROPS(17)
      IF (S.LE.SS) THEN
      H=THIRD*PROPS(15)*(ONE-S/SS)**1.5D0
      ELSE
      H=ZERO
      END IF
C*************************************************************************
C Determine the annealed value of S. Although in general it is a
C function of temperature, in the present version it is input directly
C and considered constant.
C*************************************************************************
      SA=PROPS(19)/SQART3
C*************************************************************************
C Calculate RDOT.
C*************************************************************************
      SD=(S/SA)-ONE
      IF (SD.GT.ZERO) THEN
      RDOT=AMU*THIRD*PROPS(18)*CON2*SD**PROPS(20)
      ELSE
      RDOT=ZERO
      END IF
C*************************************************************************
      RETURN
      END
```

# APPENDIX E

## ABAQUS input files

```
*HEADING
LOAD BOUNDARY CONDITIONS - 20000 N
*NODE
1,0.0,0.0
2,0.00635,0.0
3,0.00635,0.009525
4,0.0,0.009525
*ELEMENT,TYPE=CAX4H
1,1,2,3,4
*BOUNDARY
1,1,2
2,2
4,1
*EQUATION
2
3,2,1.,4,2,-1.
*MATERIAL
*USER MATERIAL,CONSTANTS=20
.01D0    ,0.75D0 ,0.D0   , 60.0D6 ,1073.14D0 ,32.0D9 ,1.59D11 ,16.6D-6
7.3D3    ,0.44D3,6.346D11,3.7569D4 ,5.1125D0 ,0.0D0  ,3774.D6 ,125.1D6
.06869D0,0.0D0   , 60.0D6,1.0D0
*DEPVAR
4
*AMPLITUDE,VALUE=A,TIME=V,NAME=TOPLOAD
0., 0., 10.,  -20000,  20.   , -20000,  30.   , 0.
*STEP,NLGEOM,AMP=RAMP,INC=1500,CYCLE=6,SUBMAX
*VISCO,PTOL=1.0,CETOL=1.0E-5
0.0001,30.0,,.06
*CLOAD,AMPLITUDE=TOPLOAD
4,2,1.
*EL FILE,FREQ=1
2,1
2,1,1
*EL PRINT,FREQ=1000
2,1
2,1,1
*NODE PRINT,FREQ=1000
*PRINT,RESIDUAL=NO,FREQ=100
*END STEP
```

```
*HEADING
ALUMINUM GRADIENT SPECIMEN
** NEUTRAL FILE GENERATED ON: 26-MAR-86     09:38:09  PATRAN VERSION: 1.6B
** SUMMARY DATA:
**      52 NODES,     36 ELEMENTS,  0 MATERIALS,  0 PHYSICAL PROPERTIES
*NODE, NSET=CF0000
    1     0.0         0.0
    4     0.01270     0.0
   49     0.0         0.04041
   52     0.00374     0.04041
*NGEN,NSET=LSIDE
1,49,4
*NGEN,NSET=RSIDE
4,52,4
*NGEN
1,4,1
5,8,1
9,12,1
13,16,1
17,20,1
21,24,1
25,28,1
29,32,1
33,36,1
37,40,1
41,44,1
45,48,1
49,52,1
*NSET,NSET=TOP
49,50,51,52
*ELEMENT, TYPE=CAX4H
 1,  1,  2,  6,  5
*ELGEN
1,3,1,1,12,4,3
*BOUNDARY
    1     1     2   .000E+00
    2     2         .000E+00
    3     2         .000E+00
    4     2         .000E+00
    5     1         .000E+00
    9     1         .000E+00
   13     1         .000E+00
   17     1         .000E+00
   21     1         .000E+00
   25     1         .000E+00
   29     1         .000E+00
   33     1         .000E+00
   37     1         .000E+00
   41     1         .000E+00
   45     1         .000E+00
   49     1         .000E+00
*EQUATION
2
52,2,1.,49,2,-1.
2
51,2,1.,49,2,-1.
2
50,2,1.,49,2,-1.
*MATERIAL
*USER MATERIAL, CONSTANTS=20
.01D0,  0.75D0 ,0.D0     , 35.0D6  , 573.16D0 ,25.0D9 ,0.70D11 ,22.0D-6
2.753  ,1.00D3 ,1.906D7 ,2.1086D4 ,4.2831D0  ,0.0D0  ,1115.D6 ,18.9D6
.07049D0,0.0D0  , 35.0D6 ,1.0D0
```

```
*DEPVAR
4
*PLOT
*DRAW
*STEP,NLGEOM,AMP=RAMP,INC=1,CYCLE=6,SUBMAX
*VISCO,PTOL=1.0,CETOL=1.E-4
0.0000065,0.0000065,0.0000065
*BOUNDARY
TOP,2,,-0.00000001
*NODE PRINT
*PRINT,RESIDUAL=NO
*END STEP
*RESTART,WRITE,FREQ=300
*STEP, NLGEOM, AMP=RAMP,INC=300,CYCLE=6,SUBMAX
*VISCO,PTOL=5.0, CETOL=1.0E-4
0.001, 8.0,,.08
*BOUNDARY
TOP,2,,-0.0080
*EL FILE,FREQ=49
    2    2    1    1
    2    2    1    1
    2    2    2    2
*NODE FILE,FREQ=49
    2    1    1    1    1    2
*EL PRINT,DEPVAR,FREQ=49
2,1
2,1,1
*NODE PRINT,FREQ=49
*PRINT,RESIDUAL=NO
**                          PLOTTING SECTION
*PLOT,FREQ=49
*DISPLACED
1,1.0
*CONTOUR
**                          VON MISES STRESS
9,10
**                          INTERNAL VARIABLE
81,10
*END STEP
```